Exploiting Oxidative Stress as a Therapeutic Option in Rhabdomyosarcoma

---

Dissertation

zur

Erlangung der naturwissenschaftlichen Doktorwürde
(Dr. sc. nat.)

vorgelegt der

Mathematisch-naturwissenschaftlichen Fakultät

der

Universität Zürich

von

Eva Brack

aus Deutschland

Promotionskommission

Prof. Dr. Beat Schäfer (Vorsitz)

Prof. Dr. Martin Pruschy

Prof. Dr. Alex Hajnal

Zürich, 2018

STATEMENT OF AUTHORSHIP

The experimental work presented in this thesis was performed at the Department of Oncology and Children's Research Center, University Children's Hospital Zurich. I declare that I have used no other sources and aids other than those indicated. All passages quoted from publications or paraphrased from these sources are indicated as such, i.e. cited and/or attributed. This thesis was not submitted in any form for another degree or diploma at any university of other institution of tertiary education.

Zurich, May 2018

Eva Brack

To Christoph and Antonie who supported me along my journey

- and to my patients, who just deserve better

Any living cell carries with it the experiences of a billion years of experimentation by its ancestors. You cannot expect to explain so wise an old bird in a few simple words.

Max Delbrück, geneticist, 1966

Summary

Rhabdomyosarcomas are the most common soft tissue sarcomas and account for around 7% of childhood malignancies. Within this group, alveolar rhabdomyosarcoma (aRMS) is a highly malicious subtype, which is characterized by a specific chromosomal translocation encoding the oncogenic transcription factor PAX3-FOXO1. Standard treatment for children with aRMS comprises surgery, chemotherapy, and radiotherapy. Despite this aggressive treatment approach, survival rates remain poor, especially in the case of recurrences. Further, due to the high toxicity of the different treatment modalities, short-, as well as long-term side-effects are common, which subsequently greatly influence the patients' quality of life.

In an attempt to find new therapeutic agents from a large drug library screen, we have previously identified the compound fenretinide (retinoic acid p-hydroxyanilide), to affect both PAX3-FOXO1 expression as well as aRMS cell viability. Fenretinide is a Vitamin A derivate and already in clinical use since many years but has up-until-now not been used in the context of rhabdomyosarcoma.

In this thesis my aim was to characterize the mode of action of fenretinide in aRMS in detail and to find treatment modalities that act in combination with fenretinide.

We were able to show that fenretinide induced the production of reactive oxygen species (ROS). Further exploration revealed that the fenretinide-induced ROS derived from an interaction of fenretinide downstream of complex II of the mitochondrial respiratory chain, leading to mitochondrial ROS (superoxides) which were able to trigger cell death, as ROS scavenging completely abolished cell death.

To identify the mode of cell death involved, we next co-treated cells with commonly used pharmacological inhibitors of specific cell death pathways including Z-vad (pan-caspase inhibitor-apoptosis inhibitor), Necrostatin-1 (RIP-1 kinase inhibitor-necroptosis inhibitor), 3-Methyadenine (3-MA) (phosphatidylinositol 3-kinase inhibitor-autophagy inhibitor) and Ferrostatin-1

(ferroptosis inhibitor). Interestingly, none of these inhibitors was able to rescue cells from cell death. Moreover, CRISPR/Cas9 mediated depletion of key players in the apoptotic and necroptotic pathway (Bak, Bax and RIPK1) confirmed our pharmacological data. These findings indicate that a different, less well characterized cell death pathway might be involved. Surprisingly, electron microscopic images of fenretinide treated cells revealed an excessive accumulation of cytoplasmic vacuoles. Morphologically, these vacuoles were distinct from autophagosomes and swollen endoplasmic reticulum, as observed during autophagy, oncosis, or paraptosis.

Subsequent flow cytometry and fluorescence microscopy experiments pointed at a hyperstimulated macropinocytosis which shows accumulation of enlarged early and late endosomes due to impaired endosomal trafficking. However and most notable, pharmacological inhibition of the classical endosomal pathways (clathrin and caveolae mediated endocytosis) did not influence cell death. In contrast, pharmacological inhibition as well as genetic knockdown of the large GTPase dynamin completely abolished the fenretinide induced vacuolization, indicating a new form of dynamin-dependent cell death.

In the second part of this thesis, we concentrated on treatment modalities that would enhance cell death in combination with fenretinide. To expand the treatment regime in this difficult to treat tumours is one of the main ambitions connecting laboratory and clinical research. We focused on ionizing radiation (IR), as this treatment form is already part of the standard treatment regime of patients with aRMS. However, IR is prone to induce many side-effects including growth-restriction, infertility and the development of secondary malignancies. Hence, identification of radio sensitizers is highly desirable and would allow to reduce the applied doses. Our study showed, that the combinatorial treatment potentiated cell death and led to an impaired clonogenic growth. This was due to an enhanced production of a different type of ROS, namely production of hydrogen peroxide whereas fenretinide mainly induces superoxides. Further, we detected

augmented DNA damage and impaired cell cycle progression in the co-treated cells, most likely due to enhanced ROS damage.

Finally, we analysed the underlying cell death mechanisms and found an induction of apoptosis together with increased macropinocytosis. However, IR alone did not influence macropinocytosis which is specific for fenretinide.

Taken together, our data identify fenretinide to demonstrate high potential for treatment of aRMS, as it induces a new form of dynamin dependent cell death mediated through the production of ROS. Further in combination with IR, fenretinide is a very promising radio-sensitizer able to significantly enhance cell death.

Zusammenfassung

Das Rhabdomyosarkom ist der häufigste Tumor aus der Gruppe der Weichteilsarkome und hat in etwa einen Anteil von 7% an allen kindlichen Krebserkrankungen. Eine Untergruppe dieser Tumore ist das hochmaligne alveoläre Rhabdomyosarkom welches durch eine spezifische chromosomale Translokation und den dadurch codierten onkogenen Transkriptionsfaktor PAX3-FOXO1 charakterisiert ist.

Das Standardbehandlungsregime für Kinder welche an aRMS erkranken beinhaltet Operation und Strahlentherapie für die lokale Kontrolle und Chemotherapie als systemische Behandlung. Trotz dieses aggressiven Vorgehens sind die Überlebensraten noch immer schlecht, dies vor allem, wenn es zu einem Krankheitsrückfall (Relapse) kommt. Darüber hinaus haben die unterschiedlichen Behandlungen, aufgrund ihrer hohen Toxizität, häufig Kurzzeit- und Langzeitnebenwirkungen, welche einen grossen Einfluss auf die Lebensqualität der Patienten haben. In unserer Arbeitsgruppe wurde im Rahmen eines Medikamentenscreens der Wirkstoff Fenretinide (retinoic acid p-hydroxyanilide) als ein Therapeutikum identifiziert, dass in den durchgeführten Versuchen sowohl die Expression von PAX3-FOXO1 als auch das Zell Überleben von aRMS Zellen beeinflusst. Fenretinide, welches zur Familie der A-Vitamine gehört, ist bereits seit vielen Jahren im klinischen Gebrauch und wurde auch in multiplen Studien integriert, eine Anwendung zur Behandlung des Rhabdomyosarkoms ist bis dato noch nicht beschrieben.

Ziel dieser Doktorarbeit war es die genaue Wirkungsweise von Fenretinide auf aRMS-Zellen im Detail zu untersuchen und zudem die Kombination von Fenretinide mit weiteren Behandlungsmodalitäten auf eine synergistische Wirkung hin zu evaluieren.

In unseren Versuchen konnten wir zeigen dass Fenretinide die Produktion von reaktiven Sauersoffradikalen (reactive oxygene species, ROS) induziert. Weitere Untersuchungen zeigten dass Sauerstoffradikale durch eine Interaktion von Fenretinide mit dem Komplex-II der

mitochondrialen Atmungskette hervorgerufen wurden und so für die Entstehung von mitochondrialen ROS (Superoxiden) sorgen. Weiter zeigte sich, dass diese Superoxide den eintretenden Zelltod induzieren. Dies konnte durch anschliessende Neutralisationsversuche bewiesen werden, da die Induktion des Zelltods komplett aufgehoben werden konnten. Um den genauen Zelltodmechanismus der diesen Beobachtungen zugrunde liegt zu identifizieren, behandelten wir unsere Zellen zusätzlich mit pharmakologischen Inhibitoren der gängigsten Zelltod Wege zusammen mit Fenretinide. Zu diesen Inhibitoren der verschiedenen Zelltodmechanismen zählen Z-vad (pan-caspase Inhibitor-Apoptose Inhibitor), Necrostatin-1 (RIP-1 kinase Inhibitor- Nekroptose Inhibitor), 3-Methyadenine (3-MA) (Phosphatidylinositol 3-kinase Inhibitor- Autophagy Inhibitor) und Ferrostatin-1 (Ferroptose Inhibitor). Interessanterweise konnte keiner dieser Inhibitoren den Zelltod verhindern. Darüber hinaus konnten wir mit Hilfe der CRISPR/Cas9 vermittelten Ausschaltung von Schlüsselmolekülen des apoptotischen, als auch des nekroptotischen Zelltods (Bak, Bax und RIPK1) unsere pharmakologischen Daten bestätigen. Diese Forschungsergebnisse weisen darauf hin, dass voraussichtlich ein weniger gut charakterisierter Zelltod an der Wirkung von Fenretinide beteiligt ist. Elektronenmikroskopische Aufnahmen von Fenretinide behandelten Zellen zeigten eine exzessive Anhäufung von Vakuolen im Zytoplasma. Morphologisch stellten sich diese Vakuolen jedoch unterschiedlich zu Autophagosomen oder zum geschwollenem endoplasmatischen Retikulum dar, wie sie während Autophagy, Oncosis oder Paraptosis beobachtet werden können.

Weiterführende Durchflusszytometrie und Fluoreszenzmikroskopie Untersuchungen deuteten in die Richtung einer überstimulierten Makropinozytose. In diesem Fall führt eine eingeschränkte Beweglichkeit von vergrösserten frühen-als auch späten Endosomen zu einer Anhäufung derselben. Am bemerkenswertesten war jedoch dass eine pharmakologische Inhibition der klassischen endosomalen Wege, via Clathrin und Caveolin vermittelte Endozytose, keinen Einfluss auf den induzierten Zelltod hatten. Unsere weiterführenden Experimente zeigten, dass

eine pharmakologische Inhibition als auch das genetisches Abschalten der grossen GTPase Dynamin den durch Fenretinide induzierten vakuolisierenden Zelltod komplett aufheben konnten, was auf einen neuen Dynamin-abhängigen Zelltod Mechanismus hinweist.

Im zweiten Teil meiner Doktorarbeit habe ich mich auf die Untersuchung von Behandlungsmodalitäten konzentriert die zusammen mit Fenretinide die Wirkung auf aRMS Zellen noch verstärken. Das Behandlungsregime für diesen schwer zu behandelnden Tumor auszuweiten und damit eine direkte Verbindung der Laborarbeit und der klinischen Behandlung und Wissenschaft zu schaffen war eines meiner Hauptziele meiner Doktorarbeit.

Wir fokussierten uns hier auf die Strahlentherapie da diese Behandlungsform bereits Teil der Standardbehandlung bei Patienten mit aRMS ist. Gerade die Strahlentherapie ist zwar effektiv, weisst jedoch ein hohes Risiko für verschiedenste Nebenwirkungen je nach Lokalisation der Applikation aus. Hierzu zählen Wachstumseinschränkung, Unfruchtbarkeit, bis hin zur Entwicklung von Zweitmalignomen. Aus diesem Grund ist es besonders wünschenswert Therapeutika zu finden die als Sensibilisatoren für die ionisierende Strahlung fungieren um die zu applizierende Strahlendosis möglichst reduzieren zu können.

Wir konnten zeigen dass die kombinierte Behandlung den induzierten Zelltod analog zur Behandlungsintensität potenzierte und das klonale Wachstum einschränkte. Dies ist zurückzuführen auf eine verstärkte Produktion von verschiedenen reaktiven Sauerstoffradikalen. Eine detaillierte Analyse dieser Mechanismen ergab dass Strahlentherapie vor allem die Produktion von Wasserstoffperoxid, und Fenretinide, wie bereits erwähnt, vor allem die Produktion von Superoxiden hervorruft.

Des Weiteren beobachteten wir eine verstärkte DNA Schädigung und ein eingeschränktes Voranschreiten des Zellzyklus in den kombiniert behandelten Zellen, dies am wahrscheinlichsten auch hervorgerufen durch ROS Schäden. Als letztes haben wir noch den zugrunde liegenden

Zelltodmechanismus im Detail analysiert. Hier konnten wir zum einen die Induktion von Apoptose und zum anderen eine vermehrte Makropinozytose in den kombiniert behandelten Zellen nachweisen. Die Strahlentherapie allein hatte jedoch keinen Einfluss auf die Makropinozytose und somit ist dieses Phänomen einzigartig für Fenretinide.

Zusammenfassend, zeigen unsere Daten dass Fenretinide ein hohes Potential als ein zusätzliches Therapeutikum in der Behandlung des alveolären Rhabdomyosarkoms hat. Hier zeigte sich auf molekularer Basis eine neue Form des Zelltods basierend auf der Anhäufung von Vakuolen im Plasma, welcher durch Sauerstoffradikale aus der mitochondrialen Atemkette induziert wird. Des Weiteren präsentiert sich Fenretinide als vielversprechender Partner für die Strahlentherapie, da es als Sensibilisator für ionisierende Strahlung wirkt wodurch es aufgrund der kombinatorischen und synergistischen Wirkung zu einer Potenzierung des induzierten Zelltods und damit der Wirkung auf den Tumor kommt.

List of Abbreviations

AA	Acyls-arachidonoyl
ACD	Accidental cell death
ACD	Autophagy-dependent cell death
ALK	Anaplastic Lymphoma Kinase
ALK	Anaplastic Lymphoma Kinase
ALL	Acute lymphoblastic leukaemia
AML	Acute myelogenous leukaemia
AMPK	5' adenosine monophosphate-activated protein kinase
AP2	Adaptor protein 2
ARE	Antioxidant-responsive elements
ARF	Alternate reading frame protein
ARMS	Alveolar rhabdomyosarcoma
Arp2/3	Actin-related protein 2/3
ASK1	Apoptosis signal-regulating kinase 1
ATG	Autophagy-related genes
ATM	Ataxia telangiectasia mutated
ATP	Adenosine triphosphate
ATRA	All Trans retinoic acid
AURKA	Aurora kinase A
BAK	BCL2 antagonist/killer 1
BAR	Bin-Amphiphysin-Rvs
BAX	BCL2 associated X apoptosis regulator
BCL2	B-cell lymphoma 2 family
BCL-XL	BCL2 like 1
BER	Base Excision Repair
BH	BCL2 homology
BID	BH3-interacting domain death agonist
Brca	Breast cancer gene
BSE	Bundle signalling element
BSO	L-Buthionine-sulfoximine
C	Cytosine
CAR	Chimeric antigen receptor
Caspases	Cysteine-dependent aspartate-directed proteases
CavME	Caveolae-mediated endocytosis
CCP	Clathrin-coated pits
CCV	Clathrin coated vesicles
CD3-zeta	Zeta chain of the TCR/CD3 complex
CDK	Cyclin-dependent kinase
cDNA	Complementary Deoxyribonucleic acid
CDR	Circular dorsal ruffles

CI	Confidence Interval
cIAP	Cellular inhibitor of apoptosis protein
CIE	Clathrin independent endocytosis
CK1	Casein Kinase 1
CLASP	Clathrin associated sorting protein
CLIC	Clathrin-independent carriers
CME	Clathrin mediated endocytosis
CMV	Cytomegalovirus
CNS	Central Nervous System
CSF-1	Colony-stimulating factor-1
CWS	Cooperative Weichteilsarkom Studiengruppe
CYTC	Cytochrome c
DAPI	4', 6-Diamidino-2-Phanylindole
DD	Death domain
DES1	Dihydroceramide desaturase 1
DIABLO	Diablo IAP-binding mitochondrial protein
DISC	Death-inducing signalling complex
DMSO	Dimethylsulphoxide
DNA	Deoxyribonucleic acid
DNA-PKcs	DNA-dependent protein kinase catalytic subunit
DSB	Double-strand breaks
e.g.	Exempli gratia, for example
EFS	Event free survival
EGF	Epidermal growth factor
ENDOG	Endonuclease G
EpSSG	European paediatric Soft tissue sarcoma study group
ERK	Extracellular signal-regulated kinase
eRMS	Embryonal rhabdomyosarcoma
ETC	Electron transport chain
FADD	FAS-associated protein with a death domain
FDA	Food and Drug Administration
FOXO	Forkhead box O
FSRT	Fractionated Stereotactic Radiotherapy
FTS	Farnesylthiosalicylic acid
G	Guanosine
GAP	GTPase-activating protein
GAPDH	Glyceraldehyde 3-phosphate dehydrogenase
GCL	Glutamylcysteine ligase
GCR	Gross chromosomal rearrangement
GDP	Guanosine diphosphate
GEEC	GPI-AP enriched endosomal compartments

GEF	Guanine nucleotide exchange factor
GPI	Glycosylphosphatidylinositol
GPX	Glutathione peroxidases
GR	Glutathione reductase
GSSG	Oxidized glutathione
Gy	Gray
H/K/NRAS	Rat sarcoma oncogene (H: Harvey sarcoma virus, K: Kirsten sarcoma virus, N:human neuroblastoma)
H2O2	Hydrogen peroxide
HIFa	Hypoxia induced factor alpha
HRR	Homologous Recombination Repair
HSC70	Heat shock cognate 70
HTRA2	High temperature requirement protein A2
ICCC-3	International Classification of Childhood Cancer, 3rd edition
ICD-O	International Classification of Diseases for Oncology
IFN	Interferon
IGFR	Insulin-like growth factor receptor
IGRT	Image-guided radiotherapy
IL2	Interleukin 2
IMRT	Intensity-modulated radiotherapy
IMS	Mitochondrial intermembrane space
IR	Ionizing Radiation
IRS	Intergroup Rhabdomyosarcoma study
JNK	c-Jun amino-terminal kinase
KEAP1	Kelch-like ECH-associated protein 1
LC3	Microtubule-associated protein 1 light chain 3
LET	Linear energy transfer
LOX	Lipoxygenases
MAPK	Mitogen activated protein kinase
MHC	Major Histocompatibility complex
MKK	MAP kinase kinase
MLKL	Mixed lineage kinase domain-like
MOMP	Mitochondrial membrane permeabilization
MRC	Mitochondrial respiratory chain
MRN	M complex of Mre11-Rad50-Nbs1
mRNA	Messenger ribonucleic acid
mTOR	Mammalian target of rapamycin
NAC	N-acetylcysteine
NADPH	Reduced Nicotinamide adenine dinucleotide phosphate

NCCD	Nomenclature Committee on Cell Death
NF-kB	Nuclear factor-kappa B
NGF	Nerve-growth factor
NHEJ	Nonhomologous End Joining
NICER	Nationales Institut für Krebsepidemiologie und –registrierung).
NMYC	Myelocytomatosis oncogene, N-neuroblastoma
NOXs	NADPH oxidase complex
NRF2	Nuclear Factor Erythroid 2-like 2
NS-1	Necrostatin 1
NTRK3	Neurotrophin receptor neurotrophic receptor tyrosine kinase 3
O2-	Superoxide anion
OH.	Hydroxyl radical
OMM	Outer mitochondrial membrane
PAK1	p21-activated kinase 1
PAMP	Pathogen associated molecular patterns
PCD	Programmed cell death
PDGF	Platelet-derived growth factor
PE	Phosphatidylethanolamine
PEITC	Phenethylisothiocyanate
PH	Pleckstring homology
PHD	Prolyl hydroxylases
PI3K	Phosphatidylinositol 3-kinase
PIP	Phosphatidylinositol phospholipids
PPM1B	Protein phosphatase Mg2+/Mn2+ dependent 1B
PPP	Pentose phosphate pathway
PR	Peripheral ruffle
PRD	Proline- and arginine-rich domain
PRR	Pathogen recognition receptors
PRX	Peroxiredoxins
PTCH1	Patched 1
PtdIns(3)P	Phosphatidylinositol 3-phosphate
PTEN	Phosphatase and tensin homolog
PTP	Protein tyrosine phosphatase
PUFA	Phosphatidylethanolamine-containing polyunsaturated fatty acids
qRT-PCR	Quantitative Real-Time Polymerase Chain Reaction
Rab	Ras-like proteins from rat brain
RAR	Retinoic acid receptor
RARA	Retinoic acid receptor alpha
RARE	Retinoic acid responsive elements
RB	Retinoblastoma

RBBP	Retinoblastoma binding protein
RCD	Regulated cell death
RIP	Receptor-interacting serine/threonine-protein kinase
RNA	Ribonucleic acid
ROS	Reactive Oxygen species
RT	Radio therapy
RXRE	Retinoid X response elements
SC	Stem Cell
scFv	Single chain variable fragment
SDS	Sodium dodecyl sulfate
SEER	Surveillance, Epidemiology and End Results
sgRNA	Small guide RNA
SH3	SRC homology 3
SHH	Sonic hedgehog
shRNA	Small hairpin RNA
siRNA	Small interfering RNA
SMAC	Second mitochondrial activator of caspases
SMN	Secondary malignant neoplasms
SOD	Superoxide dismutase
SSB	Single-strand breaks
ssDNA	Single strand DNA
STAT3	Signal transducer and activator of transcription 3
STUB1	STIP1 homology and U-box containing protein 1
tBID	Truncated mitochondrion-permeabilizing fragment
TKO	Triple knockout
TLR	Toll-like receptor
TNFR1	TNFα receptor 1
TNFSF10	TNF ligand superfamily member 10
TNFα	Tumour necrosis factor α
TNM	Tumour node metastasis state
TR	Thioredoxin reductase
TRAIL	Tumor Necrosis Factor Related Apoptosis Inducing Ligand
TRAILR	TRAIL receptor
TRX	Thioredoxin
ULK	Unc-51-like kinases
UNC5A-D	Netrin receptors
VEGF	Vascular endothelial growth factor
VHL	Von Hippel-Lindau protein

WASp/WAVE 2	Wiskott Aldrich syndrome protein/WASP-family verprolin homologous protein 2
WIPI2	WD-repeat protein interacting with phosphoinositides-2
xCT	Cysteine/glutamate antiporter
ZBP1	Z-DNA binding protein 1
Δψm	Mitochondrial transmembrane potential

Table of Contents

I. Introduction

1. Cancer

1.1 Classification

The term cancer does not defines just one disease, but comprises a collection of diseases with one common feature: the uncontrolled division and invasion of certain cells. The first recorded cases of cancer can be traced back to 2500BC, when the Egyptian physician Imhotep described "*a bulging mass in the breast*". Yet, it took another 2000 years, until cancer got its current name, given by the Greek physician Hippocrates who first named a mass of cancerous cells *karkinos*, the Greek word for crab. Neoplasms can be classified either by the site of origin or based on the histological type of the tumour, after the "International Classification of Diseases for Oncology (ICD-O)". According to the latter, neoplasms may be classified into four major categories: Carcinomas are malignant neoplasms of epithelial origin and account for 80 to 90% percent of all cancer cases. Sarcomas are neoplasms that originate in supportive and connective tissues such as bones, tendons, cartilage, muscle, and fat and commonly occur in adolescents and young adults. Then neuroectodermal tumours, which originate from the embryonal neural crest. And lastly, the hematopoietic malignancies, which comprise solid lymphomas that arise in the lymphatic system and leukaemias, also referred as "*liquid cancers*" or "*blood cancers*". Hematopoietic malignancies originate in the bone marrow and are associated with the overproduction of immature blood cells. There is still an ongoing debate around the origin of tumour cells. The most popular model hypothesize a monoclonal origin of tumour cells, i.e., the cells start with a single mutated cell and gradually acquire more and more mutations [1]. This hypothesis, however, has lately been challenged by publications claiming a polyclonal origin for at least in some cancer types [2]. Another well recognized model is the cancer stem cell (SC) model, which states that normal SCs

may suffer an initial oncogenic transformation followed by more and more mutations and eventually become cancer stem cells [3]. Undebatable is the role of oncogenes and tumour suppressor genes in the development of cancer. During genome wide sequencing studies, 125 driver gene mutations were discovered, of which 71 affect tumour suppressor genes and 54, oncogenes. Further sub classification allowed the allocation of these driver gene mutations into 12 major pathways affecting cell fate, cell survival, and genome maintenance [4].

1.2 Hallmarks of Cancer

Cancer is a dynamic and heterogeneous disease, with each malignancy possessing certain characteristics of malignant cells. First described by Hanahan and Weinberg in 2000 [5], the hallmarks and definition of cancer have been revised and extended by the two authors through subsequent researches leading to a better understanding of the genomic landscape of tumours and the role of the immune system in cancer development [6]: “Evading growth suppressors, avoiding immune destruction, enabling replicative immortality, tumour promoting inflammation, activating invasion & metastasis, inducing angiogenesis, genome instability & mutation, resisting cell death, deregulating cellular energetics and sustaining proliferative signalling”. This 10-piece set of functional capabilities allows the tumour uncontrolled proliferation. Hence, recognition of this skill set, will help the researcher develop new strategies to fight cancer.

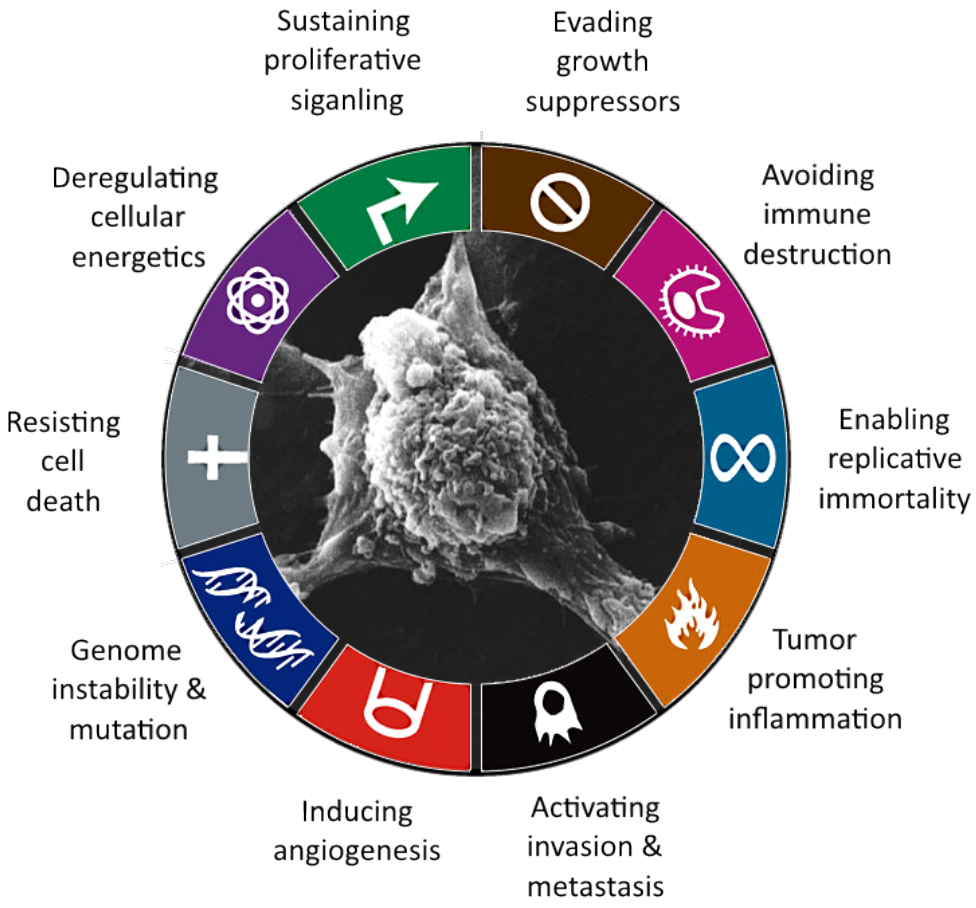

Figure 1 The Hallmarks of cancer, adapted from [6]

1.3 Epidemiology

According to the World Health Organization WHO, cancer is the second leading cause of death globally, and is responsible for approximately 8.8 million deaths annually. Each year, 35,000 people are diagnosed with cancer in Switzerland, of which, 16,000 will die. This is more than one quarter (26.3 %) of the total number of annual deaths (NICER, Nationales Institut für Krebsepidemiologie und -registrierung).

2 Childhood Cancer

2.1 Overall incidence and mortality

Childhood cancers are markedly different from those occur in adults [7]. According to the ICD-O-3 classification of tumours in adults, the International Classification of Childhood Cancer, third edition (ICCC-3), classifies tumours into 12 main groups, which are further subdivided into 47 subgroups [8]. Childhood cancer is relatively uncommon, with approximately 1 to 2 per 10000 children aged 14 years and younger affected annually. However, it remains the leading cause of disease-related mortality among children 1 to14 years of age. For children under one year, the most common malignancy was neuroblastoma (28.6%), followed by leukaemia (14.4%). For the age group 1 to 14, leukaemia is the most common malignancy (25%), followed by neoplasm of the central nervous system (CNS) (17%) [9].

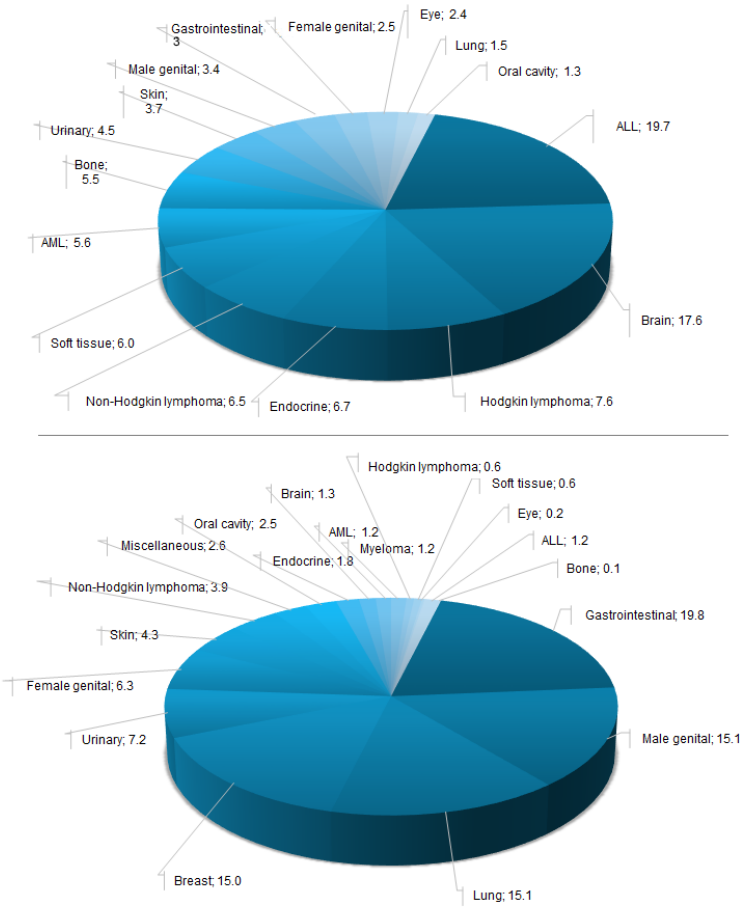

Figure 2 The frequency of cancer types in children (above) and adults (below) on the basis of 2012 Surveillance, Epidemiology and End Results (SEER) data [7].

Since the 1960s, when the estimated five-year cancer survival rate was 28%, the cancer survival rate in children 0 to 14 years has dramatically improved. Currently the overall ten-year survival rate for children diagnosed with cancer is approximately 87%. The increase in survival rate varied significantly among different diagnostic groups and was most striking for acute lymphoblastic leukaemia (ALL), which was considered incurable in the early sixties and nowadays has an overall survival rate of over 80%. As positive these statistics may sound, some malignancies, e.g., neuroblastomas and soft tissue sarcomas, still have a very poor prognosis with less than 70% cure rate - and worse after recurrence. (All data retrieved from Swiss Childhood Cancer Registry, Annual Report 2015-2016)

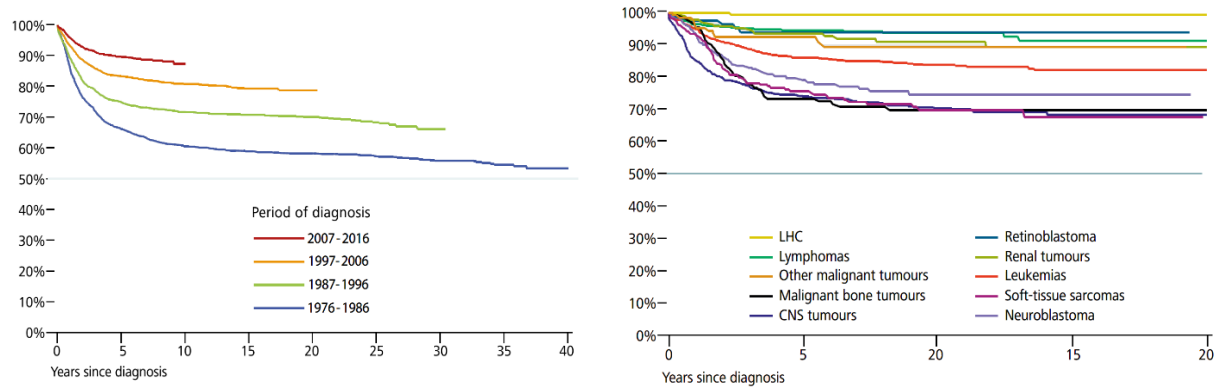

Figure 3 Survival of patients in the SCCR. Swiss residents; age at diagnosis 0-14 years; n = 7043. Left: Period of diagnosis 1976-2016. Right: Survival according to type of cancer.

2.2 Molecular and genetic basis

Cancer is a genetic disease, and genetic aberrations can either be germline or somatic [4]. The proportion of paediatric cancers with clear hereditary background is small, with about 5% [10]. “Hereditary” refers to an inherited genetic alteration, which was passed on by the parents or occurred before fertilization in the oocyte or sperm cell. the most frequently recorded diagnoses with a hereditary background are: retinoblastoma (37% of all retinoblastoma cases), Wilms' tumour (7%), leukaemia- associated with Down's syndrome (3%), and brain tumours - associated

with neurofibromatosis (2%) [10], however the list of other inherited predispositions to cancer is long [11].

Childhood malignancies are often the products of somatic mutations. Such mutations frequently have gross chromosomal rearrangements (GCR) leading to interstitial deletions, amplifications, inversions, and translocations. These can subsequently result in the expression of proto-oncogenes, deletion of tumour-suppressor genes, or the generation of oncogenic fusion genes. Most of the chromosomal translocations can be found in hematologic malignancies and sarcomas [7, 12].

2.3 Treatment of childhood malignancies

The multidisciplinary and standard approach over the last 40 years to treat childhood malignancies is multimodal, integrating chemotherapy, surgery, radiotherapy, and hematopoietic stem cell transplantation. The first pillar of treatment is chemotherapy, the goal of chemotherapy is to eradicate all cancer cells. It has been shown in the past that, chemotherapy is most efficient when administered in combination regimens. This is due to an overcoming of drug resistances to individual agents, that is already present in up to 50% at diagnosis [13]. Most of the conventional chemotherapeutic agents are non-selective cytotoxic substance that targets vital structures or pathways of the cancer cells. In the process, however, normal cells are also affected, leading to severe and undesirable toxic side effects.

Surgery is the second pillar of cancer treatment. Better staging through advanced radiology technologies and sophisticated resection techniques have helped minimizing mutilating operations and surgery-associated mortality. Further, these new techniques have helped surgeons to more accurately take biopsies, which is essential for subsequent treatment.

Radiotherapy, the third pillar of conventional anti-cancer treatment, is next to surgery the oldest treatment for cancer. Ionizing radiation interacts both directly and indirectly (through the production of reactive oxygen species) with the cells' DNA [14]. Improvements in the techniques in delivering radiation have led to a significant reduction of radiation damages on normal tissues

[15-18]. A better understanding of radiobiology has also led to the development of multiple radio-sensitizers that allow a reduction of the radiation dosage [19].

Targeted cancer therapy targets specific proteins involved in tumorigenesis. This form of treatment mainly focuses on specific molecular changes that are unique to the particular cancer. While targeted therapy is well established in the treatment of adulthood malignancies, several paediatric trials are now being conducted with compounds targeting multiple cancer pathways. These include the epidermal growth factor receptor pathway, the vascular endothelial growth factor pathway, anaplastic lymphoma kinase, insulin-like growth factor receptor (IGFR), hedgehog signalling, the mammalian target of rapamycin, protein kinase B, c-secretase, Janus kinase, fms-like tyrosine kinase and others [20, 21].

Gaining nowadays more importance in the treatment of paediatric malignancies is the use of immunotherapy. There is a wide variety of immunotherapies that work in different ways to either boost the body's immune system or educate the immune system to fight malignant cells. For example, monoclonal antibodies are used to target certain tumour-associated antigens. This form of immunotherapy is well established in the treatment of neuroblastoma, with the use of monoclonal antibodies targeting GD2 - a tumour-associated disialoganglioside found on the surface of neuroblastoma cells or in the treatment of non-Hodgkin Lymphoma [22]. Other promising new therapies such as the recently FDA-approved CAR (chimeric antigen receptor) T-cell therapy are also being developed. CAR T-cells are autologous T lymphocytes transduced with a modified lentiviral vector expressing CARs with an anti-CD19 scFv (single chain variable fragment) and the zeta chain of the TCR/CD3 complex (CD3-zeta). After transfusion back into the patient, the CAR-T-cells direct the host T lymphocytes to the CD19-expressing tumour cells, causing selective toxicity [23].

3. Rhabdomyosarcoma

3.1 Pathology and molecular biology

Rhabdomyosarcomas are malignant tumours of mesenchymal origin, committed to the skeletal muscle lineage. RMS belong to the broad group of small round blue cell tumours. The characteristic feature of RMS is the skeletal myogenic origin with the identification of muscle-specific proteins like myosin, desmin, myoglobin, Z-Band protein and Myo-D [24, 25]. In 1958 Horn and Enterline first classified RMS into four histopathological groups (embryonal, botryoid, alveolar, and pleomorphic) [26]. Since then, multiple modifications to this classification have been made. Nowadays, histopathologically RMS are divided into four major subtypes, embryonal, alveolar, pleomorphic, and sclerosing/spindle cell RMS [27-29]. The embryonal (eRMS) and alveolar (aRMS) are the two most common subtypes with frequencies of 60%-70% and 20% , respectively [29]. The term embryonal refers to the fact that eRMS histopathologically contain features of embryonic rhabdomyogenesis, whereas the term alveolar refers to the morphological resemblance of aRMS histology to foetal lung alveoli. eRMS tumours show elongated and rather loose packed cells, compared to aRMS tumours with densely packed cells, organized in nests around fibrovascular stroma, resembling alveoli [24, 27]. The outcome of children with eRMS is much more favourable than the outcome of children with aRMS (5-year EFS 43% versus 29%) [30].

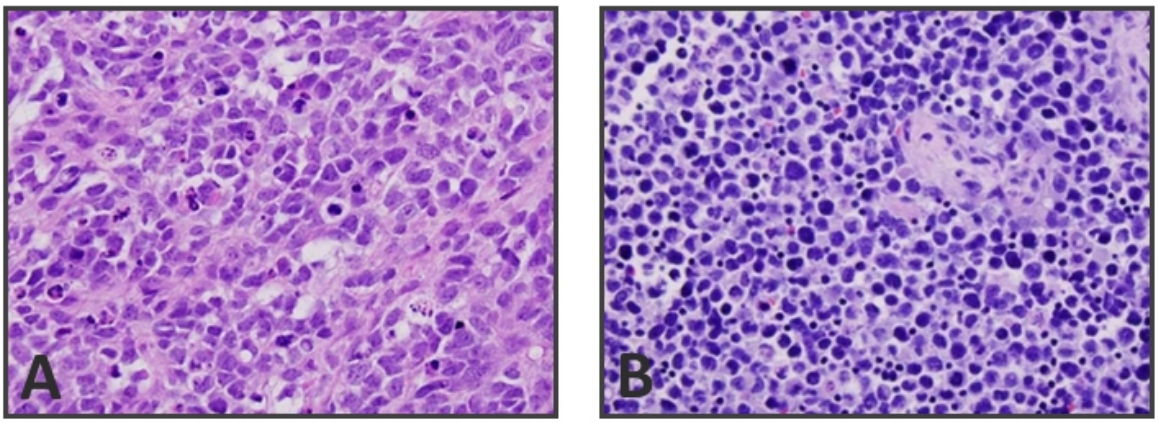

Figure 4 Cytological details of rhabdomyosarcoma. A) Embryonal rhabdomyosarcoma (eRMS). B, Alveolar rhabdomyosarcoma (ARMS) [27].

Advances in genetic techniques allowed karyotyping studies that revealed a series of genetic aberrations and non-random chromosomal translocations. Such events have caused the fusion of DNA sections, leading to a further subclassification of RMS. In eRMS cases, genetic aberrations such as loss of heterozygosity at 11p15.5, point mutations in TP53, NRAS, KRAS, HRAS, PIK3CA, CTNNB1, NF1, and FGFR4, as well as MDM2 amplifications and aneuploidy are commonly found [31, 32]. Whereas in aRMS two genotypes are mainly present, the more frequent chromosomal translocation PAX3/FOXO1 t(2;13) (q35;q14), and the less frequent variant PAX7/FOXO1 t(1;13)(p36;q14). PAX3, PAX7, and FOXO1 wild type all encode transcription factors. When either PAX3 or PAX7 gene is fused to the FOXO1 gene through translocation, chimeric transcription factors PAX3/7-FOXO1 are formed. At their N-termini, they contain the PAX-derived paired domain and homeodomain responsible for DNA binding, and at the C-termini, the FOXO1 transactivation domain [31]. Rarely, two additional rearrangements of the PAX3 gene can be found in aRMS tumours: The in-frame fusion with the nuclear receptor coactivator NCOA1 t(2;2)(q35;p23) [33] or the fusion with the chromatin remodelling gene INO80D [31]. Along with the chromosomal translocation observed in these tumours, other genetic alterations in aRMS cases are rare and sometimes even the only genetic alteration. Occasionally observed alterations include

CDK4, miR-17-92 and MYCN amplifications, as well as the uniparental disomy 11p15.5 at the IGF2 locus [32]. This highlights the importance of chromosomal translocations as driver of tumorigenesis. It was shown, that introduction of PAX3-FOXO1 into chicken embryo fibroblast and expression of the protein in these cells leads to transformation and anchorage-independent growth [34]. Further, downregulation of *PAX3-FOXO1* induced apoptosis [35] and decreased the proliferation rate in RMS cell lines [36].

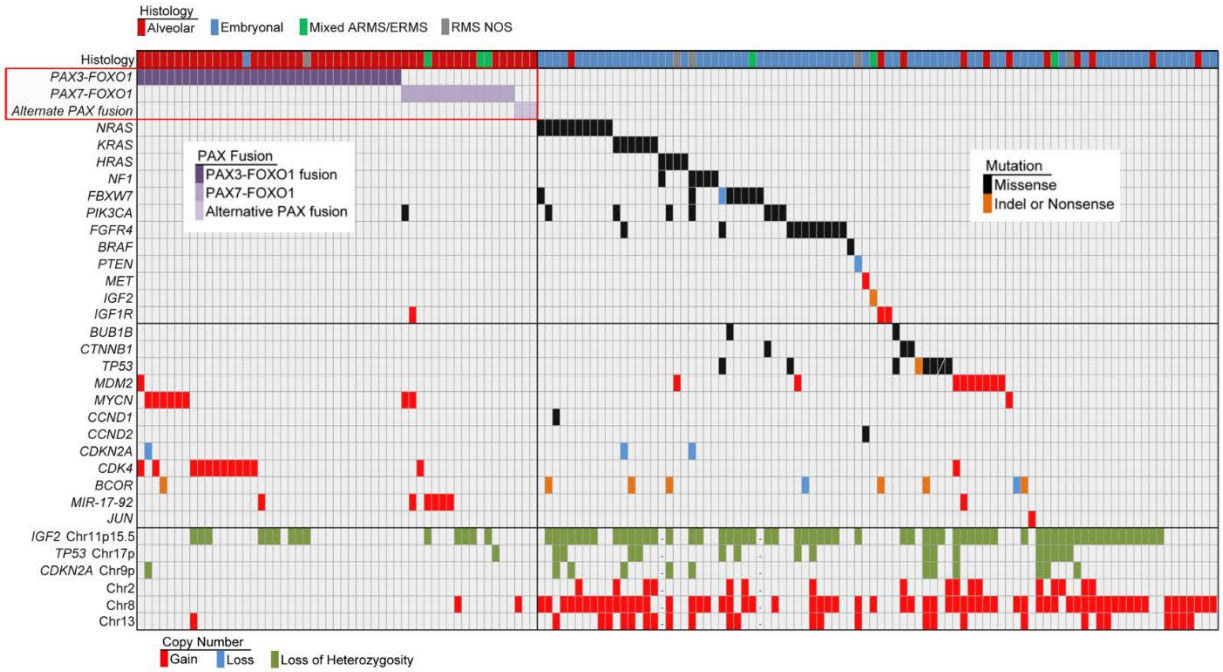

Figure 5 The Genomic Landscape of paediatric RMS [31].

The ability of PAX3-FOXO1 to act as driver of tumorigenesis is at least partially due to its ability to alter transcription of its target genes. Microarray studies have revealed a whole battery of potential target genes, which are mainly myogenic signalling and differentiation genes such as the transcriptions factors MYOD1, MYOG, and SIX1 [37, 38]. In addition, several receptor tyrosine kinases involved in cell growth, such as FGFR4, ALK, and MET, were upregulated [32]. According to gene ontology criteria, several target genes were found downregulated which are involved in muscle development and regulation of muscle contraction [37].

Comparing the genetic landscape of fusion positive and fusion negative RMS samples, 93% of all tumours revealed an overlap between some of the *PAX3-FOXO1* target genes and genes mutated in eRMS. Both tumours through either mutation or translocation alter the function of the common receptor tyrosine kinase/RAS and receptor tyrosine kinase/PIK3CA axis [31].

Previously, pathophysiological classification and subtype discrimination were the main factors for risk and outcome prediction, but nowadays, through the evaluation of patient data to include the genetic background of the tumour, it is believed that the fusion status rather than histology predicts the prognosis more accurately [30].

3.2 Epidemiology and Outcome

Soft tissue sarcomas are a heterogeneous group of malignancies comprising around 7.4% of all childhood malignancies. Within this group, Rhabdomyosarcoma (RMS) is the most frequent one, accounting for 50% of all soft tissue sarcomas. The annual incidence is estimated at 4.5 cases per million children, with a significant male dominance of 5.2 to 3.8 cases per million children. 70% of the cases involved children under ten years and the two main subtypes are the embryonal RMS (2.6 cases per million) and the alveolar RMS (1 case per million children) [39, 40]. The outcome of children with RMS differs significantly between subtypes. ERMS has a more favourable prognosis with a three year survival rate of around 75%, whereas aRMS is highly malignant with a poor overall survival rate of less than 30% [29].

Moreover, the recurrence rate in children with aRMS is high with more than 48%. Further, the remaining 5-year post-relapse survival rate is only about 21% [41-43].

3.3 Hereditary syndromes

Several germ-line genetic disorders are associated with a higher risk to the development of sarcomas.

Li-Fraumeni syndrome, first described in 1969, has the highest predisposition to develop rhabdomyosarcoma. About 10% of RMS are associated with Li-Fraumeni syndrome, which is caused by germ-line mutations in the P53 tumour suppressor gene [44]. Further germ-line mutations in the retinoblastoma gene 1 not only predispose the subject to the development of bilateral retinoblastomas, but also to osteo- and rhabdomyosarcomas [45]. Costello syndrome, a condition caused by mutations of the HRAS gene at 11p15.5, is associated with the development of embryonal rhabdomyosarcomas. Another example is the Beckwith–Wiedemann syndrome, which causes overgrowth in children and a higher incidence of developing rhabdomyosarcomas. Here the genetic background is complex, with mutations mainly involving the 11p15.5 locus [12].

3.4 Clinical Presentation and risk stratification

The term *oncology* - the field of medicine dealing with cancer - originates from ancient Greek. The word onkos describes in Greek theatre a tragic mask, which was worn by an actor as a symbol of physical burden. Oncology refers to the discipline of medicine that deals with patients with cancer.

Patients with rhabdomyosarcoma usually present with a painless mass lesion or with a disturbance of a normal body function through an outwardly invisible tumour mass. 35-40% of tumours are found around the head and neck, 25% in the genitourinary tract, 20% at extremities, and the rest from truncal primaries [43]. Around 15% to 25% newly diagnosed patients already present with metastasis, mainly to the lungs and less common to the bone marrow, bones, and lymph nodes [46]. Staging is a critical step after the cancer diagnosis, as therapy and prognosis are directly linked to the tumour stage. Currently there is no international consensus on tumour staging and the European CWS studies mainly follow the postsurgical Intergroup Rhabdomyosarcoma study (IRS) staging [47]. The second commonly applied staging system is the pre-treatment, site-modified TNM staging system (tumour-nodes-metastasis).

In order to predict the patient's individual prognosis, several factors are considered. The main factor for risk stratification of rhabdomyosarcomas remains the histopathological confirmed diagnosis (aRMS vs eRMS). Further, the IRS and lymph node state (TNM state), the primary tumour site, size of the tumour (< 5cm vs. > 5cm) and the age of the patient (< 10 years vs. > 10 years) are considered. According to these factors, the patients are assigned a risk group, which then determines their treatment strategy.

3.5 Treatment

As patient numbers are low, most children are treated according to risk-adapted, cooperative and multiinstitutional trials. These trials are designed to guide the treating physicians and to collect important patient data to improve treatment and quality of care. In Europe, the "*Cooperative Weichteilsarkom Studiengruppe*" (CWS) and the "*European paediatric Soft tissue sarcoma study group*" (EpSSG) are responsible to conduct these trials.

As mentioned above, according to the patient's risk group assignment, the patient is allocated to a treatment arm, which always consists of local surgical treatment and a vincristine, actinomycin based chemotherapy, and in case of higher stages, additional ifosfamide therapy. Radiotherapy belongs to the standard treatment and is only omitted in the very low risk group [48]. In patients with metastatic disease, high dose chemotherapy followed by autologous stem cell presentation was evaluated against standard chemotherapy with the addition of oral maintenance therapy in the HD CWS-96 trial. The study suggested that there was no role for high-dose chemotherapy in patients with metastatic RMS, but that maintenance chemotherapy might be beneficial [49]

In case of recurrence, adapted regimens are given, including targeted agents such as bevacizumab or temsirolimus [50, 51]. But as direct targeting of transcriptions factors is considered impossible due to their low enzymatic activity and their huge interacting surface between transcription factor and DNA, alternative focuses have been set on targeting the involved signalling pathways [52, 53].

Unfortunately, the EpSSG supported BERNIE phase II study, which evaluated the addition of bevacizumab to standard high risk treatment with ifosfamide, vincristine, actinomycin and doxorubicin or to maintenance chemotherapy with cyclophosphamide and vinorelbine in patients with metastatic RMS, did not see a benefit to the addition of bevacizumab [51]. Also, the COG supported trial that evaluated the addition of temsirolimus to cixutumumab in patients with RMS and other solid tumours, did not reveal any benefit.

Taken together, there is an ongoing interest and effort to improve treatment strategies in patients with RMS. So far, besides standard chemotherapy and radiation therapy, no new and more targeted agents have been identified that significantly augment treatment outcome and survival.

4. Fenretinide

In late 1960's, the pharmaceutical company Johnson & Johnson first developed fenretinide as a potential treatment for breast cancer, which was never brought to the market. In 2007, it was approved by the European Commission and the Food and Drug Administration (FDA) for the treatment of childhood sarcomas.

4.1 Pharmacology

Fenretinide is also known as N-(4-hydroxyphenyl) retinamide or 4HPR. Fenretinide is a synthetic phenylretinamide analogue of all-trans-retinoic acid (ATRA) also called just vitamin A (molecular formula: C26H33NO2). Upon exchanging the amide-linked 4-hydroxyphenyl group for the carboxyl group of ATRA, side effects such as skin and liver toxicity were markedly reduced (PubChem, open Chemistry database).

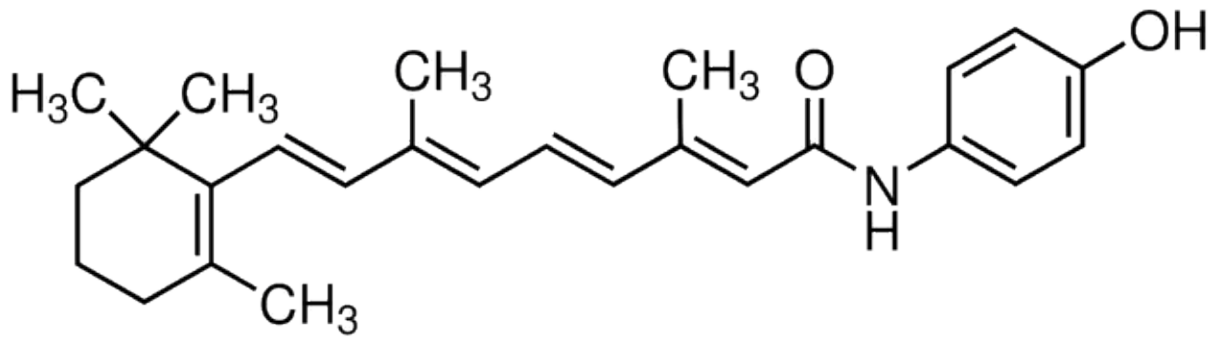

Figure 6 Molecular structure of fenretinide

Fenretinide is administered either orally or intravenously. In vivo as well as in vitro, fenretinide is metabolized into different analogues including N-(4-methoxyphenyl)retinamide (4-MPR) through a structural change at the hydoxyphenyl ring and to 4-oxo-N-(4-hydroxyphenyl)retinamide (4-oxo-4-HPR) through oxidation at the cyclohexenyl ring [54-56]. The metabolite 4-MPR accumulates mainly in fatty tissue but is also well detected in the plasma. Even though it is considered as non-toxic to cancer cells, it only accumulates in cells sensitive to fenretinide and so serves as an ideal biomarker [55, 56]. 4-oxo-4-HPR is present in much smaller concentrations as 4-MPR and 4-HPR nevertheless, it is much more cytotoxic than 4-HPR in multiple cell lines, even in some that are resistant to 4-HPR [54, 57].

Despite the promising results from in vitro studies, the transition of 4-HPR into clinical use was difficult, as fenretinide has low bioavailability caused by poor solubility in aqueous solution and high affinity to plasma proteins and lipids [57-59]. Multiple attempts have been made to increase the bioavailability of fenretinide through chemical modifications. One of such modification is the coupling of fenretinide to nanoparticles, which enhanced its drug release and cell entry in vitro and resulted in better bioactivity [60, 61], however clinical trials using this formulation are pending. In another approach to increase the bioavailability, fenretinide was packed into a lipid matrix which enhanced the bioactivity in vitro. [62]. As a result of these promising data, a phase I trial of orally given fenretinide in this new organized lipid complex in children with relapsed

Neuroblastoma showed that this new formulation achieved higher plasma levels, minimal toxicity, and evidence of anti-tumour activity, compared to the old capsule formulation [63]. However, when this new formulation was evaluated in adults, the mean plasma levels of fenretinide using the LYM-X-SORB formulation were the same than the capsules, and gastrointestinal side effects caused a study drop out of 7 out of the 20 patients [64].

The addition of ketoconazole to fenretinide significantly increased the 4-HPR plasma levels through an inhibition of the metabolism of 4-HPR in mice [65]. This formulation is currently under clinical trial for usage in children with relapsed neuroblastoma, and as the study has just closed, results are pending (NCT02163356). Two other trials that administered fenretinide via intravenous infusion reported much higher plasma levels compared to the oral formulation and a promising anti-cancer activity [66, 67].

The side effect profile of fenretinide is favourable, involves mainly the skin, (dermatitis), the eyes (development of nyctalopia), the liver (elevation of the liver enzymes and bilirubin), and the intestines (diarrhoea and nausea). Further pseudo tumour cerebri was also reported once. However grade four (limiting) toxicities are rare [58, 68].

4.2 Fenretinide-mediated anti-cancer activity: A literature summary

The fat-soluble Vitamin A or all-trans-retinoic acid is essential for the maintenance of health. As it is not de novo synthetized in the body, it needs to be taken up through the diet.

Vitamin A plays an essential role in the photosensitivity of the eye [69]. ATRA is a direct ligand for nuclear retinoic acid receptors (RARs), which belong to the steroid hormone receptor superfamily. So far six genes coding for different RARs have been identified. Their expression differs in different cells, but with the same functionality. Upon binding to the so called RAR elements (RARE) or retinoid X response elements (RXREs) located within the promoter of target genes, they function as heterodimers. More than 500 genes have been suggested to be regulatory targets of retinoic acid either directly or mediated by other transcription factors [69]. The target

genes play essential roles in the preservation of immune function, vision, and the development and maintenance of multiple body tissues during embryogenesis and later in life. The link between fenretinide and RARs is still a controversy according to the literature. Sheik et al reported that fenretinide was active in breast cancer cell lines resistant to RA and that binding of fenretinide to RARs was poor, hence only a minimal activation of the retinoic acid receptor element (RARE) and retinoid X receptor response elements (RXREs) was seen, implying a RAR independent mechanism of action [70]. Similar findings were seen in hematopoietic cell lines [71]. Other studies however, showed a direct interaction of fenretinide with RARs. Fanjul et al suggested that fenretinide is a highly selective activator of retinoid receptors [72] and Sani et al suggested that the hydroxyl group of fenretinide was responsible for the binding to RARs [73]. Further, fenretinide was able to induce apoptosis in liver carcinoma cells in a RAR beta dependent manner [74].

Most of the published data, suggest that the fenretinide induced cell death occurs mainly through apoptosis in most of the cell lines. This is achieved either through the production of reactive oxygen species (ROS) or the involvement of lipid second messengers.

Due to the fact that in many cancer cell lines, fenretinide induced cell death can be inhibited by the addition of antioxidants such as Vitamin C and E and N-acetylcysteine (NAC), it is suggested that ROS and oxidative stress play an important role [67, 75-78]. The exact source of ROS is still being debated in the literature. However, most studies agree that the mitochondrial respiratory chain (MRC) must be the site of ROS production. Cuperus et all were able to show that ROS production occurred via complex II of the MRC [79], other groups suggested that rather complex III or sites between I and II were responsible [75, 80]. Several studies further report that the endoplasmic reticulum is rather a target of ROS than a source [81-84]

Not only is the source of ROS controversial, what exact kind of ROS are produced is also under discussion. While Hail and Suzuki et al propose that fenretinide induces the production of

hydrogen peroxide, others favour the production of mitochondria derived superoxides [67, 75, 79, 85].

Downstream of ROS, multiple signalling pathways have been described for the induction of apoptosis. The activation of mitogen activated protein kinase (MAPK), c-Jun amino-terminal kinase (JNK), p38, extracellular signal-regulated kinase ERK1/2, GADD153, as well as nuclear factor-kappa B (NF-κB) have all been implicated in apoptosis induction [76, 81, 86-90]. Further, the members of the pro-apoptotic BH3 family and the anti-apoptotic BCL-2 family, survivin (a member of the inhibitor of apoptosis family), as well as the release of the downstream effector cysteine-dependent aspartate-directed proteases (caspases) 3, 8 and 9 play critical roles in fenretinide induced apoptosis [87, 89, 91-99]. Fang et al found recently that combining fenretinide with the BH3 mimetic ABT-737 further enhanced both the extrinsic and the intrinsic apoptosis pathway, suggesting fenretinide's critical role in apoptosis induction [94]. Interestingly, Cao et al showed that fenretinide can either induce apoptosis or autophagy depending on the concentration used and therefore the amount of ROS produced. Here the DJ-1 (a multifunctional oxidative stress response protein) and the ASK-1-p38 MAPK pathway are the main regulators of either apoptosis or autophagy induction [100].

Besides ROS production, lipid second messengers are thought to be targets of fenretinide. Ceramide, a sphingolipid second messenger, can either be de novo generated within a cell or through hydrolysis of sphingomyelin. Ceramides are implicated as signalling molecules during cell death [101]. Previously it was believed that fenretinide directly elevates ceramide, however newer studies using liquid chromatography-tandem mass spectrometry showed that fenretinide rather elevated dihydroceramide, the precursor of ceramide [102-104]. This is achieved through an inhibition of the dihydroceramide desaturase 1 (DES1) by fenretinide [105]. Two studies in pancreatic cancer cells and leukaemia cells showed that ROS and ceramide production are two independent events in fenretinide induced cell death [106, 107].

5 Reactive Oxygen Species (ROS)

The role of reactive oxygen species and antioxidants in the development and maintenance of malignant cells and in the abatement of malignancies is still a centre of debate. ROS and oxidative stress are considered as a promoter of malignancies and antioxidants protective or even curative, but some newer studies suggest that ROS may be anti-cancer molecules.

5.1 Biology and sources of reactive oxygen species and their regulation

Molecular oxygen is relatively unreactive. ROS are derived from the incomplete reduction of molecular oxygen and may include: superoxide anion (O_2^-), hydrogen peroxide (H_2O_2), and hydroxyl radical ($OH^{\cdot}$)[108]. Intracellularly, ROS are generated mainly in the mitochondria and the membrane bound NADPH oxidase complex (NOXs) [109].

In aerobic organisms and during cellular respiration, electrons are passed through a chain of mitochondrial complexes onto molecular oxygen, the final electron acceptor. In the mitochondria, 10 different sites are known to produce ROS, whereupon complex I, II and III, produce the lion's share [110]. Through the leakage of electrons from the electron transport chain (ETC), molecular oxygen can be reduced, giving rise to superoxide anions. Released into the mitochondrial matrix, superoxide anions are rapidly dismutased into hydrogen peroxide by superoxide dismutase 2 (SOD2). Superoxide anions released into the mitochondrial intermembrane space are converted by superoxide dismutase 1 (SOD1) into freely diffusible hydrogen peroxide [111]. A third and extracellular superoxide dismutase (SOD3) is the major SOD in the vascular extracellular space and dismutases superoxides there [112]. Dismutases therefore prevent oxidation damage of macromolecules.

The second source of ROS is the NOX complex, which catalyses the generation of superoxide anions from molecular oxygen and NADPH. NOX primarily locates in the plasma membrane, but

also can be found on the membrane of nucleus, mitochondria, and endoplasmic reticulum [113]. Also here, SOD 1 and 3 convert the superoxide anions to hydrogen peroxide [112].

Last, a minor source for ROS production is the Fenton reaction. Here hydroxyl radicals are formed when hydrogen peroxide reacts with ferrous or cuprous ions through the Fenton reaction. Hydroxyl radicals are highly reactive and toxic leading to lipid, protein, and DNA damage [114].

In an attempt to maintain redox homeostasis and avoid damage to macromolecules, the cell has developed a complex and sophisticated ROS scavenging network, besides the above-mentioned SODs. Spatially segregated in peroxisomes, the enzyme catalase converts hydrogen peroxide to water and molecular oxygen with an extremely high substrate turnover rate, scavenging around 6 million molecules of hydrogen peroxide per minute [115].

Glutathione peroxidases (GPXs), a group of five isoforms, catalyse the reaction between hydrogen peroxide and reduced glutathione (GSH) to form oxidized glutathione (GSSG). Glutathione reductase (GR), on the opposite, uses NADPH as an electron donor to reduce oxidized GSSG to GSH [116]. GSH, being the most abundant peptide in cells, is able to directly scavenge HO·, singlet oxygen, and plays an important role in the regeneration of other antioxidants such as vitamin C and E to their active forms [117].

Peroxiredoxins (PRXs) are highly abundant and spatially distributed in the cytosol, peroxisome, endoplasmic reticulum, and mitochondria. Six isoforms of PRXs are known and their active cysteine site serves as an oxidant acceptor to reduce hydrogen peroxide [118]. Oxidized PRXs are further reduced by thioredoxin (TRX), which, as a result, becomes oxidized. Thioredoxin reductase (TR) also uses NADPH as an electron donor to reduce oxidized TRXs [119].

Several transcription factors participate in orchestrating the activity and the production of the above described antioxidants. The key transcription factor is Nuclear Factor Erythroid 2-like 2 (NRF2). Under normal condition, NRF2 is located in the cytoplasm and associated with Kelch-like ECH-associated protein 1 (KEAP1) and the Cul3-based E3 ubiquitin ligase and so targeted

for proteasomal degradation [120, 121]. Under oxidative stress, KEAP1 is oxidized by H_2O_2 at its cysteine residues enabling a dissociation from NRF2 [122]. Subsequently stabilized NRF2 translocates into the nucleus, where it binds to antioxidant-responsive elements (AREs) within the regulatory region of around 200 target genes including CAT, GPXs, PRXs, SOD2 and TRX [123, 124]. Moreover, NRF2 is involved in the de novo synthesis of GSH through the NRF2-mediated expression of the cysteine/glutamate antiporter (xCT), which regulates the cysteine homeostasis and the expression of glutamylcysteine synthetase components [120]. Lastly, NRF2 induces the expression of regulatory enzymes in the pentose phosphate pathway (PPP) and serine biosynthesis, leading to an enhanced NADPH production, the substrate for TR and GR [125].

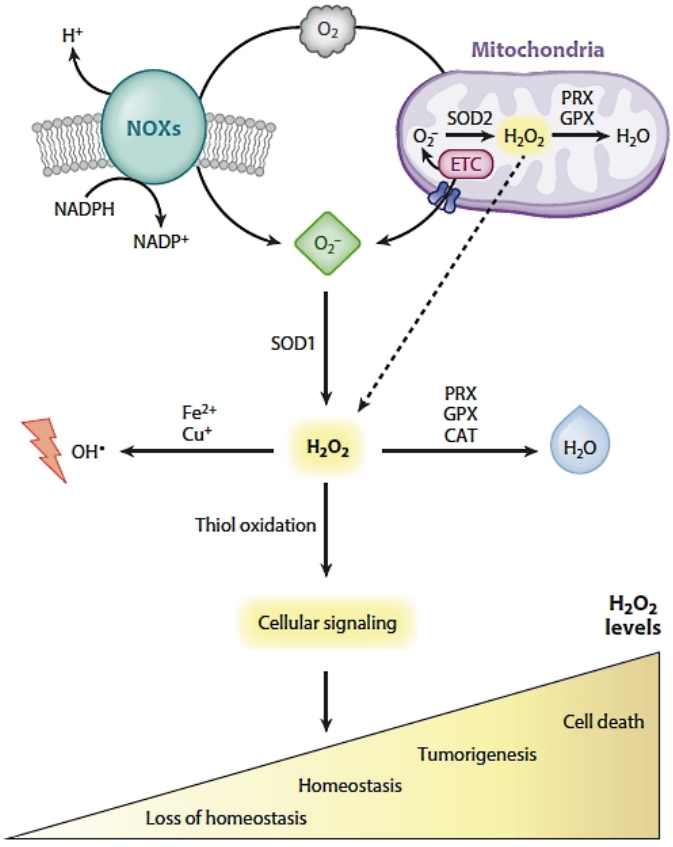

Figure 7 Sites of ROS generation and regulation [126]

5.2 ROS and cancer

Misbalance in the cellular redox state is associated with multiple diseases such as neurodegeneration, atherosclerosis, autoimmune diseases, and aging [127, 128]. The role of ROS in tumorigenesis has been debated for decades. ROS serve as important signalling molecules in normal as well as in cancer cells. Whereas low levels of ROS are responsible for controlled metabolic adaption, proliferation, and differentiation [129], high levels of ROS can hyper-activate signalling pathways and could eventually lead to transformation and tumorigenesis [130]. Multiple studies have shown an elevated level of intracellular ROS in many types of cancer cells [131]. The increased level of ROS reflects the disruption of redox homeostasis, either due to an upregulated ROS production or a reduced ROS-scavenging capacity, leading to persisting oxidative stress in cancer cells [132]. Multiple ways of increasing ROS level in cancer cells have been identified. Irani et al showed that, H-ras-transformed fibroblasts produce large amount of superoxides through the activation of NOX [133]. Other studies point out the association of the tumour suppressor p53 in increased ROS production: Loss of the tumour suppressor p53 leads to an increased ROS production in Trp53-knockout mice, however, dietary supplementation with NAC in these mice prevented the occurrence of frequent lymphomas and further slowed the growth of lung cancer xenografts in these animals [134]. Likewise, breast cancer 1 (Brca1) and p53-heterozygous deficient animals showed increased levels of ROS and a higher incidence of carcinomas in their forestomach and oesophagus [135]. Conflicting findings suggest a complex redox regulation in cancer cells concerning the regulation of scavenging mechanisms. Cancer cells need to adapt to the increased levels of ROS, in order to promote proximal pro-tumorigenic signalling. However, in some cancer cells, an increase in ROS levels is associated with a decreased production of antioxidants such as SOD2, CAT and GPX1. This decrease helps the cancer cell to maintain high ROS levels [136-138]. Upregulation of NRF2 through mutations in NRF2 itself, in KEAP1, or in the oncogenes K-ras and Myc is a well-documented phenomenon in cancer cells. This upregulation

leads to an increased expression of ROS scavenging molecules, and so to the maintenance of ROS homeostasis in cancer cells. This ensures cancer cell survival through an inhibition of the otherwise ROS-activated JNK/p38 death-inducing pathway [139, 140]. This reflects an adaption of cancer cells to oxidative stress and allows cancer cells to activate proximal pro-tumorigenic signalling pathways, nonetheless oxidative stress can also have anti-tumorigenic effects.

5.3 ROS signalling

Superoxides are highly reactive with iron-sulfur clusters; however, when reacting with thiols, the rate is too low to be relevant for signalling [141]. Moreover, due to their negative charge and their poor stability, they are almost unable to travel through membranes [142]. Hydrogen peroxide are not as reactive as superoxides but more stable and diffuses easily through membranes, which renders them potent signalling molecules [141, 143].

5.3.1 Pro-tumorigenic Role of ROS

Higher level of ROS can lead to oxidative inactivation of the phosphatase and tensin homolog (PTEN), the protein tyrosine phosphatase (PTP), and MAPK phosphatases. As these phosphatases are all negative regulators of the PI3K/AKT and MAPK pathways, the PI3K/AKT/mTOR and MAPK/ERK signalling cascades are stimulated in a ROS dependent manner [133, 144-146]. The PI3K/AKT pathway is not only upregulated in various cancer types, AKT can further increase ROS production to promote proliferation and cancer cell survival [147]. Moreover, Weinberg et al was able to show that disruption of the mitochondrial function caused a lower level of ROS, which in turn led to reduced tumorigenesis in an oncogenic mouse model of lung cancer, and that increased level of mitochondrial ROS was responsible for K-ras-induced anchorage-independent growth of the lung cancer cells through the MAPK/ERK pathway [148]. ROS not only promoted survival through hyperactivation of the pro-survival pathways, it is capable of activating nuclear factor kappa B (NFκB) signalling pathway, which in return leads to an upregulation of genes, such

as caspase inhibitors or members of the B-cell lymphoma 2 family (BCL2), involved in cell survival [149-151].

Last, ROS can promote angiogenesis and metastasis, which are often associated with an aggressive tumour growth. In fast growing tumours, limited blood supply translates into poor oxygen und nutrient supply- a condition that promotes ROS production. Through AMPK activation, NADPH production by one-carbon metabolism is enhanced, despite the impairment of the pentose phosphate pathway [152, 153]. Moreover, ROS stabilizes hypoxia induced factor alpha (HIFα) through the inhibition of prolyl hydroxylases (PHDs) under hypoxic stress: While PHDs under normal conditions mark HIFα for proteasomal degradation [154, 155], under hypoxic stress, HIFα dimerizes with its beta subunit, translocates to the nucleus and induces the expression of proangiogenic genes like vascular endothelial growth factor (VEGF), genes involved in glycolysis and cell survival [156-158].

Neoangiogenesis allows cancer cells to migrate. Tochhawng et al showed that cancer cells are capable to detach from primary tumour through a series of cellular events, including cytoskeletal remodelling and degradation of the extracellular matrix, which requires the activation of several signalling pathways including MAPK, PI3K/Akt, and transcriptional activation of HIFα and Snail [159]. Moreover, ROS mediated oxidation and so activation of v-Src lead to a more aggressive cancer phenotype showing increased invasion and anchorage- and growth factor independent growth [160].

5.3.1 Anti-tumorigenic Role of ROS

When oxidative stress becomes too high, cell cycle arrest and cell death pathways are induced.

As a sensor for redox stress, apoptosis signal-regulating kinase 1 (ASK1) mediates the activation of JNK and p38 MAPK, which eventually leads to cell death [161]. ASK1 is coupled to TRX1 in its inactive state. However, on TRX1 oxidation by ROS at two cysteine sites, ASK1 dissociates

from TRX1 and thus facilitates the suppression of anti-apoptotic factors through the activation of the downstream MAP kinase kinase (MKK)4/MKK7/JNK and MKK3/MKK6/p38 pathways [161, 162]. However multiple human tumours harbour inactivating mutations in JNK and p38 and thus avoid cell death signalling [163].

5.3.2 Exploiting oxidative stress as a therapeutic option in cancer

In order to exploit the possibility of integrating ROS in a treatment option and taking into consideration the two opposite roles of ROS in cancer, several approaches have been applied in the past. As cancers cells have higher basal levels of ROS, they are more sensitive to a higher level of ROS compared to normal cells. Once a certain threshold is reached, cell death in induced (Figure 9). Therefore, one option is to increase ROS levels in cancer cells either directly or indirectly through interference with their antioxidant system. The other option is to decrease ROS levels in hope to disable protumorigenic signalling.

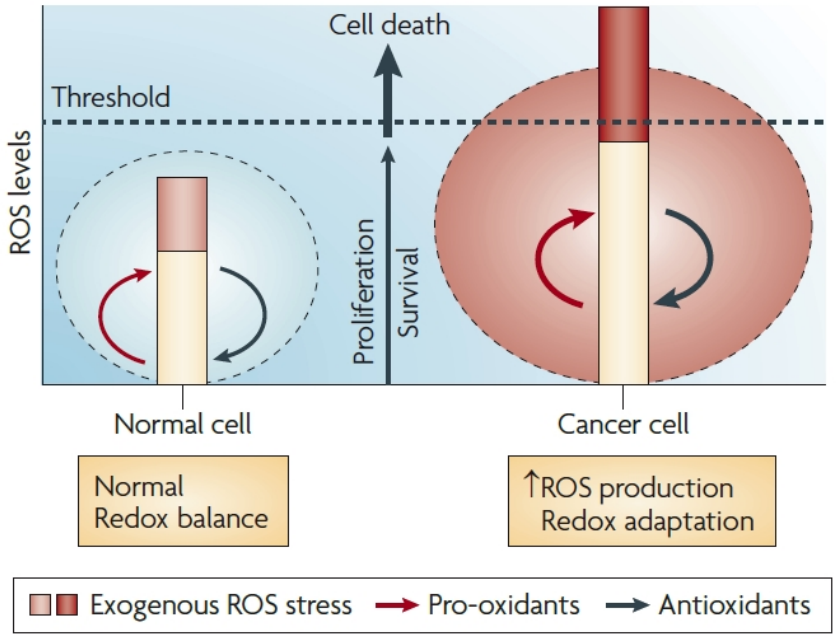

Figure 8 Cancer redox biology: a biological basis for therapeutic selectivity [131]

Many classical chemotherapeutic agents and ionizing radiation, function by increasing the ROS level within the cancer cell. Drugs like taxanes, vincalkaloids, platinum, anthracyclines, and antimetabolites induce mitochondrial damage through interference with the ETC and thus induce superoxide production, which eventually leads to the release of cytochrome c and triggers cell death [164]. Alternatively, ROS levels can be indirectly increased through the inhibition of the scavenging pathways. As the GSH metabolism seems to be important in protecting cancer cells from cell death, targeting this scavenging pathway seems promising. A recent publication of Yun et al showed that high levels of Vitamin C in K-ras and B-raf muted cancer cells led to oxidative stress, as intracellular oxidised vitamin C was reduced to vitamin C by glutathione and thus depleted glutathione. Thus, reactive oxygen species accumulate and inactivate glyceraldehyde 3-phosphate dehydrogenase (GAPDH), which leads to metabolic crisis in the cancer cells [165]. Another compound, namely, Phenethylisothiocyanate (PEITC) conjugates with GSH through electrophile-nucleophile interactions and depletes GSH from the pool. In addition, PEITC is able to inhibit GPX activity. These two examples cited so far caused a build-up of ROS and led to cell death in a preclinical mouse model of H-ras transformed ovarian cancer cells [166, 167]. The compound L-Buthionine-sulfoximine (BSO) inhibits glutamylcysteine ligase (GCL) and so targets GSH synthesis. In combination with ROS inducing agents such as 2-deoxy-D-glucose or carboplatin, BSO serves as a sensitizer and enhances cell death [168, 169].

The Glutathione pathway is not the only promising candidate for increasing redox stress; inhibitors against TRX, TR, and SOD1 also have been shown to be of great value [167, 170, 171].

Lastly, NRF2, the key player in antioxidant regulation, presents an interesting target. NRF2 is stabilized by multiple oncogenes like K-ras, PI3K, and Myc, mutations in NRF2 or in its negative regulator KEAP1 are often found in cancer cells [172, 173]. Moreover, NRF2 is upregulated in multiple cancer types and responsible for chemotherapy and radiation therapy failure [174, 175]. So far, two different strategies have been employed that either inhibit or induce the production of

NRF2. NRF2 inhibitors may be effective against NRF2-addicted cancer cells in which NRF2 is abnormally activated. But due to insufficient specificity, these inhibitors are not established yet. Moreover drugs that induce NRF2 are in use for non-malignant conditions but are also not yet established for cancer [176, 177].

6. Endocytosis

Endocytosis is the process that cells use to internalize surface proteins and macromolecules. Once internalized, the molecules are sorted and transferred to different compartments depending on their composition and designated destination: Either they can be recycled and routed back to the plasma membrane, passed to late endosomes and lysosomes for degradation, to the trans Golgi network also for degradation, or even sent across endothelial cells at the blood-brain barrier in a process that is called transcytosis for the delivery of macromolecules to the brain [178, 179]. Under physiological conditions, endocytic processes are essential for the maintenance of cell polarity and the physiological composition of proteins and lipids in the plasma membrane, which are important for cell surface receptor regulation, signalling, and motility. Certain viruses, pathogens, and bacterial toxins exploit endocytosis as a mechanism for entering cells and cancer cells may use endocytic process to induce their motility leading to their metastasis transformation [180].

Endocytic pathways can be broadly divided in to pinocytosis and phagocytosis. Particles larger than 500nm are usually taken up by phagocytosis or if soluble macropinocytosis. Pinocytosis can be further divided into clathrin-mediated endocytosis (CME), caveolae-mediated endocytosis, and those independent of clathrin (clathrin-independent endocytosis, CIE) [181]

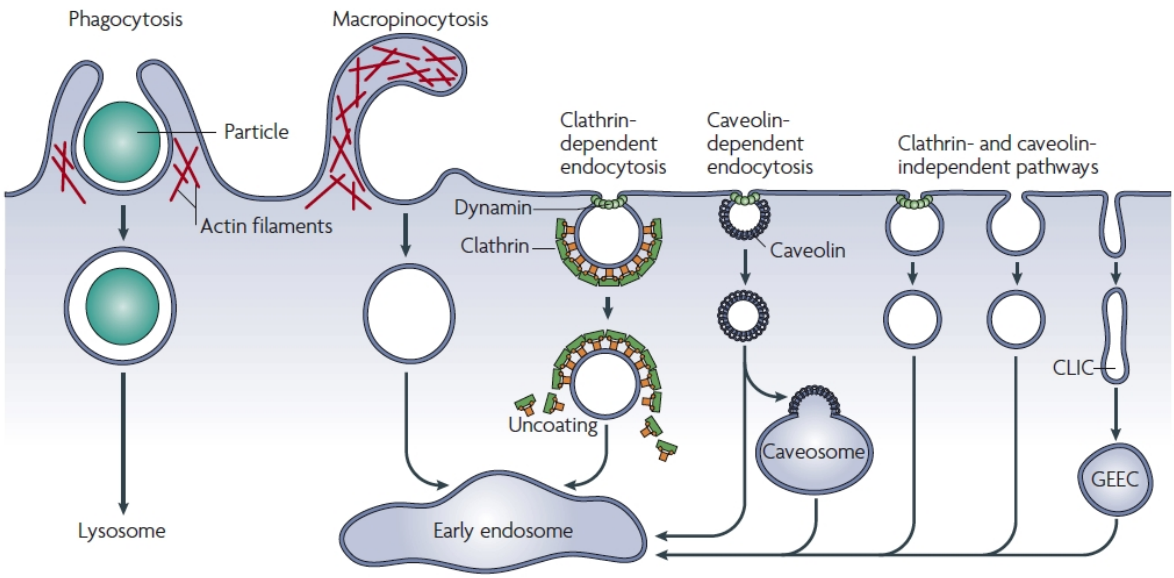

Figure 9 Different endocytic pathways [182]

6.1 Clathrin mediated endocytosis

CME occurs through the initial formation of clathrin-coated pits (CCP) and ends with the formation of clathrin coated vesicles (CCV). This process involves the following steps: the initiation of CCP formation, selection of the cargo, clathrin coat formation, CCP maturation, membrane invagination, CCV scission, and finally, the release and the uncoating of the vesicles [183]. Each step requires certain key-components to proceed. The initiation of the CCP formation begins with the recruitment of the four subunits of the heterotetrameric adaptor protein 2 (AP2) complex to the plasma membrane [184]. The AP2 complex is on the one hand responsible for cargo-recognition and on the other hand for recruiting clathrin to the plasma membrane in the next step of CME. Clathrin consists of heavy and light chains that form heterodimers; which are then assembled into trimers, forming a triskeleton [185]. The triskeletons gather like a net around the CCV, interconnected with the AP2 complex. Besides clathrin and AP2, in total, about 150 proteins are involved in the CCV formation; they are subsumed as CLASPs (clathrin associated sorting proteins) and interact with both the cargo and the AP2 complex to increase the sorting capacity

[186]. In a next step, clathrin polymerization stabilizes the curvature of the pit. However, for complete curvature forming and CCP progression, other proteins are also necessary and these include the BAR (Bin-Amphiphysin-Rvs) domain-containing proteins endophilin, amphiphysin, sorting nexin 9, and epsin. Successful budding of the CCV requires, the coordinated effort of several proteins: The binding of the BAR proteins to the large dynamin GTPase via their SRC homology 3 (SH3) domain (details on dynamins see below). This binding not only activates but also enables dynamin to assemble around the necks of the CCV. This assembly in turn causes the GTP hydrolysis, which drives the budding of the CCV. Once released, the clathrin coat is disassembled and now the vesicle is free to fuse with endosomes [181, 186-189].

6.2 Clathrin independent endocytosis

The term clathrin independent endocytosis (CIE) summarizes several pathways where the endocytic vesicles do not have a distinct coating. These pathways can be either dynamin dependent or dynamin independent. Dynamin dependent pathways comprise the RhoA dependent pathway and the Caveolae-mediated endocytosis CavME pathway (see below). The RhoA dependent pathway was first identified to be involved in the uptake of Inteleukin 2 (IL2) receptor and was later shown to be also involved in the uptake of other cytokine receptors such as EGFR. Several other proteins involved in the formation of the vesicles are Rac1, Pak, and the phosphatidylinositol 3-kinase (PI3K). As mentioned above, the vesicle budding occurs in a dynamin-dependent manner [182, 190].

Dynamin independent pathways comprise the Cdc42 dependent pathway and a pathway involving the GTPase Arf6.

The Cdc42 dependent pathway is responsible for the uptake of large amount of fluid into cells and leads to the formation of so-called clathrin-independent carriers (CLICs). The newly formed CLICs eventually fuse to specialized early endosomes which are enriched with glycosylphosphatidylinositol (GPI) anchored proteins called the GPI-AP enriched endosomal

compartments (GEECs). In that sense, this process is mainly termed the CLIC/GEEC pathway [182, 186, 190]. And last the Arf6-dependent pathway that was first associated with the uptake and recycling of the Major Histocompatibility Antigen I. However, other cargo like beta-1 integrin, E-cadherin and others followed. Arf6 activates phosphatidylinositol-4-phosphate-5-kinase to produce phosphatidylinositol-4,5-biphosphate which is involved in actin assembly and has been associated with regulating endosome recycling. However the role of Arf6 as an independently acting pathway is not yet fully established and might be greatly dependent of the cell type [182].

6.3 Caveolae-mediated endocytosis

Caveolae-mediated endocytosis (CavME) is involved in signalling, lipid metabolism, and cell surface tension sensing [186]. CavME is a highly regulated process and occurs after the binding of ligands to their respective receptors which accumulate in caveolae. Caveolae are hydrophobic membrane domains rich in cholesterol and sphingolipids. They are formed by the assembly of the integral membrane protein caveolin, which is inserted into the inner leaflet of the membrane bilayer in a wedge-like fashion that shapes the membrane curvature. Caveolin binds to cholesterol through its N-terminus and the rest serves as a scaffold for the binding of signalling proteins. The budding of the caveolae is not yet well understood but involves the regulated interplay of kinases and phosphatases. However, for the scission of the caveolae from the membrane the dynamin GTPases are the main drivers [181, 186, 191].

6.4 The large GTPase Dynamin

The GTPase Dynamin was first discovered in 1989 [192] shortly after its role in endocytic processes was described [193]. In mammals, three different Dynamin genes are known, and the proteins share a homology of 80% with very different expression patterns spatially. Dynamin 1 is found solely in neuronal tissues; Dynamin 2 is expressed ubiquitously; and Dynamin 3 is expressed in the brain, the testes, and the lungs [194].

Dynamin is a 100kDa GTPase composed of a catalytic G domain that binds and hydrolysis GTP and a four helix bundle called bundle signalling element (BSE). The BSE is a flexible connector between the stalk and the G domain. Further a phosphinositide-4.5.-biphophate binding pleckstrin homology (PH) domain and at the C-terminus a proline- and arginine-rich domain (PRD) through which dynamin partners interact (Figure 10) make-up the whole molecule [195]. Under physiological conditions, the stalk of dynamin dimerizes to form a cross. The two G-domains of the dimer are oriented in opposite directions and form the basic dynamin unit. The PH domain is responsible for phospholipid and PI(4,5)P2 binding and the PRD contains multiple binding sites for SH3 domain containing proteins. These SH3 domain-containing proteins are responsible for guiding dynamins to endocytic sites and for its coordination with other factors during scission processes.

Dynamins polymerize into helical structures, which is essential for their function. The polymerization of the dynamins results from the side-by-side apposition of the dimers through an interaction of the corresponding stalks. In that sense, the stalks shape the core of the dynamin ring and depending on their angle, the diameter of the ring is set. The BSE and G-domains reach towards the adjoining rungs of the dynamin helix. This is crucial, as the GTP hydrolysis of the G-domains can only occur across adjoining rungs and explains the strong onset of GTP hydrolysis upon polymerization [196].

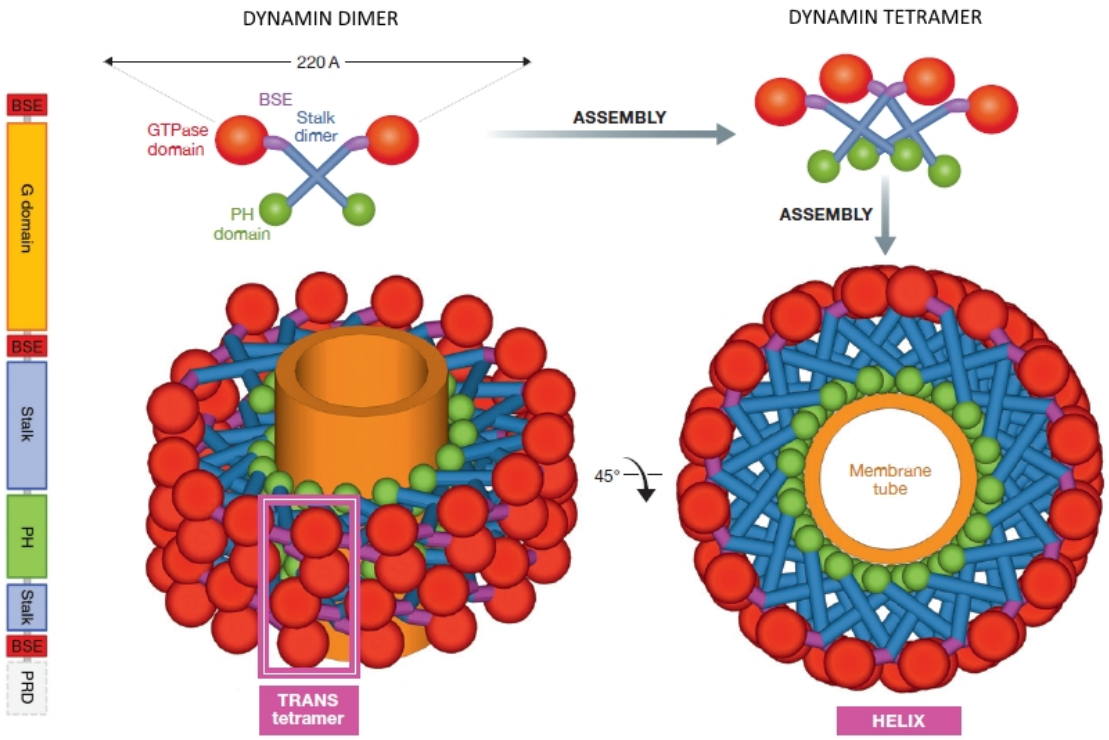

Figure 10 Structure and assembly of dynamin [187, 194]

Concerning the dynamin's fission mechanism, several models have been suggested. Generally researchers agree that dynamin helical oligomers use the energy derived from GTP hydrolysis to constrict and cut membrane tubules from the membrane. When bound to guanosine triphosphate, the opposing G domains dimerize and their GTPase activity is activated. Upon GTP hydrolysis, the position of the G domain changes relative to the BSE; the resulting mechanical energy is transferred to constrict the helix [197].

The "two stage model for dynamin-catalysed fission" model suggests that in stage one, when G domains across the adjoining rungs have the highest affinity, the polymerized dynamins implement a super-constricted state that causes the formation of hemi-fission intermediates. In stage two, subsequent hydrolysis to the GDP-bound form loosens the scaffold to a constricted state, leaving the hemi-fission intermediates proceed to complete fission [198].

The “constrictase/ratchet model” suggests that the energy released from the hydrolysis of GTP drives dynamins, which act as a molecular motor, to mechanically slide the adjacent turns of the helix. This sliding of the helical turns would occur repeatedly leading to the constriction and twisting of the helix (association/power stroke/dissociation) [197].

As mentioned above, dynamins are involved in multiple endocytic pathways. Even there are significant differences between the pathways, similarities exist when it comes to the function of dynamins. During early formation of the endosomal pit, several adapter proteins and scaffolding proteins are recruited to the PI(4,5)P2 enriched plasma membrane. The cargo is accumulated, and the vesicles grow and mature. At this stage, dynamins also accumulates around the growing vesicles. During CME, BAR-domain containing proteins bind dynamins and guides them to the neck of the vesicle to mediate the fission (see above) [196].

Another poorly understood function of dynamins is their interaction with the cytoskeleton. Dynamins are directly linked to the cytoskeleton and colocalize to the actin meshwork and interact with their regulators N-WASP/WAVE and Arp2/3, which are important in the formation of lamellipodia, circular dorsal ruffle, invadopodia, and actin comets (see also the section on circular dorsal ruffles). Actin might play a role in guiding dynamins to the right position or it might do so by generating membrane tension at the neck of the endosomes to facilitate the dynamin-induced scission [196, 199].

It has also been suggested that dynamin 2 modulates the function and localization of Rac, a Rho family member. Under normal conditions, Rac is involved in lamellipodia formation, transcytosis, and macropinocytosis. Schlunck et al showed, that disruption of the dynamin function impairs lamellipodia formation and thus inhibits cell spreading and platelet-derived growth factor-induced macropinocytosis. Rac was found misplaced into abnormal dorsal ruffles and led to the accumulation of abnormally shaped tubulated structures with membrane-bound Rac. The authors suggested that the disruption of dynamin function inhibits the internalization of Rac from the

plasma membrane which leads to the accumulation of activated Rac in abnormal membrane ruffles, depleting Rac from the pool [200].

Armstrong et al also suggested that the interaction of dynamins, Rac, and actin are essential for transcytosis and that an inhibition of dynamin leads to the translocation of active Rac from the plasmalemma, leading to the loss of cortical actin and the formation of intercellular gaps [201].

Many studies on dynamin rely on the use of dynamin mutants, dynamin knock-out mice, or dynamin inhibitors [187, 195, 202]. Depending on the target site of the Dynamin inhibitors, the inhibitors alter different functions of the dynamin protein. Binding to the GTPase domain of dynamin decreases the GTPase activity and binding to the PH domain effects the recruitment of dynamin to the membrane.

Multiple compounds have been developed over the last twenty years targeting different dynamin domains with different sensitivity and specificity[187]. The compound dynasore hydrate, or just dynasore was identified by Macia et al during a high-throughput screening of ~ 16 000 compounds for their ability to inhibit the GTPase activity of dynamin 1. They showed that Dynasore inhibited the GTPase activity of dynamin and abolished the uptake of the transferrin and low-density lipoprotein receptor [203]. The authors assumed that dynasore inhibits the basal and the stimulated rates of GTP hydrolysis in a non-competitive manner, without having an influence on GTP binding or dynamin assembly [203]. However, using a recently developed highly sensitive GTPase assay, Mohanakrishnan found that while dynasore had no influence on the basal GTPase activity of unassembled dynamin, it inhibited the GTPase activity of the assembled dynamin. These findings speak against the GTPase domain as the target of dynasore [204] and the exact target of dynasore remains to be elucidated.

As it was shown that dynasore had some undesirable side-effects including the binding to serum proteins which depleted dynamin availability and a high affinity to the detergent tween, which reduced its potency. Further at higher concentrations, dynasore had some cytotoxic effects [187].

Several new compounds were developed to improve the efficacy of dynasore; for example dyngo-4a. Dyngo-4a displayed a decreased cytotoxicity and a 32-fold higher inhibitory potency towards the assembly stimulated GTPase activity of dynamin [205].

Multiple studies have proved the efficacy of dynasore and dyngo-4a in inhibiting endocytosis in various cell systems [206, 207]. However, new studies have now suggested dynamin-independent effects of dynasore and dyngo-4a. Park et al first described in murine dynamin 1-3 triple knockout (TKO) fibroblasts that fluid phase endocytosis was not inhibited, whereas addition of dynasore abolished the uptake [202]. Recently, Persaud et al showed that dynasore and dyngo-4a were able to inhibit the Ras-like GTPase RagA in dynamin TKO cells and so prevented an activation of mTORC1 signalling [208]. Although there is growing evidence suggesting that dynasore and dyngo-4a may interfere with cholesterol homeostasis and may target lipid rafts independent of dynamins, the exact mechanisms remain to be resolved [209].

7. Cell Death Mechanisms

Cell death is part of life and crucial for all multicellular organisms. Cell death is essential in many processes, including tissue sculpting during embryogenesis, the maintenance of the immune system, and the destruction of aged, diseased, infected, or damaged cells.

The first descriptions of programmed cell death mechanisms were published in the early 1950s [210, 211]. In 1973, Schweichel and Merker proposed the first classification on cell death based on morphological features [212]. According to this classification, three different forms of cell death could be distinguished: type I cell death, also called apoptosis; type II cell death, also called autophagy; and type III cell death, also called necrosis (Figure 11) [213].

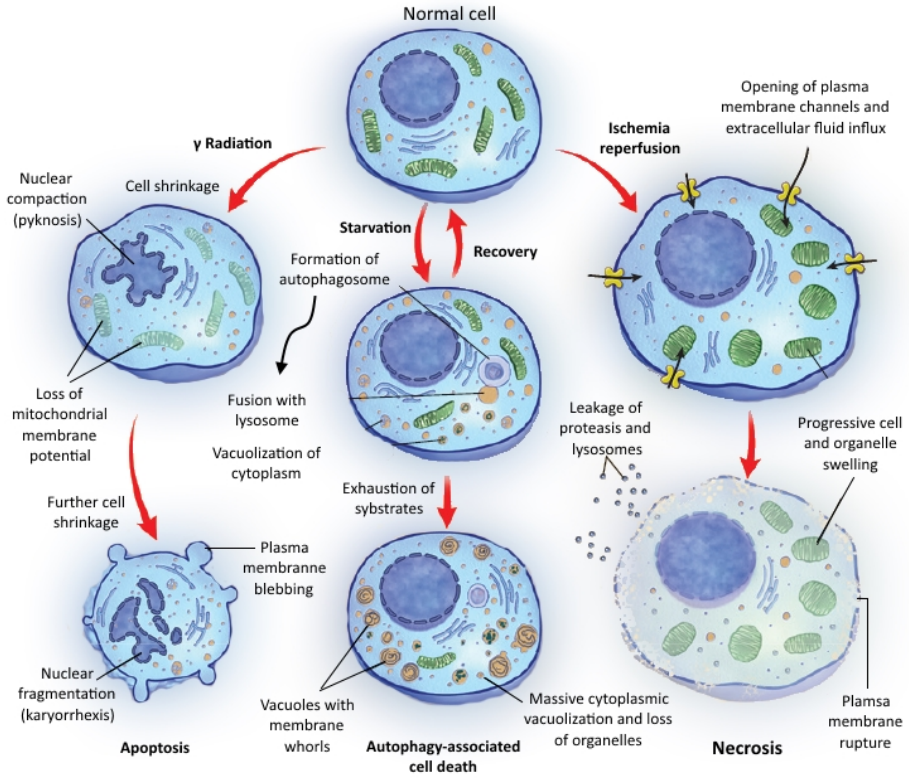

Figure 11 Schematic diagram showing 3 possible pathways of cell death [213]

The first classification relied on morphological features solely, but now with modern biochemical methods and techniques, the field has been revolutionised. Over the last 6 decades, scientists have gained profound insights into the molecular pathways on the initiation, regulation, and execution of different kinds of cell death. The majority of cell deaths do not proceed randomly but rather in a highly organised manner and are genetically programmed. Because of this, the term regulated cell death (RCD) or programmed cell death (PCD) was coined. This process is in clear contrast to accidental cell death (ACD), which is the sudden and catastrophic death of cells when exposed to severe, external insult [214]. Some features of the different PCD forms partially overlap and whether a cell dies from one or the other PCD form depends on the cell death stimulus, the tissue type and the cell's microenvironment. The same stimulus may also trigger different forms of PCD in the same cell depending on the intensity of the stimulus; or the same stimulus could trigger different forms of PCD in different cells [215].

The Nomenclature Committee on Cell Death (NCCD) has so far defined 12 major kinds of PCD and surely more will follow (Figure 14) [216].

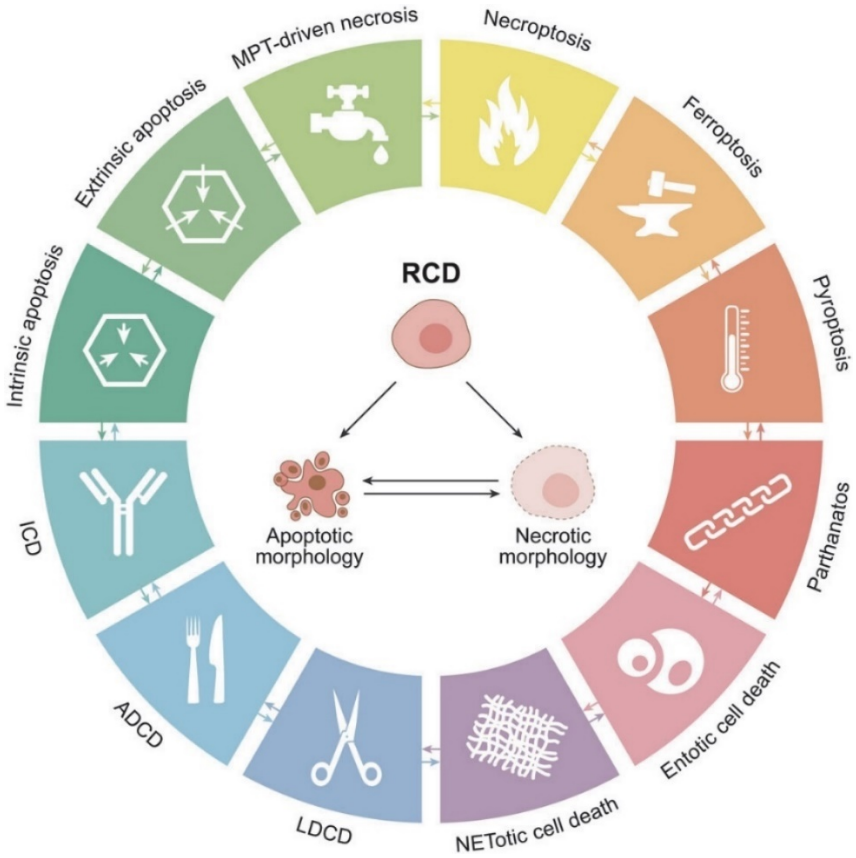

Figure 12 Major cell death subroutines. (RCD: regulated cell death, ADCD: autophagy-dependent cell death, ICD: immunogenic cell death, LDCD: lysosome-dependent cell death, MPT: mitochondrial permeability transition [217].

7.1 Apoptosis

The term Apoptosis is derived from the Greek word "ἀπόπτωσις" - meaning falling off, which usually suggests "leaves falling from a tree". It was first used by Kerr et al in 1972 to describe a morphologically distinct form of cell death [218]. Apoptosis is surely the best characterized form of cell death and can be subdivided into extrinsic apoptosis and intrinsic apoptosis. Apoptosis is initiated following an insult or preprogramed for certain physiological conditions, such as during embryogenesis and development [218-220].

The executioners of apoptosis are the caspases. This energy-dependent proteolytic cascade of cysteine-aspartate specific proteases (caspases) is the final step of apoptosis. Caspases are dimeric endoproteases that become activated through proteolysis by upstream caspases and once activated cleave downstream caspases themselves [221].

7.1.1 Morphology of apoptosis

During apoptosis, typical morphological changes can be visualized by light or electron microscopy. As early events, cell shrinkage and chromatin condensation (pyknosis) occur. The cells appear smaller, denser, and the organelles are tightly packed. The most characteristic feature of apoptosis is the condensation of the chromatin. As apoptosis proceeds, nuclear fragmentation (karyorrhexis), extensive plasma membrane blebbing and budding occurs which involves the separation of the cell fragments into apoptotic bodies (Figure 13). During this whole process, the organelle integrity and the plasma membrane are maintained. This is essential, as in that way hardly no inflammatory reaction will occur. Eventually, the apoptotic bodies are phagocytosed by macrophages and degraded within phagolysosomes [222, 223].

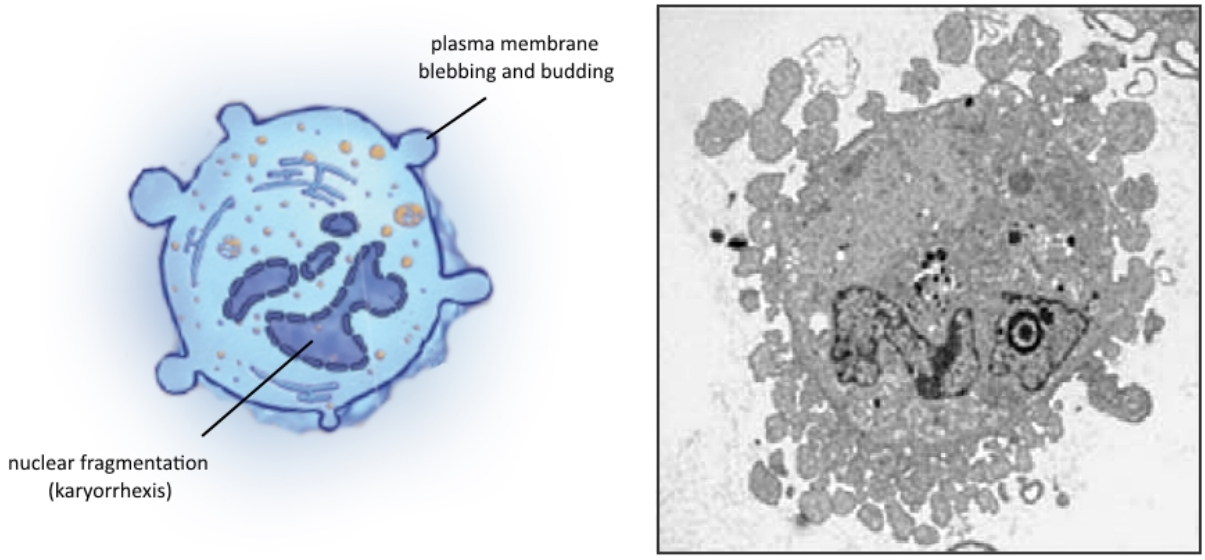

Figure 13 Electron microscopy image of taurolidine induced apoptosis in a glioma cell [213, 224]

7.1.2 Extrinsic Apoptosis

Extrinsic apoptosis is induced by extracellular stress signals that are transmitted through a battery of specific transmembrane receptors. The cell death program is initiated upon binding of death ligands to their corresponding death receptors, such as FAS/CD95 ligand (FASL/CD95L) to FAS/CD95, tumour necrosis factor α (TNFα) to TNFα receptor 1 (TNFR1), and TNF ligand superfamily member 10 (TNFSF10, also termed TRAIL), to the TRAIL receptor (TRAILR) [225, 226].

All different death receptors function by eliciting signals that lead to extrinsic apoptosis. In a similar way, upon ligand binding to its corresponding receptor, the receptor is stabilized and undergoes a conformational change. This facilitates the formation of a multiprotein complex at the cytosolic tail, the so-called death domain (DD) [227].

Several proteins are subsequently recruited to the DD, causing the formation of the supramolecular death-inducing signalling complex (DISC). These proteins include receptor-interacting protein kinase 1 (RIP1), FAS-associated protein with a DD (FADD), c-FLIP, cellular inhibitor of apoptosis proteins (cIAPs), and pro-caspase-8 or 10 [228, 229]. Aggregation of the DISC causes conformational changes that unleash the catalytic activity of caspase-8 or 10.

In type I cells, including lymphocytes and thymocytes, caspase 8 cleavage directly triggers the caspase 3 dependent executioner phase independent of mitochondria activation. Whereas in type II cells, including hepatocytes, pancreatic β cells and most of the cancer cells, caspase-8 cleavage induces the proteolytic cleavage of BH3-interacting domain death agonist (BID), to the truncated mitochondrion-permeabilizing fragment (tBID). TBID translocates to the outer mitochondrial membrane (OMM) and activates BCL2 associated X apoptosis regulator (BAX) and BCL2 antagonist/killer 1 (BAK) [230-232].

This activation is controlled by pro-apoptotic and anti-apoptotic members of the apoptosis regulator (BCL2) protein family, a group of proteins containing one to four shared BCL2 homology (BH) domains.

Through the homodimerization of Bak and Bax, mitochondrial pore formation is initiated which leads to mitochondrial membrane permeabilization (MOMP) and the release of several proteins from the mitochondrial intermembrane space (IMS). These proteins include cytochrome c (CYTC), diablo IAP-binding mitochondrial protein (DIABLO or second mitochondrial activator of caspases (SMAC)), endonuclease G (ENDOG), and cytoplasmic adaptor protein APAF1 [233, 234].

MOMP can be antagonized by anti-apoptotic members of the BCL2 family, including BCL2 and BCL2 like 1 (BCL-XL). They directly bind to and inhibit the pro-apoptotic BCL2 members [235, 236].

CYTC and APAF1 bind to procaspase 9 forming the supramolecular complex apoptosome, which activates caspase 9. The activated caspase 9 catalyses the proteolytic activation of the two executioner caspases 3 and 7, and thus completes the apoptotic demise of cells [214, 216, 237-240].

7.1.2 Intrinsic Apoptosis

Intrinsic apoptosis is initiated by a multitude of internal stress factors, including oxidative stress, ER stress through accumulation of unfolded proteins or DNA damage [241, 242]. Multiple stress factors can initiate intrinsic apoptosis and they all share one common step, the irreversible MOMP. MOMP is thoroughly controlled by pro-apoptotic and anti-apoptotic members of the BCL2 family (see above) [231, 235, 236, 238, 240]. If the pro-apoptotic signals dominate, Bak and Bax homodimerize at the OMM and initiate the pore formation. Once the point of no return is reached, MOMP not only leads to the release of lethal proteins from the IMS (see above), it also leads to the dissipation of the mitochondrial transmembrane potential ($\Delta\psi m$), with cessation of

mitochondrial ATP synthesis through an inhibition of the MRC [238, 240, 243]. Then as described above, eventually the apoptosome is formed, which preludes the last steps of apoptosis.

The release of proteins from the IMS is caspase-independent and is responsible for further pro-apoptotic effects: The release of AIF and ENDOG and their relocation to the nucleus, leads to the cleavage of DNA into nucleosomal fragments (nucleosomal fragmentation) [244, 245]. SMAC/DIABLO is important for the activation of the caspases for its ability to eliminate the inhibitory effect of IAPs [246-248].

In that sense the NCCD suggests to define ‘intrinsic apoptosis' as a cell death process that is always mediated by MOMP but may proceed in a caspase-dependent and caspase-independent manner [214].

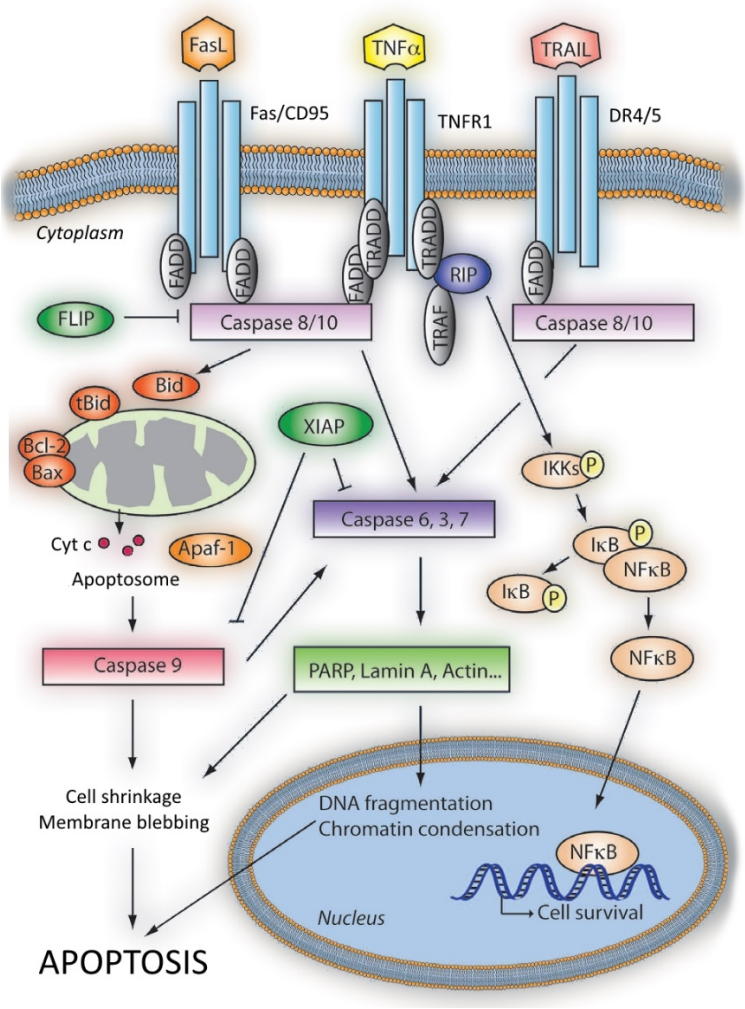

Figure 14 Schematic overview of the apoptosis pathway [249]

7.2 Necroptosis

For a long time, apoptosis was seen as the only form of RCD, and other cell death forms were considered unregulated accidental cell deaths (ACD)s, and therefore, subsumed as necrosis [218]. With the discovery of genetic, biochemical, and functional evidences, the term "necrosis" is understood as a molecularly controlled, regulated form of cell death (RCD), which includes various cell-death modalities such as parthanatos, ferroptosis, mitochondrial permeability transition (MPT)-dependent necrosis, and necroptosis [250, 251]. Among these, necroptosis is the best studied form of regulated necrosis and is clearly defined by a tightly regulated activation and inhibition process.

7.2.1 Morphology of Necroptosis

Necroptotic cell death was historically referred to as the type III cell death (Figure 11). It is characterized by early cellular rounding and swelling and an increased cytoplasmic granularity, while the nuclei remain intact. Towards the end, the disintegration and rupture of the mitochondrial and lysosomal plasma membrane is accompanied with the ejection of cellular contents in a ruptured balloon-like morphology [252].

7.2.2 Molecular mechanism

Apoptosis is not only the main form of induced RCD after an insult, it is also the main cell death form under physiological conditions [220]. The role of necroptosis during embryogenesis, differentiation, and maturation is limited to few reports. It is further not clear, if necroptosis is not only induced as a backup for an impaired apoptosis [253, 254].

Necroptosis mainly occurs during pathophysiological conditions of infection and disease. Upon cellular stress, a range of proteins can trigger necroptosis. These include TNF, FasL, TRAIL, interferon (IFN), lipopolysaccharides, dsRNA, cytosolic DNA, ER stress, viral infection and chemotherapeutic agents. Their corresponding receptors (Fas, TNFR1, pathogen recognition receptors (PRRs) like toll-like receptor 3 and 4 (TLR 3 and 4) and Z-DNA binding protein 1

(ZBP1)) are responsible for signal transduction [255-264]. The key molecules during necroptosis are the RIP kinases (receptor-interacting protein kinases), a class of serine/threonine protein kinases. RIP1 possesses several domains which are capable to activate different signalling pathways. Its N-terminal kinase domain is required for canonical necroptosis, its death domain (DD) is essential for TRADD association and its C-terminal RHIM domain is responsible for the recruitment of RIP3. RIP3 is homologous to RIP1, also containing an N-terminal kinase domain and a C-terminal RHIM domain [265].

One prototypic signalling pathway is mediated through TNF stimulation: TNF induces the recruitment of RIP1 and TRADD to TNFR1, which is then called complex 1. Ubiquitination and phosphorylation of RIP1 hinders a dissociation of complex 1 from the receptor, resulting in an inhibition of cell death and a pro-survival NF kappa B signalling [266].

Whereas, upon dissociation of complex I from the receptor, different pro-cell death complexes (complex IIa, IIb and the necrosome) are formed depending on the availability and abundance of accompanying proteins, which can either induce apoptosis or necroptosis [267]. If caspase 8 is available, it associates with complex II and induces apoptosis, however if caspase 8 is not available or dysfunctional, RIP3 is recruited to form the necrosome.

Complex IIa further recruits FADD, TRADD, and RIP1, whereas complex IIb can be formed independent of TRADD. In order to activate RIP3 by RIP1 through phosphorylation, their physical interaction between their RHIM domains is essential. [260, 268-270]. After its activation, RIP3 phosphorylates mixed lineage kinase domain-like (MLKL) at several sites (Figure 15) [271-273]. The exact mechanism of action of MLKL is still unknown and controversially discussed. Common understanding is that MLKL delocalizes to the plasma membrane once phosphorylated, where it binds specific phosphatidylinositol phosphate species and prompts an influx of ions, either directly by the formation of ion channels or pores or indirectly through the interaction with ion channels. This ion influx will eventually lead to the cell's demise [273-275].

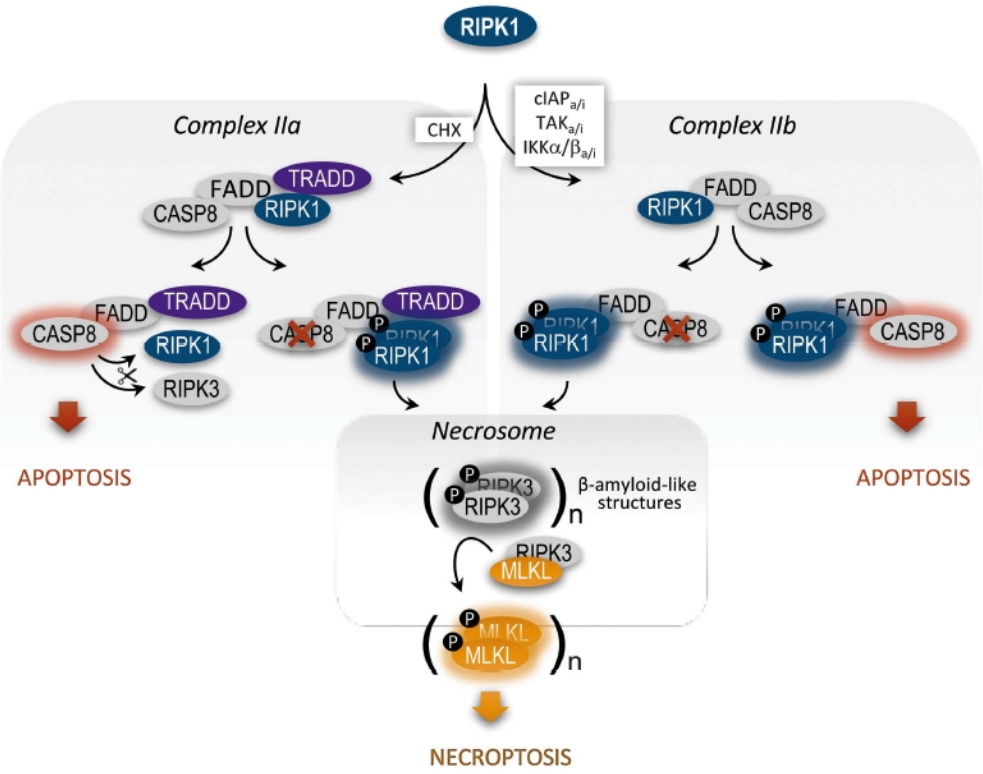

Figure 15 Signal transduction complexes in TNF-induced necroptosis [276].

Alternatively to the canonical necrosome formation, RIP3 can be activated through the TLR3, TLR4 and ZBP1. Here dsRNA, cytosolic DNA and pathogen associated molecular patterns (PAMPs) are the inducing molecules. Once RIP3 is activated, MLKL is phosphorylated independent of the RIP1 kinase activity and necroptotic cell death can proceed [256, 277].

7.3 Ferroptosis

Ferroptosis, a new form of RCD, was described by Dixon et al in 2012 [278]. Ferroptosis is an oxidative, iron-dependent form of cell death leading to lethal accumulation of toxic lipid ROS through lipid peroxidation and the depletion of plasma membrane polyunsaturated fatty acids [279, 280]. At the genetic, biochemical, and morphological level, ferroptosis can be distinguished from other RCDs, [278]. Up to now, ferroptosis has been associated with normal physiological functions such as embryogenesis and differentiation [281].

7.3.1 Morphology of Ferroptosis

Morphologically, ferroptotic cell death has only few distinct cellular features. In the early phase, the mitochondria become smaller with increased membrane density, reduced or no cristae, and ruptured OMM (Figure 16). As the process progresses, the cells show a necrotic and rather indistinct appearance [251, 278].

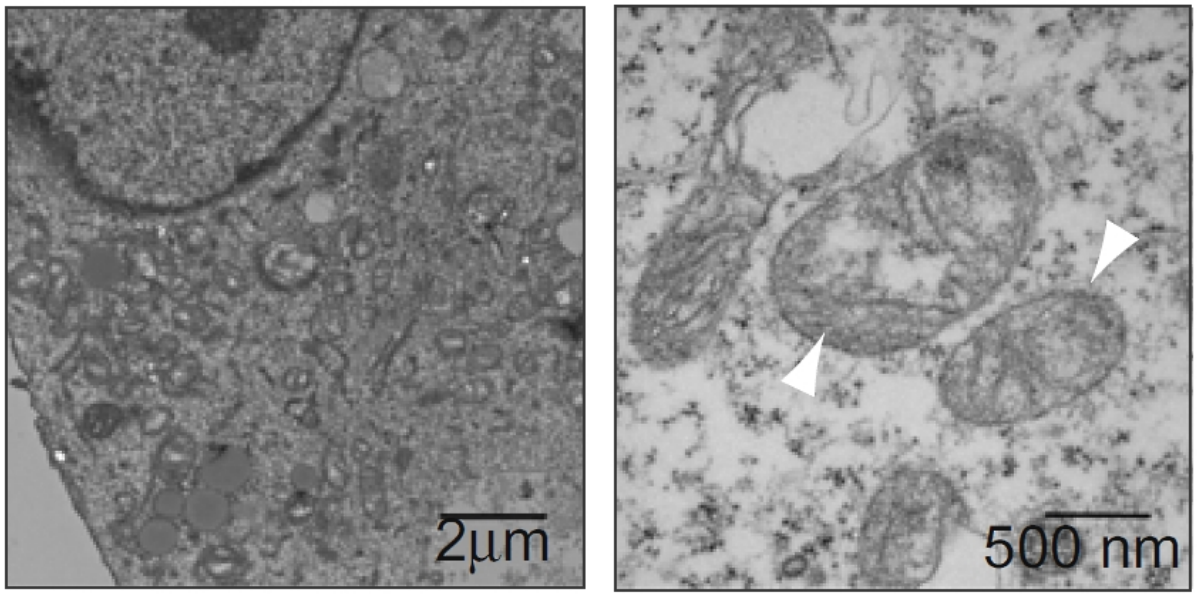

Figure 16 Transmission electron microscopy of BJeLR cells treated with erastin and undergoing ferroptosis. Single white arrowheads indicate shrunken mitochondria [278]

7.3.2 Molecular mechanism

Ferroptosis can be triggered by small molecules that inactivate the cellular glutathione (GSH)-dependent antioxidant defence system [282]. The reduced glutathione (GSH)-dependent enzyme glutathione peroxidase 4 (GPX4) is the most important ferroptosis inhibitor. It catalyses the GSH-dependent reduction of lipid hydroperoxides to lipid alcohols [283]. Compounds that affect Glutathione homeostasis seem promising as agents that induce ferroptosis. The first ferroptosis inducing compound Erastin inhibits the cysteine/glutamate antiporter system xc- and so consequently depletes cysteine [278]. Tyrosine kinase inhibitor sorafenib seems to have the same function. Sorafenib also depletes cysteine via inhibiting the cysteine/glutamate antiporter system

xc- and induces ferroptotic cell death in multiple cancer cell lines [284]. Kagan et al was able to show that lipid peroxidation preferentially occurred at certain phosphatidylethanolamine-containing polyunsaturated fatty acids (PUFAs). Here, lipid peroxidation is catalysed by lipoxygenases (LOX). Lipid peroxides further decompose into reactive derivatives, which target proteins, nucleic acids and other macromolecules [285, 286].

The iron-dependency of ferroptosis has been shown in several ways: Iron depletion by iron chelators abrogates ferroptosis whereas increased iron availability through an increased import by the iron carrier transferrin or increased degradation of the iron storage pool ferritin promotes ferroptosis [278, 283, 287, 288]. This iron-dependency might be explained by two different mechanisms. First LOX contain a di-iron centre at their catalytic sites, which renders them iron dependent [289] and second heavy metals are prone to promote non-enzymatic lipid oxidation via the Fenton reaction [290, 291]. Which of the two mechanisms is the most important one remains to be elucidated.

7.4 Autophagy

Autophagic cell death is historically referred to as type II cell death. The term autophagy-dependent cell death (ACD) is somehow misleading as autophagic responses mediate cytoprotection rather than cell death. It was shown that inhibition of the autophagic machinery accelerates rather than prevents cell death [292, 293]. ACD is involved in physiological cell death as observed during the development of D. melanogaster [294] and has been observed in some cancer cells as a response to chemotherapeutic agents. The latter seems to be especially true when the cells lack key proteins of the apoptotic pathway such as Bak, Bax, and caspases [295].

7.4.1 Morphology of autophagy

During ACD, much of the cytoplasm are sequestered into autophagosomes. These large autophagosomes are responsible for the cell's characteristic vacuolated appearance (Figure 17) [214]. Autophagosomes are double-membraned and may contain cytosol and intact cytoplasmic

organelles such as mitochondria and ER. After the fusion of autophagosomes with lysosomes, these develop into autolysosomes with a single layer of membrane that contain degraded cytoplasmic organelles [296].

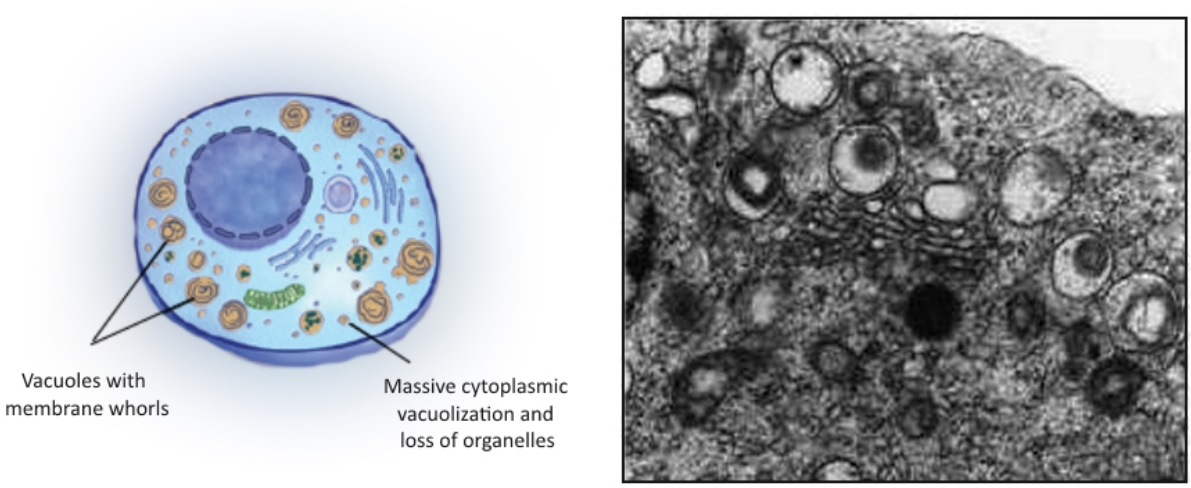

Figure 17 Human epithelial cancer (HeLa) cell treated thapsigargin and undergoing autophagic cell death. Accumulation of double-membraned cytoplasmic vacuoles containing organelles or parts of the cytosol [297].

7.4.2 Molecular mechanism

The autophagic process can be divided into distinct steps, each involving different key proteins. Key players of the autophagic machinery are the autophagy-related (Atg) genes, that orchestrate the autophagic process [298]. The degradative autophagy pathway is induced during cellular stress, which can be caused by conditions such as nutrient and growth factor deprivation [298]. The protein kinases mTOR negatively regulates autophagy through inhibitory phosphorylation of the Unc-51-like kinases ULK1 and ULK2 (mammalian homologues of Atg1) while AMPK activates autophagy through phosphorylation of ULK 1&2 and by inhibiting mTOR [299-301]. Upon induction of autophagy ULK is dephosphorylated, which leads to the phosphorylation of Beclin-1 (mammalian homologue of Atg6) and eventually to the generation phosphatidylinositol 3-phosphate (PtdIns(3)P) [302, 303]. Autophagosome formation requires two ubiquitin-like conjugation systems, which are directly linked with expansion of autophagosomal membranes

[304, 305]. These complexes activate Atg3, which covalently attaches microtubule-associated protein 1 light chain 3 (better known as LC3/Atg8) onto the surface of autophagosomes [306]. Lipidated LC3 is essential for the closure of the autophagosomes and assists the attachment of specific cargos and adaptor proteins [307, 308]. The regulation and timing of the fusion of the autophagosome with a lysosome is essential and requires among others SNARE proteins and Ras-like proteins from rat brain (Rab) protein [298]. Finally, bit by bit, the contents of the autolysosome are degraded, and their building blocks recycled [309].

7.5 Methuosis

Methuosis is derived from the Greek word methuo, which means to drink to intoxication. Maltese and Overmayer used the word to describe a novel type of cell death, which occurs in cells accumulating large fluid-filled cytosolic vacuoles [310]. Although methuosis can be initiated by various triggers, such as genetic manipulation, small molecules, and antibodies, these triggers share the same feature of an increased macropinocytosis [311-321]. In the latest NCCD review, methuosis was not considered as a form of RCD, as it has not been described yet in a physiological context [216].

7.5.1 Morphology of methuosis

The most prominent feature of methuosis is the congestion of the cytoplasm with large clear, fluid-filled vacuoles of different sizes. The membrane of the vacuoles is single-layered, in contrast to the double-membraned autophagosomes. The nucleus stays intact without signs of chromatin condensation or fragmentation. At the final stage, the cell membrane ruptures, resembling the final stage of necroptosis [310, 311].

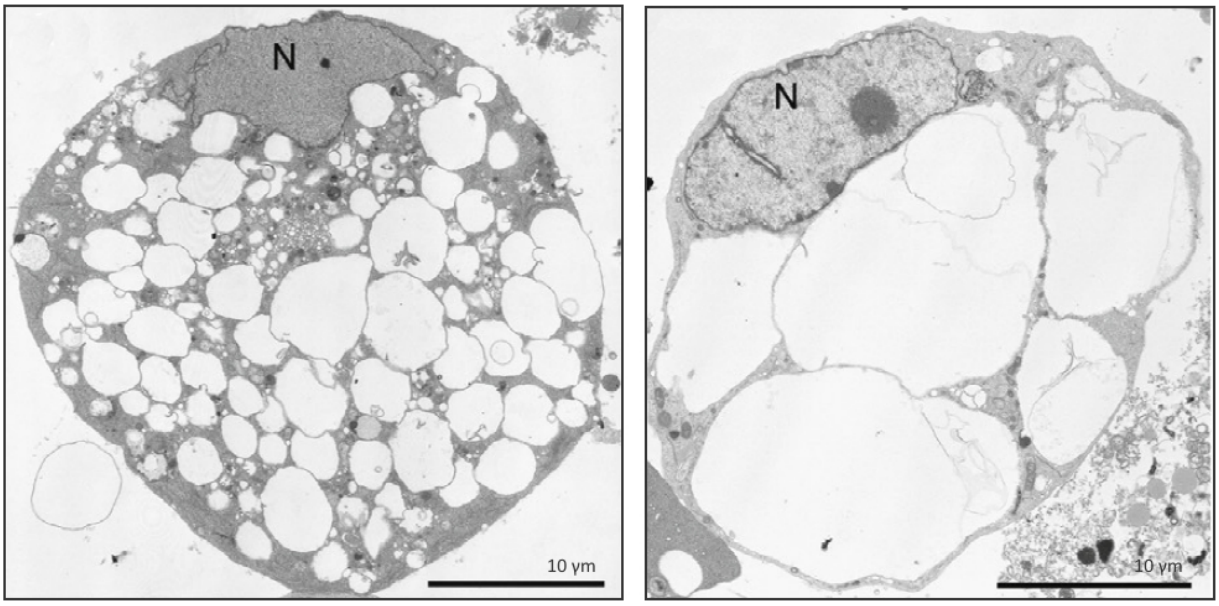

Figure 18 GBM cells undergoing methuosis triggered by ectopic expression of activated Ras [322].

7.5.2 Molecular mechanism

7.5.2.1 Macropinocytosis during physiological processes

Macropinocytosis is a regulated clathrin-independent from of endocytosis that mediates the internalization of soluble molecules, nutrients, and antigens. Macropinocytosis is involved in cell motility, migration, and metastasis [323]. Evolved from surface membrane ruffles, the so called macropinosomes are formed by closure of the plasma membrane through an actin-dependent process [323]. First described by Lewis in 1931, macropinocytosis is caused by external stimuli such as CSF-1, epidermal growth factor (EGF) and platelet-derived growth factor (PDGF) signalling through receptor-tyrosine kinase signalling [324-327].

Two distinct forms of macropinocytosis can be distinguished: Macropinocytosis derived from peripheral ruffle (PR) formation, referred to as macropinocytosis, and macropinocytosis derived from circular dorsal ruffle formation, referred to as circular dorsal ruffles (CDR). While macropinocytosis is very well studied, CDR is less explored, and many open questions remain.

7.5.2.1.1 Macropinocytosis from peripheral ruffles

Once formed, the macropinosomes undergo a maturation process, which is different for different cells. Here, key molecules are various Rab GTPases. Known as the Rab cascade, upstream Rab GTPases recruit certain GEFs (guanine nucleotide exchange factors) that activate and recruit a downstream Rab GTPase. The downstream Rab GTPase then recruits a GAP (GTPase-activating proteins) to the upstream Rab, which is consequently deactivated [186].

Most of the cargo is directly recycled back to the plasma membrane via early endosomes with Rab5 GTPase as the key endosomal component. The remaining early endosomes mature to late endosomes. The formation of a new late endosomes is preceded by acquisition of a Rab7 GTPase. This leads to the transient formation of a hybrid Rab5/Rab7 endosome. The removal of Rab5 and its replacement with Rab7 require its GAP activity. The Rab7 positive late endosomes become more and more acidified (the luminal pH drops from 6 down to 4.9) and finally fuse with lysosomes. During this stage, the late endosomes accumulate Lamp1, a late endosomal/lysosomal protein. Nearly all of the cargo in the late endosomes is degraded within the lysosome and only a minority serves for the maintenance and generation of lysosomes themselves [328]. Phosphatidylinositol phospholipids (PIP) are important components of the membranes and are heavily involved in endocytosis. Phosphorylation and dephosphorylation at the 3, 4, and 5 positions of the inositol ring directs certain binding proteins to the PIPs. PI(4,5)P2 is mainly present on the plasma membrane and prominent binding partners include AP2 and dynamin, whereas PI(3)P is enriched in endosomes with their own binding partners. [329]. PIPs and Rab GTPases are closely connected. PIPs are able to recruit GEFs and GAPs to the Rab GTPases and either activate or inactivate the Rab GTPase. PIPs are therefore crucial for the directional flow of membrane cargoes [186].

Besides the above mentioned Rab GTPases, other members of the RAS superfamily are significantly involved in macropinocytosis [330]. Rac1 and Cdc42 are essential for membrane

ruffling and macropinosome formation [326, 331-333], while RhoB localizes to intracellular endosomes, where it controls vesicle transport through regulating actin assembly on vesicle membranes. Last, RhoG, is involved in the formation of dorsal membrane ruffles [326, 331-335]. The involvement of Ras in membrane ruffling and macropinocytosis has gained more and more importance since it has been shown to be involved in membrane ruffling and macropinocytosis but also driving methuosis [310, 311, 317, 336-340]. Last, the Arf GTPases are also involved in membrane trafficking. Arf6 guides Rac1 to the plasma membrane and initiates the activation of phospholipase D1, which is required for macropinosome formation [341, 342].

7.5.2.1.2 Circular dorsal ruffles

Suggested functions of CDRs embrace the directed internalization of receptors and the gross internalization of soluble substrates and molecules through macropinocytosis. Further CRD is involved in cell motility in a specific mode, namely mesenchymal migration [333, 343].

CDRs are phenomena observed on the dorsal surface of cells. They extend vertically from the cell membrane to form closed, ring-shaped vesicles. After TRK stimulation, they appear, constrict, enclose, and disappear within 30minutes [344]. The signalling events are not fully understood. However, the phosphatidylinositol 3-kinase (PI3K) and the small GTPase Rac seem to be involved downstream of TRK stimulation [345]. After growth factor stimulation, expression of guanosine diphosphate (GDP)-bound dominant negative forms of Ras, Rac and Rab5 inhibit the induction of CDRs. Further members of the Arf family have been found localized to CDR and overexpression of their GAPs strongly inhibits CDR formation [346, 347].

The regulation of actin polymerization is controlled by a group of interacting proteins. The key step is N-WASP 1 or Cortactin mediated activation of Arp 2/3 [199, 348]. More than 20 membrane-binding proteins are associated with CDR. Among these, Dynamin 2 plays an essential role. While Dynamin 2 overexpression strongly induces CDR formation, dominant-negative

mutant Dynamin 2 expression and Dynamin 2 depletion abolishes CDR formation [199, 200, 346, 349-351].

7.5.2.2 Macropinocytosis during methuosis

The first description of hyperstimulated macropinocytosis dated back to 1999 when Chi and Kitanka observed a caspase-independent form of cell death. They reported such cell death to be accompanied by massive accumulation of fluid-filled vesicles after ectopic expression of the constitutively active oncoprotein, H-Ras (G12V) in glioblastoma cells [337, 352]. They misinterpreted the vesicles to be autophagosomes.

Almost 10 years later, Overmayer and Maltese showed that ectopic expression of oncogenic H-Ras induces the formation of single-membraned non-acidic vacuoles. These vacuoles resemble macropinosomes in that they incorporate fluid-phase tracer dextran 488, via increased macropinocytosis. Further, they showed that these macropinosomes contained Rab 7 and Lamp1 but failed to fuse with lysosomes, indicating an impaired maturation. To further pin down the involved pathway, they expressed mutant and constitutively active Rac1 in glioblastoma cells and saw that this mutant also induced an increased fluid-phase dye uptake and eventually cell death, indicating its relevance [310, 311]. Moreover, they were able to show that this new phenotype was distinct from autophagy, apoptosis, and necroptosis. The macropinosomes did not contain the autophagosomal marker LC3, however, caspase 3 activation was observed, but the phenotype could not be inhibited by either knockdown of Beclin-1 (autophagy essential protein), pharmacological inhibition with the pan-caspase inhibitor Z-vad, nor the necroptosis inhibitor Necrostatin (NS-1) [310].

Two follow up studies in glioblastoma and osteosarcoma cell lines revealed that methuosis occurs independent from activation of phosphatidylinositol-3-kinases (PI3K), Cdc42 and Raf signalling [311]. Further, they showed that active Rac1 stimulates GIT1, a negative regulator of the GTP-binding protein Arf6, which is a well-known regulator of endosomal recycling. Pharmacological

inhibition of Rac1 or shRNA-dependent silencing of GIT1 prevented the vacuolization and loss of cell viability [336].

Since these early descriptions of methuosis in cancer cells with ectopic H-Ras expression, several groups have demonstrated induction of methuosis through different compounds in various cell systems. After application of methamphetamine to neuroblastoma cells, Nara et al observed the formation of large cytoplasmic vacuoles that were not co-localized with autophagosome or the ER markers. Co-localization experiments revealed Ras and Rac1 on the vacuoles and co-treatment with the Ras inhibitor, farnesylthiosalicylic acid (FTS), and the Rac1 inhibitor, EHT1864 inhibited the formation of macropinosomes. Further an increase in the lysosomal marker LAMP1 and a decrease in Cathepsin L were observed, indicating either an impaired endosomal maturation or an impaired lysosomal function triggered by Ras/Rac1 [353, 354].

Chunhui et al, found that a combination of ectopic expression of TrkA and nerve-growth factor (NGF) treatment in medulloblastoma cells also hyperstimulated macropinosomes. However, these vacuoles carried the autophagosomal marker LC3, whereas knock-down experiments of autophagy key players did not block the NGF-induced macropinocytosis. Interestingly, the Casein Kinase 1 (CK1) inhibitor D4476 completely blocked the observed phenomenon and induction of cell death [355]. Their follow-up study then showed that RhoA is activated by Src. Further CK1 phosphorylates RhoB, leading to the release of actin stress fibres, which enables the activated RhoA to reorganize actin required for generation of macropinosomes [356].

Other small molecules have been shown to induce macropinocytosis through various pathways. These include the indol-based chalcone-related small molecules MIPP and MOMIPP in different cancer cell lines and in a Ras and Rac1 independent fashion. Nevertheless, also here a block in endosomal maturation is suggested [313, 357]. Further development of these chalcones identified some agents that induce massive accumulation of vacuoles, however fail to induce cell death. This

unexpected uncoupling of vacuolization and cell death suggests that other pathways and key molecules must be involved than the ones explored so far [315, 358, 359].

Another compound studied in the context of methuosis is Vacquinol, which further decreases ATP levels and induces a rupture of the cell membrane. An unbiased shRNA screen showed that the activity of MAP kinase kinase 4 (MKK4) was required, however its exact role remains unclear and the publication was later retracted due to unreproducible animal studies [360]. Despite being promising in the cell culture setting, this compound failed to effectively reduce tumour size or prolong overall survival in a glioblastoma mouse model [319, 361].

Last, Manara et al discovered that upon CD99 mAB triggering, methuosis is induced in Ewing sarcoma through activation of Insulin Growth Factor Receptor 1 (IGFR1), Ras and Rac1 [317].

Although multiple studies have by now well documented methuosis in malignant cancer cells, many questions remain. Are tumour cells in general more prone to disruptions of the endocytic pathway as they often rely on sustained growth factor signalling? What are the exact signalling pathways involved and at which step is the endosomal maturation blocked? Most importantly, how does increased macropinocytosis lead to the induction of cell death?

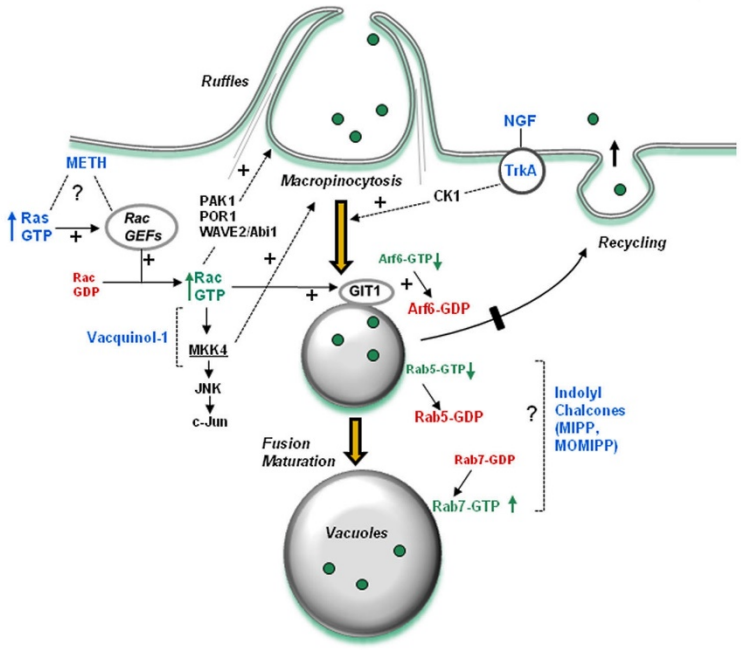

Figure 19 Overview of signalling pathways involved in hyperstimulation of macropinocytosis [362]

8 Ionizing Radiation

8.1 Physics and Chemistry

The German physicist Wilhelm Conrad Röntgen was the first to discover that x-ray exposure blackens photographic films in 1895. One year later, the first medical use of x-ray was published (Lancet, 1896) [363]. Radiation oncology is the clinical field dealing with the application of radiation as a therapeutic option in the treatment of malignancies. Alongside with surgery, radiation therapy was the first established treatment for cancer patients.

The term radiobiology refers to the study of ionizing radiation and its effect on living organisms. Depending on the amount of energy, radiation either elevates an electron in an atom to a higher energy level (excitation) or if the energy level is higher, ejects orbital electrons from the atom (ionization). Along with the ejection of the electrons a large amount of energy is released [364]. The delivered radiation dose is internationally measured in Gray (Gy) and defined as the amount of radiation depositing 1 Joule of energy in 1 kilogram of matter. Different kind of ionizing radiation can be distinguished; these include electromagnetic radiations (x-rays and gamma-rays) and particulate radiations (electrons, protons, α-particles, heavy charged particles, neutrons). All charged particles cause direct radiation effects, meaning that the radiation directly excites or ionizes the target atom through a high linear energy transfer (LET). X-rays, gamma-rays, and neutrons, on the other hand, indirectly interact with the target: they react with molecules in the cell (e.g., hydrolysis of water) and cause the production of free radicals that eventually damage the target [14]. Hydrolysis of the water results in a hydrogen and a hydroxyl (free radical) molecule. Upon recombination of two hydroxyl molecules, unstable hydrogen peroxide is formed. Hydrogen peroxide eventually decays into a peroxide hydroxyl, which combines with an organic compound to form a stable organic hydrogen peroxide molecule, which damages the cell [14, 365].

Fractionated radiation means the delivery of the required radiation dosage in multiple smaller doses, over several weeks. Through this protracted application, the differences between healthy

and tumour tissue are best utilized in the sense of damage repair and response of the microenvironment [15]. To be able to describe effects of different fractionation regimes, the linear quadratic model is applied and shows the effects of fractionated radiation on cell survival. By reducing the dose per application, higher cumulative dose levels can be administered. This spares the normal tissue without reducing the radiation effect on cancerous tissue [366, 367]. This model has lately been challenged by the observation that target cells show a hypersensitivity to dosages below 0.5Gy and radio resistance to higher doses. Differences in DNA damage repair might be responsible for this observation. Interestingly, tumour cells that are generally more radio resistant show the greatest sensitivity to low dose radiation [368].

8.2 Five R's of Radiobiology

The five R's of radiobiology are used to explain the biological factors that influence treatment response of different patients to fractionated radiation. Originally described as the four R's of radiobiology by Withers in 1975, the four key principles upon which radiation parameters are based are explained: repair of normal cells to sublethal doses of radiation damage, redistribution of cells within the cell cycle, repopulation of surviving tumour cells, and reoxygenation of hypoxic areas within in the tumour [369].

Repair after sublethal doses of radiation mainly involves the repair of single and double strand breaks (SSB/DSB). Healthy tissues have greater capability to launch the repair program compared to irradiated tumorous tissue. Redistribution refers to the different sensitivity of cells during cell cycle and the different repair programs that are started depending on the cell cycle phase (see below). Repopulation is the observation that surviving tumour cells accelerate in regrowth after radiation. To avoid this, short radiation intervals have to be chosen.

Reoxygenation exploits the capability of tumour cells to enhance their intratumoral oxygenation, which significantly improves the radiation efficacy.

The fifth R was later added by Steel in 1989, highlighting the importance of radio sensitivity of cells [370]. Radiation sensitivity is dependent on intrinsic and extrinsic factors. Actively dividing cells are more radiosensitive than non-dividing cells. Cell cycle can be divided into four phases: mitosis or M phase (division of cells), gap 1 or G1 phase (preparation for replication), synthesis or S phase (DNA synthesis by replication), and gap2 or G2 phase (preparation for re-entering mitosis). M and G2 phase are the most radiosensitive phases, when chromosomes are condensed and paired [371]. Further radio sensitivity correlates with a cell's ability to start its DNA repair program or its activation of apoptotic pathways. Other factors that influence radiation sensitivity are the microenvironment and the vasculature that determine oxygenation and nutrient availability. Oxygen supply is one of the main factors determining radio sensitivity. The relative radio sensitivity of euoxic to hypoxic cells is about 1.5 to 2.5, meaning that the dose required to achieve a certain effect must be 1.5 to 2.5 higher for euoxic than hypoxic cells [372]. Oxygen is needed for the formation of reactive oxygen species. Further, it is believed that oxygen transfers free radical–induced DNA damage into a more permanent state. Intratumoral regions with poor oxygen supply are relatively radio resistant and tend to be more aggressive. Hypoxia can select for tumour cells harbouring p53 mutations which are so associated with a bad prognosis [373-375].

8.3 DNA and Chromosome Damage Repair and cell death

Ionizing radiation produces a range of DNA lesions, which eventually can cause cell death and mutations. In mammalian cells, 1 to 2 Gy causes around 1000 base damages and single-strand breaks (SSBs) and around 40 double-strand breaks (DSBs) [376]. Low dose radiation or indirect radiation causes mainly SSBs damages through hydroxyl radicals, generated from the hydrolysis of water [377], whereas direct radiation mainly causes DSBs and thus the cleavage of DNA in two. SSBs are by far less important compared to DSBs to cause cell death. DSBs are thought to be the most important lesions as one single double strand break can already engage the damage-sensing

process that can lead to cell death. Large lesions causing the formation of dicentric and acentric DNA fragments can induce mitotic cell death during division [366].

To handle DNA damage, cells developed sophisticated DNA damage repair mechanisms. SSBs and base damages are usually repaired by base excision repair (BER) and DSBs by either nohomologous end joining (NHEJ) or by homologous recombination repair (HRR) [376]. During BER the undamaged complementary strand functions as a template. First, the damaged base along with the associated sugar is removed by an endonuclease, followed by the insertion and ligation of a replacement nucleotide by the DNA polymerase beta [376]. If several SSBs more than three nucleotides apart are present on opposing strands of DNA, BER can accidently cause a double-strand break. This mechanism is thought to be responsible for the indirect radiation damage through ROS [377].

When a DSB occurs during S or G2 phase the HRR is launched, while during G1 phase NHEJ repair program is initiated. During NHEJ, a sensor repair program is triggered that guides the sensors ATM (ataxia telangiectasia mutated) and MRN (mammalian complex of Mre11-Rad50-Nbs1) to the DSB. To guide repair, microhomologies (short homologous DNA fragments present in single-stranded DNA overhangs at the end of the DSB) are used. After recruitment of the DNA-dependent protein kinase catalytic subunit (DNA-PKcs), processing or end-bridging and ligation is performed. A precise repair can occur only when the overhangs are compatible, otherwise translocations and telomere fusions can occur [376, 378].

For HRR, a complement DNA strand is required as a template. This can be found during S/G2 phase when a sister chromatid is available. ATM and MRN are also recruited to the site of the DSB. The DNA is resected by the endonuclease MRE11, resulting in two 3’-single stranded DNA (ssDNA), that serves as binding sites for Rad51. ATM phosphorylates BRCA1 leading to the recruitment of BRCA2. BRCA2 in return recruits Rad51 that is responsible for the strand exchange with the undamaged chromosome leading to so called Holliday junctions. In this model, the

ssDNA strands first invade and base-pair with the undamaged sister chromatid. The ssDNA strands from the damaged chromatid are then elongated by a DNA polymerase, using the sister chromatids as templates. Once the Holliday junctions are resolved, the gap filling and DNA ligation can be performed [379].

As discussed above, the main target of radiation therapy is DNA. Nevertheless, the so called bystander effect demonstrates that neighbouring unirradiated tissues are also affected by their irradiated neighbour tissue and display chromosomal damage in up to 30% after radiation [380]. It is thought that the bystander effect is mediated through cytokines, for example, tumour necrosis factor, interleukin 8, or reactive oxygen species. A direct cell-to cell contact was not needed, whereas gap-junctions play an important role [381]. The bystander effect has also been observed in vivo: Khan et al reported upper lung damage in rats that had only received radiation to the lower parts of the lung. It is believed that this effect was also mediated by ROS [382].

If a cell experiences lethal radiation and damages can no longer be repaired, different kinds of cell death programs can be triggered.

Mitotic cell death or mitotic catastrophe is the most commonly observed cell death after radiation. It occurs when large DNA lesions lead to the formation of dicentric and acentric DNA fragments or through failure of the mitotic checkpoints. Morphological changes that can be observed are unique nuclear changes, like multinucleation and macronucleation as consequences of chromosomal missegregation. Further micronucleation most likely resulting from the persistence of acentric chromosomes can be observed [217]. The molecules involved in sensing the impaired mitosis and eventually triggering mitotic death are still unclear, but most likely p53 plays a role [383]. The fate of cells experiencing mitotic catastrophe is either mitotic cell death or senescence. However, according to recommendations of the Nomenclature Committee on Cell Death, neither mitotic death nor senescence are considered RCD [217].

During senescence, cells stop proliferation, but remain metabolically active and viable. Morphologically, their cytoplasm flattens, and nuclei enlarge. Further, an intracellular vacuolization and altered chromatin structure can be observed [384]. In the German language we refer to them as “fried eggs, sunny side up”. The molecular steps leading to senescence include the inhibition of multiple cyclin-dependent kinases (CDKs), a dephosphorylation and activation of retinoblastoma (RB) proteins and ARF, and the activation of p53 [385]. As they stay metabolically active, senescent cells may secrete a variety of immunomodulatory and mitogenic cytokines and growth factors. These in return can promote the growth of neighbouring tumour cells [385].

Along with mitotic cell death, radiation can further induce apoptosis. Here changes in mitochondria, followed by caspase activation and MOMP can be observed. Initiation of the apoptotic pathways mainly occurs through direct and indirect DNA damage and p53 activation, which in turn leads to an upregulation of proapoptotic proteins like BAK and BAX, cell death ligands or receptors [366].

8.4 Radiation induced toxicity

Radiation effects can be divided into acute reactions, subacute reactions, and late effects. Acute reactions occur within seconds to days after radiation, while the timing of subacute reactions and late effects is dependent on the dosage per fraction and the total dose administered. The time course and severity of clinical signs and symptoms are a function of the overall body volume irradiated and the radiation intensity [386]. Radiation fast-responding cells are mainly cells that are actively dividing. Epithelial and mucosa cells, stem cells, and haematopoietic cells are examples [386]. Here, as acute radiation induced side-effects, dermatitis, mucositis and neutropenia can be observed.

Besides the radiation intensity and total dosage, patient-specific factors may also influence the degree of toxicity. Such factors include the individually associated therapeutic regimen, nutritional status, and individual genetic background. Patients with Ataxia teleangiectatica, Nijmegen-

Breakage-Syndrome or Fanconi's Anaemia in general have a significantly increased vulnerability to radiation, most likely due to their impairment in DNA repair [387].

Depending on the age of the patient and the treatment site, the long-term side effects may vary. These include cardiomyopathy, neurocognitive sequelae, growth restriction through growth hormone deficiency, infertility, and the development of secondary malignant neoplasms (SMN) [388-392].

The likelihood to develop secondary malignancies is much higher in children than in adults, as the risk remains throughout their entire lifetime. SMNs are best studied in children with Hodgkin's disease and leukaemia. In Hodgkin's disease an overall incidence of up to 25% within 30 years after radiation has been recorded [393], and in women with radiation to the chest, the incidence of developing breast cancer can reach 35% [394].

8.5 Types of radiation devices and radiosensitizing agents

To reduce or to avoid side effects, multiple strategies have been developed. More precise radiotherapy techniques, such as the three-dimensional conformal radiotherapy was first developed in Japan by Shinji Takahashi in the 1960s. With this new technique, a better conformation of the radiation doses to the target, while sparing the surrounding tissue, was achieved [16, 395]. Since then further improvements of these techniques have led to the development and implementation of intensity-modulated radiotherapy (IMRT) and image-guided radiotherapy (IGRT) [396, 397]. IMRT treatment uses a flexible shielding and multiple radiation beams coming from different directions. This allows a precise sculpturing of the radiation beams around the shape of the tumour, and therefore, the high-dose area is confined to the tumour while sparing the surrounding tissue [398].

Proton therapy uses protons instead of photons as the source of radiation to treat malignancies. Due to their large mass, protons have minimal side scatter in the tissue. The penetration range of protons depends on their intrinsic energy and only small amounts penetrate beyond their calculated

range. Furthermore, protons reach a maximum peak dose (Bragg peak) only within the last millimetres of their range, which is localized to the target tissue [17]. Therefore, protons reach maximum effect in the target, which decreases the dose in the surrounding tissue. First studies in children on treatment outcome and treatment related side effects after PT have been promising [18].

In order to increase the efficiency and reduce the side effects of RT, radiosensitizers may be administered simultaneously with the therapy [399]. Radiosensitizing agents are compounds that render cancer cells more vulnerable to radiation therapy. Further radiosensitizing agents are capable of broadening the therapeutic window and selectively augment radiation effects in tumour cells while sparing the surrounding tissue.

According to their chemical structures, radiosensitizers can be classified into three categories, namely, small-molecule chemicals, nanostructures, and macromolecules [19]. A broader approach to explain different ways to combine medication with radiotherapy was proposed by Bentzen et al [400]. They proposed five potential exploitable mechanisms: spatial cooperation, cytotoxic enhancement, biological cooperation, temporal modulation, and normal tissue protection. Through cytotoxic enhancement, the combinatorial treatment "*aims to enhance the cell killing by modulating the induction or repair of cellular DNA damage*" [400].

8.6. Radiation therapy in the treatment of rhabdomyosarcoma

As previously mentioned, radiotherapy is the third pillar of treating children with RMS [401-404]. Depending on the IRS risk group allocation, the timing, duration, and radiation dose administered changes. Due to the dismal prognosis of children with aRMS, they are all allocated to radiotherapy treatment [404].

Since the addition of RT to the treatment regimen in the Intergroup Rhabdomyosarcoma Study I and III, event free survival (EFS) and overall survival have substantially improved. The best improvement was observed in IRS-III when RT was used in conjunction with intensified

chemotherapy [401]. Nevertheless, radiation-induced side effects and toxicity remain a major problem [405]. In an attempt to reduce radiation induced morbidity, the Intergroup Rhabdomyosarcoma Study-IV focused on hyperfractionated radiation to determine if dose escalation would improve outcomes without increasing late side-effects. The study resulted in observing no difference in local or regional control, and a comparison of the late effects was not done [43, 406]. On the contrary, Wolden et al. showed that IMRT in parameningial aRMS resulted in an excellent local tumour control with IRS-comparable acute toxicity rates despite the use of reduced margins [407]. A newer study from Combs et al evaluated the outcome and toxicity profile of IMRT and fractionated stereotactic radiotherapy (FSRT) in children with head-and-neck-rhabdomyosarcoma. They reported excellent outcomes with low incidence of treatment-related side effects. A difference in outcome between aRMS and eRMS was not observed [408].

Since proton beam therapy has become more accessible, it has gained importance in the treatment of aRMS. Dosimetric studies show an enhanced conformity through proton administration and increased sparing of the healthy surrounding tissues [409]. First results from proton therapy in patients with orbital RMS, showed a superior dose conformation to the tumour and a reduced radiation exposure of the adjacent normal structures [410], with the 5-years overall survival rate comparable to that of photon therapy [18].

Although there is ongoing research on new radiosensitizing agents for the treatment of aRMS, up to now no compound is permanently established in the international treatment protocols.

Subject of Investigation

Even though survival rates and outcome of children with cancer has significantly improved over the last 50 years, the current treatment strategies are still accompanied with high toxicity and often low specificity. Further, treatment failure due to resistance development is still a major problem. Hence to improve treatment strategies, agents with less toxicity and more targeted focus have to be found. Many paediatric malignancies harbour genetic aberrations, giving rise to oncogenic transcription factors. ARMS also belong to these group of malignancies with the oncogenic fusion protein PAX3-FOXO1. Being able to directly target these would be highly desirable, but as transcription factors are considered undruggable due to their lack of an enzymatic binding pocket, other strategies have to be exploited. Therefore, a small-compound library screen was previously performed in our laboratory, to find drugs which target the fusion protein without being generally toxic. Here, fenretinide was identified as top hit.

Hence my first aim was to characterize the mode of action of fenretinide in aRMS cells, with a specific focus on its possible interaction with the fusion gene/protein. The second aim was to identify and characterize the induced cell death, since we observed that fenretinide triggered a new and not yet described form of cell death. Finally, we aimed to identify other treatment modalities that work in concert with fenretinide and characterize their combinatorial effect. This work will help to potentially place fenretinide into one of the international treatment trials to augment outcome and decrease treatment-related side-effects in patients with aRMS.

II. Results

Manuscript I & II

Manuscript I

Fenretinide induces a new form of dynamin-dependent cell death in pediatric sarcoma

Eva Brack[1, 2], Marco Wachtel[1, 2], Anja Wolf [1, 2], Beat W. Schäfer[1, 2],

[1] Department of Oncology and [2]Children's Research Center,
University Children's Hospital Zurich, Zurich, Switzerland

Corresponding Author: Beat W. Schäfer
University Children's Hospital Zurich
Steinwiesstrasse 75, 8032 Zurich
Switzerland

Conflict of interest: The authors declare no conflict of interest

Abstract

Alveolar rhabdomyosarcoma (aRMS) is a highly malicious childhood malignancy characterized by a specific chromosomal translocation encoding the oncogenic transcription factor PAX3-FOXO1 and therefore also referred to as fusion-positive RMS (FP-RMS). Previously, we have identified the compound fenretinide (retinoic acid p-hydroxyanilide) from a large drug library screen, to affect both PAX3-FOXO1 expression levels as well as FP-RMS cell viability. Here, we characterized the mode of action of fenretinide in more detail. First, we demonstrate that fenretinide induced the generation of reactive oxygen species (ROS) depending on complex II of the mitochondrial respiratory chain. ROS scavenging as well as complexing of iron ions completely abolished cell death.

To identify the mechanisms of cell death, we co-treated cells with fenretinide and a range of pharmacological inhibitors of specific cell death pathways including Z-VAD (apoptosis), Necrostatin-1 (necroptosis), 3-Methyadenine (3-MA) (autophagy) and Ferrostatin-1 (ferroptosis). Surprisingly, none of these inhibitors was able to prevent cell death. Genetic depletion of key players in the apoptotic and necroptotic pathway (Bak, Bax and RIPK1) with CRISPR/Cas9 confirmed the pharmacological data. Interestingly, electron microscopic examination of fenretinide treated cells revealed an excessive accumulation of cytoplasmic vacuoles which were distinct from autophagosomes. Further flow cytometry and fluorescence microscopy experiments suggested a hyperstimulation of macropinocytosis, leading to an accumulation of enlarged early and late endosomes. Surprisingly, pharmacological inhibition as well as genetic depletion of the large GTPase dynamin completely abolished fenretinide induced vacuolization and subsequent cell death, suggesting a new form of dynamin-dependent programmed cell death.

Taken together, our data identify a new form of cell death mediated through the production of ROS by fenretinide treatment. Hence, this data further underscore the value of fenretinide for treatment of sarcoma patients including FP-RMS.

Introduction

Rhabdomyosarcoma (RMS) is the most common soft tissue malignancy of children and young adolescents accounting for 5-10% of all cancers in this age group [1]. RMS are highly malignant tumors of mesenchymal cell origin and can be subdivided into two major subtypes, of which the alveolar rhabdomyosarcoma (aRMS) is the most unfavorable one [2]. The majority of aRMS are characterized by a tumor-specific chromosomal translocation, giving rise to the chimeric transcription factor PAX3/7-FOXO1 and are therefore referred to as fusion-positive RMS (FP-RMS) [3]. The overall survival rate of patients suffering from this malignancy is poor with less than 30%, and the recurrence rate is high with more than 48%. Further, the remaining 5-year post-relapse survival rate is only about 21% [2, 4]. Resistance of FP-RMS to conventional treatments including chemotherapy and radiation therapy, which mainly lead to induction of apoptosis, is a main cause of failure [5-8]. Hence, one of the major resistance mechanisms is the intrinsic or acquired ability to prevent apoptosis [9].

Importantly, during the last decade a range of non-apoptotic cell death pathways have been described [10], opening the exciting possibility to eliminate cancer cells via alternative routes. Besides apoptosis, regulated necrosis comprising among others necroptosis and ferroptosis are the best studied and understood alternative forms of cell death [11]. A number of agents have been discovered that are capable to reactivate such alternative death pathways in several different cell types [12-17] and therefore have an anti-neoplastic action.

Several types of cell death are associated with accumulation of cytoplasmic vesicles including methuosis, paraptosis or oncosis [18-25]. Methuosis is a rather new form of cell death and is characterized by an accumulation of phase lucent vesicles generated by increased macropinocytosis. This type of cell death is widely investigated in several types of cancers and can be induced through multiple compounds such as vacuolin-1 [18-21]. However, a cell death mode characterized by accumulation of vacuoles has not yet been reported for FP-RMS.

To explore alternative forms of cell death in FP-RMS, we previously screened a library of 1280 mostly FDA approved compounds using PAX3-FOXO1 activity as read-out [26]. From this screen, we identified fenretinide (retinoic acid p-hydroxyanilide) as the most effective small-molecule compound. Importantly, fenretinide treatment also induced a strong reduction of FP-RMS tumor growth in mouse xenograft experiments.

Here we describe the detailed mechanism of cell death provoked by fenretinide treatment in FP-RMS cells. Fenretinide activated a novel form of non-apoptotic cell death which was associated with extensive accumulation of cytoplasmic vesicles [18, 27]. Strikingly, this novel cell death mechanism is pharmacologically and genetically dependent on the function of the GTPase dynamin which controls endocytosis. These findings, together with a long experience of fenretinide treatment in clinics for the treatment of multiple malignancies, rejuvenate the application of this drug in FP-RMS.

Results

We previously demonstrated that fenretinide-induced cell death is associated with a reduction in PAX3-FOXO1 levels in FP-RMS cells [26]. Since expression of PAX3-FOXO1 is essential for survival [28], we first explored whether the effect of fenretinide is dependent of fusion protein depletion. For this, we used a doxycycline inducible lentiviral shRNA vector system directed against endogenous PAX3-FOXO1 together with a CMV-promoter driven vector for expression of an shRNA-insensitive variant of PAX3-FOXO1 (P3F mut) in Rh4 cells (Supplementary Figure 1A). Upon induction of shRNA, endogenous P3F protein levels were reduced to about 20 percent, while levels of ectopic PAX3-FOXO1 matched the ones of the endogenous protein (Supplementary Figure 1B). As expected, treatment of these cells with fenretinide did not induce a decrease in exogenous PAX3-FOXO1 protein levels, demonstrating that they are not regulated at the post-translational level. Furthermore, ectopic expression of PAX3-FOXO1 reduced the levels of cleaved PARP, suggesting that it indeed can rescue cells from apoptosis. Unexpectedly and most importantly however, ectopic PAX3-FOXO1 did not protect from fenretinide induced cell death as measured by WST assay and by Western blot (Figure 1A). Taken together, these results suggest that induction of apoptosis after fenretinide treatment is linked to a reduction in PAX3-FOXO1 levels, while under conditions of sustained PAX3-FOXO1 expression fenretinide might induce an alternative mode of cell death.

To further explore this hypothesis, we next studied different well characterized cell death pathways to evaluate their relevance for fenretinide mediated cytotoxicity using a pharmacological approach. We treated two FP-RMS cell lines (Rh4 and Rh30) with fenretinide in combination with the apoptosis inhibitor Z-VAD, the necroptosis inhibitor Necrostatin (NS1), the autophagy inhibitor 3-Methyadenine (3-MA), the ferroptosis inhibitor Ferrostatin-1 (FS) and the iron chelator Deferoxamin (DFO) [29, 30] and assessed cell viability after 48h. Surprisingly, none of the

specific cell-death inhibitors was able to rescue from cell death (Figure 1B), suggesting that neither induction of apoptosis, necroptosis, ferroptosis or autophagy play a major role in fenretinide induced cell death. Interestingly however, the iron chelator DFO almost completely rescued cell viability. While both FS and DFO act as reactive oxygen species (ROS) scavengers, FS is lipid-soluble and claimed to protect from membrane lipid-peroxidation during ferroptosis, while DFO has a broader ROS-protecting activity, suggesting that more broadly produced ROS species might play an important role.

Since pharmacological inhibition is prone to certain off-target effects, we aimed next to confirm these results using a genetic approach. We used the CRISPR/Cas9 system in both cell lines to knockout essential apoptotic/necroptotic pathway genes to create death pathway ablated tumour cells. To block apoptosis, we combined sgRNAs directed against BAK and BAX, two key players in the intrinsic apoptotic pathway, and to inhibit necroptosis we used sgRNAs directed against RIPK1, the central kinase in the necroptotic pathway. We achieved nearly complete knockouts for BAK and BAX and a significant reduction of RIPK1 as determined by Western Blot (Supplementary Figure 1C). In parallel, we also combined the different sgRNAs and depleted all three genes in one single cell population. All knockout cells were then treated with fenretinide. In Rh4 cells, combined knockout of BAX and BAK resulted in a nearly complete inhibition of Caspase-7 and PARP-1 cleavage, while in Rh30 cells both PARP-1 and Caspase-9 cleavage were less affected by the genetic manipulations, suggesting that other apoptotic pathways are (also) involved. Similar results were seen for the triple-knockouts of BAK/BAX/RIPK1 (Figure 1C). Interestingly, we found that Rh4 cells do not express Caspase-8, while Rh30 cells do (Supplementary Figure 1D) which might explain the difference in apoptotic downstream effects between the two cell lines. Next, we determined dose-response curves with all knockout cells after treatment with fenretinide. In agreement with the pharmacological approach, we observed only a very small, non-significant rescue from cell death in deleted versus wild-type cells, which was

slightly more pronounced in the triple knockout cells (Figure 1D) and in Rh30 cells compared to Rh4 cells. Nevertheless, these results suggest that while fenretinide engages some apoptotic features including caspase activation, cells execute mainly an alternative death pathway if apoptosis is blocked.

Based on the ability of the ROS inhibitor DFO to rescue FP-RMS cells from fenretinide-induced cell death, we wondered whether and what kind of ROS might be induced and whether these would be responsible for induction of cell death.

First, we confirmed ROS accumulation after 20hrs of fenretinide treatment with the fluorogenic pan-ROS probe CellRox by observing a strong perinuclear accumulation in the treated compared to control cells (Figure 2A). To evaluate the kinetics of ROS accumulation, we captured time lapse fluorescence microscopy images of fenretinide treated and untreated Rh4 cells stained with CellRox (Supplementary Figure 2A). This revealed that cells stained positive for ROS already 20hrs after fenretinide treatment, and started to detach and undergo cell death 6hrs later, demonstrating that ROS production precedes initiation of cell death. Similar time lapse experiments with BAK/BAX/Rip1 knock out cells and propidium iodide (PI) as marker for cell death showed that knock-outs delay onset of cell death for about 10 hours (Supplementary Figure 2A), validating that fenretinide is able to initiate apoptosis, but cells undergo a different mode of cell death if apoptosis is blocked.

To quantify induced ROS, we measured CellRox fluorescence after 18hrs of fenretinide treatment by flow cytometry (Figure 2B). This analysis showed that ROS levels increased by about 2.5-fold. Staining of cells with a mitochondria specific ROS probe (MitoSox) revealed a similar increase of about three-fold (Figure 2B), suggesting that at least a part of fenretinide-induced ROS species originate from mitochondria.

To determine the relevance of ROS for induction of cell death, we used different ROS inhibitors including the antioxidant Vitamin C, DFO, FS and the mitochondria-specific ROS scavenger MitoTempo. The extent of reduction in ROS levels differed between the different inhibitors, with DFO and MitoTempo reducing ROS levels below 50 percent, while Vitamin C and FS were considerably less effective (Figure 2C and D and Supplementary Figure 2B). In agreement with these scavenging potencies, similar to DFO (Figure 1B) also MitoTempo was able to completely inhibit fenretinide induced cell death (Figure 2D), while Vitamin C and FS had only minor effects. Taken together, these findings suggest that fenretinide induces mitochondrial ROS generation which are involved in the induction of cell death.

One of the major sources of ROS production is the mitochondrial respiratory chain (MRC). As the MRC is the major source of ATP production in the cell, any interference is fatal for the tumour cell and reduces the mitochondrial membrane potential ($\Delta\psi m$). Hence, we next evaluated whether the mitochondrial ROS induced by fenretinide are produced by one of the MRC complexes. We co-treated Rh4 cells with fenretinide and different inhibitors targeting the five complexes of the MRC and measured the amount of produced ROS. Inhibitors against complex I (Rotenone), III (Antimycin), IV (Sodium Azid) and V (CCCP) did not cause a decrease in ROS levels (Supplementary Figure 3A). Instead, inhibitors of complex II, namely TTFA and Carboxin significantly reduced ROS production in both Rh4 and Rh30 cells (Figure 3A and B). These findings indicate that the main target of fenretinide for ROS production lies downstream of complex II of the MRC.

To further characterize fenretinide induced cell death, we next investigated morphological changes at the ultrastructural level using electron microscopy (EM). For this, we treated Rh4 and Rh30 cells with fenretinide in combination with Z-VAD for 48hrs (Figure 4A). Interestingly, this

analysis revealed that fenretinide induced an enormous vacuolization within the cytoplasm which was even further enhanced in combination with Z-VAD. The vacuoles had different sizes, were phase lucent and contained only one single membrane, suggesting that they do not represent autophagosomes. In contrast, features of apoptosis were only rarely detected, most pronounced with a combination of fenretinide and Necrostatin (data not shown), whereas we could readily identify chromatin condensation and membrane blebbing after treatment with the PLK1 inhibitor Volasertib, which is known to induce apoptosis in RMS cells [31] (Supplementary Figure 4A). These findings further strengthen our hypothesis that fenretinide is able to trigger multiple types of cell death.

The observed features of the phase lucent vesicles were consistent with macropinosomes and reminiscent of cell death forms which are associated with accumulation of endosomes [18, 27]. We therefore wondered whether fenretinide induced cell death involves disturbance of macropinocytosis or endocytosis. To study macropinocytosis, we followed the uptake of fluid phase dyes like Acridine Orange and Lucifer Yellow [21] by flow cytometric analysis. Fenretinide indeed induced the uptake of Acridine Orange and Lucifer Yellow (>4fold increase, Figure 4B and Supplementary Figure 4B and 4C). Co-treatment with the ROS scavengers Vitamin C and MitoTempo almost completely abolished this uptake, indicating that the fenretinide induced increase in dye uptake is downstream of ROS induction and mediated through macropinocytosis. Addition of Z-VAD to fenretinide treated cells did not further enhance this effect. Validation of these results by fluorescent microscopy after 48hrs of fenretinide treatment confirmed the strong increase in Lucifer Yellow uptake (Figure 4C). Hence, these findings are in accordance with the EM images and suggest that the observed vesicles derive from an increased accumulation of endosomes, similar to the ones described for other cytoplasmic vacuolization associated cell death forms [18, 27, 32].

To further characterize the endosomal origin of the vesicles, we stained fenretinide treated cells with antibodies directed against the early endosomal marker Rab5, the late endosomal marker Rab7, and the lysosomal marker LAMP-1. Compared to untreated control, an accumulation of early and late endosomes but not of lysosomes was observed (Figure 5A and 5B). Interestingly, even though the vesicles are acidic enough to allow Acridine Orange emission to change from green to red (Figure 4B, 5C Supplementary Figure 4B, 5C), they are unable to further mature and fuse with lysosomes, indicating that later maturation steps are blocked.

Based on this, we next aimed to further substantiate the relevance of disturbed endocytosis for fenretinide induced cell death. We blocked the different endocytosis processes by chemical compounds and measured cell viability. Neither inhibition of macropinocytosis by EIPA, clathrin-independent endocytosis by Filipin and Genistein nor clathrin-mediated endocytosis by Chlorpromazin influenced cell viability upon fenretinide treatment (Supplementary Figure 5A). Interestingly however, the Dynamin inhibitors dynasore and dyngo-4a nearly completely rescued from cell death (Figure 5C and 5D and Supplementary Figure 5B), both at the physiological (Figure 5C) and the morphological level (Figure 5D). Moreover, we also observed a significant inhibition of Acridine Orange uptake by co-treatment with dynasore (Figure 5E and Supplementary Figure 5 C).

To exclude, that dynasore acts via ROS scavenging, we co-treated Rh4 and Rh30 cells for 48hrs and measured mitochondrial ROS by flow cytometry. In Rh4 cells ROS levels were unaffected by dynasore, while we measured an almost 50 percent reduction in ROS levels in Rh30 cells (Supplementary Figure 5D), suggesting that dynasore does not generally act as ROS scavenger and the reduction of ROS levels in Rh30 cells might occur indirectly.

To evaluate whether dynasore specifically rescued fenretinide mediated cell death, we screened a small molecule library with 204 mostly FDA-approved drugs in Rh4 cells alone and in combination with dynasore or Vitamin C and assessed cell viability (Supplementary Figure 5E).

Within the top cytotoxic drugs (reducing viability to 10-50%), we identified 12 drugs that exerted a ROS dependent cytotoxic effect (cell viability change >25%), including MLN2238, MLN9708, Rigosertib, Verdinexor, BI-847325, Ponatinib, MK-1775, VX-680, Doxorubicin, Ispinesib, Elesclomol and OTX015. In none of these cases however, dynasore could significantly enhance survival, indicating that dynasore acts specifically on fenretinide induced cell death and not simply as ROS scavenger.

In order to validate the involvement of the GTPase Dynamin in fenretinide induced accumulation of endosomes, we used the CRISPR/Cas 9 system to knock-out Dynamin-1 and -2 in both Rh4 and Rh30 cells. As determined by Western Blot analysis, the knock out in Rh4 cells was nearly complete for both Dynamins, while knock-out efficiency was reduced in Rh30 cells (Supplementary Figure 6A). Examining the uptake of Acridine Orange after fenretinide treatment into the Dynamin knock-out cells revealed a significant lower uptake compared to scrambled control cells (Figure 6A and F and Supplementary Figure 6B and C), demonstrating significant reduction of endocytic processes in knockout cells. Importantly, upon treatment of these knockout cells with different concentrations of fenretinide we also detected a significant rescue from cell death using a cell viability assay (Figure 6B, Supplementary Figure 6D). Rescue was further confirmed by phase contrast images (Figure 6C). Taken together these findings indicate that the vesicle accumulation during fenretinide treatment is directly dependent on the Dynamin GTPases. Furthermore, these results suggest that the accumulation of the endosomes is causally and directly linked to cell death.

Discussion

One of the biggest therapeutic challenges in FP-RMS treatment is intrinsic or acquired resistance towards conventional therapies, which is the main cause for the high recurrence rates of this type of tumor. Since survival rates of patients with relapsed FP-RMS are still very poor [4], there is an urgent need to identify new agents that are effective against such resistant cells. Drugs that re-sensitize cells towards chemotherapy induced apoptosis as well as compounds that activate alternative, non-apoptotic cell death pathways represent potential opportunities in this context [33, 34].

Here, we characterized the cytotoxic effect of fenretinide on FP-RMS cells. Originally, fenretinide was detected as hit in a large compound library screen designed to identify drugs affecting PAX3-FOXO1 activity [26]. While fenretinide indeed affects PAX3-FOXO1 transcript levels, the more detailed characterization of the mechanism of action performed in this study suggests that its cytotoxic effects in FP-RMS cells do not depend on reduction of PAX3-FOXO1 levels and therefore this effect might be a more downstream event following induction of cell death. Interestingly, fenretinide induced cell death was found to include a mechanism other than apoptosis, necroptosis, autophagy and ferroptosis, as neither commonly used inhibitors directed against these pathways nor their genetic ablation of key molecules had a positive influence on survival of cells after fenretinide treatment. In contrast, inhibition of ROS completely protected FP-RMS cells from fenretinide mediated toxicity, as already described in other cellular systems [35-38]. While it is not clear at this point how fenretinide treatment leads to ROS induction, our study clearly demonstrates that ROS originating from the mitochondria plays an important and early role in fenretinide mediated cell death in FP-RMS cells. Downstream of ROS, fenretinide induces the formation and accumulation of cytoplasmic vesicles. These vesicles are surrounded by a single membrane and therefore do not originate from the autophagy pathway which gives rise to double membrane autophagosomes. Instead, the vesicles morphologically resembled endosomes,

an interpretation which was further substantiated by fluid phase dye uptake studies showing strong enhancement of these processes by fenretinide. Furthermore, pharmacologic as well as genetic interference with Dynamins blocked vesicle accumulation and rescued from fenretinide induced cell death. The Dynamin family of GTPases are major mediators of endosome fission at the plasma membrane. They are involved in both clathrin-dependent and -independent endocytosis, but some evidence suggests that they also play a role in a specific macropinocytosis pathway involving circular dorsal ruffles (CDR) [39, 40] We found that inhibitors of clathrin and caveolin-mediated endocytosis like Chlorpromazin, Filipin und Genistein failed to block fenretinide mediated cell death. Furthermore, ultrastructural analysis by EM showed that fenretinide induced vesicles have a variable size with a dimeter of up to 7 μm, which is comparable to the described diameter of macropinosomes of 0.2 to 5 μm [19]. Taken together, these data indicate that these vesicles most likely derive through an increased or impaired macropinocytosis.

Interestingly, blocking of Caspase activity by Z-VAD further enhanced the number of vesicles in presence of fenretinide. Hence, a part of the cells might succumb by an apoptotic mechanism but shift the mode of cell death cell when this route is blocked. This is in accordance with a delay in the onset of cell death in presence of Z-VAD by about 10 hours as seen in our time lapse experiments. When compared to other cell death mechanisms, apoptosis has been shown to be a relatively fast process [41, 42]. Accordingly, non-apoptotic regulated modes of cell death such as necroptosis have only been detected after specific inhibitors of apoptosis became available [43, 44].

For induction of this vesicle associated type of cell death in FP-RMS cells a special type of ROS stress seems to be relevant, since induction of ROS-dependent cell death with other drugs including the proteasome inhibitors MLN2238 and MLN9708, the microtubule-destabilizing agent Rigosertib or the tyrosine-kinase inhibitor Bosutinib were not blocked by Dynamin inhibitors. The mechanisms behind this difference needs further clarification in the future.

The role of reactive oxygen species as important regulators of tyrosine kinase receptor signalling cascades [45-48], might be another possible explanation to the formation of CDRs after fenretinide treatment.

Importantly, similar cellular phenotypes have been described in the context of different relatively vaguely described cell death mechanisms called paraptosis, oncosis and methuosis [25, 27, 32]. In case of methuosis vesicle accumulation has been associated with disturbance of endosomal maturation and/or recycling. Several different stimuli have been described that induce this phenotype. These include different small molecules with less understood links to macropinocytosis as well as activation of Ras, which stimulates marcopinosmome formation via over-activation of Rac1 and concomitant decline in Arf6 and at the same time impedes their recycling (for review see Maltese et al [18]). Ultimately, this manifests as vesicle accumulation as seen in different cells like glioblastoma, Ewing sarcoma and epithelial cells [21, 27, 49]. Whether Ras mutant tumors compensate this effect and are less prone for methuosis is currently unclear. FP-RMS tumors anyway are not associated with Ras mutations. Similar to methuosis, we observed an impaired recycling of endosomes with a maturation stop at the level of early/late endosome formation, as the vesicles acquire markers such as Rab5 and Rab7 but not the lysosomal marker LAMP-1. However, since pharmacological inhibition and knock-out of Rac1 as well as Arf6 in FP-RMS cells neither affected fenretinide mediated cell death nor dye uptake (data not shown), this pathway does not seem to play a role in these cells. Hence, while the exact mechanism leading to the maturation stop of the endosomes in FP-RMS cells needs further characterization, it seems that different upstream pathways might be able to induce the same vacuolization phenotype associated with cell death. Importantly however, while in all the described cases vesicle accumulation and cell death correlate, a causal link of the two effects has not been established yet.

Overall our results provide evidence that fenretinide induced mitochondrial ROS interferes with regulation of Dynamin-dependent macropinocytosis leading to vesicle accumulation in the

cytoplasm of the cells. This is associated with strong cytotoxic effect in FP-RMS cells. The fact that fenretinide engages a novel form of cell death which is not exploited by conventional chemotherapy agents defines it as a promising combinatorial partner for the treatment of FP-RMS patients. Agents for a potential combination treatment might be drugs that induce canonical apoptosis or necroptosis or even other forms of cell death like autophagy or ferroptosis. Since fenretinide is already in clinical use in children (Clinicaltrials.gov ID NCT02163356) and has only moderate side-effects both in short and long term treatment regimens [50, 51] our findings might stimulate expansion of the clinical application of fenretinide to FP-RMS therapy in the future.

Material and Methods

Cell culture

The alveolar rhabdomyosarcoma cell lines RH4 and Rh30 (provided by Peter Houghton, Greehey Children's Cancer Research Institute, San Antonio, Texas, USA) and the HEK293T (ATCC, LGC Promochem, Wesel, Germany) were maintained in Dulbecco's Modified Eagle Medium (DMEM, Sigma-Aldrich-Aldrich, Buchs, Switzerland), with 100 U/mL penicillin/streptomycin (Invitrogen, ThermoFisher, Waltham, Massachusetts, USA), 2 mM L-glutamine ((BioConcept, Allschwil, Switzerland) or Glutamax (Gibco, ThermoFisher, Waltham, Massachusetts, USA) and 10% fetal bovine serum (FBS) (Sigma-Aldrich-Aldrich, Buchs, Switzerland), in 5% CO2 at 37°C. ARMS cell lines were regularly tested for Mycoplasma infection, authenticated by short tandem repeat analysis (STR profiling) in 2011/2014 and positively matched with reference data [52].

Cell proliferation assay

Cells were seeded at a concentration of 150'000 cells/ml (Rh4) or 100'000 cells/ml (Rh30) in 384 well polystyrol microplates (Greiner Bio One, Kremsmünster, Austria) format in 20µL medium. For determination of dose response curves with single compounds (see Table 1 in Supplementary Material and Methods), drugs were added to the cells using a HP D300 digital dispenser (Hewlett-Packard Development Company, L.P., Houston, Texas, USA).

To assess metabolic activity 10µL colorimetric water-soluble tetrazolium (WST-1) (Sigma-Aldrich-Aldrich, Buchs, Switzerland), diluted 1:1 with DMEM, was added. After 30 minutes of incubation at 37°C in the dark, absorbance at 440 and 640 nm were measured with a Synergy™ HT multi-detection microplate reader (BioTek, Winooski, Vermont, USA). The difference of the two values was calculated (delta optical density; ΔOD) and values from pure medium were subtracted as background.

Small molecule library screen

Cells were seeded at a concentration of 150’000 cells/ml (Rh4) or 100’000 cells/ml (Rh30) in 384 well polystyrol microplates (Greiner Bio One, Kremsmünster, Austria) format in 20µL medium. Drugs were diluted to a final concentration of 500nM and manually added in duplicates to the cells (see Table 5 in the Appendix), 12 DMSO controls were included. After 48 hours treatment, effects of drugs were determined by cell viability assay.

Flow Cytometry

For all Flow Cytometry experiments, 150000 cells/ml (Rh4) or 100000 cells/ml (Rh30) were seeded in Corning Costar 6-well plates (Sigma-Aldrich-Aldrich, Buchs, Switzerland). After treatments, cells were detached from the plates using Trypsin, washed once with PBS and re-suspended in 0.5 ml indicated buffer. Data was acquired with the LSRII Fortessa (BD Biosciences, San Jose, California, USA) flow cytometer or the BD FACS Canto system (BD Biosciences, San Jose, California, USA).

The data was analysed with FlowJo Software, Version 9.9.6 (Tree Star Inc., Ashland, Orlando, USA). The used fluorescent stains can be found in Table 2 in Supplementary Material and Methods.

Pan ROS measurement

Cells were seeded and treated with compounds according to table 1 in Supplementary Material and Methods for 20-48 hours. At the same time, CellROX Deep red (ThermoFisher, Waltham, Massachusetts, USA) solution (4µM) was added to the media. Cells were collected, washed in PBS (Sigma-Aldrich-Aldrich, Buchs, Switzerland) and resuspended in FluoroBrite DMEM live cell fluorescence imaging medium (ThermoFisher, Waltham, Massachusetts, USA). CellRox

(ThermoFisher, Waltham, Massachusetts, USA) signal (50’000 events per sample) was acquired with Excitation laser 640 nm and Emission filter 670/14.

Mitochondrial ROS measurement

Cells were seeded and treated with the desired compounds according to table 1 in Supplementary Material and Methods for 20-48 hours. Cells were collected, washed in PBS and resuspended in MitoSox (ThermoFisher, Waltham, Massachusetts, USA) Solution (10µM MitoSox in PBS) for 30min at 37°C in the dark. MitoSox signal (50’000 events per sample) was acquired with Excitation laser 561 nm, and Emission filter 570 LP, 525/50.

Acridine Orange (AO) and Lucifer Yellow (LY) Uptake

Cells were seeded and treated with compounds according to Table 1 in Supplementary Material and Methods for 48 hours. Acridine Orange (2.7 µM, Sigma-Aldrich-Aldrich, Buchs, Switzerland) and Lucifer Yellow (820 µM, ThermoFisher, Waltham, Massachusetts, USA) in FluoroBrite DMEM live cell fluorescence imaging medium (ThermoFisher, Waltham, Massachusetts, USA) was added to the cells 4 h prior to their preparation for flow cytometry after removal of the culture medium. Cells were collected, washed in PBS and resuspended in PBS. Signals (50’000 events per sample) were acquired with Excitation laser 488 nm and 561, Emission filter 505 LP, 530/30 and 635LP, 670/30 for AO and with Excitation laser 405nm, Emission laser 505LP, 525/50 for LY.

Epifluorescence microscopy

All images were taken with the Zeiss Axio Observer (Zeiss, Oberkochen, Germany) equipped with the Hamamatsu Orca Flash 4.0 V2, sCMOS, (Hamamatsu, Hamamatsu City, Japan) cooled fluorescence camera and an objective with 20x magnification. The violet and green fluorescent

filters were used for the imaging of DAPI, Lucifer Yellow, Rab5/7 and Lamp1 stained structures, respectively. Fluorescent stains are listed in Table 2 in Supplementary Material and Methods.
For Data Processing, the images were exported as TIFF files and the mean integrated density was quantified with the image processing program Fiji [53]. The integrated density value of an image was divided by the number of cells (counted on the phase image). A minimum of four pictures were taken for each treatment.

Rab 5, Rab7 and Lamp-1 immunofluorescence staining

50000 cells/ml were seeded in 4 well-Falcon™ chambered cell culture slides (Thermo Scientific, ThermoFisher, Waltham, Massachusetts, USA) and treated with 3µM fenretinide for 48 h. After washing, cells were fixed with 4 % paraformaldehyde (PFA) (CarlRoth, Karlsruhe, Germany) washed and quenched with 0.1 M Glycin (Sigma-Aldrich-Aldrich, Buchs, Switzerland) in PBS. After fixing, cells were permeabilized with 0.1% Triton X-100 (Sigma-Aldrich-Aldrich, Buchs, Switzerland) in PBS and then blocked with 4% horse serum (Sigma-Aldrich-Aldrich, Buchs, Switzerland) in 0.1% Triton X-100/PBS before they were incubated with the respective primary antibody in 0.1% Triton X-100 in PBS and 4% horse serum at 4°C overnight in a humid chamber. Primary Antibodies used for immunofluorescence localization of rabbit anti-Rab 5 (Cat #2143) and rabbit anti-Rab 7(Cat #9367) were obtained from Cell Signaling Technology (Danvers, Massachusetts, USA) and mouse anti-LAMP1 was obtained from the Developmental Studies Hybridoma Bank (University of Iowa, Ames, Iowa, USA) respectively. After three washing steps, cells were incubated with donkey anti-rabbit IgG-Alexa 488 (Rab 5/7) or chicken anti-mouse IgG-Alexa 488 (Lamp1) 2° Antibody (1:200) (both from ThermoFisher, Waltham, Massachusetts, USA) in PBS with 4% horse serum for 1 hour at RT. After washing, the chamber walls were removed and Vectashield mounting medium with 4′, 6-Diamidin-2-phenylindol (Vector Laboratories, Burlingame, California, USA) was added.

Live cell time-lapse microscopy

80000cells were seeded in 400µl of a 8-well 15u- Ibidi chambered cell culture slide (Ibidi GmbH, Planegg, Germany) and treated with or without 3µM fenretinide and different stains in FluoroBrite DMEM with 10% FBS and 1% Pen/Strep and Glutamin. CellRox (4µM) was used for panROS detection, propidium iodide (1µg/ml) (Sigma-Aldrich-Aldrich, Buchs, Switzerland) was used for detection of dead cells. For time lapse image acquisition, the slides were kept in a thermally stabilized and CO2 controlled chamber incubator (5% CO2 at 37 °C) (Ibidi GmbH, Planegg, Germany) and images were automatically taken every 20 min over a 60 hours period.

LY fluorescence microscopy

50000 cells were seeded per well of a 4-well Falcon™ chamber slide and treated with 3/4µM (for Rh4/Rh30) fenretinide for 48h and subsequently stained with Lucifer Yellow (820µM) in FluoroBrite DMEM for 4 h at 37°C, 5% CO2. Afterwards, cells were washed with PBS and fixed with 4 % PFA for 15 min at room temperature. After three PBS washes, the chamber was removed and the cells were mounted in Vectashield mounting medium with 4′, 6-Diamidin-2-phenylindol.

Electron microscopy

300000 (Rh4) or 200000 cells (Rh30) cells were seeded per well of a Corning Costar 6-well plate (Sigma-Aldrich-Aldrich, Buchs, Switzerland) and treated with 3 or 5µM fenretinide in combination with either 100µM Z-VAD-FMK, 30µM dynasore, 25µM Necrostatin or 0.0065µM Volasertib for 48h at 37°C, 5% CO2. Treated and untreated control cells were then fixed with 2.5 % glutaraldehyde (EMS Electron Microscopy Sciences, Hatfield, Pennsylvania, USA) in 0.1 M cacodylate buffer (pH 7.35) (Merck AG, Zug, Switzerland) for at least on hour. Adherent cells were scraped off the culture dish using a cell scraper, combined with floating cells, pelleted by centrifugation and sequentially treated with 1% OsO4 in 0.1 M cacodylate buffer for 1 hour at 0°C

and 2% uranyl acetate (Merck AG, Zug, Switzerland) in H2O overnight at 4°C. The final pellet was immobilized with 2% of Difco Noble Agar (BD Biosciences, Allschwil, Switzerland) in H2O, subsequently dehydrated in an ethanol absolute series (VWR International GmbH, Dietikon, Switzerland) and embedded in Epon/Araldite (Sigma-Aldrich-Aldrich, Buchs, Switzerland). Ultrathin (50 nm) sections were contrasted with uranyl acetate and examined with a CM100 transmission electron microscope (Thermo Fisher Scientific, Eindhoven, The Netherlands) at an acceleration voltage of 80 kV using an Orius 1000 digital camera (Gatan, Munich, Germany), or a Talos 120 transmission electron microscope at an acceleration voltage of 120 KV using a Ceta digital camera and the MAPS software package (Thermo Fisher Scientific, Eindhoven, The Netherlands).

Immunoblotting

Whole cell extracts were prepared from cells lysed with RIPA buffer (50 mM Tris-Cl (pH 7.5), 150 mM NaCl, 1% NP-40, 0.5% Na-deoxycholate, 1 mM EGTA, 0.1% SDS, 50 mM NaF, 10 mM sodium β-glycerolphosphate, 5 mM sodium pyrophosphate, 1 mM sodium orthovanadate and supplemented with Complete Mini Protease Inhibitor cocktail (all from Sigma Aldrich, Buchs, Switzerland). Proteins were separated using NuPAGE™ Novex™ 4-12% Bis-Tris gels (ThermoFisher, Waltham, Massachusetts, USA) and transferred to nitrocellulose membranes (GE Healthcare Life Sciences). Membranes were blocked with 5% milk powder in TBS/0.05% Tween and subsequently incubated with respective primary antibodies overnight at 4°C. After three time washing in TBS-0.05% tween, membranes were incubated with horseradish peroxidase (HRP)-linked secondary antibody for 1h at RT. After three additional washing steps with TBS/0.05% Tween, proteins were detected by chemiluminescence using either the Pierce™ ECL Western Blotting Substrate or Supersignal Western blotting reagent (both ThermoFisher, Waltham, Massachusetts, USA) and a ChemiDoc MP (BioRad Laboratories AG, Cressier, Switzerland) or

Fujifilm LAS-3000 (Biocompare, San Francisco, USA) imager. The images were analyzed with the software Image Lab Version 6.0. (BioRad Laboratories AG, Cressier, Switzerland). All used antibodies used are listed in table 3 in Supplementary Material and Methods.

CRISPR/Cas9-mediated knockout

Multi-coloured lentiCRISPR plasmids with EGFP (Addgene Cat #75159), TagBFP (Addgene Cat #75160) or mCherry (Addgene Cat #75161) fluorescent markers were kindly provided by Scott McComb. The sgRNAs sequences were designed on http://crispr.mit.edu (accessed on 9.2.2017) and ordered as complementary oligos from Microsynth AG (Balgach, Switzerland) (for sgRNA sequences see Table 4 Supplementary Material and Methods). 100µM complementary oligos were annealed in Tango Buffer (ThermoFisher, Waltham, Massachusetts, USA) by heating for 5 min to 95°C, followed by a slow cool down over 1 hour to RT. Vectors, annealed sgRNA oligos, (ThermoFisher, Waltham, Massachusetts, USA), Esp3I (BsmBI) (ThermoFisher, Waltham, Massachusetts, USA) and T4 ligase (ThermoFisher, Waltham, Massachusetts, USA) were combined in T4 Ligase buffer and the following reaction was run on a T3000 thermocycler (Biometra, Biocompare, San Francisco, USA): 10 cycles of 37°C for 5 minutes and 16°C for 10 minutes for restriction and ligation, respectively. 4µl of the ligation reaction was then used to transform StellarTM competent bacteria (Clontech, Takara, Saint-Germain-en-Laye, France) by heat shock at 42°C for 45 sec (Clontech, Takara, Saint-Germain-en-Laye, France). Colony PCR using RedTaq PCR mixture (Sigma-Aldrich-Aldrich, Buchs, Switzerland) and sgRNA specific primers was performed to identify positive clones. For the production of lentiviral particles, 293T cells were transfected with the LentiCRISPR plasmid together with pVSV.G (Addgene Cat# 8454) and pPAX (Addgene Cat# 12260) plasmids in a ratio of 2.6:1:1 using either polyethylenimine (Polysciences, Warrington Township Pennsylvania, USA) or calcium phosphate (Sigma-Aldrich-Aldrich, Buchs, Switzerland). Medium was changed after 4 hours, and virus was harvested 48

hours later. Viral supernatants were concentrated using Amicon Ultra tube Ultracel 100k (Millipore, Merck, Schaffhausen, Switzerland). For transduction of target cells, viral particles and 16µg/ml hexadimethrine bromide (Sigma-Aldrich-Aldrich, Buchs, Switzerland) were added to culture medium and left over night on the cells. 72 hours later, transduction efficiency was evaluated by flow cytometry, and positive cells were isolated by FACS sorting with a BD Aria III 4L (BD Biosciences, San Jose, California, USA). Several different sgRNAs per target gene were evaluated individually for their knock-out efficiency and the two most efficient ones were selected for further experiments.

ShRNA-mediated knockout

Custom lentiviral shRNA constructs containing a U6-tet promoter driven shRNA (scrambled (sc) or directed against PAX3/FOXO1 (target sequence: GGCCTCTCACCTCAGAATTCA)) as well as a PGK promoter driven GFP and puromycine expression cassette were purchased from Cellecta (Cellecta Inc. Mountain View, California, USA). For constitutive expression of PAX3-FOXO1, the cDNA was cloned into the multiple cloning site (NheI) following the EF1 promoter in the lentiviral plasmid pRR-CMV-Bleo-EF1-MCS (Cellecta) also carrying a Bleomycin resistance under a CMV promoter. Generation of lentiviral particles in HEK293T cells and transduction of the target cells was performed as described above for the CRISPR/Cas9 knock-outs.

Statistical analysis

The software GraphPad Prism (La Jolla, California, USA) was used for all statistical analysis (parametric paired t-test). The data were considered significant when $p \leq 0.05$.

Acknowledgements

We thank Andres Kaech and Urs Ziegler at The Center for Microscopy and Image Analysis Zurich for their excellent service and support. We also thank Silvia Jenni, Gloria Pedot and Luca Pontiggia (University Children's Hospital Zurich) for assistance with the cell sorting.

This work was supported by the Krebsliga Zurich.

Conflict of interest

The authors declare that they have no conflict of interest.

References

1. Brien D, Jacob AG, Qualman SJ,Chandler DS, Advances in pediatric rhabdomyosarcoma characterization and disease model development. Histol Histopathol, 2012; 27: 13-22.

2. Williamson D, Missiaglia E, de Reynies A, Pierron G, Thuille B, Palenzuela G, et al., Fusion gene-negative alveolar rhabdomyosarcoma is clinically and molecularly indistinguishable from embryonal rhabdomyosarcoma. J Clin Oncol, 2010; 28: 2151-8.

3. Barr FG, Gene fusions involving PAX and FOX family members in alveolar rhabdomyosarcoma. Oncogene, 2001; 20: 5736-46.

4. Dantonello TM, Int-Veen C, Schuck A, Seitz G, Leuschner I, Nathrath M, et al., Survival following disease recurrence of primary localized alveolar rhabdomyosarcoma. Pediatr Blood Cancer, 2013; 60: 1267-73.

5. Kaufmann SH,Earnshaw WC, Induction of apoptosis by cancer chemotherapy. Exp Cell Res, 2000; 256: 42-9.

6. Mesner PW, Jr., Budihardjo, II,Kaufmann SH, Chemotherapy-induced apoptosis. Adv Pharmacol, 1997; 41: 461-99.

7. Fuchs J, Urla C, Sparber-Sauer M, Schuck A, Leuschner I, Klingebiel T, et al., Treatment and outcome of patients with localized intrathoracic and chest wall rhabdomyosarcoma: a report of the Cooperative Weichteilsarkom Studiengruppe (CWS). J Cancer Res Clin Oncol, 2018; 144: 925-34.

8. Koscielniak E KT, CWS-guidance for risk adapted treatment of soft tissue sarcoma and soft tissue tumours, in children, adolescents, and young adults vol Version 1.6.1. Cooperative Weichteilsarkom Studie Group-CWS der GPOH, . 2014.

9. Hanahan D,Weinberg RA, Hallmarks of cancer: the next generation. Cell, 2011; 144: 646-74.

10. Galluzzi L, Vitale I, Abrams JM, Alnemri ES, Baehrecke EH, Blagosklonny MV, et al., Molecular definitions of cell death subroutines: recommendations of the Nomenclature Committee on Cell Death 2012. Cell Death Differ, 2012; 19: 107-20.

11. Vanden Berghe T, Kaiser WJ, Bertrand MJM,Vandenabeele P, Molecular crosstalk between apoptosis, necroptosis, and survival signaling. Mol Cell Oncol, 2015; 2.

12. McComb S, Aguade-Gorgorio J, Harder L, Marovca B, Cario G, Eckert C, et al., Activation of concurrent apoptosis and necroptosis by SMAC mimetics for the treatment of refractory and relapsed ALL. Sci Transl Med, 2016; 8: 339ra70.

13. Lin CY, Chang TW, Hsieh WH, Hung MC, Lin IH, Lai SC, et al., Simultaneous induction of apoptosis and necroptosis by Tanshinone IIA in human hepatocellular carcinoma HepG2 cells. Cell Death Discovery, 2016; 2: 16065.

14. Jing L, Song F, Liu Z, Li J, Wu B, Fu Z, et al., MLKL-PITPα signaling-mediated necroptosis contributes to cisplatin-triggered cell death in lung cancer A549 cells. Cancer Letters, 2018; 414: 136-46.

15. Dixon Scott J, Lemberg Kathryn M, Lamprecht Michael R, Skouta R, Zaitsev Eleina M, Gleason Caroline E, et al., Ferroptosis: An Iron-Dependent Form of Nonapoptotic Cell Death. Cell, 2012; 149: 1060-72.

16. Tsoi J, Robert L, Paraiso K, Galvan C, Sheu KM, Lay J, et al., Multi-stage Differentiation Defines Melanoma Subtypes with Differential Vulnerability to Drug-Induced Iron-Dependent Oxidative Stress. Cancer Cell, 2018; 33: 890-904.e5.

17. Hangauer MJ, Viswanathan VS, Ryan MJ, Bole D, Eaton JK, Matov A, et al., Drug-tolerant persister cancer cells are vulnerable to GPX4 inhibition. Nature, 2017; 551: 247-50.

18. Maltese WA,Overmeyer JH, Methuosis: nonapoptotic cell death associated with vacuolization of macropinosome and endosome compartments. Am J Pathol, 2014; 184: 1630-42.

19. Ahlstedt J, Fornvik K, Zolfaghari S, Kwak D, Hammarstrom LGJ, Ernfors P, et al., Evaluating vacquinol-1 in rats carrying glioblastoma models RG2 and NS1. Oncotarget, 2018; 9: 8391-99.

20. Li Z, Mbah NE,Maltese WA, Vacuole-inducing compounds that disrupt endolysosomal trafficking stimulate production of exosomes by glioblastoma cells. Mol Cell Biochem, 2018; 439: 1-9.

21. Manara MC, Terracciano M, Mancarella C, Sciandra M, Guerzoni C, Pasello M, et al., CD99 triggering induces methuosis of Ewing sarcoma cells through IGF-1R/RAS/Rac1 signaling. Oncotarget, 2016; 7: 79925-42.

22. Sun L, Li B, Su X, Chen G, Li Y, Yu L, et al., An Ursolic Acid Derived Small Molecule Triggers Cancer Cell Death through Hyperstimulation of Macropinocytosis. J Med Chem, 2017; 60: 6638-48.

23. Aki T, Nara A,Uemura K, Cytoplasmic vacuolization during exposure to drugs and other substances. Cell Biol Toxicol, 2012; 28: 125-31.

24. Weerasinghe P,Buja LM, Oncosis: an important non-apoptotic mode of cell death. Exp Mol Pathol, 2012; 93: 302-8.

25. Sperandio S, de Belle I,Bredesen DE, An alternative, nonapoptotic form of programmed cell death. Proc Natl Acad Sci U S A, 2000; 97: 14376-81.

26. Herrero Martin D, Boro A,Schafer BW, Cell-based small-molecule compound screen identifies fenretinide as potential therapeutic for translocation-positive rhabdomyosarcoma. PLoS One, 2013; 8: e55072.

27. Overmeyer JH, Kaul A, Johnson EE,Maltese WA, Active ras triggers death in glioblastoma cells through hyperstimulation of macropinocytosis. Mol Cancer Res, 2008; 6: 965-77.

28. Bernasconi M, Remppis A, Fredericks WJ, Rauscher FJ, 3rd,Schafer BW, Induction of apoptosis in rhabdomyosarcoma cells through down-regulation of PAX proteins. Proc Natl Acad Sci U S A, 1996; 93: 13164-9.

29. Dixon SJ, Lemberg KM, Lamprecht MR, Skouta R, Zaitsev EM, Gleason CE, et al., Ferroptosis: an iron-dependent form of nonapoptotic cell death. Cell, 2012; 149: 1060-72.

30. Dixon SJ, Patel DN, Welsch M, Skouta R, Lee ED, Hayano M, et al., Pharmacological inhibition of cystine-glutamate exchange induces endoplasmic reticulum stress and ferroptosis. Elife, 2014; 3: e02523.

31. Zheng DW, Xue YQ, Li Y, Di JM, Qiu JG, Zhang WJ, et al., Volasertib suppresses the growth of human hepatocellular carcinoma in vitro and in vivo. Am J Cancer Res, 2016; 6: 2476-88.

32. Shubin AV, Demidyuk IV, Komissarov AA, Rafieva LM,Kostrov SV, Cytoplasmic vacuolization in cell death and survival. Oncotarget, 2016; 7: 55863-89.

33. Fulda S, Targeting apoptosis resistance in rhabdomyosarcoma. Curr Cancer Drug Targets, 2008; 8: 536-44.

34. Fulda S, Therapeutic opportunities based on caspase modulation. Seminars in Cell & Developmental Biology, 2017.

35. Chen NE, Maldonado NV, Khankaldyyan V, Shimada H, Song MM, Maurer BJ, et al., Reactive Oxygen Species Mediates the Synergistic Activity of Fenretinide Combined with the Microtubule Inhibitor ABT-751 against Multidrug-Resistant Recurrent Neuroblastoma Xenografts. Mol Cancer Ther, 2016; 15: 2653-64.

36. Asumendi A, Morales MC, Alvarez A, Arechaga J,Perez-Yarza G, Implication of mitochondria-derived ROS and cardiolipin peroxidation in N-(4-hydroxyphenyl)retinamide-induced apoptosis. Br J Cancer, 2002; 86: 1951-6.

37. Cuperus R, Leen R, Tytgat GAM, Caron HN,van Kuilenburg ABP, Fenretinide induces mitochondrial ROS and inhibits the mitochondrial respiratory chain in neuroblastoma. Cell Mol Life Sci, 2010; 67: 807-16.

38. Makena MR, Koneru B, Nguyen TH, Kang MH,Reynolds CP, Reactive Oxygen Species-Mediated Synergism of Fenretinide and Romidepsin in Preclinical Models of T-cell Lymphoid Malignancies. Mol Cancer Ther, 2017; 16: 649-61.

39. Orth JD, Krueger EW, Weller SG,McNiven MA, A novel endocytic mechanism of epidermal growth factor receptor sequestration and internalization. Cancer Res, 2006; 66: 3603-10.

40. Orth JD,McNiven MA, Get off my back! Rapid receptor internalization through circular dorsal ruffles. Cancer Res, 2006; 66: 11094-6.

41. Coultas L,Strasser A, The molecular control of DNA damage-induced cell death. Apoptosis, 2000; 5: 491-507.

42. Galluzzi L, Vitale I, Aaronson SA, Abrams JM, Adam D, Agostinis P, et al., Molecular mechanisms of cell death: recommendations of the Nomenclature Committee on Cell Death 2018. Cell Death Differ, 2018; 25: 486-541.

43. Hirsch T, Marchetti P, Susin SA, Dallaporta B, Zamzami N, Marzo I, et al., The apoptosis-necrosis paradox. Apoptogenic proteases activated after mitochondrial permeability transition determine the mode of cell death. Oncogene, 1997; 15: 1573-81.

44. Degterev A, Huang Z, Boyce M, Li Y, Jagtap P, Mizushima N, et al., Chemical inhibitor of nonapoptotic cell death with therapeutic potential for ischemic brain injury. Nat Chem Biol, 2005; 1: 112-9.

45. Aslan M,Ozben T, Oxidants in receptor tyrosine kinase signal transduction pathways. Antioxid Redox Signal, 2003; 5: 781-8.

46. Ha SJ, Lee J, Park J, Kim YH, Lee NH, Kim YE, et al., Syringic acid prevents skin carcinogenesis via regulation of NoX and EGFR signaling. Biochem Pharmacol, 2018.

47. Paulsen CE, Truong TH, Garcia FJ, Homann A, Gupta V, Leonard SE, et al., Peroxide-dependent sulfenylation of the EGFR catalytic site enhances kinase activity. Nature Chemical Biology, 2011; 8: 57.

48. Irani K, Xia Y, Zweier JL, Sollott SJ, Der CJ, Fearon ER, et al., Mitogenic signaling mediated by oxidants in Ras-transformed fibroblasts. Science, 1997; 275: 1649-52.

49. Dendo K, Yugawa T, Nakahara T, Ohno SI, Goshima N, Arakawa H, et al., Induction of non-apoptotic programmed cell death by oncogenic RAS in human epithelial cells and its suppression by MYC overexpression. Carcinogenesis, 2018; 39: 202-13.

50. Cooper JP, Reynolds CP, Cho H,Kang MH, Clinical development of fenretinide as an antineoplastic drug: Pharmacology perspectives. Exp Biol Med (Maywood), 2017; 242: 1178-84.

51. Mohrbacher AM, Yang AS, Groshen S, Kummar S, Gutierrez ME, Kang MH, et al., Phase I Study of Fenretinide Delivered Intravenously in Patients with Relapsed or Refractory Hematologic Malignancies: A California Cancer Consortium Trial. Clin Cancer Res, 2017; 23: 4550-55.

52. Hinson AR, Jones R, Crose LE, Belyea BC, Barr FG,Linardic CM, Human rhabdomyosarcoma cell lines for rhabdomyosarcoma research: utility and pitfalls. Front Oncol, 2013; 3: 183.

53. Schindelin J, Arganda-Carreras I, Frise E, Kaynig V, Longair M, Pietzsch T, et al., Fiji: an open-source platform for biological-image analysis. Nat Methods, 2012; 9: 676-82.

Figure legends

Figure 1. Fenretinide activates a distinct and non-classical cell death pathway. **a** Cell viability of indicated engineered Rh4 cells treated with Doxycycline and increasing concentrations of fenretinide as determined by WST assay. Western Blot using whole cell lysates from indicated modified Rh4 cells after treatment or not with 5µM fenretinide for 48h. **b** Cell viability assay of Rh4 and Rh30 cells treated with increasing concentrations of fenretinide in combination with different cell death inhibitors (Z-VAD (100µM), NS-1 (25µM), 3-MA (2.5µM), FS (4µM), DFO (50µM) **c** Western Blot using whole cell lysates from Rh4 and Rh30 cells carrying the indicated knock-outs treated with increasing concentrations of fenretinide. PARP cleavage and Caspase 7 or 9 activity was assessed. **d** Cell viability assay of indicated knockout-cells treated with increasing concentrations of fenretinide as assessed by WST assay.

Figure 2. Fenretinide triggers the production of reactive oxygen species. a-d Fluorescence microscopy analysis and flow cytometry of fenretinide treated Rh4 cells. **a** Light microscopy images of fenretinide (3µM) treated Rh4 cells stained with a fluorogenic Pan-ROS detectant (CellRox 4µM) **b** Mean fluorescence index analysis of the flow cytometry data of Rh4 (upper) and Rh30 cells lower panel) treated with fenretinide (3/4µM). Cells were stained with CellRox 4µM and MitoSox 10µM for the detection of total ROS and mitochondrial ROS levels, respectively **c** Mean fluorescence index analysis of the flow cytometry data of Rh4 (upper) and Rh30 cells, lower panel) treated with fenretinide (3/4µM) and different ROS inhibitors including Vitamin C (50µM), Deferoxamin (50µM) and Ferrostatin (4µM). Cells were stained with MitoSox for the detection of mitochondrial ROS levels **d** Mean fluorescence index of the flow cytometry data of normalized ROS levels in Rh4 and Rh30 cells (upper and lower panel, respectively) after indicated treatments (right panel) and cell viability (left panel) of Rh4 and Rh30 cells treated with fenretinide (3/4µM)

in presence or absence of the mitochondria specific ROS scavenger MitoTempo (300µM) as determined by WST assay.

Figure 3. Fenretinide interferes with complex II of the mitochondrial respiratory chain. Flow cytometry analysis of fenretinide (3/4µM) treated Rh4 and Rh30 cells (upper and lower panel, respectively) in combination with two different inhibitors of complex II of the respiratory chain. Assessed was mitochondrial ROS by staining with MitoSox (10µM). **a** Mean fluorescence index of flow cytometry data measured in Rh4 and Rh30 cells treated with fenretinide in combination with 1500µM of complex II inhibitor Carboxin (left panel) and 500µM respectively 1000µM TTFA (right panel).

Figure 4. Fenretinide induces accumulation of cytoplasmic vesicles and uptake of fluid phase dyes. a Electron microscopy images of untreated or fenretinide (3/4µM) treated Rh4 and Rh30 cells (left and right panel) for 48 hours (lane one and three). Lane two and four show Rh4 and Rh30 cells treated with fenretinide (3/4µM) and Z-VAD (100µM) for 48 h. **b** Mean fluorescence index of the flow cytometry data of fenretinide (3/4µM) treated Rh4 and Rh30 cells in combination with different inhibitors Vitamin C (50µM), Z-VAD (100µM) and MitoTempo (300µM), stained with Acridine Orange (2.7µM) using two different bandpass filters 530/30 and 670/30 (See Suppl.Fig.4B). **c** Light fluorescence microscopy images of Rh4 and Rh30 cells treated or untreated with fenretinide (3/4µM) and stained with Lucifer Yellow (820µM). Graphs on the right show quantification of the relative mean density index assessed with Fiji software. Total integrated density value of an image was divided by the number of cells.

Figure 5. Fenretinide causes accumulation of early and late endosomes. a Cell viability assay of Rh4 and Rh30 cells (upper and lower panel, respectively) treated with increasing concentrations of fenretinide in combination with 30µM of dynasore. **b** Electron microscopy images of untreated

or fenretinide (3/4µM) treated Rh4 and Rh30 cells (upper, respective lower panel) for 48hours (lane one and three). Lane two and four show Rh4 and Rh30 cells treated with fenretinide (3/4µM) and dynasore (30µM) for 48h. **c** Relative mean fluorescence index of the flow cytometry data of fenretinide (3/4µM) treated Rh4 and Rh30 cells (upper, respective lower panel) in combination with the Dynamin inhibitor dynasore (30µM), stained with Acridine Orange (2.7µM) using two different bandpass filters 530/30 and 670/30 (See Supl.Fig.5C). **d** Light fluorescence images of Rh4 cells treated or untreated with fenretinide (3µM) and stained with antibodies against either Rab 5, Rab 7 or Lamp1. Further nuclear staining with Dapi. **e** Quantification of the relative mean density index assessed with Fiji software. Total integrated density value of an image was divided by the number of cells.

Figure 6. Inhibition of the Dynamin GTPases rescues from Fenretinide induced cell death. **a-c:** Crispr/Cas9 Dynamin depleted cells by different sgRNAs **a** Mean fluorescence index of the flow cytometry data of fenretinide (3µM) treated Rh4 and Rh30 Dynamin depleted cells (upper and lower panel, respectively), stained with Acridine Orange (2.7µM) using two different bandpass filters 530/30 and 670/30 (See Supplementary Fig 6B). **b** Cell viability assay of Rh4 and Rh30 Dynamin mutants (upper and lower panel, respectively), treated with different concentrations of fenretinide. **c** Phase contrast images of Rh4 and Rh30 Dynamin depleted cells treated or with fenretinide (3µM /4µM).

Figure 1

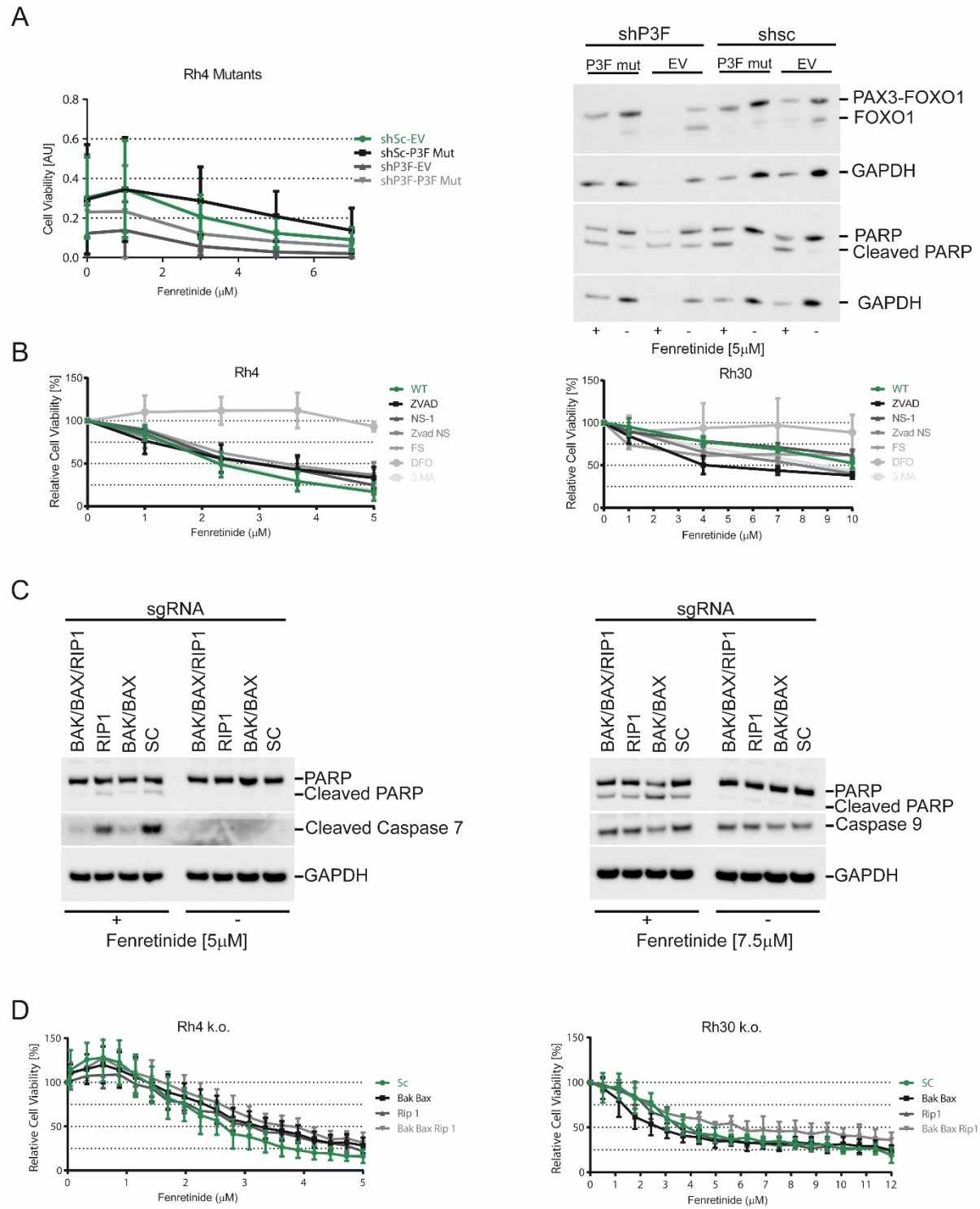
A
Rh4 Mutants
Cell Viability [AU]
Fenretinide (μM)
shSc-EV
shSc-P3F Mut
shP3F-EV
shP3F-P3F Mut
shP3F
shsc
P3F mut
EV
P3F mut
EV
PAX3-FOXO1
FOXO1
GAPDH
PARP
Cleaved PARP
GAPDH
Fenretinide [5μM]
B
Rh4
Rh30
Relative Cell Viability [%]
Fenretinide (μM)
WT
ZVAD
NS-1
Zvad NS
FS
DFO
3 MA
C
sgRNA
BAK/BAX/RIP1
RIP1
BAK/BAX
SC
PARP
Cleaved PARP
Cleaved Caspase 7
GAPDH
Fenretinide [5μM]
Caspase 9
Fenretinide [7.5μM]
D
Rh4 k.o.
Rh30 k.o.
Relative Cell Viability [%]
Fenretinide (μM)
Sc
Bak Bax
Rip 1
Bak Bax Rip 1
SC
Rip1

Figure 2

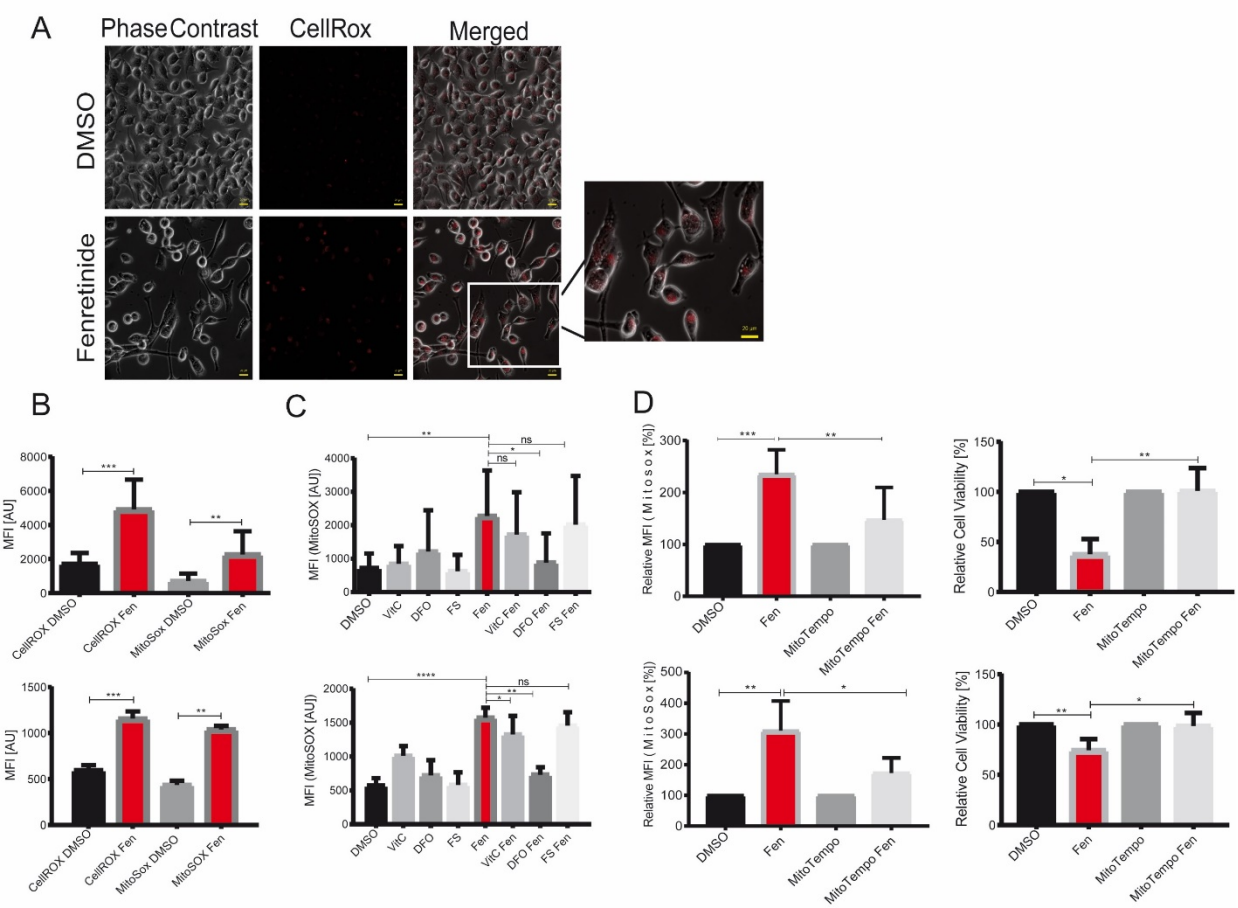
A
Phase Contrast
CellRox
Merged
DMSO
Fenretinide
B
MFI [AU]
CellROX DMSO
CellROX Fen
MitoSox DMSO
MitoSox Fen
MFI [AU]
CellROX DMSO
CellROX Fen
MitoSox DMSO
MitoSOX Fen
C
MFI (MitoSOX [AU])
DMSO
VitC
DFO
FS
Fen
VitC Fen
DFO Fen
FS Fen
MFI (MitoSOX [AU])
DMSO
VitC
DFO
FS
Fen
VitC Fen
DFO Fen
FS Fen
D
Relative MFI (M i t o s o x [%])
DMSO
Fen
MitoTempo
MitoTempo Fen
Relative Cell Viability [%]
DMSO
Fen
MitoTempo
MitoTempo Fen
Relative MFI (M i t o S o x [%])
DMSO
Fen
MitoTempo
MitoTempo Fen
Relative Cell Viability [%]
DMSO
Fen
MitoTempo
MitoTempo Fen

Figure 3

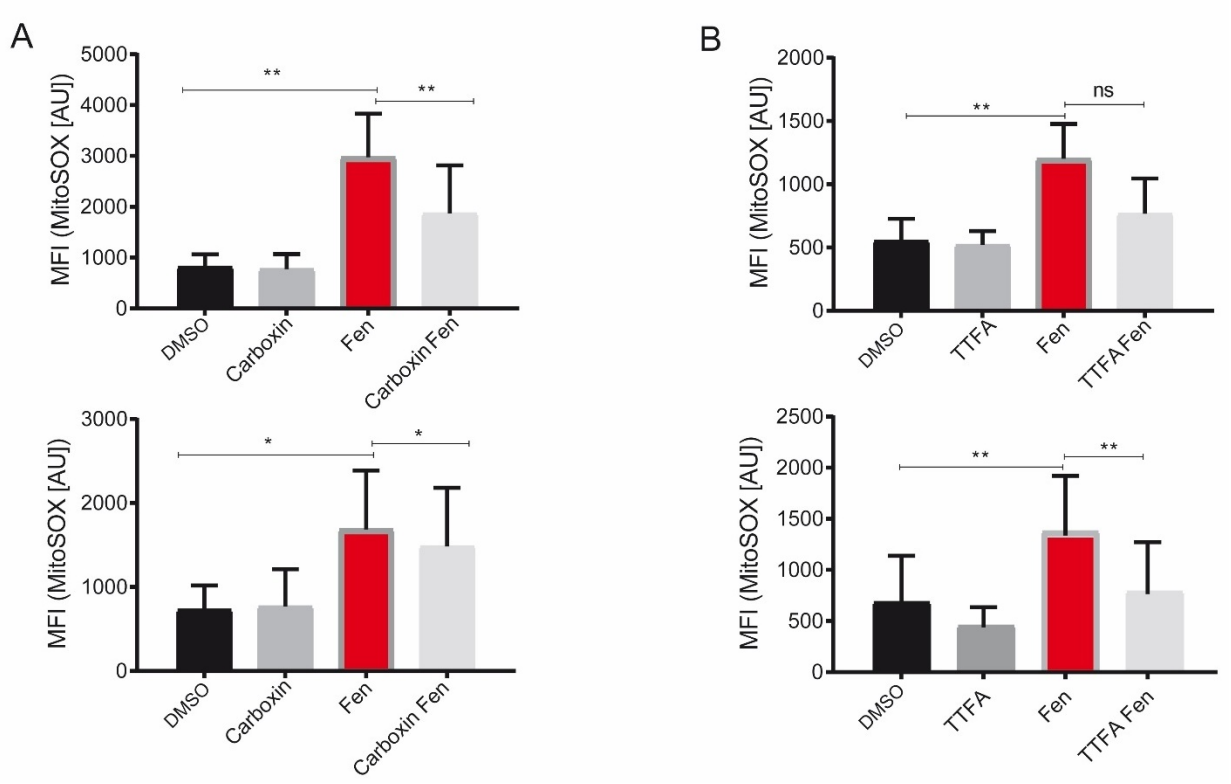
A
MFI (MitoSOX [AU])
5000
4000
3000
2000
1000
0
**
**
DMSO
Carboxin
Fen
CarboxinFen
MFI (MitoSOX [AU])
3000
2000
1000
0
*
*
DMSO
Carboxin
Fen
Carboxin Fen
B
MFI (MitoSOX [AU])
2000
1500
1000
500
0
**
ns
DMSO
TTFA
Fen
TTFA Fen
MFI (MitoSOX [AU])
2500
2000
1500
1000
500
0
**
**
DMSO
TTFA
Fen
TTFA Fen

Figure 4

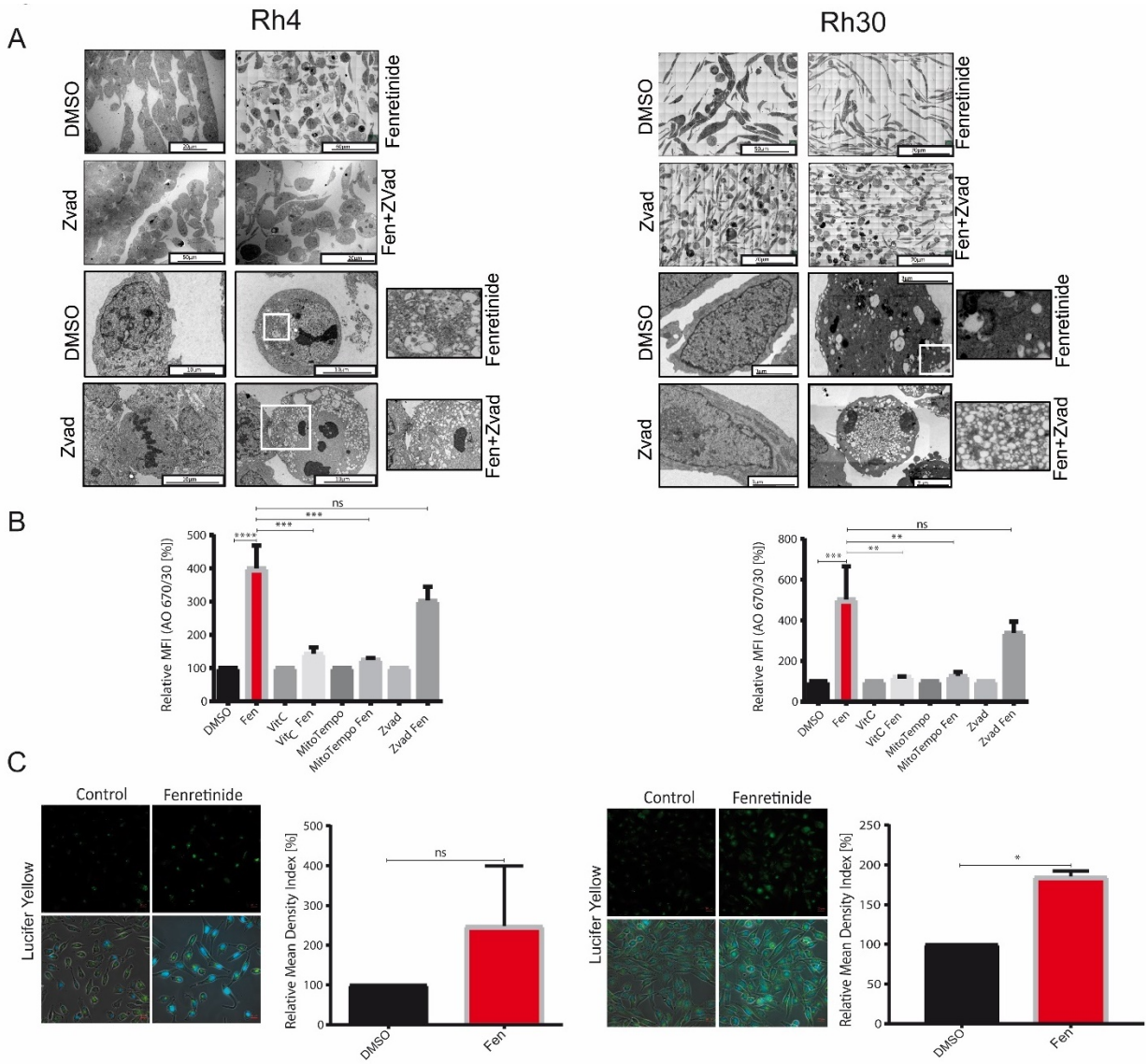
A
Rh4
Rh30
DMSO
Zvad
Fenretinide
Fen+Zvad
B
Relative MFI (AO 670/30 [%])
DMSO
Fen
VitC
VitC Fen
MitoTempo
MitoTempo Fen
Zvad
Zvad Fen
ns
C
Control
Fenretinide
Lucifer Yellow
Relative Mean Density Index [%]

Figure 5

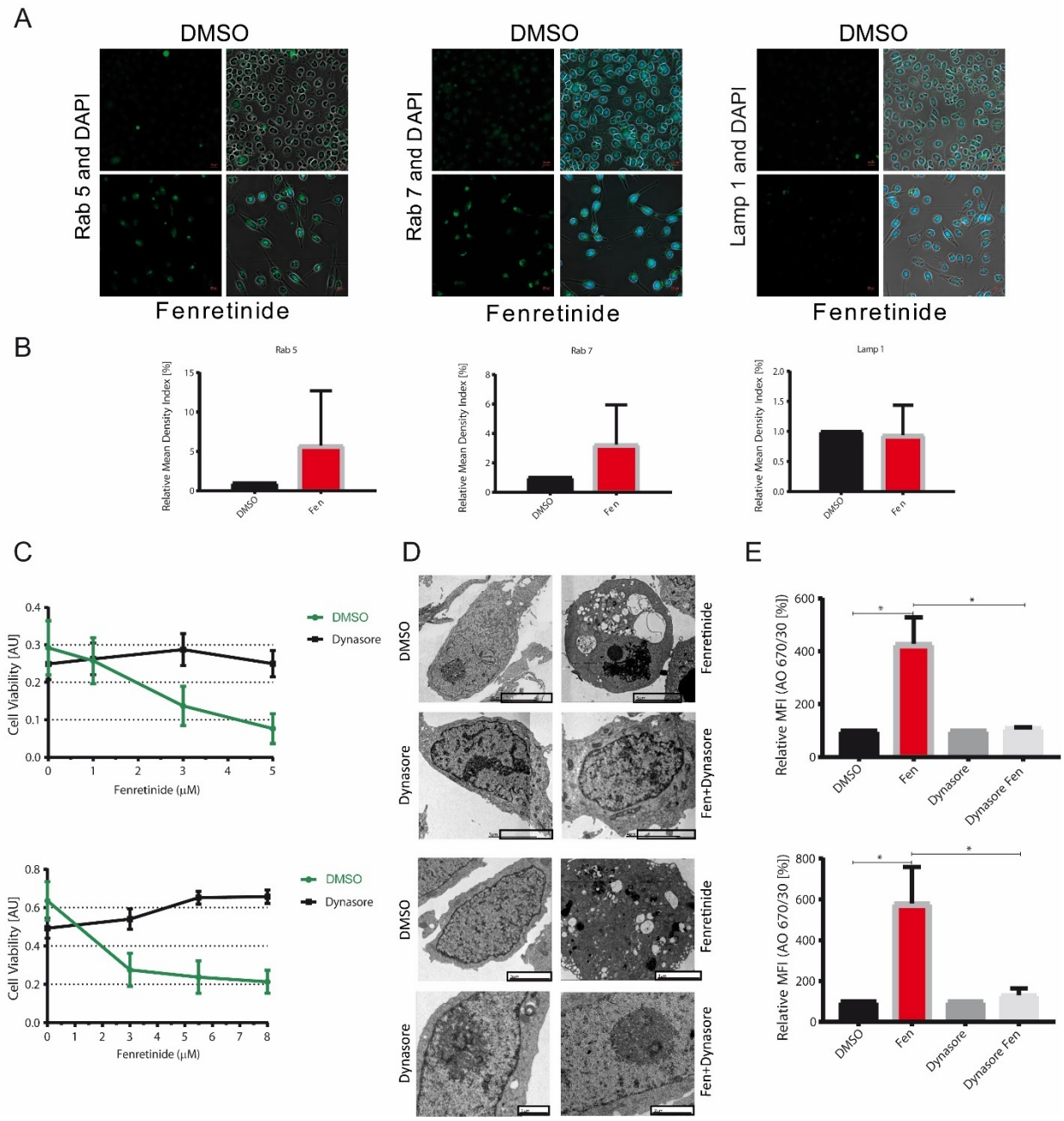
A
DMSO
DMSO
DMSO
Rab 5 and DAPI
Rab 7 and DAPI
Lamp 1 and DAPI
Fenretinide
Fenretinide
Fenretinide
B
Rab 5
Rab 7
Lamp 1
Relative Mean Density Index [%]
DMSO
Fen
C
Cell Viability [AU]
DMSO
Dynasore
Fenretinide (μM)
D
DMSO
Fenretinide
Dynasore
Fen+Dynasore
E
Relative MFI (AO 670/30 [%])
DMSO
Fen
Dynasore
Dynasore Fen

Figure 6

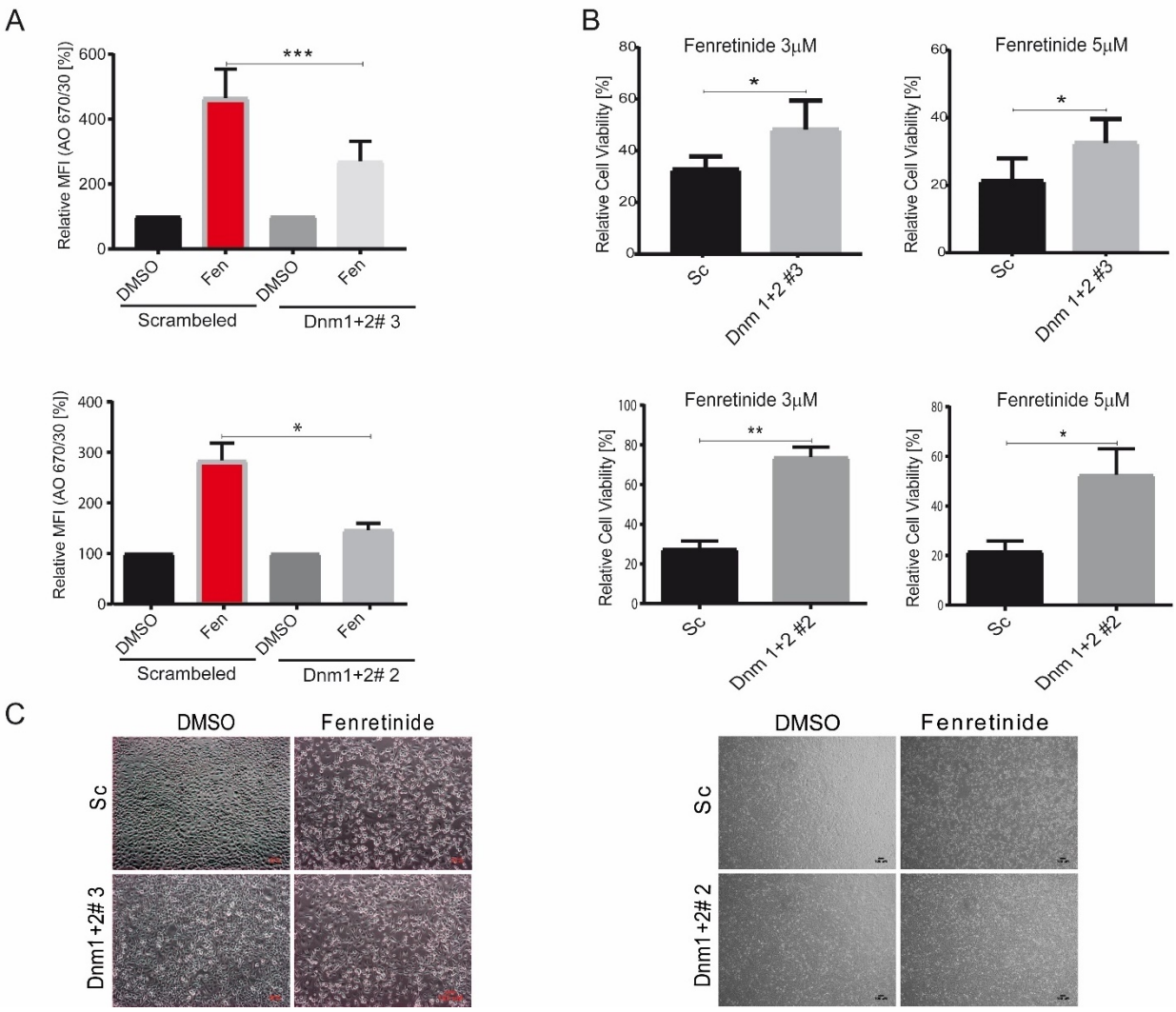
A
Relative MFI (AO 670/30 [%])
600
400
200
0
***
DMSO
Fen
DMSO
Fen
Scrambeled
Dnm1+2# 3
Relative MFI (AO 670/30 [%])
400
300
200
100
0
*
DMSO
Fen
DMSO
Fen
Scrambeled
Dnm1+2# 2
B
Fenretinide 3µM
Relative Cell Viability [%]
80
60
40
20
0
*
Sc
Dnm 1+2 #3
Fenretinide 5µM
Relative Cell Viability [%]
60
40
20
0
*
Sc
Dnm 1+2 #3
Fenretinide 3µM
Relative Cell Viability [%]
100
80
60
40
20
0
**
Sc
Dnm 1+2 #2
Fenretinide 5µM
Relative Cell Viability [%]
80
60
40
20
0
*
Sc
Dnm 1+2 #2
C
DMSO
Fenretinide
Sc
Dnm1+2# 3
DMSO
Fenretinide
Sc
Dnm1+2# 2

Supplementary Data and Figures

Sup. Fig. 1

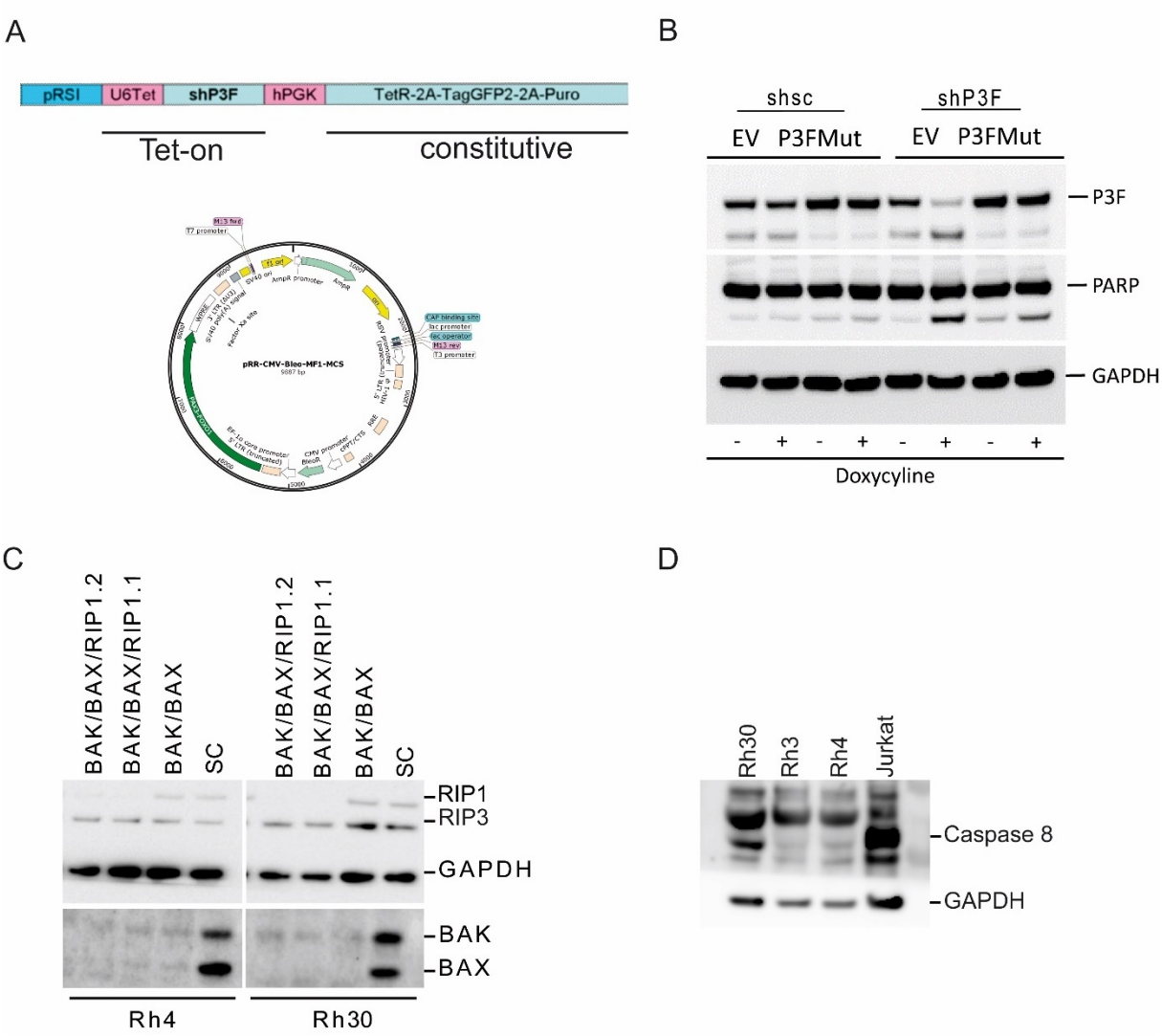

Sup. Fig. 2

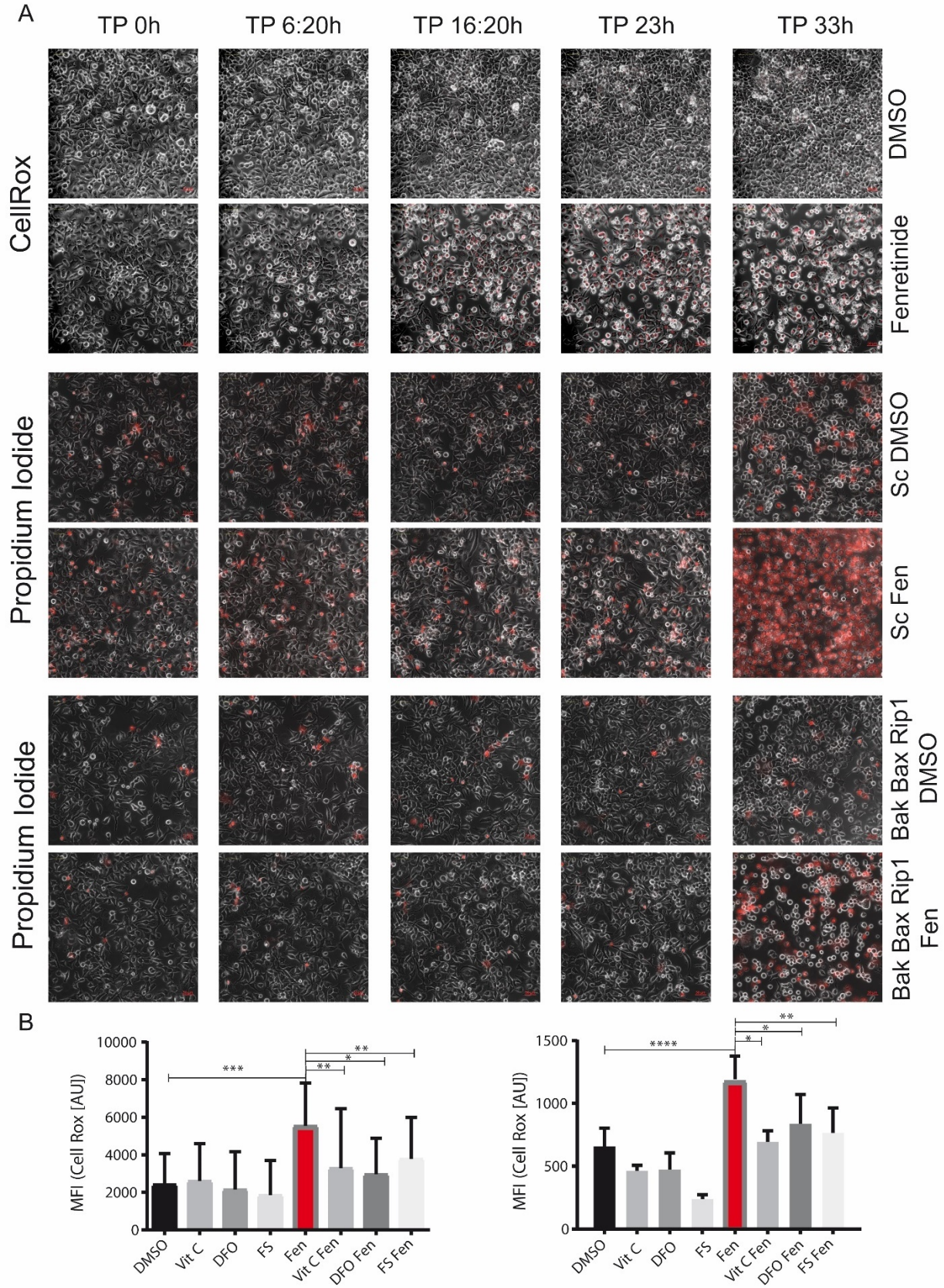
A
TP 0h
TP 6:20h
TP 16:20h
TP 23h
TP 33h
CellRox
DMSO
Fenretinide
Propidium Iodide
Sc DMSO
Sc Fen
Propidium Iodide
Bak Bax Rip1 DMSO
Bak Bax Rip1 Fen
B
MFI (Cell Rox [AU])
10000
8000
6000
4000
2000
0
***
**
*
**
DMSO
Vit C
DFO
FS
Fen
Vit C Fen
DFO Fen
FS Fen
MFI (Cell Rox [AU])
1500
1000
500
0
****
**
*
*
DMSO
Vit C
DFO
FS
Fen
Vit C Fen
DFO Fen
FS Fen

Sup. Fig. 3

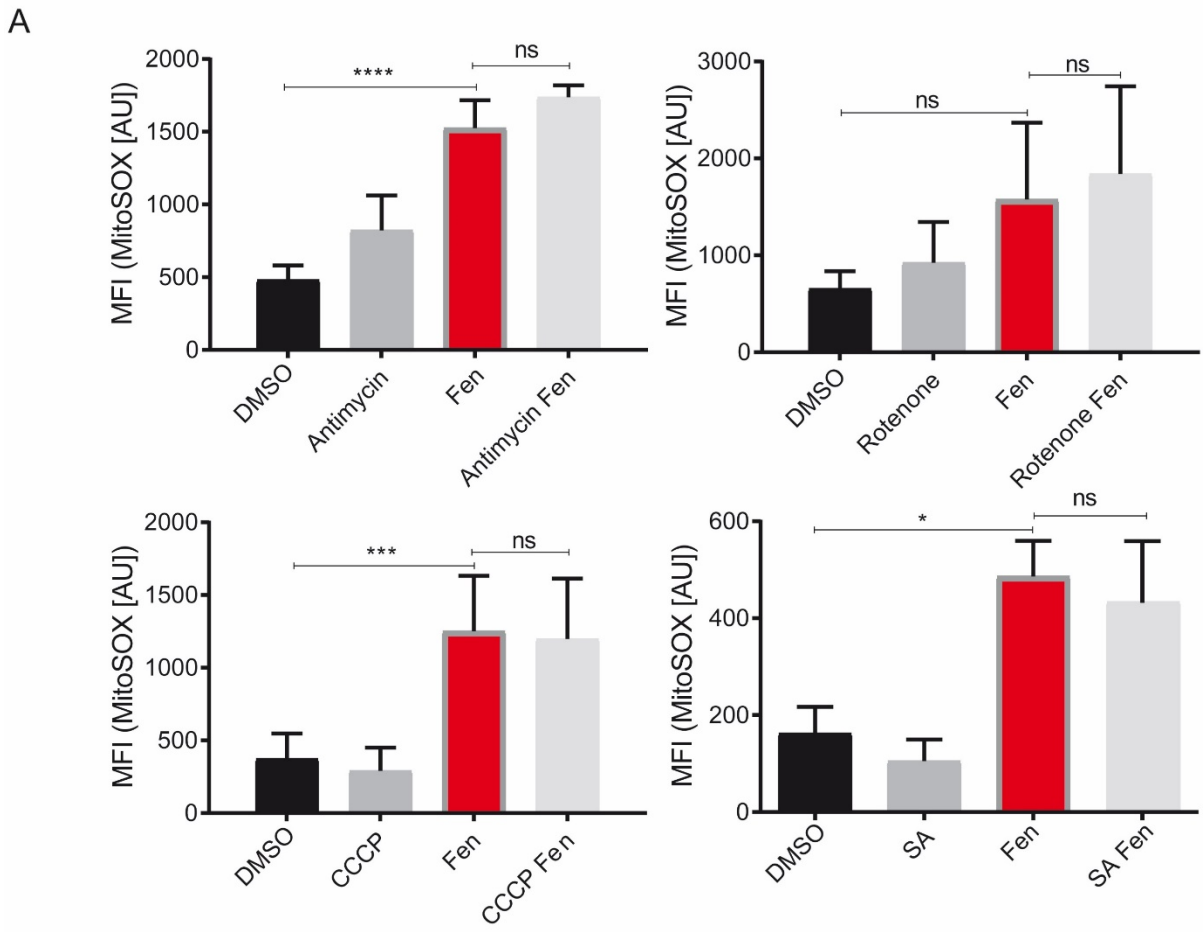
A
MFI (MitoSOX [AU])
2000
1500
1000
500
0
****
ns
DMSO
Antimycin
Fen
Antimycin Fen
3000
2000
1000
0
ns
ns
DMSO
Rotenone
Fen
Rotenone Fen
***
ns
DMSO
CCCP
Fen
CCCP Fen
600
400
200
0
*
ns
DMSO
SA
Fen
SA Fen

Sup. Fig. 4

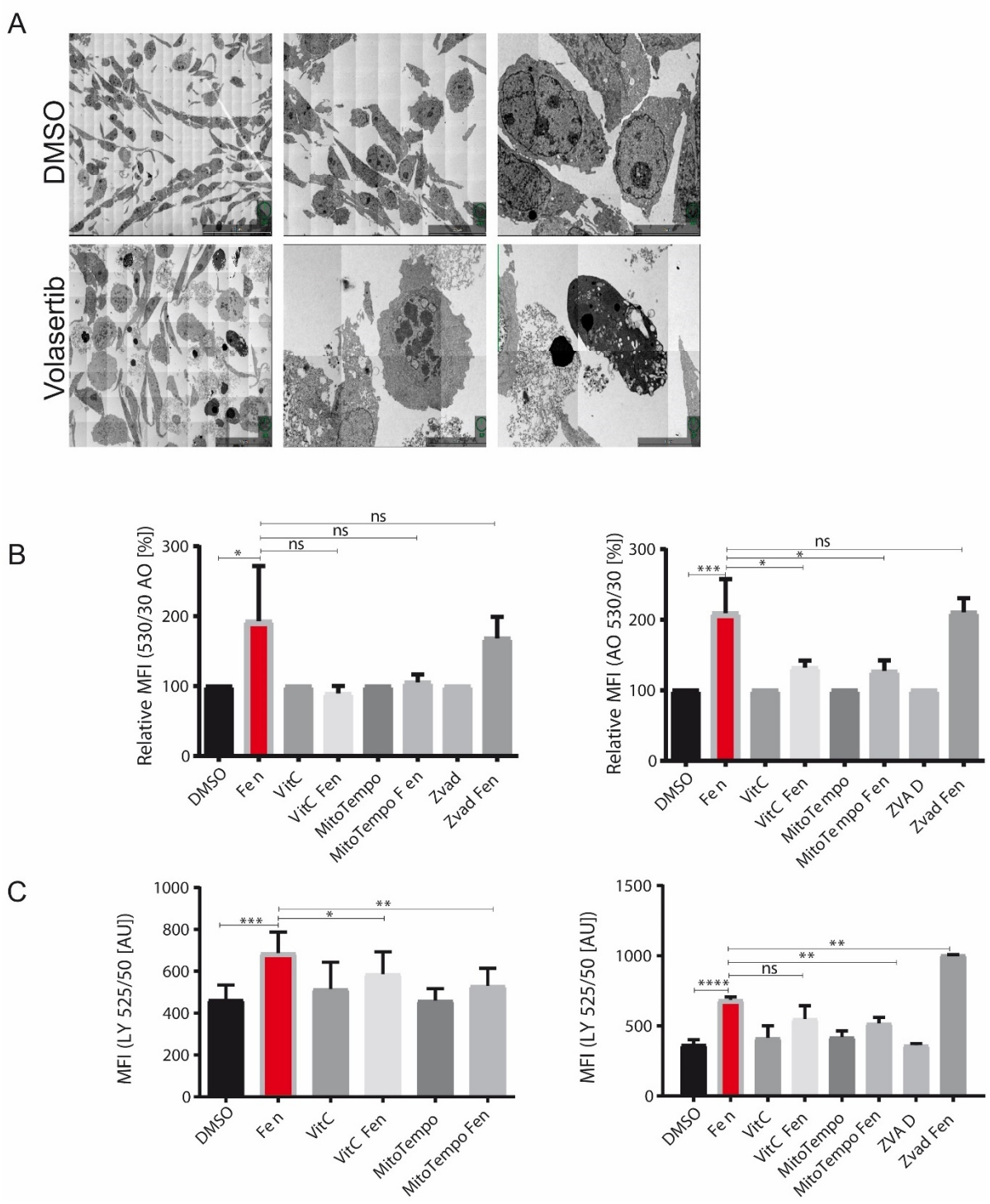
A
DMSO
Volasertib
B
Relative MFI (530/30 AO [%])
300
200
100
0
*
ns
ns
ns
DMSO
Fe n
VitC
VitC Fen
MitoTempo
MitoTempo F en
Zvad
Zvad Fen
Relative MFI (AO 530/30 [%])
300
200
100
0
***
*
*
ns
DMSO
Fe n
VitC
VitC Fen
MitoTempo
MitoTempo Fen
ZVA D
Zvad Fen
C
MFI (LY 525/50 [AU])
1000
800
600
400
200
0
***
*
**
DMSO
Fe n
VitC
VitC Fen
MitoTempo
MitoTempo Fen
MFI (LY 525/50 [AU])
1500
1000
500
0
****
ns
**
**
DMSO
Fe n
VitC
VitC Fen
MitoTempo
MitoTempo Fen
ZVA D
Zvad Fen

Sup. Fig. 5

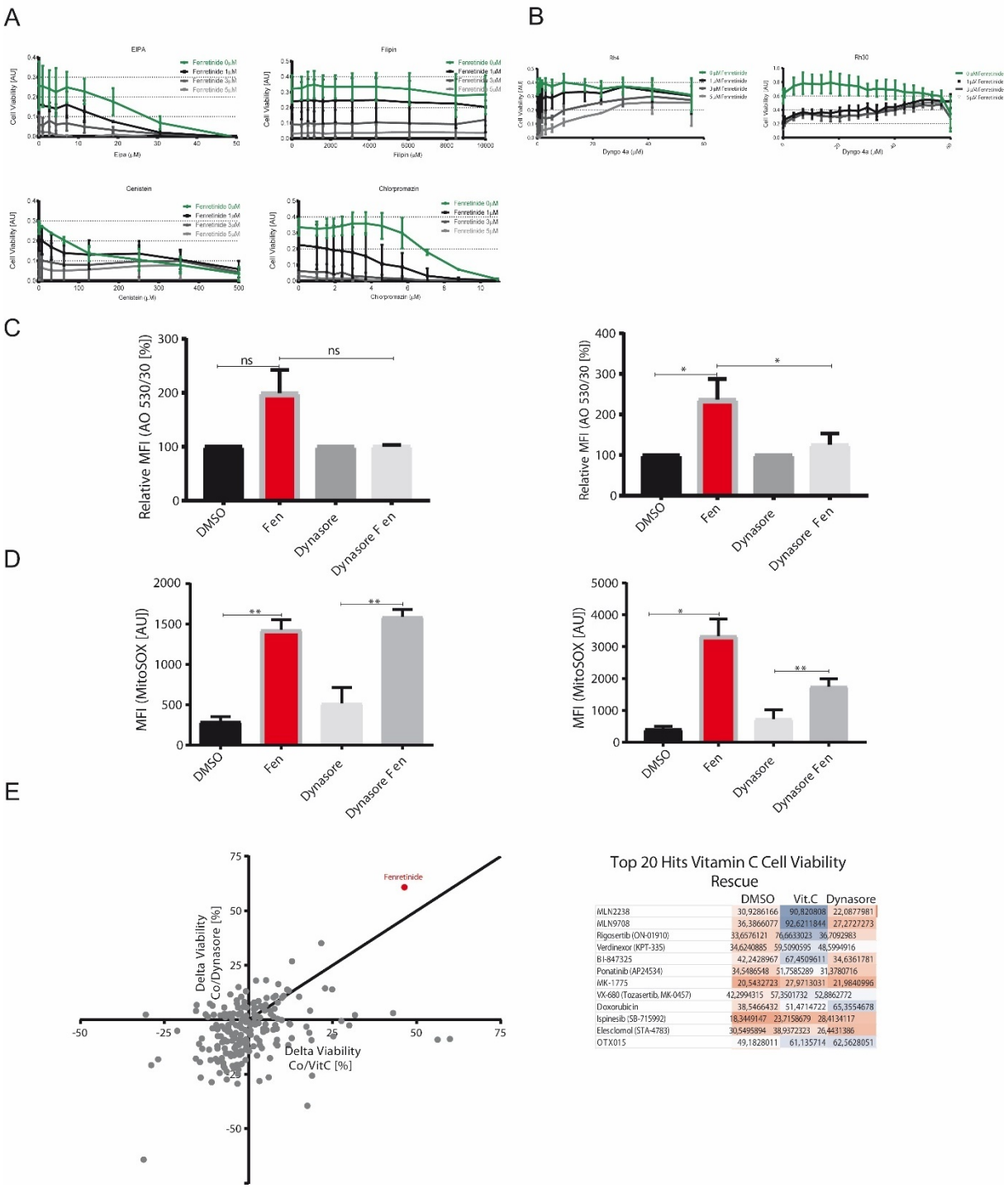

Top 20 Hits Vitamin C Cell Viability Rescue

	DMSO	Vit.C	Dynasore
MLN2238	30,9286166	90,820808	22,0877981
MLN9708	36,3866077	92,6211844	27,2727273
Rigosertib (ON-01910)	33,6576121	76,6633023	36,7092983
Verdinexor (KPT-335)	34,6240885	59,5090595	48,5994916
BI-847325	42,2428967	67,4509611	34,6361781
Ponatinib (AP24534)	34,5486548	51,7585289	31,3780716
MK-1775	20,5432723	27,9713031	21,9840996
VX-680 (Tozasertib, MK-0457)	42,2994315	57,3501732	52,8862772
Doxorubicin	38,5466432	51,4714722	65,3554678
Ispinesib (SB-715992)	18,3449147	23,7158679	28,4134117
Elesclomol (STA-4783)	30,5495894	38,9372323	26,4431386
OTX015	49,1828011	61,135714	62,5628051

Sup. Fig. 6

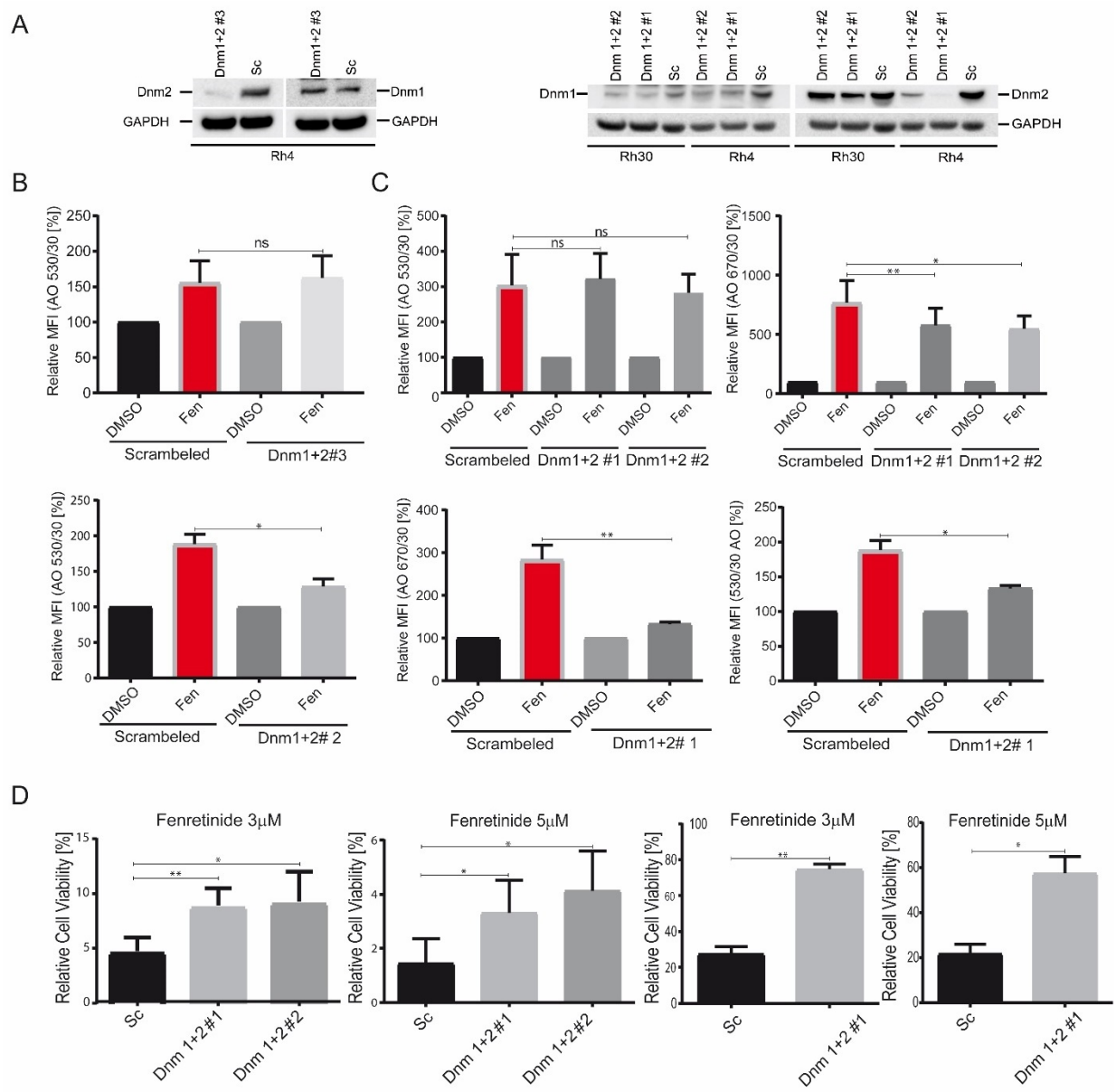
A
Dnm1+2 #3
Sc
Dnm2
GAPDH
Dnm1
Rh4
Dnm 1+2 #2
Dnm 1+2 #1
Rh30
B
C
Relative MFI (AO 530/30 [%])
Relative MFI (AO 670/30 [%])
DMSO
Fen
Scrambeled
Dnm1+2#3
Dnm1+2 #1
Dnm1+2 #2
Dnm1+2# 2
Dnm1+2# 1
ns
D
Fenretinide 3µM
Fenretinide 5µM
Relative Cell Viability [%]
Sc
Dnm 1+2#1
Dnm 1+2#2

Legends supplementary figures

Supplementary Figure 1. Fenretinide induced cell death is not dependent on PAX3-FOXO1 expression. a Scheme of the two-vector system designed to simultaneously silence endogenous PAX3-FOXO1 (Doxycycline-inducible) while overexpressing PAX3-FOXO1. **b** Western Blots using extracts from indicated modified Rh4 cell treated with Doxycycline (0.1ug/ml) or not to induce shRNA-mediated silencing of endogenous PAX3-FOXO1. Blots were probed for PAX3-FOXO1 and PARP cleavage (shP3F-EV: empty expression vector, P3F Mut: pRR plasmid driving expression of shRNA-insensitive form of P3F, shsc-EV: shRNA vector with control shRNA, shP3F: Silencing vector driving expression of P3F-directed shRNA). **c** Western Blot using whole cell lysates from Rh4 cells having the indicated knock-outs of key players of the apoptotic and necroptotic pathway (Bak, Bax, RIPK1 and RIPK3). **d** Western Blot using whole cell lysates from Rh4, Rh3, Rh30 and Jurkat control cells. Caspase 8 presence was assessed.

Supplementary Figure 2. Fenretinide triggers the production of reactive oxygen species. a Light microscopy time lapse images of fenretinide (3µM) treated Rh4 cells or control cells stained with a fluorogenic Pan-ROS detectant (CellRox 4µM) (upper two rows). Mid two rows show fenretinide (3µM) treated Rh4 cells or control cells stained with Propidum Iodide (3µl/ml) – a cell death marker; lower two rows show Rh4 Bak/Bax/Rip knockout cells, treated or untreated with fenretinide (3µM) and stained with Propidum Iodide (3µl/ml). **b** Mean fluorescence index analysis of the flow cytometry data of Rh4 and Rh30 cells (left and right panel) treated with Fenretinide (3/4µM) and different ROS inhibitors including Vitamin C (50µM), Deferoxamin (50µM) and Ferrostatin (4µM). Cells were stained with CellRox (4µM) for the detection of Pan ROS levels.

Supplementary Figure 3. Fenretinide does not interfere with other complexes of the mitochondrial respiratory chain than complex II. Flow cytometry analysis of fenretinide (3µM) treated Rh4 cells in combination with inhibitors of each complex of the respiratory chain. **a** Mean fluorescence index analysis of flow cytometry data measured with Rh4 cells treated with fenretinide in combination with 0.25µM of complex I Inhibitor Rotenone, 2.5µM of complex III Inhibitor Antimycin, 15µM of complex IV inhibitor Sodium Azid (SA) and 0.5µM of the uncoupler CCCP. Staining with MitoSox (10µM) to assess mitochondrial ROS.

Supplementary Figure 4. Fenretinide induces accumulation of cytoplasmic vesicles and induces the uptake of fluid phase dyes. a Electron microscopy images of untreated and Volasertib (6.5nM) treated Rh4 cells for 48 hours**. b** Mean fluorescence index analysis of the flow cytometry data of fenretinide (3/4µM) treated Rh4 and Rh30 cells (left and right panel) in combination with different inhibitors Vitamin C (50µM), Z-VAD (100µM) and MitoTempo (300µM), stained with Acridine Orange (2.7µM) using two different bandpass filters 530/30 and 670/30 (See.Fig.4B). **c** Mean fluorescence index analysis of the flow cytometry data of fenretinide (3/4µM) treated Rh4 and Rh30 cells (left and right panel) in combination with different inhibitors Vitamin C (50µM), Z-VAD (100µM) and MitoTempo (300µM), stained with Lucifer Yellow (820µM).

Supplementary Figure 5. Fenretinide treatment induces accumulation of fluid phase dyes in early and late endosomes. a Cell viability assays of Rh4 cells treated with increasing concentrations of fenretinide in combination with different inhibitors of the different endocytic pathways (EIPA-Macropinocytosis, Filipin/Genistein-Clathrin independent endocytosis, Chlorpromazin-Clathrin mediated endocytosis) in increasing concentrations as depicted**. b** Cell viability assays of Rh4 and Rh30 cells treated with increasing concentrations of fenretinide in

combination with the Dynamin inhibitor Dyngo 4a in increasing concentrations as depicted**. c** Relative Mean fluorescence index analysis of the flow cytometry data of fenretinide (3/4µM) treated Rh4 and Rh30 cells (left and right panel) in combination with the Dynamin inhibitor dynasore (30µM), stained with Acridine Orange (2.7µM) using two different bandpass filters 530/30 and 670/30 (See Fig.5 C) **d** Mean fluorescence index analysis of the flow cytometry data of fenretinide (3/4µM) treated Rh4 and Rh30 cells (left and right panel), dynasore (30µM) was added as depicted and stained with MitoSox (10µM). **e** Cell viability assay of Rh4 cells treated with a custom-made small compound and drug containing library comprising 206 agents (each 0.5µM, except fenretinide 3µM) in combination with Vitamin C (50µM) or dynasore (30µM). Depicted is the difference of cell viability of only library treated cells and cells treated with either Vitamin C (50µM) or dynasore (30µM). The table on the right shows the top twenty Vitamin C rescued compounds.

Supplementary Figure 6. a Western Blot using whole cell lysates from Rh4 and Rh30 cells in which either Dynamin 1 or Dynamin 2 was knocked out using the CrisprCas 9 system. In each case three different guides (#1, 2, and 3) are shown. Dynamin 1 respectively Dynamin 2 and GAPDH activity was assessed. **b** Mean fluorescence index analysis of the flow cytometry data of fenretinide (3/4µM) treated Rh4 and Rh30 mutants (upper and lower panel), stained with Acridine Orange (2.7µM) using two different bandpass filters 530/30 and 670/30 (See Fig 6 A). **c** Mean fluorescence index analysis of the flow cytometry data of fenretinide (3µM) treated Rh4 and Rh30 mutants (upper and lower two panels), stained with Acridine Orange (2.7µM) using two different bandpass filters 530/30 and 670/30 (right and left panel). **d** Cell viability assay of Rh4 and Rh30 Dynamin mutants (two left respectively two right graphs) treated with different concentrations of fenretinide

Supplementary Tables

Compound Name	Product information
3-Methyladenine (3-MA)	M9281, Sigma-Aldrich
Deferoxamine Mesylate (Deferoxamine, DFO)	D9533, Sigma-Aldrich
Hydroxy- dynasore (Dyngo 4a)	SML0340 Sigma-Aldrich
Dynasore hydrate (dynasore)	D7693, Sigma-Aldrich
Ethylisopropylamiloride (EIPA)	A3085, Sigma-Aldrich
Ferrostatin-1 (FS)	A4371, APExBIO
Genistein	G6649, Sigma-Aldrich
Filipin complex from filipinensis	F9765, Sigma-Aldrich
Chlorpromazin hydochloride	C8138, Sigma-Aldrich
L-Ascorbinsäure (Vitamine C)	A4403, Sigma-Aldrich
MitoTempo (MT)	SML0737, Sigma-Aldrich
Necrostatin-1 (NS-1)	A4213, APExBIO
Retinoic acid p-hydroxyanilide (Fenretinide, Fen)	H7779, Sigma-Aldrich
Z-VAD-FMK	A1902, APExBIO
Carboxine	45371, Sigma-Aldrich
2-Thenoyltrifluoroacetone	T27006, Sigma-Aldrich
Rotenone	R8875, Sigma-Aldrich
Antimycin	A8674, Sigma-Aldrich
Carbonyl cyanide 3-chlorphenyl-hydrazone (CCCP)	C2759, Sigma-Aldrich
Sodium Azid	S2002, Sigma-Aldrich

Table 1 Compounds used for WST-1 cell viability assays and Flow Cytometry

Stain	Product information
Acridine Orange (hemi zinc chloride salt)	158550, Sigma-Aldrich
CellRox Deep Red Reagent	C10422, ThermoFisher
Lucifer Yellow	L453, ThermoFisher
MitoSox Red	M36008, ThermoFisher
Propidium Iodide	4170, Sigma-Aldrich

Table 2 Fluorescent stains for flow cytometry and fluorescence microscopy

Antibody	Product information
Mouse anti-caspase 8	Cell Signaling, Cat# 9746
Rabbit anti-Bak	Cell Signaling, Cat #3792
Rabbit anti-Bax	Cell Signaling, Cat# 2774
Rabbit anti-cleaved caspase-7	Cell Signaling, Cat# 9491
Mouse anti-caspase 9	Cell Signaling, Cat#9508
Rabbit anti-PARP	Cell Signaling, Cat# 9542
Rabbit anti-GAPDH	Cell Signaling, Cat#2118
Mouse anti-RIP1	BD Biosciences, Cat# 51-6559
Rabbit anti-RIP3	Abnova, Cat# PAB0287
Rabbit anti-dynamin1	ThermoFisher, Cat# PA1-660
Rabbit anti-dynamin 2	GeneTex, Cat# C2C3
Horseradish peroxidase-conjugated goat anti-mouse	Cell Signaling, Cat# 7076

Horseradish peroxidase-conjugated goat anti-rabbit	Cell Signaling, Cat# 7074

Table 3 Antibodies used for WB

Gene Name	Primer Sequence
RIPK1-1	ACACCTCCCGAAGCCTCCGCTGTCT
RIPK1-2	ACACCTGTGAAAGTCACGATCAACG
Scrambled	GCACTACCAGAGCTAACTCA
Bak	ACGGCAGCTCGCCATCATCG
Bax	CAAGCGCATCGGGGACGAAC
Dynamin 1 #1	ACACCGCAGGTCGAGGTCCGCGTTC
Dynamin 1 #2	ACACCCATTGTCACCCGACGTCCCC
Dynamin 2 #1	ACACCCCCGCTGGTCAACAAACTGC
Dynamin 2 #2	ACACCGTGACGATTCCTGAACCGCG
Dynamin 1 #3	AAGGCGCACCTCCTCGAAGT
Dynamin 2 #3	CGTGTGGCGAGTAGACTCGA

Table 4 Lenti-CRISPR primers (insert sequences)

Product Name	Target
Veliparib (ABT-888)	PARP
Axitinib	VEGFR, PDGFR, c-Kit
Saracatinib (AZD0530)	Src, Bcr-Abl
FG-4592	HIF
Afatinib (BIBW2992)	EGFR
Bortezomib (PS-341)	Proteasome
Bosutinib (SKI-606)	Src
Dovitinib (TKI-258, CHIR-258)	c-Kit, FGFR, Flt, VEGFR, PDGFR
Dasatinib	Src, Bcr-Abl, c-Kit
Erlotinib HCl (OSI-744)	EGFR
Gefitinib (ZD1839)	EGFR
Lapatinib (GW-572016)	EGFR, HER2
Lenalidomide (CC-5013)	TNF-alpha
Nilotinib (AMN-107)	Bcr-Abl
Pazopanib HCl	VEGFR, PDGFR, c-Kit
Rapamycin (Sirolimus)	mTOR
Sorafenib Tosylate	VEGFR, PDGFR, Raf
Sunitinib Malate	VEGFR, PDGFR, c-Kit, Flt
Vandetanib (ZD6474)	VEGFR
Vorinostat (SAHA, MK0683)	HDAC
VX-680 (Tozasertib, MK-0457)	Aurora Kinase
Y-27632 2HCl	ROCK
Elesclomol (STA-4783)	HSP
Entinostat (MS-275)	HDAC
Enzastaurin (LY317615)	PKC
Olaparib (AZD2281, Ku-0059436)	PARP

GDC-0941	PI3K
SB431542	TGF-beta/Smad
Crizotinib (PF-02341066)	c-Met, ALK
AUY922 (NVP-AUY922)	HSP
PHA-665752	c-Met
SB216763	GSK-3
MK-2206 2HCl	Akt
Vismodegib (GDC-0449)	Hedgehog, P-gp
KU-55933 (ATM Kinase Inhibitor)	ATM
GSK1904529A	IGF-1R
MLN8054	Aurora Kinase
Danusertib (PHA-739358)	Aurora Kinase, FGFR, Bcr-Abl, c-RET, Src
GSK690693	Akt
JNJ-38877605	c-Met
Palbociclib (PD-0332991) HCl	CDK
Cabozantinib (BMS-907351)	VEGFR, c-Met, Flt, Tie-2, c-Kit
Everolimus (RAD001)	mTOR
BMS-754807	IGF-1R
YM155 (Sepantronium Bromide)	Survivin
Alisertib (MLN8237)	Aurora Kinase
AT9283	Bcr-Abl, JAK, Aurora Kinase
Barasertib (AZD1152-HQPA)	Aurora Kinase
Roscovitine (Seliciclib,CYC202)	CDK
Lenvatinib (E7080)	VEGFR
Valproic acid	GABA Receptor, HDAC
CYC116	Aurora Kinase, VEGFR
XAV-939	Wnt/beta-catenin
Thalidomide	Others
Decitabine	DNA/RNA Synthesis
PIK-75	PI3K, DNA-PK
2-Methoxyestradiol (2-MeOE2)	HIF
Vemurafenib (PLX4032, RG7204)	Raf
Rigosertib (ON-01910)	PLK
Ruxolitinib (INCB018424)	JAK
Resveratrol	Sirtuin
Ispinesib (SB-715992)	Kinesin
AEE788 (NVP-AEE788)	EGFR, Flt, VEGFR, HER2
PHA-793887	CDK
Ponatinib (AP24534)	Bcr-Abl, VEGFR, FGFR, PDGFR, Flt
AT7519	CDK
MK-1775	Wee1
Quizartinib (AC220)	Flt
AZD7762	Chk
R406 (free base)	Syk
Org 27569	Cannabinoid Receptor

EX 527 (Selisistat)	Sirtuin
Pomalidomide	TNF-alpha, COX
KU-60019	ATM
BIRB 796 (Doramapimod)	p38 MAPK
RO4929097	Y-Secretase
Tie2 kinase inhibitor	Tie-2
Azacitidine	DNA/RNA Synthesis
Acadesine	AMPK
Nicorandil	Others
PF-573228	FAK
Lovastatin	HMG-CoA Reductase
LDE225 (Erismodegib)	Smoothened
PF-4708671	S6 Kinase
MLN2238	Proteasome
MLN9708	Proteasome
SGI-1776 free base	Pim
AZ 960	JAK
Apatinib	VEGFR
Volasertib (BI 6727)	PLK
Degrasyn (WP1130)	DUB, Bcr-Abl
BKM120 (Buparlisib)	PI3K
Imatinib (STI571)	PDGFR,c-Kit, v-Abl
Mifepristone	Estrogen/progestogen Receptor
LY2603618	Chk
NU7441 (KU-57788)	DNA-PK, PI3K
MK-0752	Gamma-secretase
Trametinib (GSK1120212)	MEK
Ibrutinib (PCI-32765)	Src
NVP-BSK805 2HCl	JAK
GDC-0980 (RG7422)	mTOR, PI3K
A-769662	AMPK
AMG-900	Aurora Kinase
Crenolanib (CP-868596)	PDGFR
AZ 3146	Kinesin
PHA-767491	CDK
CUDC-907	HDAC, PI3K
NVP-BVU972	c-Met
SB705498	TRPV
Tofacitinib (CP-690550)	JAK
Dabrafenib (GSK2118436)	Raf
GDC-0068	Akt
Torin 2	mTOR
TAE226 (NVP-TAE226)	FAK
TPCA-1	IKK
Carfilzomib (PR-171)	Proteasome

T0070907	PPAR
WZ811	CXCR
IOX2	HIF
Evacetrapib (LY2484595)	CETP
Pazopanib	VEGFR
Rimonabant	Cannabinoid Receptor
Cabozantinib malate	c-met, VEGFR2
Spironolactone	Androgen Receptor
JNK-IN-8	Free Base
QNZ (EVP4593)	NF-κB
Tofacitinib (CP-690550) Citrate	JAK
GDC-0152	IAP
AZD3514	Androgen Receptor
AZ20	ATM/ATR
GSK126	Histone Methyltransferase
EPZ5676	Methyltransferase
GSK J4 HCl	Others
LDK378	ALK
IWP-2	Wnt/beta-catenin
GSK2334470	PDK-1
PF-3758309	PAK
HSP990 (NVP-HSP990)	HSP (e.g. HSP90)
AZD3463	ALK
EPZ-6438	Histone Methyltransferase
PYR-41	E1 Activating
PR-619	DUB
P5091 (P005091)	DUB
BMS-833923	Hedgehog/Smoothened
AZD1080	GSK-3
C646	Histone Acetyltransferase
10058-F4	c-Myc
AVL-292	BTK
IOX1	Histone demethylases
OG-L002	Histone demethylases
SGC-CBP30	Epigenetic Reader Domain
CNX-774	BTK
MM-102	Histone Methyltransferase
JIB-04	Histone demethylases
PFI-2	Histone Methyltransferase
CPI-203	Epigenetic Reader Domain
GSK2606414	PERK
6H05	Rho
K-Ras(G12C) inhibitor 9	Rho
SH-4-54	STAT
OTX015	BET
LEE011	CDK

LDC000067	CDK
PI-1840	Proteasome
JNK Inhibitor IX	JNK
GNF-5837	Trk receptor
Afuresertib (GSK2110183)	Akt
GDC-0994	ERK
UNC0379	Histone Methyltransferase
GSK-LSD1 2HCl	Histone Demethylase
GSK J1	Histone Demethylase
INCB024360	IDO
BRD4770	Histone Methyltransferase
BV-6	IAP
EI1	Histone Methyltransferase
MI-2 (Menin-MLL Inhibitor)	Histone Methyltransferase
LDC1267	Axl
CPI-360	Histone Methyltransferase
CH5183284 (Debio-1347)	FGFR
YK-4-279	DNA/RNA Synthesis
AZD6738	ATM/ATR
Verdinexor (KPT-335)	CRM1
EPZ015666	Histone Methyltransferase
Pexmetinib (ARRY-614)	p38 MAPK
Pexidartinib (PLX3397)	CSF-1R
BI-847325	MEK
PFI-4	Epigenetic Reader Domain
Epacadostat (INCB024360)	IDO
NSC 23766	Rac
BMS-345541	IκB/IKK
Pacritinib (SB1518)	JAK
Idasanutlin	MDM2/p53
iBet762	BET
ABT-263	BCL2, BCL-XL, BCL-w
ABT-199	BCL2
Obatoclax	BCL2-family
dynasore	Dynamin
Dyngo4a	Dynamin
GDC-0973	MEK
Fenretinide	Retinoid Acid Receptor
JQ-1	BET
Birinapant	IAP
Doxorubicine	DNA
Vincristine	Microtubuli
Etoposide	Topoisomerase

Table 5 Compounds of the drug screen library

Manuscript II

Fenretinide acts as potent radiosensitizer for treatment of rhabdomyosarcoma

Eva Brack[1,2], Sabine Bender [3], Marco Wachtel [1,2], Martin Pruschy[3], Beat W. Schäfer [1,2*]

[1]Department of Oncology and [2]Children's Research Center,
University Children's Hospital Zurich, Zurich, Switzerland

[3]Department of Radiology Biology, Radio-Oncology, University Hospital Zurich, Switzerland

Corresponding Author: Beat W. Schäfer
Steinwiesstrasse 75
8032 Zurich
Switzerland

Keywords: Rhabdomyosarcoma, fenretinide, radiation therapy, radiosensitizer, reactive oxygen species

Conflict of interest: The authors declare no conflict of interest.

Abstract

Alveolar rhabdomyosarcomas (aRMS) are highly aggressive childhood malignancies that are mainly treated by conventional chemotherapy, surgery and radiotherapy. Since radiotherapy is associated with a high burden of side effects, addition of radio-sensitizers would be beneficial. Here, we thought to assess the role of fenretinide, a potential agent for aRMS treatment, as radio-sensitizer for aRMS treatment.

Survival of human aRMS cells was assessed after combinatorial treatment with fenretinide and ionizing radiation (IR) by cell viability and clonogenic assays. Further, the underlying mechanisms of action and cell death modality were studied.

The combinatorial treatment with fenretinide and IR significantly reduced cell viability further compared to single agent treatment. Mechanistically, this was accompanied by enhanced production of reactive oxygen species, initiation of cell cycle arrest and induction of apoptosis. Interestingly, the combinatorial treatment also triggered a new form of dynamin-dependent macropinocytosis, which was previously described in fenretinide-only treated cells.

Our data suggest that fenretinide acts in combination with IR to induce cell death in aRMS cells and might act as novel radio-sensitizer for the treatment of this disease.

Introduction

Radiation therapy (RT) applying ionizing radiation (IR) is along with chemotherapy and surgery part of the standard therapeutic regiment for many malignancies. In the pediatric patient population this treatment is used e.g. in neuroblastoma, medulloblastoma, Ewings and soft tissue sarcomas (1). Rhabdomyosarcoma (RMS) is the most common soft tissue malignancy in children and young adolescents. Especially the alveolar rhabdomyosarcoma subgroup (aRMS) is associated with a poor outcome due to its aggressiveness and a high risk of relapse (2-5).

Earlier, we identified the small molecule fenretinide (retinoic acid p-hydroxyanilide) as a potential additional treatment option for this malignancy, as it was found to have strong cytotoxic effects on aRMS cells (6). In follow-up experiments, we further elucidated the underlying mechanism of cell death which depends on enhanced production of reactive oxygen species, an increased accumulation of cytoplasmic vesicles resembling the characteristics of macropinocytosis (First manuscript), a recently described new form of cell death (7, 8).

The effectiveness of ionizing radiation is well studied and has direct and indirect effects on cancer cells. As direct action, IR damages DNA, proteins and lipids, which eventually results in genomic instability, cell cycle arrest and cell death (9). Indirect effects occur through radiolysis of water and the production of reactive oxygen species (ROS). The unpaired electrons in ROS are highly reactive and can induce DNA single- and double-strand breaks (10-13). Further, they act as a signaling molecules driving cells towards cell death.

On the other hand, ionizing radiation is associated with considerable side effects and induces damages to non-diseased tissues and organs depending on the dose administered and absorbed. This may cause relevant side effects especially in pediatric patients which become apparent only later in life such as growth retardation, reduced neurocognitive development, infertility, and most importantly the risk to develop secondary malignancies (14, 15). One current goal in radiobiology is therefore to minimize these side effects, while at the same time maximizing radiation benefits

against tumor cells. Image-guided and intensity-modulated RT for example have led to significant improvements in the field (16, 17).

Another well recognized option to achieve this goal is the simultaneous administration of radiosensitizers (18). Drugs are defined as radiosensitizing agents when they render cancer cells more vulnerable to radiation therapy. Wang et al categorizes radiosensitizers based on their structures into three categories: small-molecule chemicals, nanostructures, and macromolecules (19). Bentzen and colleagues explained the different mechanisms by using the term cytotoxic enhancement, where the combinatorial treatment in general modulates response to DNA damage (20).

Fenretinide is a small-molecule compound that is well established in the treatment for multiple malignancies during adulthood and is also already in clinical use in children (Clinicaltrials.gov ID NCT02163356) (21, 22). Moreover its side-effect profile is very favorable with no limiting toxicities (23).

Multiple studies suggest that the fenretinide induced cell death occurs mainly through apoptosis in most of the cell lines. This is achieved either through the production of reactive oxygen species (ROS) or the involvement of lipid second messengers (24-28).

So far, fenretinide has not been investigated together with RT in the treatment of rhabdomyosarcoma. However, fenretinide combined with radiation therapy is currently under investigation for the treatment of diffuse intrinsic pontine glioma (DIPG) and suggests promising results in mice (29).

In the current study we therefore aimed to characterize the potential use of the fenretinide as radiosensitizer. Additionally, we described the underlying mechanisms of cell death occurring during combination treatment in more detail. The study highlights this combination as potential novel treatment option for aRMS.

Material and Methods

Gamma Irradiation

Irradiation was performed using an Xstrahl 200 kV X-Ray unit (Ratingen, Germany) at 100 cGy/minute. Depending on the question, different intensities of radiation was applied to the cells.

Cell Culture

The alveolar rhabdomyosarcoma cell line Rh4 (provided by Peter Houghton, Greehey Children's Cancer Research Institute, San Antonio, Texas, USA) was maintained in high glucose Dulbecco's Modified Eagle Medium (DMEM, Sigma-Aldrich, Buchs, Switzerland), supplemented with 100 U/mL penicillin/streptomycin (Invitrogen, ThermoFisher, Waltham, Massachusetts, USA), 2 mM L-glutamine (BioConcept, Allschwil, Switzerland) or Glutamax (Gibco, ThermoFisher, Waltham, Massachusetts, USA) , and 10% fetal bovine serum (FBS, Sigma-Aldrich, Buchs, Switzerland), in 5% CO2 at 37°C. ARMS cell lines were regularly tested for Mycoplasma infection, authenticated by short tandem repeat analysis (STR profiling) in 2011/2014 and positively matched with reference data (30).

Cell viability assay

80000 Rh4 cells/ml were seeded in 96 well format (TC-Plate, Standard F, Sarstedt, Nümbrecht, Germany) in 100µL medium. The studied compounds (see Table 6) were added for 72hours. For measurement of cell viability, 10µl WST-1 reagent (Sigma-Aldrich-Aldrich, Buchs, Switzerland) was added. After 30 minutes incubation at 37°C in the dark, absorbance at 440 and 640 nm were measured with a Synergy™ HT multi-detection microplate reader (BioTek, Winooski, Vermont, USA). The difference of the two values was calculated (delta optical density; ΔOD) and values from pure medium were subtracted as background.

Clonogenic cell survival assays

Clonogenic cell survival was determined by the ability of single cells to form colonies in vitro (31). 50000 cells were seeded in 10cm dishes format (TC-Dish, 100, Standard, Sarstedt, Nümbrecht, Germany). The following day, the cells were treated with the desired concentration of fenretinide in DMEM, high glucose supplemented with 100 U/mL penicillin/streptomycin ,2 mM Glutamax and 10% FBS, and irradiated with the desired intensity. After 12 days of culturing in 5% CO2 at 37°C the medium was removed and the cells fixed with glutaraldehyde (6.0%) and stained with crystal violet (0.5%).

Flow Cytometry

For all flow cytometry experiments, 150000 Rh4 cells were seeded per well in Corning Costar 6-well plates (Sigma-Aldrich-Aldrich, Buchs, Switzerland). After treatments, cells were detached from the plates using Trypsin, washed once with PBS and re-suspended in 0.5 ml indicated buffer. Data was acquired with the LSRII Fortessa (BD Biosciences, San Jose, California, USA) flow cytometer or the BD FACS Canto system (BD Biosciences, San Jose, California, USA). Acquired data was analysed with FlowJo Software, Version 9.9.6 (Tree Star Inc., Ashland, Orlando, USA). All used fluorescent stains are listed in Table 7 in Supplementary Material and Methods.

Pan ROS measurement

Cells were seeded and treated with the desired compounds according to table 6 (in the Supplementary Material and Methods). Simultaneously 4µM CellRox Deep red (ThermoFisher, Waltham, Massachusetts, USA) solution was added to the medium. One hour after drug treatment, cells were irradiated with the desired intensity. After 18 hours cells were collected, washed in PBS and re-suspended in FluoroBrite live cell fluorescence imaging medium DMEM (ThermoFisher,

Waltham, Massachusetts, USA). CellRox signal (50’000 events per sample) was acquired with excitation laser 640 nm and Emission filter 670/14.

Mitochondrial ROS measurement

Cells were seeded and treated with the desired compounds according to table 7. One hour after drug treatment, cells were irradiated with the desired intensity. After 18 hours, cells were collected, washed in PBS and re-suspended in MitoSox (ThermoFisher, Waltham, Massachusetts, USA) Solution (10µM MitoSox in PBS) for 30min at 37°C in the dark. MitoSox signal (50’000 events per sample) was acquired with excitation laser 561 nm, and Emission filter 570 LP, 525/50.

Cell cycle Analysis

Cells were seeded and treated with the desired concentration of fenretinide. One hour after drug treatment, cells were irradiated with the desired intensity. After 24h and 48h, cells were, collected, washed with PBS and fixed with ice cold 70 % ethanol for four hours at -20°C. Then cells were washed with PBS three times and incubated for 30 min with propidium iodide 20 mg/ml (Sigma-Aldrich, Buchs, Switzerland) and RNAse A (200mg/ml) (Qiagen, Hilden, Germany) in TritonX-PBS 0.1% (Sigma-Aldrich, Buchs, Switzerland). PE signal (50’000 events per sample) was acquired with excitation laser 488 nm, and Emission filter 585/42.

Acridine Orange (AO) Staining

Acridine Orange (Sigma-Aldrich-Aldrich, Buchs, Switzerland) (AO) was used to measure fluid-phase endocytic uptake induced by fenretinide treatment and IR after 48h. Cells were seeded and treated with the desired compounds according to table 6 in Supplementary Material and Methods. One hour after drug treatment, cells were irradiated with the desired intensity. After 48 hours Acridine Orange (2.7 µM) in FluoroBrite DMEM live cell fluorescence imaging medium

(ThermoFisher, Waltham, Massachusetts, USA) was added to the cells 4 h prior to their preparation for flow cytometry. Cells were collected, washed in PBS and re-suspended in PBS. AO signal (50’000 events per sample) were acquired with excitation laser 488 nm and 561, emission filter 505 LP, 530/30 and 635LP, 670/30.

Epifluorescence microscopy

All images were taken with the Zeiss Axio Observer (Zeiss, Oberkochen, Germany) equipped with a Hamamatsu Orca Flash 4.0 V2, sCMOS cooled fluorescence camera (Hamamatsu, Hamamatsu City, Japan) and an objective with 20x magnification. All fluorescent stains used can be found in table 2 in Supplementary Material and Methods. For data processing, images were exported as TIFF files and the mean integrated density was quantified with the image processing software Fiji (32). The integrated density value of an image was divided by the number of cells (counted on the phase image). Per treatment a minimum of four pictures was taken.

LY fluorescence microscopy

50000 cells/ml were seeded in Falcon™ chambered cell culture slides (4 wells, Corning) (Thermo Scientific, ThermoFisher, Waltham, Massachusetts, USA) and treated with 3µM fenretinide. One hour after drug treatment, cells were irradiated with the desired intensity. After 48h, cells were subsequently stained with Lucifer Yellow (820µM) in FluoroBrite DMEM for 4 h at 37°C, 5% CO2 after removal of the culturing medium. Afterwards, cells were washed with PBS and fixed with 4 % PFA for 15 min at room temperature. After three PBS washes, the chamber was removed, and the cells were mounted in Vectashield mounting medium with 4′,6-Diamidin-2-phenylindol (Vector Laboratories, Burlingame, California, USA).

Immunoblot

Whole cell extracts were prepared from cells lysed with RIPA buffer (50 mM Tris-Cl (pH 7.5), 150 mM NaCl, 1% NP-40, 0.5% Na-deoxycholate, 1 mM EGTA, 0.1% SDS, 50 mM NaF, 10 mM sodium β-glycerolphosphate, 5 mM sodium pyrophosphate, 1 mM sodium orthovanadate and supplemented with Complete Mini Protease Inhibitor cocktail (all from Sigma Aldrich, Buchs, Switzerland). P Proteins were separated using NuPAGE™ Novex™ 4-12% Bis-Tris gels (ThermoFisher, Waltham, Massachusetts, USA) and transferred to nitrocellulose membranes (GE Healthcare Life Sciences). Membranes were blocked with 5% milk powder in TBS/0.05% Tween and subsequently incubated with respective primary antibodies overnight at 4°C. After three time washing in TBS-0.05% tween, membranes were incubated with horseradish peroxidase (HRP)-linked secondary antibody for 1h at RT. A

Following antibodies were used: Rabbit, anti-phospho-Histone H2A.X (Ser139) (Cat# 9718), rabbit anti-cleaved-Caspase 7 (Cat# 9491), rabbit anti-cleaved PARP (Cat# 5625), rabbit anti-GAPDH (Cat#2118) all from Cell Signaling (Cell Signaling Technology, Danvers, Massachusetts, USA). Horseradish peroxidase-conjugated goat anti-rabbit from Cell Signaling (Cat# 7077) were used as secondary antibodies. After three additional washing steps with TBS/0.05% Tween, proteins were detected by chemiluminescence using either the Pierce™ ECL Western Blotting Substrate (ThermoFisher, Waltham, Massachusetts, USA) or Supersignal Western blotting reagent (ThermoFisher, Waltham, Massachusetts, USA) and a ChemiDoc MP (BioRad Laboratories AG, Cressier, Switzerland) imager. The images were analysed with the software Image Lab Version 6.0. (BioRad Laboratories AG, Cressier, Switzerland).

Statistics

The software GraphPad Prism (La Jolla, California, USA) was used for all statistical analyses. Comparisons of differences between two groups were analysed by parametric paired t-test. The data were considered significant when $p \leq 0.05$.

Results

We previously demonstrated that fenretinide alone efficiently induces a novel dynamin-dependent cell death in aRMS cells (Manuscript 1), which we also confirmed here (Figure 1A, left panel, Table 1). As radiotherapy is part of the aRMS standard treatment regimens, we questioned if the combination radiotherapy with fenretinide would enhance the anti-tumor effect on aRMS cells. In a first step, we therefore co-treated Rh4 cells with different single doses of radiation (5 and 10Gy) and two low doses of fenretinide (IC10 and IC20, equals to 1.9 and 2.6µM) and assessed cell viability after 72h by WST-1 assay. Indeed, for all combination treatments, cell viability decreased significantly at this time point. We found a dose dependent combinatorial effect of fenretinide with IR, whereby the combination at the lower radiation dose reduced cell viability to levels comparable to cells treated at higher radiation doses alone (Figure 1A, Table 1 and 2). Next, we assessed the combinatorial effect on clonogenic cell survival. In this setting, we observed a strong combinatorial effect already at lower concentrations of fenretinide (0.5µM) together with low radiation doses of 2Gy (Figure 2B).

In a next step, we investigated the mechanisms of cell death that were induced by the combination treatment. Western blot analysis of cleaved Caspase 7 and cleaved PARP revealed induction of apoptosis in single treated cells, which was enhanced by the combination treatment. The addition of Z-vad, a pan-caspase inhibitor abolished both caspase 7 and PARP cleavage (Figure 2C). Next, we were interested to see whether the combination would induce enhanced phosphorylation of the histone H2AX (γH2AX) as a well-established marker for DNA double-strand breaks (33).Western blot analysis showed enhanced phosphorylation of γH2AX in the combinatorically treated cells, most prominently after 30 minutes and rapidly decreasing over the next four hours (Figure 1D). Based on these findings, we further investigated the effect of fenretinide and IR on cell cycle distribution. Fenretinide alone did not change the cell cycle distribution after 24 hours. In contrast, single treatment of IR induced a dose-dependent G2/M arrest (Figure 1F, left panel) which was

further increased by the combination in a dose-dependent manner. After 48h, we still saw a slight G2/M arrest but also an emerging Sub-G1 peak, which indicates the induction of cell-death after that treatment period (Figure 1F, right panel). These data suggest that fenretinide combined with IR enhances a G2/M cell cycle arrest which eventually leads to cell death.

Next, we wanted to see whether the combination treatment affected reactive oxygen species (ROS) production. Indeed, increasing concentrations of fenretinide and increasing doses of IR significantly enhanced ROS production (pan-ROS) compared to the control cells. This was also significantly more prominent in the combination treatment (Figure 2A, Table 3). To confirm specificity, we co-treated cells with the hydrogen-peroxide scavenger N-Acetylcysteine (NAC) and observed a significant reduction of ROS production (Figure 2A, Table 3). Since we previously found mitochondrial derived ROS to be the main source of ROS under fenretinide treatment, we also analyzed cells with the specific MitoSox staining. We observed a significant dose-dependent increase of mitochondrial ROS both upon fenretinide treatment alone, as well as a further increase under combination treatment. Interestingly, radiation alone, did not enhance mitochondrial ROS production (Figure 2B, Table 4).

To further characterize and validate the impact of ROS species on cell death, we treated the cells additionally with Vitamin C as a well-recognized pan-ROS scavenger and MitoTempo, a mitochondrial-specific ROS Scavenger. We observed an almost complete rescue from cell-death by both Vitamin C and MitoTempo (Figure 2C, Table 5).

Taken together, fenretinide and IR induce the production of reactive oxygen species whereas mitochondrial derived superoxides are mainly produced by fenretinide.

Previously, we could demonstrate that fenretinide induced the formation of large phase lucent cytoplasmic vesicles, which derive from increased macropinocytosis. Therefore, our next aim was

to clarify whether fenretinide would also enhance accumulation of those cytoplasmic vesicles when combined with IR. Hence, we co-treated cells either with dynasore, Vitamin C or Z-vad and measured Acridine Orange (AO) staining to assess endocytosis (Figure 3, A-C and Supplementary Figure 1, A-C). These experiments revealed a significant increase in dye uptake in the fenretinide-only treated cells which was further enhanced by IR treatment. Interestingly, IR treatment alone only minimally affected the uptake of AO. In addition, co-treatment of the cells with Vitamin C and dynasore decreased the dye uptake in treated cells (Figure 3A+B, Supplementary Figure 1 A+B). No change was observed in the IR-only treated cells (Figure 3A and 3B, Supplementary Figure 1 A+B). As expected, the addition of Z-vad did not change the levels of endocytosis as measured by AO dye uptake (Figure 3C, Supplementary Figure 1A).

Finally, to validate these findings we used the fluid phase dye Lucifer Yellow and performed fluorescence microscopy. We confirmed a non-significant increase of dye uptake when cells were treated with IR alone, whereas a significant increase was observed in the combination treatments (Figure 3D). These findings suggest that the combination of IR with fenretinide significantly enhanced the uptake of fluid phase dyes whereas IR alone does not. Further, enhanced endocytosis might depend on mitochondrial ROS production and involve dynamin GTPases as most likely triggering factors.

Discussion

The aim of this study was to evaluate the potential of fenretinide as a radiosensitizer for co-treatment of aRMS cells. In radiation therapy, timing, duration, and dose are crucial factors for its effectiveness and to minimize long term side effects. Therefore, identification of combinations of agents and treatment modalities that act synergistically is most desirable. Radiosensitizing agents are capable to broaden the therapeutic window and selectively augment radiation effects in tumour cells while also sparing the surrounding tissue. Fenretinide combined with radiation therapy is under investigation for the treatment of diffuse intrinsic pontine glioma (DIPG) and shows promising results in mouse experiments (29). However, up-to-now there are only few other studies exploring this combinatorial effect in additional tumors.

We already showed that fenretinide has a strong anti-tumour effect in aRMS cells through the production of mainly mitochondrial derived reactive oxygen species, which induced a new form of a dynamin-dependent vesicular cell death (manuscript one). Here, first experiments demonstrated an increased dose-dependent combinatorial anti-tumor effect. This enabled us to reduce both treatment dosages with a persisting effect already at 2Gy which also impaired clonogenic growth.

The underlying cell death mechanism was identified in part as apoptosis. However, it also led to induction of ROS and subsequent DNA damage. Radiation therapy is known to induce G2 cell cycle arrest following DNA damage (34), which was confirmed in our findings. It is also known that fenretinide can induce cell cycle arrest (35). Our results also showed impaired cell cycle progression with mainly G2/M arrest most pronounced in the combination treatment. This is an important finding as it is one of the hallmarks of cancer that tumour cells sustain proliferative signalling even after DNA damage (36), and therefore restoration of a normal physiological response – induction of cell death - is desirable.

Our experiments using a pan-ROS detectant, further revealed a significant increase of ROS production in irradiated cells. In our previous experiments we were able to show that fenretinide alone induces mitochondrial derived ROS. Here, irradiation mainly induced the production of hydrogen peroxide, as we were able to scavenge them with NAC. Hence triggering different ROS species in our treatment combination is important in the context of resistance development, as cancer cells are known to upregulate antioxidant pathways (37).

To identify the cell death mechanism in more detail we evaluated whether IR would also trigger dynamin-dependent increased macropinocytosis as found previously as the prominent mode of action of fenretinide. As shown above, we were able to identify increased macropinocytosis in the co-treated cells. In the irradiated-only cells, this increase was minimal when assessed by flow cytometry and a bit more prominent when assessed with light microscopy. The discrepancy between flow cytometry and light microscopy might actually be an analysis bias and explained by the fact that ionizing irradiation induces cell cycle arrest and senescence (as observed on microscopy imaging) and subsequently a morphologically apparent change of cells. As they become bigger, they are capable to take up more dye and the analysis will show an increased integrated mean density index per cell. Due to the gating strategy applied in flow cytometry, the cell size is not relevant. However, in the irradiated-only cells the dye uptake could be inhibited neither with a Dynamin Inhibitor nor a ROS-scavenger, as was the case for fenretinide treated cells. Based on these findings it is unlikely that radiation induced cell death is a result of increased macropinocytosis, however this cell death mode can be triggered and enhanced upon additional fenretinide treatment, most likely from the interaction of a distinct population of ROS.

Taken together our findings support the hypothesis that fenretinide acts as a promising radiation sensitizer in co-treatment of alveolar rhabdomyosarcoma cells. Different modes of cell death mechanism are activated and enhanced by these two treatment modalities. Reactive oxygen species

and DNA damage are the main underlying triggering factors, whereas macropinocytosis as seen in fenretinide treatment plays only a minor role in IR-only treated cells. A combinatorial treatment with both modalities however may help to reduce development of resistances and increases the therapeutic window in the local treatment. Hence, it might be a promising treatment regimen in paediatric patients with alveolar rhabdomyosarcoma.

References

1. Koscielniak E KT. CWS-guidance for risk adapted treatment of soft tissue sarcoma and soft tissue tumours, in children, adolescents, and young adults vol Version 1.6.1. Cooperative Weichteilsarkom Studie Group-CWS der GPOH, . (2014)

2. Brien D, Jacob AG, Qualman SJ,Chandler DS. Advances in pediatric rhabdomyosarcoma characterization and disease model development. *Histol Histopathol* (2012) 27: 13-22.

3. Williamson D, Missiaglia E, de Reynies A, Pierron G, Thuille B, Palenzuela G, et al. Fusion gene-negative alveolar rhabdomyosarcoma is clinically and molecularly indistinguishable from embryonal rhabdomyosarcoma. *J Clin Oncol* (2010) 28: 2151-8. doi: 10.1200/jco.2009.26.3814

4. Dantonello TM, Int-Veen C, Schuck A, Seitz G, Leuschner I, Nathrath M, et al. Survival following disease recurrence of primary localized alveolar rhabdomyosarcoma. *Pediatr Blood Cancer* (2013) 60: 1267-73. doi: 10.1002/pbc.24488

5. Fuchs J, Urla C, Sparber-Sauer M, Schuck A, Leuschner I, Klingebiel T, et al. Treatment and outcome of patients with localized intrathoracic and chest wall rhabdomyosarcoma: a report of the Cooperative Weichteilsarkom Studiengruppe (CWS). *J Cancer Res Clin Oncol* (2018) 144: 925-34. doi: 10.1007/s00432-018-2603-y

6. Herrero Martin D, Boro A,Schafer BW. Cell-based small-molecule compound screen identifies fenretinide as potential therapeutic for translocation-positive rhabdomyosarcoma. *PLoS One* (2013) 8: e55072. doi: 10.1371/journal.pone.0055072

7. Maltese WA,Overmeyer JH. Methuosis: nonapoptotic cell death associated with vacuolization of macropinosome and endosome compartments. *Am J Pathol* (2014) 184: 1630-42. doi: 10.1016/j.ajpath.2014.02.028

8. Overmeyer JH, Kaul A, Johnson EE,Maltese WA. Active ras triggers death in glioblastoma cells through hyperstimulation of macropinocytosis. *Mol Cancer Res* (2008) 6: 965-77. doi: 10.1158/1541-7786.mcr-07-2036

9. Powell S,McMillan TJ. DNA damage and repair following treatment with ionizing radiation. *Radiotherapy and Oncology* (1990) 19: 95-108. doi: 10.1016/0167-8140(90)90123-E

10. Ward JF. Biochemistry of DNA lesions. *Radiat. Res.* Suppl. 8 (1985) S103–S11.

11. Diehn M, Cho RW, Lobo NA, Kalisky T, Dorie MJ, Kulp AN, et al. Association of reactive oxygen species levels and radioresistance in cancer stem cells. *Nature* (2009) 458: 780. doi: 10.1038/nature07733 https://www.nature.com/articles/nature07733#supplementary-information

12. Lu L, Dong J, Wang L, Xia Q, Zhang D, Kim H, et al. Activation of STAT3 and Bcl-2 and reduction of reactive oxygen species (ROS) promote radioresistance in breast cancer and overcome of radioresistance with niclosamide. *Oncogene* (2018) doi: 10.1038/s41388-018-0340-y

13. Hatzi VI, Laskaratou DA, Mavragani IV, Nikitaki Z, Mangelis A, Panayiotidis MI, et al. Non-targeted radiation effects in vivo: A critical glance of the future in radiobiology. *Cancer Letters* (2015) 356: 34-42. doi: https://doi.org/10.1016/j.canlet.2013.11.018

14. Jaffray DA, Lindsay PE, Brock KK, Deasy JO,Tomé WA. Accurate Accumulation of Dose for Improved Understanding of Radiation Effects in Normal Tissue. *Int J Radiat Oncol Biol Phys* (2010) 76: S135-9. doi: 10.1016/j.ijrobp.2009.06.093

15. Jaffray DA, *Delineating Organs at Risk in Radiation Therapy*. 2014: Springer Science & Business Media.

16. Raziee H, Moraes FY, Murgic J, Chua MLK, Pintilie M, Chung P, et al. Improved outcomes with dose escalation in localized prostate cancer treated with precision image-guided radiotherapy. *Radiotherapy and Oncology* (2017) 123: 459-65. doi: https://doi.org/10.1016/j.radonc.2017.04.003

17. Kong F, Ying H, Zhai R, Du C, Huang S, Zhou J, et al. Clinical outcome of intensity modulated radiotherapy for carcinoma showing thymus-like differentiation. *Oncotarget* (2016) 7: 81899-905. doi: 10.18632/oncotarget.11914

18. Bentzen SM. Preventing or reducing late side effects of radiation therapy: radiobiology meets molecular pathology. *Nat Rev Cancer* (2006) 6: 702-13. doi: 10.1038/nrc1950

19. Wang H, Mu X, He H,Zhang XD. Cancer Radiosensitizers. *Trends Pharmacol Sci* (2018) 39: 24-48. doi: 10.1016/j.tips.2017.11.003

20. Bentzen SM, Harari PM,Bernier J. Exploitable mechanisms for combining drugs with radiation: concepts, achievements and future directions. *Nat Clin Pract Oncol* (2007) 4: 172-80. doi: 10.1038/ncponc0744

21. Maurer BJ, Kang MH, Janeba J, Villablanca JG, Groshen S, Matthay KK, et al. Phase I Trial of Fenretinide Delivered Orally in a Novel Organized Lipid Complex in Patients with Relapsed/Refractory Neuroblastoma: A Report from the New Approaches to Neuroblastoma Therapy (NANT) Consortium. *Pediatr Blood Cancer* (2013) 60: 1801-8. doi: 10.1002/pbc.24643

22. Mohrbacher AM, Yang AS, Groshen S, Kummar S, Gutierrez ME, Kang MH, et al. Phase I Study of Fenretinide Delivered Intravenously in Patients with Relapsed or Refractory Hematologic Malignancies: A California Cancer Consortium Trial. *Clin Cancer Res* (2017) 23: 4550-55. doi: 10.1158/1078-0432.ccr-17-0234

23. Garaventa A, Luksch R, Lo Piccolo MS, Cavadini E, Montaldo PG, Pizzitola MR, et al. Phase I trial and pharmacokinetics of fenretinide in children with neuroblastoma. *Clin Cancer Res* (2003) 9: 2032-9.

24. Chen NE, Maldonado NV, Khankaldyyan V, Shimada H, Song MM, Maurer BJ, et al. Reactive Oxygen Species Mediates the Synergistic Activity of Fenretinide Combined with the

Microtubule Inhibitor ABT-751 against Multidrug-Resistant Recurrent Neuroblastoma Xenografts. *Mol Cancer Ther* (2016) 15: 2653-64. doi: 10.1158/1535-7163.mct-16-0156

25. Suzuki S, Higuchi M, Proske RJ, Oridate N, Hong WK,Lotan R. Implication of mitochondria-derived reactive oxygen species, cytochrome C and caspase-3 in N-(4-hydroxyphenyl)retinamide-induced apoptosis in cervical carcinoma cells. *Oncogene* (1999) 18: 6380-7. doi: 10.1038/sj.onc.1203024

26. Osone S, Hosoi H, Kuwahara Y, Matsumoto Y, Iehara T,Sugimoto T. Fenretinide induces sustained-activation of JNK/p38 MAPK and apoptosis in a reactive oxygen species-dependent manner in neuroblastoma cells. *Int J Cancer* (2004) 112: 219-24. doi: 10.1002/ijc.20412

27. Goto H, Takahashi H, Fujii H, Ikuta K,Yokota S. N-(4-Hydroxyphenyl)retinamide (4-HPR) induces leukemia cell death via generation of reactive oxygen species. *Int J Hematol* (2003) 78: 219-25.

28. Tosetti F, Vene R, Arena G, Morini M, Minghelli S, Noonan DM, et al. N-(4-hydroxyphenyl)retinamide inhibits retinoblastoma growth through reactive oxygen species-mediated cell death. *Mol Pharmacol* (2003) 63: 565-73.

29. Tsoli M, Yeung N, Valvi S, Joshi S, Franshaw L, Shen H, et al. DIPG-05. Combination of Synthetic Retinoid Fenretinide with Receptor Tyrosine Kinase Inhibitor as a Potential New Approach Against Diffuse Intrinsic Pontine Glimoma. *Neuro Oncol* (2017) 19: iv5-6. doi: 10.1093/neuonc/nox083.020

30. Hinson AR, Jones R, Crose LE, Belyea BC, Barr FG,Linardic CM. Human rhabdomyosarcoma cell lines for rhabdomyosarcoma research: utility and pitfalls. *Front Oncol* (2013) 3: 183. doi: 10.3389/fonc.2013.00183

31. Franken NAP, Rodermond HM, Stap J, Haveman J,van Bree C. Clonogenic assay of cells in vitro. Nature Protocols (2006) 1: 2315. doi: 10.1038/nprot.2006.339

32. Schindelin J, Arganda-Carreras I, Frise E, Kaynig V, Longair M, Pietzsch T, et al. Fiji: an open-source platform for biological-image analysis. Nat Methods (2012) 9: 676-82. doi: 10.1038/nmeth.2019

33. Bonner WM, Redon CE, Dickey JS, Nakamura AJ, Sedelnikova OA, Solier S, et al. γH2AX and cancer. Nature reviews. *Cancer* (2008) 8: 957-67. doi: 10.1038/nrc2523

34. Strasser-Wozak EM, Hartmann BL, Geley S, Sgonc R, Bock G, Santos AJ, et al. Irradiation induces G2/M cell cycle arrest and apoptosis in p53-deficient lymphoblastic leukemia cells without affecting Bcl-2 and Bax expression. *Cell Death Differ* (1998) 5: 687-93. doi: 10.1038/sj.cdd.4400402

35. Cowan AJ, Frayo SL, Press OW, Palanca-Wessels MC, Pagel JM, Green DJ, et al. Bortezomib and fenretinide induce synergistic cytotoxicity in mantle cell lymphoma through apoptosis, cell-cycle dysregulation, and IkappaBalpha kinase downregulation. *Anticancer Drugs* (2015) 26: 974-83. doi: 10.1097/cad.0000000000000274

36. Hanahan D,Weinberg RA. Hallmarks of cancer: the next generation. *Cell* (2011) 144: 646-74. doi: 10.1016/j.cell.2011.02.013

37. Schumacker PT. Reactive oxygen species in cancer cells: Live by the sword, die by the sword. *Cancer Cell* (2006) 10: 175-76. doi: https://doi.org/10.1016/j.ccr.2006.08.015

Figures

Figure 1

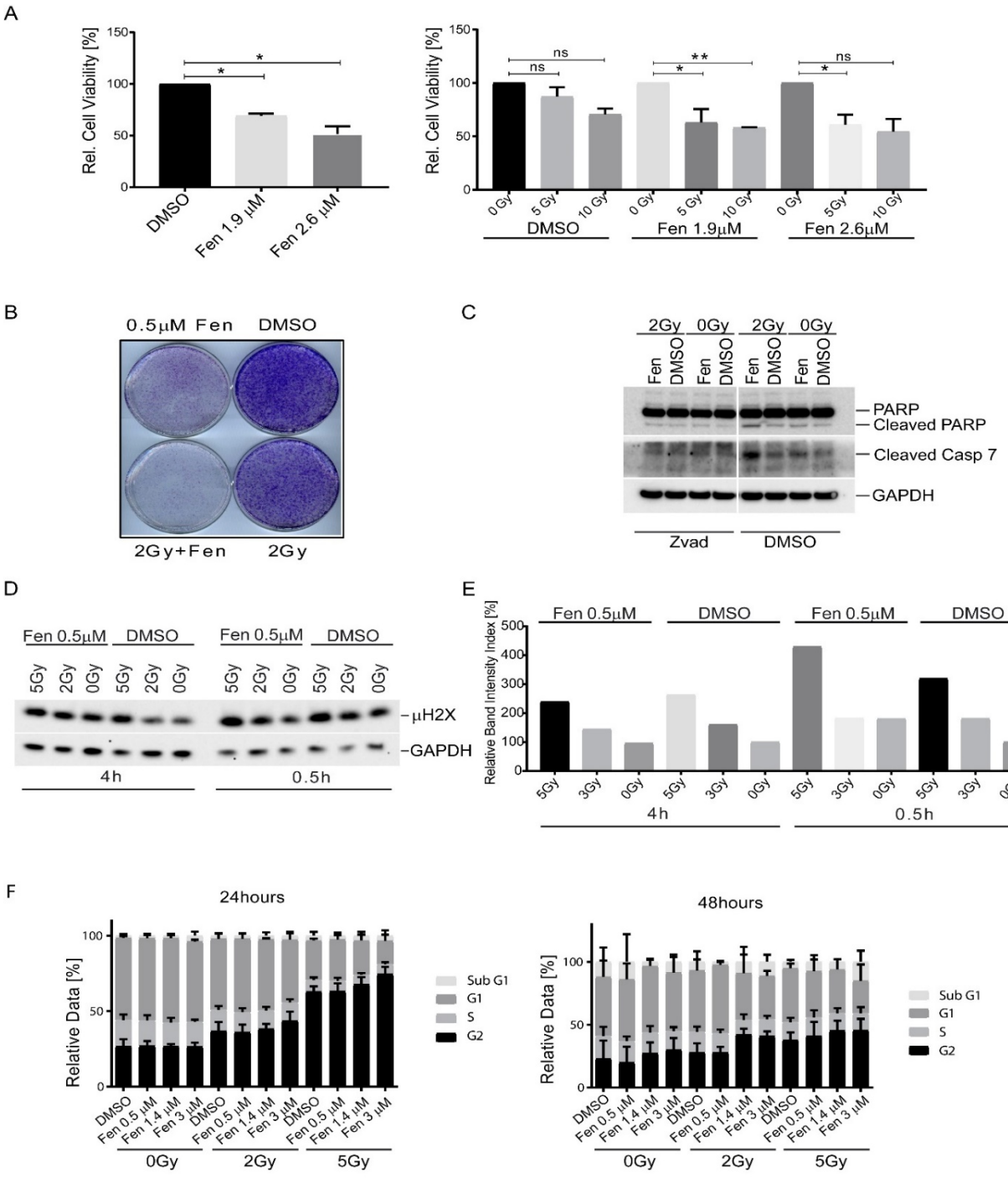

Figure 1: The combinatorial treatment of fenretinide and radiation therapy leads to an enhanced cell death. A) Cell viability of Rh4 cells treated with fenretinide alone (left panel) and cell viability assay of fenretinide and ionizing radiation at the indicated concentrations and dosages as determined by WST assay (right panel). **B)** 12 days clonogenicity assay of Rh4 cells treated with fenretinide and ionizing radiation at the indicated concentrations and dosages **C)** Western Blot using whole cell lysates from Rh4 cells treated with 0.5µM fenretinide and 2Gy radiation. Cleaved PARP, Caspase 7 and GAPDH activity was assessed **D)** Western Blot using whole cell lysates from Rh4 cells treated with 0.5µM fenretinide and either 2Gy or 5Gy radiation. Phosph-H2X and GAPDH activity was assessed (upper panel). Quantification of individual band intensities assessed by BioRad Software: Depicted are the normalized ratios of yH2X and GAPDH (lower panel). **E)** Cell cycle analysis determined by Flow Cytometry of Rh4 cells after 24h and 48h treated with fenretinide and radiation at the indicated concentrations and dosages. Staining with propidium iodid (20mg/ml).

Figure 2

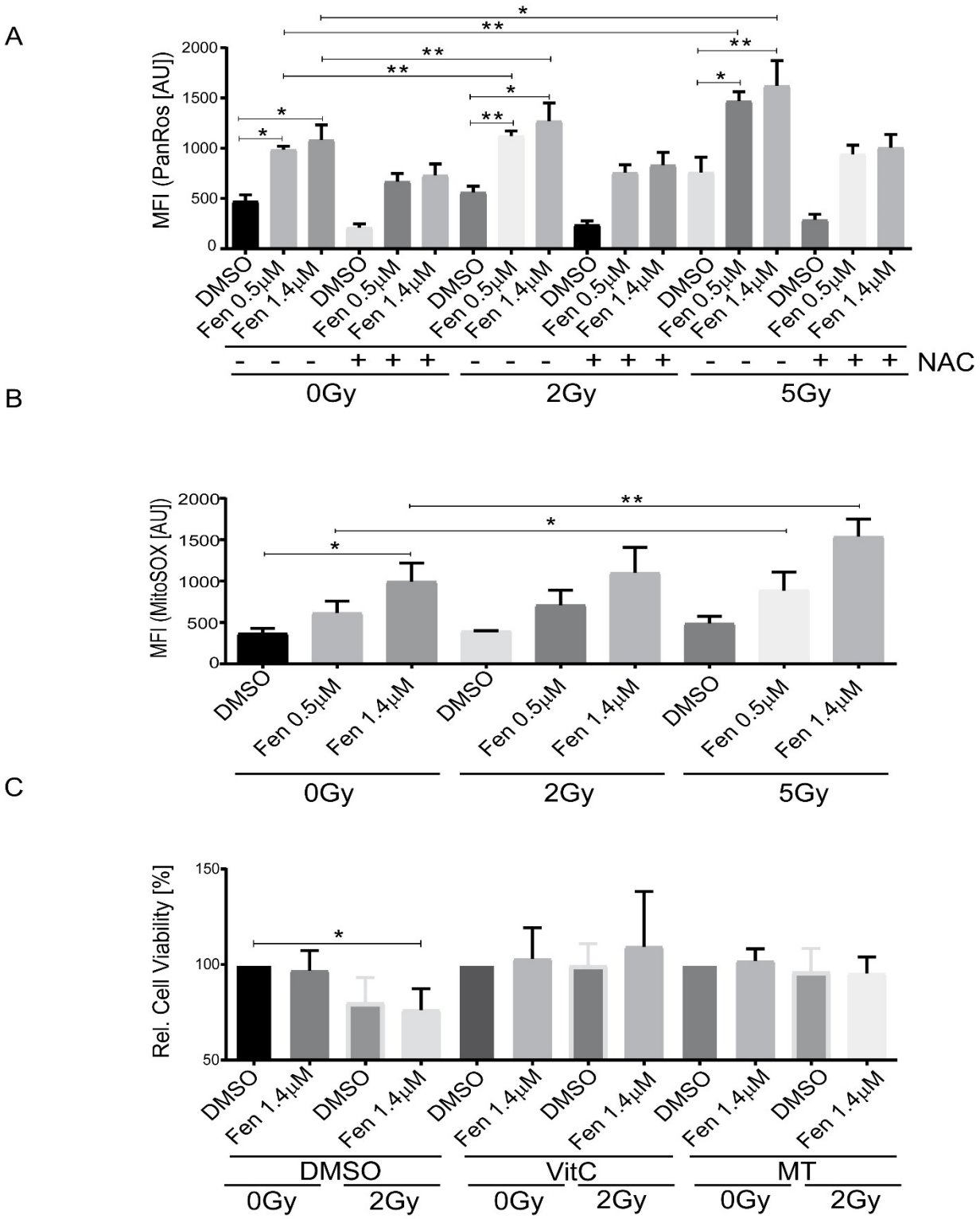
A
MFI (PanRos [AU])
2000
1500
1000
500
0
DMSO
Fen 0.5µM
Fen 1.4µM
NAC
0Gy
2Gy
5Gy
B
MFI (MitoSOX [AU])
C
Rel. Cell Viability [%]
150
100
50
DMSO
VitC
MT

Figure 2: The combination of fenretinide and ionizing radiation enhances the production of reactive oxygen species. A+B: Mean fluorescence index analysis of the flow cytometry data of Rh4 cells treated with fenretinide (0.5/1.4µM) and ionizing radiation (2/5Gy), further co-treatment with N-Acetylcysteine 15mM. Cells were stained with CellRox (4µM) **(A)** and MitoSox (10µM) **(B) C)** Cell viability of Rh4 cells treated with fenretinide (1.4µM) and ionizing radiation (2Gy) in presence or absence of the mitochondria specific ROS scavenger MitoTempo (300µM) or Vitamin C (50µM) as determined by WST assay.

Figure 3

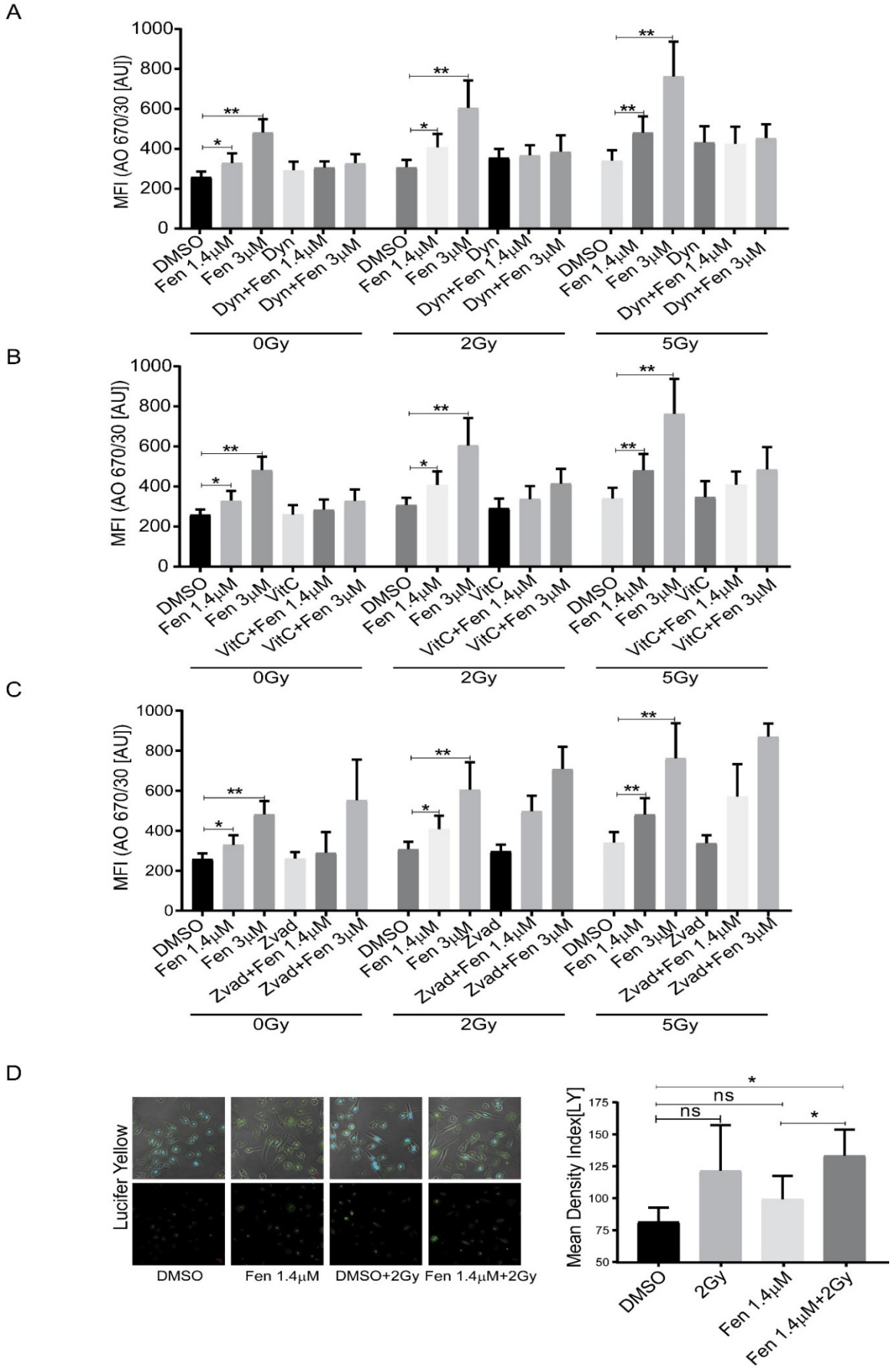
A
MFI (AO 670/30 [AU])
1000
800
600
400
200
0
DMSO
Fen 1.4μM
Fen 3μM
Dyn
Dyn+Fen 1.4μM
Dyn+Fen 3μM
0Gy
2Gy
5Gy
B
MFI (AO 670/30 [AU])
DMSO
Fen 1.4μM
Fen 3μM
VitC
VitC+Fen 1.4μM
VitC+Fen 3μM
0Gy
2Gy
5Gy
C
MFI (AO 670/30 [AU])
DMSO
Fen 1.4μM
Fen 3μM
Zvad
Zvad+Fen 1.4μM
Zvad+Fen 3μM
0Gy
2Gy
5Gy
D
Lucifer Yellow
DMSO
Fen 1.4μM
DMSO+2Gy
Fen 1.4μM+2Gy
Mean Density Index[LY]
175
150
125
100
75
50
ns
ns
*
*
DMSO
2Gy
Fen 1.4μM
Fen 1.4μM+2Gy

Figure 3: The combinatorial treatment of fenretinide and radiation therapy leads to an enhanced uptake of phase lucent dyes. A-C) Mean fluorescence index analysis of the flow cytometry data of fenretinide (1.4/3μM) and gamma radiation (2Gy/5Gy) treated Rh4 cells and co-treatment with dynasore (30μM) **(A),** Vitamin C (50μM) **(B)** or Z-VAD (100μM) **(C)**, stained with Acridine Orange (2.7 μM) using two different bandpass filters, here 530/30 (Bandpass filter 670/30 Supplementary Figure 1 A-C) **D)** Light fluorescence images of Rh4 cells treated or untreated with fenretinide (1.4μM) and gamma radiation (5Gy), stained with Lucifer Yellow (820μM). Quantification of the Relative Mean Density Index assed with Fiji software: Total integrated density value of an image was divided by the number of cells.

Supplementary Figure 1

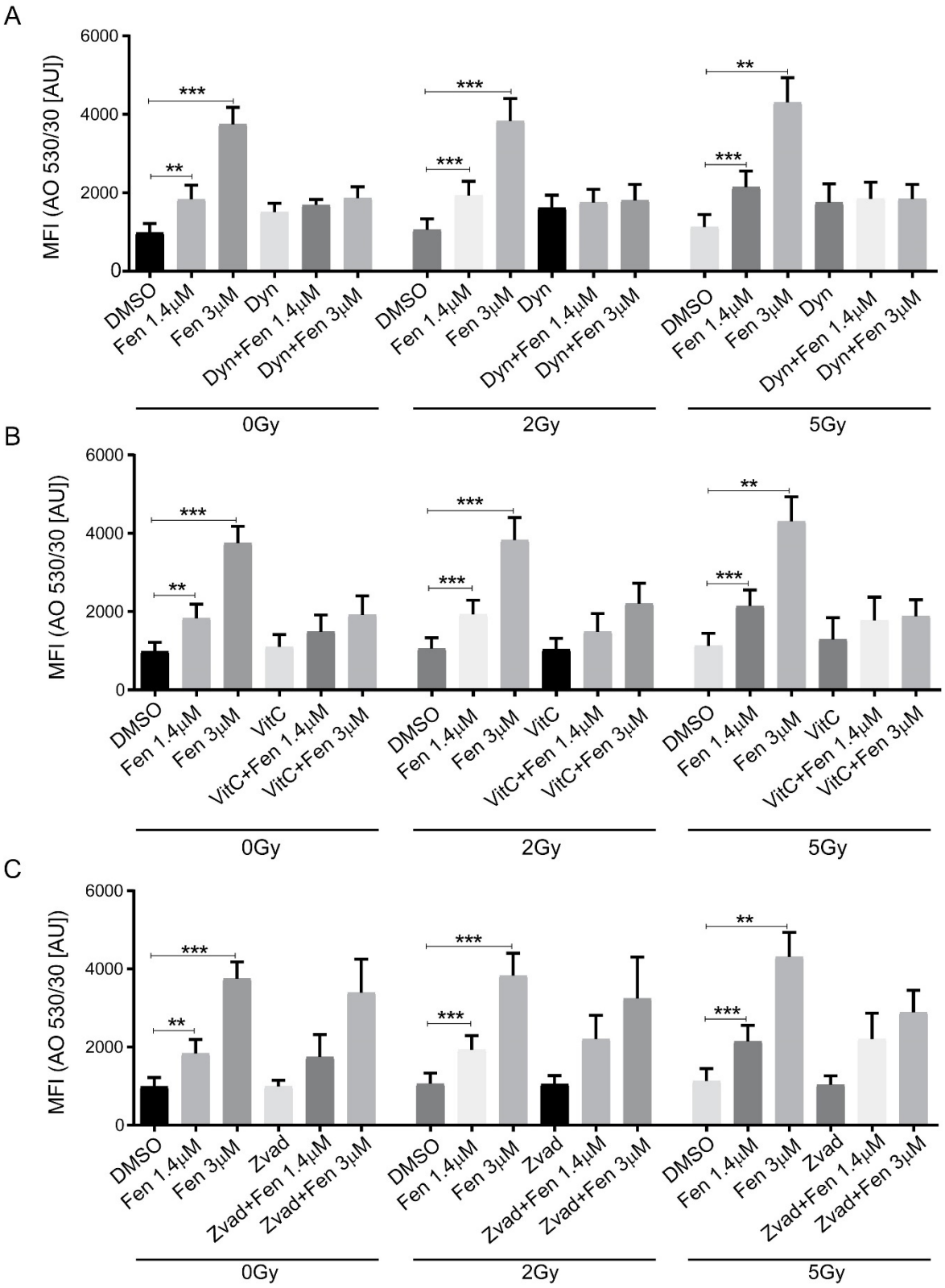

Supplementary Figure 1: The combinatorial treatment of fenretinide and radiation therapy leads to an enhanced uptake of phase lucent dyes. A-C) Mean fluorescence index analysis of the flow cytometry data of fenretinide (1.4/3μM) and gamma radiation (2Gy/5Gy) treated Rh4 cells and co-treatment with dynasore (30μM) **(A),** Vitamin C (50μM) **(B)** or Z-vad (100μM) **(C)**, stained with Acridine Orange (2.7μM) using two different bandpass filters, here 670/30 (Bandpass filter 530/30 Figure 3 A-C).

Supplementary Tables

Statistical Analysis

Table 1 Statistical analysis with paired Students t-test of cell viability assay using the software Prism 7

Treatment A	Treatment B	p-Value	Significance
DMSO, 0Gy	Fen 1.9µM, 0Gy	0.0018	**
DMSO, 0Gy	Fen 2.6µM, 0Gy	0.0079	**

Table 2 Statistical analysis with paired Students t-test of cell viability assay using Prism 7

Treatment A	Treatment B	p-Value	Significance
DMSO, 0Gy	DMSO, 5Gy	0.1313	ns
DMSO, 0Gy	DMSO, 10Gy	0.0826	ns
DMSO, 5Gy	Fen 1.9µM, 5Gy	0.0150	*
DMSO, 5Gy	Fen 2.6µM, 5Gy	0.0001	***
DMSO, 10Gy	Fen 1.9µM, 10Gy	0.1813	ns
DMSO, 10Gy	Fen 2.6µM, 10Gy	0.4102	ns
Fen 1.9µM, 0Gy	Fen 1.9µM, 5Gy	0.0365	*
Fen 1.9µM, 0Gy	Fen 1.9µM, 10Gy	0.0033	**
Fen 2.6µM, 0Gy	Fen 2.6µM, 5Gy	0.0190	*
Fen 2.6µM, 0Gy	Fen 2.6µM, 10Gy	0.1132	ns

Table 3 Statistical analysis with paired Students t-test of MFI analysis using Prism 7

Treatment A	Treatment B	p-Value	Significance
PAN-ROS NAC			
DMSO, 0Gy	DMSO, 2Gy	0.0343	*
DMSO, 0Gy	DMSO, 5Gy	0.0300	*
DMSO, 2Gy	Fen 0.5µM, 2Gy	0.0042	**
DMSO, 2Gy	Fen 1.4µM, 2Gy	0.0125	*
DMSO, 5Gy	Fen 0.5µM, 5Gy	0.0114	*
DMSO, 5Gy	Fen 1.4µM, 5Gy	0.0045	**
Fen 0.5µM, 0Gy	Fen 0.5µM, 2Gy	0.0053	**
Fen 0.5µM, 0Gy	Fen 0.5µM, 5Gy	0.0062	**
Fen 1.4µM, 0Gy	Fen 1.4µM, 2Gy	0.0099	**
Fen 1.4µM, 0Gy	Fen 1.4µM, 5Gy	0.0119	*
DMSO, 0Gy	NAC, DMSO, 0Gy	0.0043	**

Fen 0.5µM, 0Gy	NAC, Fen 0.5µM	0.0403	*
Fen 1.4µM, 0Gy	NAC, Fen 1.4µM	0.0123	*
DMSO, 2Gy	NAC, DMSO, 2Gy	0.0018	**
Fen 0.5µM, 2Gy	NAC Fen 0.5µM, 2Gy	0.0405	*
Fen 1.4µM, 2Gy	NAC Fen 1.4µM 2Gy	0.0123	*
DMSO, 5Gy	NAC, DMSO, 5Gy	0.0148	*
Fen 0.5µM, 5Gy	NAC Fen 0.5µM 5Gy	0.0308	*
Fen 1.4µM, 5Gy	NAC Fen 1.4µM, 5Gy	0.0182	*

Table 4 Statistical analysis with paired Students t-test of MFI analysis using Prism 7

Treatment A	**Treatment B**	**p-Value**	**Significance**
MitoSox			
DMSO, 0Gy	DMSO, 2Gy	0.5531	ns
DMSO, 0Gy	DMSO, 5Gy	0.0249	*
Fen 0.5µM, 0Gy	Fen 0.5µM, 2Gy	0.0523	ns
Fen 0.5µM, 0Gy	Fen 0.5µM, 5Gy	0.0289	*
Fen 1.4µM, 0Gy	Fen 1.4µM, 2Gy	0.1624	ns
Fen 1.4µM 0Gy	Fen 1.4µM, 5Gy	0.0036	**

Table 5 Statistical analysis with paired Students t-test of cell viability assay using Prism 7

Treatment A	**Treatment B**	**p-Value**	**Significance**
Different Inhibitors			
DMSO, 0Gy	1.4µM Fen, 0Gy	0.5022	ns
DMSO, 0Gy	DMSO, 2Gy	0.1198	ns
DMSO, 0Gy	Fen 1.4µM, 2Gy	0.0459	*
Fen 1.4µM, 0Gy	VitC, Fen 1.4µM, 0Gy	0.3080	ns
Fen 1.4µM, 0Gy	MT, Fen 1.4µM, 0Gy	0.9648	ns
DMSO, 2Gy	VitC, DMSO, 2Gy	0,1674	ns
DMSO, 2Gy	MT, DMSO, 2Gy	0,3227	ns
Fen 1.4µM, 2Gy	VitC, Fen 1.4µM 2Gy	0,2351	ns
Fen 1.4µM, 2Gy	MT, Fem 1.4µM, 2Gy	0,8130	ns
VitC, DMSO, 0Gy	VitC, Fen 1.4µM, 0Gy	0,2199	ns

VitC, DMSO, 0Gy	VitC, DMSO, 2Gy	0,9317	ns
VitC, DMSO, 0Gy	VitC, Fen 1.4µM, 2Gy	0,6376	ns
MT, DMSO, 0Gy	MT, Fen 1.4µM, 0Gy	0,1270	ns
MT, DMSO, 0Gy	MT, DMSO, 2Gy	0,6383	ns
MT, DMSO, 0Gy	MT, Fen 1.4µM, 2Gy	0,1036	ns

Drugs and Stains

Table 6 Drugs used during the experiments

	Product information
dynasore hydrate (dynasore)	D7693, Sigma
L-Ascorbinacid (Vitamine C)	A4403, Sigma
MitoTempo (MT)	SML0737, Sigma
Retinoic acid p-hydroxyanilide (fenretinide, Fen)	H7779, Sigma
Z-vad-FMK	A1902, APExBIO
N-Acetylcysteine	A7250, Sigma

Table 6 Fluorescent stains for flow cytometry and fluorescence microscopy

	Product information
Acridine Orange (hemi zinc chloride salt)	158550, Sigma
CellRox Deep Red Reagent	C10422, Thermo Fisher
Lucifer Yellow	L453, Thermo Fisher
MitoSox Red	M36008, Thermo Fisher
Propidium Iodide	4170, Sigma

III. Discussion

Sarcomas form the third biggest group of childhood malignancies. Within this group, aRMS is a rare but highly malicious subtype. The occurrence of metastasis already at early stages and high recurrence rates demand a multimodal and aggressive treatment approach comprising surgery, chemotherapy and radiotherapy. Despite this aggressive treatment, survival rates remain poor and therapy-related side effects still have a great impact on the children's quality of life [42]. Despite abundant research on new anti-cancer agents for treatment of aRMS, only few new compounds are permanently established in the international treatment trials [48]. Reasons for the failure of new agents are mainly high toxicity and side-effects, unsatisfying tumour responses and development of resistances.

Hence it remains one of the biggest challenges to overcome intrinsic or acquired resistances towards conventional treatment, which is responsible for the high recurrence rates seen in aRMS [411, 412].

Along these lines, drugs that re-sensitize cells towards chemotherapy induced apoptosis or activate alternative, non-apoptotic cell death pathways, while exhibiting a low toxicity profile are highly desirable [412, 413].

ARMS is characterised by its chromosomal translocation, which leads to the expression of the chimeric transcription factor PAX3-FOXO1 [31]. It is believed that PAX3-FOXO1 is the main tumorigenic driver in aRMS and tumour cell survival is dependent on its expression [35]. However, as a transcription factor it is considered undruggable and so alternative treatment strategies have to be exploited.

In this thesis, we characterized the cytotoxic effect of fenretinide on aRMS cells in great detail.

In a previous work and in an attempt to find new compounds with an improved therapeutic selectivity, we screened a small compound library thereby focusing on compounds which affected the transcriptional activity of PAX3-FOXO1. During this screen fenretinide was identified as the

top hit affecting PAX3-FOXO1 activity levels without exhibiting a broad and unspecific toxicity [99].

The work presented in the first manuscript focused on the mode of action of fenretinide in aRMS cells and described and characterized a new form of cell death induced in response to fenretinide treatment. In the second manuscript we presented data of fenretinide combined with ionizing radiation, assessed the effectiveness of this combinatorial treatment on cancer cell survival pointing out a role of fenretinide as radiosensitizer.

1. Activation of a distinct and non-classical cell death pathway

As expression of PAX3-FOXO1 is essential for aRMS and the previous screen had revealed that fenretinide affected PAX3-FOXO1 transcript levels, we first studied this interrelation in more detail. By using an inducible lentiviral vector system directed against endogenous PAX3-FOXO1 together with one overexpressing PAX3-FOXO1 in Rh4 cells, we demonstrated that, upon fenretinide treatment, apoptosis was induced which was accompanied with a reduction of PAX3-FOXO1 protein levels. However, ectopic PAX3-FOXO1 did not protect from fenretinide induced cell death indicating that Fenretinide might induce an alternative mode of cell death.

Interestingly, further studies showed that the fenretinide induced cell death was distinct from apoptosis, necroptosis, autophagy and ferroptosis, as neither pharmacological inhibition of these death pathways nor their genetic ablation rescued cell survival after fenretinide treatment. However, inhibitors directed against reactive oxygen species completely abrogated the fenretinide mediated toxicity, indicating the importance of ROS in fenretinide induced cell death.

2. Trigger to the production of reactive oxygen species

As previously shown in other cellular systems, fenretinide is capable to induce production of different kinds of reactive oxygen species, which are responsible for the observed cell death [67,

80, 90, 414]. In our cell system, we found that fenretinide treatment led to the production of mitochondria derived ROS as an early event, preceding the induction of cell death. Further, rescue experiments clearly showed that these mitochondrial ROS also mediated cell death. This observation was not surprising, since the mitochondrial respiratory chain (MRC) is on the one hand the major sources of ATP production, but on the other hand also the major source of ROS production and so depicts a vulnerable system when the equilibrium is disturbed [110, 111, 130, 154, 238, 240]. Our results are in accordance with the findings of Cuberus et al [79] who also suggested that fenretinide-induced ROS production occurred via complex II of the MRC, which is further in agreement with our own findings, which indicate that the main target of fenretinide to cause ROS production lies downstream of complex II of the MRC.

However, in contrast to our data where an uncoupling of the MRC with CCCP at complex V had no influence on ROS production, Suzuki et al. [75] suggested that fenretinide inhibits the MRC at complex V in cervical carcinoma cells. Nevertheless, while at this point it is not exactly clear how fenretinide induces ROS production, their role in triggering cell death is undebatable.

3. Accumulation of cytoplasmic vesicles and uptake of fluid phase dyes induction

On electron microscopy images, we observed that fenretinide treatment induced formation and accumulation of cytoplasmic vesicles. This phenomenon has been previously described in multiple other cellular systems in the context of paraptosis, oncosis, methuosis and autophagy [298, 310, 415, 416]. During paraptosis as well as during oncosis, the ER shows distinct vacuolization and the mitochondria are swollen [415, 417], both features that we did not observe in our fenretinide treated cells. Moreover, the vesicles observed in aRMS cells are surrounded by a single membrane and therefore did not originate from autophagy, which gives rise to double membrane autophagosomes [298]. The cytoplasmic vesicles are of variable size with diameters of up to 7µm,

which is comparable to the described diameter of macropinosomes which reach a diameter up to 5µm [361]. Morphologically the vesicles mostly resembled endosomes, an interpretation which was further verified by increased fluid phase dye uptake stimulated by fenretinide treatment. Interestingly co-treatment with ROS scavengers abolished vesicle formation substantiating an effect downstream of ROS. Further inhibition of apoptosis by Z-vad, led to enhanced accumulation of vesicles, which suggests that alternative death pathways can be engaged if the classical ones like apoptosis are impaired. Moreover, this is in accordance with a delay in the onset of cell death in presence of Z-vad by about 10 hours as seen in our time lapse experiments.

4. Accumulation of early and late endosomes in a dynamin-dependent manner

Attempts to block the fenretinide mediated cell death with commonly used endocytosis inhibitors like chlorpromazin, filipin and genistein revealed an independence of the clathrin and caveolin-mediated endocytosis. However, in contrast to other published descriptions on vesicular mediated cell death, we observed that pharmacologic as well as genetic interference with the Dynamin GTPases completely abolished vesicle accumulation and rescued from fenretinide induced cell death. The Dynamin family of GTPases are profoundly involved in endosome fission at the plasma membrane, both during clathrin-dependent and -independent endocytosis. More recent studies also suggest a role of dynamins during circular dorsal ruffle (CDR) formation, which is considered a specific type of the macropinocytosis pathway [343, 418, 419]. In this context, Orth et al was able to show, that formation of CDR at the plasma membrane mainly serves the internalization of EGFRs, following stimulation of TRKs and proceeds in a highly organized manner [418]. Here, dynamin and its binding partner cortactin, as well as multiple other cytoskeleton associated proteins are involved in vesicle formation [419]. Interestingly, tumor cells seem to form less CDR than normal cells, which might lead to unchecked growth [419], and so stimulation of CDR in tumor cells might have a negative influence on their growth which could be exploited.

Reactive oxygen species are known to activate PTEN and MAPK phosphatases and so act as negative regulators of tyrosine kinase receptor signaling cascades [133, 144-146, 420-422], which might be a possible link to the formation of CDRs after fenretinide treatment.

Also very interesting in this context is the observation that induction of ROS-dependent cell death with other drugs including the proteasome inhibitors MLN2238 and MLN9708, the microtubule-destabilizing agent rigosertib or the tyrosine-kinase inhibitor bosutinib neither induced the formation of cytoplasmic vesicles nor was the cells' demise blocked by Dynamin inhibitors.

When comparing our findings with other similar cellular phenotypes that have been described in the literature, the greatest resemblances are found in a cell death form termed methuosis [310, 415, 416]. Since the description and denomination of methuosis by Overmayer et al [310] in glioblastoma cells, several different stimuli have been described that induce this phenotype and are associated with a disturbance of the endosomal maturation. These stimuli include various small molecules with different pathways involved, including activation of Ras, as well as ectopic Ras expression per se, which stimulates marcopinosmome formation via over-activation of Rac1 and at the same time impedes their recycling (for review see Maltese et al [423])[317]. While Ras activation seems to be crucial in vesicle formation of several cell types including glioblastoma, Ewing sarcoma and epithelial cells [310, 317, 338], Ras pathway mutations are not associated with aRMS [424]. Further pharmacological inhibition as well as knock-out of Rac1 and Arf6 in aRMS cells neither affected fenretinide mediated cell death nor dye uptake (data not shown in the thesis), indicating that this pathway does not seem to play a role in these cells.

However similar to methuosis, we also observed an impaired recycling of endosomes with a maturation stop at the level of early/late endosome formation, as the vesicles acquire markers such as Rab5 and Rab7 but not the lysosomal marker LAMP-1. However, the exact mechanisms leading to a maturation stop of the endosomes has not yet been understood and needs further elucidation. Nevertheless, the different studies suggest that various upstream pathways might be engaged to

induce a similar vesicular phenotype associated with cell death, while none of the studies were able to draw a causal link between vesicle accumulation and cell death. Further very important in this context is the fact, that none of the compounds used in the mentioned studies is yet in clinical use. So clinical and pharmacological data regarding bio distribution, tolerability, side-effects and also efficacy are not available. However, due to the long clinical experiences with fenretinide and also the fact that it is already FDA approved sets it apart from those other compounds. The finding that fenretinide engages a new form of cell death which is not exploited by conventional chemotherapy agents makes it as a promising combinatorial partner for the treatment of aRMS patients, as resistance development against two different death pathways is much less likely than the development against only one. Agents for a potential combination treatment might either be stimuli that further enhance ROS production to trigger cell death even further or stimuli that induce other forms of cell death like canonical apoptosis or necroptosis.

5. Fenretinide and radiation therapy combination enhances cell death

We considered ionizing radiation as potential combination therapy for fenretinide treatment. Moreover, radiotherapy is already in use as the third pillar in the standard treatment plan for patients with aRMS along with chemotherapy and surgery and therefore represents a rational choice [401-404]. But viewed from the other side, it seems even more important to identify radiosensitizers to potentially reduce radiation doses. Fenretinide which has a low toxicity profile and promising anti-cancer activity, therefore represents an ideal candidate.

RT is associated with significant late effects in survivors [425]. Depending on the treatment site, the side effects comprise neurocognitive sequelae, growth restriction through growth hormone deficiency, infertility and secondary malignancies [388-390]. In this context, duration and dose administered is crucial and based on the patient's risk-group. While in low risk patients RT can be

omitted, high risk patients have a far worse prognosis and addition of RT to the treatment regimen has substantially improved EFS and overall survival [401, 426].

So far multiple strategies have been investigated to reduce RT-related morbidity in aRMS patients, including intensity-modulated RT (IMRT) and hyperfractioned radiation [396, 397]. While hyperfractionation did not bring a benefit in local nor regional control [43, 406], IMRT resulted in an excellent local tumor control in parameningial aRMS, with comparable side-effects than conventional RT [407]. Radiosensitizing agents are capable to broaden the therapeutic window and selectively augment radiation effects in tumor cells while also sparing the surrounding tissue. In pediatric trials, radiosensitizers are so far not implemented. Several chemotherapeutic agents as anthracyclines and actinomycin D are known to render the tumor tissue more radiosensitive, cause however a significant toxicity so that these chemotherapeutic agents must indeed be avoided in conjunction with radiotherapy. Other agents like platinum-derivates or 5-fluoruracil also potentiate the radiation effect but have not yet been studied in the context of radiotherapy and aRMS.

Tumor hypoxia is a commonly found feature in tumor masses, which becomes more severe with increasing size of the mass. Hypoxic tumor cells are not only more chemotherapy-resistant but also often resistant to radiation therapy. Further, hypoxia leads to a more malignant phenotype and increases metastasis [427]. To target tumor hypoxia and increase radiosensitivity has been a major focus of radiobiologists over the last years and different approaches to increase radiosensitivity have been made. These include hyperbaric oxygen, nitroazole sensitizers and hypoxic cytotoxins like tirapazamine [428]. However, none of these strategies was proven effective in clinical trials. Hydrogen peroxide is currently under intense investigation as a potential radiosensitizer in multiple malignancies (ClinicalTrials.gov NCT02757651). When hydrogen peroxide is injected into the tumor, it is degraded into water and oxygen and decreases tumor hypoxia [429]. As fenretinide induces superoxides which might be reduced to hydrogen peroxide by SODs an anti-

hypoxic effect might also be seen with fenretinide treatment. This question has not been addressed yet and opens the possibility of further investigations.

Fenretinide combined with radiation therapy is under investigation for the treatment of diffuse intrinsic pontine glioma (DIPG) and suggest promising results in mice [430]. Up-to-date, there are only few other studies exploring the combinatorial effect of fenretinide with radiation therapy and so far, radiosensitizing agents for the treatment of aRMS, are not established in international treatment trials. Therefore, new treatment strategies are needed to better exploit the benefits of RT while reducing their side-effects.

During our first experiment with RT combined with fenretinide, we saw an increasing, dose-dependent combinatorial effect on cell-viability. This effect was so strong, that almost no colonies survived. Subsequently, we were able to reduce both treatment dosages with a persisting effect at 2 Gy on clonogenic growth.

We saw a strong enhancement of induction of apoptosis in the combination treatment. The underlying cause for the induction of apoptosis most likely result from DNA damage and consequently induction of cell cycle arrest. Cell cycle arrest is frequently observed following DNA damage and radiotherapy [431], and is also observed after fenretinide treatment [432]. Our results also showed an impaired cell cycle progression with a G2/M arrest with a clear combinatorial effect. This is an important finding as it is one of the hallmarks of cancer that tumor cells sustain proliferative signaling even after DNA damage [6], and hence restoration of the normal response – induction of cell death - is desirable.

In the context of those findings and when taking toxicities in consideration, fenretinide with its low toxicity profile seems the perfect drug in the combination with RT.

6. Combination with ionizing radiation, ROS-production and vacuolizing cell death

In the first manuscript, we were able to show that fenretinide triggers mitochondrial ROS (superoxides). In the combination treated cells, we identified further increase in ROS production. Interestingly however, we saw that RT alone mainly triggered the production of hydrogen peroxide. So obviously in the combined treated cells, two different kinds of ROS species are responsible for the enhanced cell death. This finding, to trigger different ROS species, is important in the context of resistance development, as cancer cells are known to upregulate antioxidant pathways and different ROS species are scavenged by their own antioxidants [433].

Also interesting in this context are studies that use hydrogen peroxide as a radiosensitizer [429]. Here hydrogen peroxide serves indirectly as an oxygen donor in the tumor cell during its dismutation to H_2O and O_2. As superoxides are also reduced to hydrogen peroxide, fenretinide might serve in the same way as an indirect oxygen donor for tumorous tissues. However, this has not been investigated yet.

In summary, we were able to show that downstream of ROS, the combination of RT and fenretinide triggered increased macropinocytosis, as assessed via fluid phase dye uptake experiments by flow cytometry.

In contrast, single treatment with RT did not induce macropinocytosis and scavenging with Dynamin inhibitors had no influence. In contrary, by light microscopy only a non-significant increase in macropinocytosis was seen. This minor increase in dye uptake might however exhibit an analysis bias as the mean integrated density value of an image sums all of the pixels within a region and gives you a total value. This value is then divided by the number of cells counted on the phase image. This analysis does not take into consideration the size of the cell.

RT however induces cell cycle arrest and senescence and subsequently a morphological appearance-change of the cells with an increased cell size. This eventually will lead to an increased

integrated density value for the enlarged cell as they are capable to uptake more dye per cell and the evaluation is expected to show an increased mean density index per cell, compared to smaller cells. Due to the gating strategy applied in the flow cytometry analysis, the cell size is not relevant. However, in the irradiated-only cells neither a Dynamin Inhibitor nor a ROS-scavenger could inhibit the dye uptake, as was the case for fenretinide treated cells. Based on these findings it is unlikely that irradiation induced cell death is a result of an increased macropinocytosis.

These findings suggest that a distinct population of ROS are responsible for the induction of macropinocytosis through fenretinide, which is not induced by RT alone. Hence, while the exact mechanism leading to the increased macropinocytosis remains to be elucidated, the fact that fenretinide engages this new form of vesicular cell death which is neither exploited by conventional chemotherapy agents nor RT defines them as promising combinatorial partners. Moreover, our data clearly show that addition of fenretinide to RT enhances cell death, meaning that a reduction of the administered doses could be possible, while maintaining the same anti-cancer response. In the context of normal tissue toxicity and radiation related side-effects this is an encouraging finding to translate the combination into clinics.

7. Conclusion

Taken together our results provide evidence that fenretinide induces mitochondrial ROS through an interference with the MRC downstream of complex two. Further, these distinct ROS species induce dynamin-dependent macropinocytosis leading to an enormous vesicle formation and accumulation in the cytoplasm. These vesicles have a strong and effective cytotoxic potential in aRMS cells.

Further our findings support that fenretinide acts as a promising radiation sensitizer in alveolar rhabdomyosarcoma cells. Here, different modes of cell death mechanism are activated and enhanced by these two treatment modalities.

Since fenretinide is already in clinical use in children (Clinicaltrials.gov ID NCT02163356) with a promising toxicity profile [66, 434], a combinatorial treatment of both may help to reduce the development of resistances and increases the therapeutic window in the local radiotherapy treatment and so is a promising treatment regime in pediatric patients with alveolar rhabdomyosarcoma.

Acknowledgements

I would like to thank Prof. Dr. Beat Schäfer for giving me the opportunity to pursue my MD-Ph.D. thesis in his laboratory. His support, suggestions and advice have helped me along the way to follow my work to the end. I would like to further thank the members of my thesis committee, Prof. Dr. Alex Hajnal and Prof. Dr. Martin Pruschy for the interesting discussions, the thoughtful input and suggestions. Here, a special thanks goes to Prof. Dr. Martin Pruschy, for hosting me in his lab and for all the good scientific ideas for my radiation project.

A great and deep thank you goes to Dr. Marco Wachtel. For all his great suggestions, his mindful thoughts, his support when things went wrong, his patience and explanations to all my questions during the PhD. Most of the things I learned, were taught to me by him. Marco, you always took time for me and listened to my ideas and thoughts. Without you, the project would have never turned out that nice. Thank you so much.

Next, I want to thank my master student Anja Wolf. She really did a great job and contributed a lot to the finalization of this work. But also I want to thank her for being such a kind and honest person and reminding me many times, that work is not everything in life.

Further I would like to thank Dr. Sabine Bender for helping me with all the radiation experiments, for her critical thoughts and good ideas and her endurance with the clonos. I want to thank her for integrating me into their group and for the good times we shared outside the lab.

I want to thank Dr. Andres Kaech and Dr. Urs Ziegler from The Center for Microscopy and Image Analysis. The electron microscopy images turned out amazing and your support could not have been better.

Another special thanks goes to Katharina Holste, who put so much effort into our shared project and to help me out while I was on maternity leave. This friendly engagement really meant a lot to

me. Further I want to thank her for always having an open ear and open mind for my questions. I really enjoyed the nice moments we shared outside the lab. You became a good friend.

The next big thank you goes to Nagjie Alijaj. I always felt understood by you and no matter, how much work you had yourself, you always took your time to help out and explain things. Further I want to thank you for your open ear during my pregnancy and your support and all the amazing baby cloth.

Next I want to thank Johannes Ommer for being the most patient and best teacher ever. You always had an answer to my questions, and if not, you made sure, you would find an answer. I really enjoyed sharing my desk, bench and foot space with you. Further I really enjoyed the good discussions we had and the last few weeks together finishing our thesis.

Gloria, I want to thank you for being such a kind and cheerful person and helping me and Anja out with the sorter so many times. You did a wonderful job.

The last special thanks goes to Joana Marques for always having an open ear, and for always being helpful. But also outside the lab, I always enjoyed your company and I will never forget our trip to Washington. That was just wonderful.

I want to thank each member of my group; Dominik for the best mountain bike tips, Gabriele for the most cheerful laugh, Michaela for all the sweets and nice early morning meetings, Devmini for her gentle manners, Noemi for your open mind, Maria B. for becoming a good friend, Maria G. for being so direct and straight forward, Patricia for being so helpful, Vadim for always being thoughtful with my questions, Laura for always being happy to help, Chiara for bringing glamour to the lab, Blaz for having such a good spirit. En plus, je veux remercier Danaëlle et Charles pour parler en française avec moi. Ca a m'aide beaucoup.

All current and former lab colleagues from the other groups and also from the Pruschy lab I want to thank for creating such a nice working atmosphere, even though our lab is so grey and ugly. Every single one, was always kind and helpful. Thank you for the good moments we shared.

I want to thank my colleagues from the MD-PhD Program, Tanja, Anke, Sara, Andrea, Mara, Brice, Miro and Marcel. I am glad we met and the time we spend together during the courses, the retreat and after work were just great.

I want to thank my former supervisors and mentors, Prof. Kurt Leibundgut, Prof. Roland Ammann, Dr. Regula Angst und Dr. Peter Downie. You all taught me so much and in such different ways all the things I know about clinical oncology. Without your encouragement I would have not made this PhD. You guided me along my journey and helped me become the doctor I am today.

And I want to thank all my good friends outside the lab. You helped me keep up my motivation and forget work on the weekends and evenings. You are all amazing and I am the luckiest person, to have such good friends.

I want to thank my mother in law Karin, for taking care of Antonie so many times, so that I was able to finish writing this thesis. When Antonie was with you, I always knew she was in loving and caring hands and just had a wonderful time with her grandmother.

I want to thank my parents for just being the best parents one can imagine. Without your support all these years, I would never be there, where I am today. With your encouragement, you opened so many possibilities for me. You always have and had your ears and heart open for all my silly ideas, plans, all my concerns and worries. I am sure, my times you were just worried about me, and I am really sorry for that. But with creating a lovely home you gave me roots and still gave me wings to fly, you did the best job as parents.

I want to thank my big brother Hans Ulrich, without the constant battles and competitions during our childhood, I would have never become so ambitious. And my ambition has helped me through all these long years of studying and working so hard. In you, I see one of the most reliable persons I ever met and I know, no matter what will happen, you will always stand up for your little sisters.

Not to be forgotten, I want to thank my little sister Anna. With you, I feel completely understood without saying a single word. I feel the biggest trust and love and I know that you will always stand by me.

I want to thank my grandmothers. You both were always an idol for me. You had such difficult times in your life, but nevertheless achieved so much and gave us so much love and care.

My greatest thank you, goes to my husband Christoph. Finding words for the love and affection I feel for you is impossible and way to personal to write into a thesis. Without your support during the last four years of my PhD, the frustrating moments would have been much harder, the nice moments would have been less bright and the time outside the lab just sad and boring. Even so, your criticism made me angry sometimes, it helped me find and follow my way. I want to apologize for the hangry moments, when I just wasn't myself and not treated you the way you deserve it.

Last I want to thank Antonie for bringing us the biggest joy into our live. You are the greatest gift and pleasure and just the most amazing little person. Your curiosity is so inspiring and I hope you will be able to preserve it for a lifetime.

Curriculum Vitae

Eva Katharina Brack

24.04.1979

Qualifications

Specialist Qualification	Paediatric Oncologist/Haematologist, Swiss Medical Board
Year Qualified:	2015: Oral Board Exam, accreditation 2018
Country of Training:	Switzerland/Australia
Institution Awarding Qualification:	Swiss Society of Paediatrics
Specialist Qualification	Paediatrician, Swiss Medical Board
Year Qualified:	2010: Board Exam, accreditation 2016
Country of Training:	Switzerland
Institution Awarding Qualification:	Swiss Society of Paediatrics
Primary Medical Qualification	Medical Doctor
Year Qualified:	2006
Country of Training:	Germany
Medical School:	Ludwig Maximilians University Munich, Germany

Clinical Experience & Postgraduate Employments

Since 09/14	M.D.-Ph.D. student, Department of Paediatric Haematology and Oncology, University Children's Hospital Zurich. Cancer Biology Program / Life Science Zurich Graduate School, University of Zurich, Switzerland
Since 10/16	Consultant Paediatric Emergency Medicine (Part time) Kinderarzthaus Zurich, Zurich Switzerland
08/12 -07/14	Fellow, Department of Haematology and Oncology Children's Cancer Centre Melbourne, Monash Health Melbourne, Australia
10/11 - 06/12	Junior Consultant, Department of Haematology and Oncology Children's Clinic Aarau, Teaching hospital University of Zurich, Aarau, Switzerland

07/10 - 06/11 Fellow, Department of Haematology and Oncology
University Children's Clinic Berne
Berne, Switzerland

06/07 - 06/10 Resident/Registrar, Paediatric Specialist Training Program
Children's University Clinic Berne
Berne, Switzerland

06/06 - 05/07 Resident, Department of Paediatric Surgery
Children's University Clinic Berne
Berne, Switzerland

Publications

02/2018 The influence of different fever definitions on diagnostics and treatment after diagnosis of fever in chemotherapy-induced neutropenia in children with cancer. **Brack E**, Wagner S, Stutz-Grunder E, Agyeman Ph, Leibundgut K, Teuffel O, Ammann R. PLoS One. 2018 Feb 20;13(2):e0193227.

11/16 The proprotein convertase furin is required to maintain viability of alveolar rhabdomyosarcoma cells.
Jaaks P, Meier G, Alijaj N, **Brack E**, Bode P, Koscielniak E, Wachtel M, Schäfer BW, Bernasconi M. Oncotarget. 2016 Nov 22;7(47):76743-76755.

06/12 Foreign body associated Hemophagocytic lymphohistiocytosis or association with an undefined dysmorphic syndrome? A case report.
Brack E, Köhler H, Angst R. Bulletin Suisse du Cancer 2/2012. 138-142

01/12 First-day step-down to oral outpatient treatment versus continued standard treatment in children with cancer and low-risk fever in neutropenia. A randomized controlled trial within the multicenter SPOG 2003 FN study.
Brack E, Bodmer N, Simon A, Leibundgut K, Kühne T, Niggli FK, Ammann RA. Pediatric Blood Cancer 2012 Sep; 59(3):423-30

01/11 Acute lymphatic leukaemia in childhood. Review article.
Brack E, Leibundgut K. Praxis 2011 Oct. 5;100(20):1211-9.

09/06 Surfactant protein D regulates chemotaxis and degranulation of human eosinophils.
Von Bredow C, Hartl D, Schmid K, Schabaz F,
Brack E, Reinhardt D, Griese M. Clinical and Experimental Allergy. 2006 Dec; 36(12):1566-74

References

1. Vogelstein, B. and K.W. Kinzler, *The multistep nature of cancer.* Trends Genet, 1993. **9**(4): p. 138-41.
2. Parsons, B.L., *Many different tumor types have polyclonal tumor origin: evidence and implications.* Mutat Res, 2008. **659**(3): p. 232-47.
3. Chaffer, C.L. and R.A. Weinberg, *How does multistep tumorigenesis really proceed?* Cancer Discov, 2015. **5**(1): p. 22-4.
4. Vogelstein, B., et al., *Cancer genome landscapes.* Science, 2013. **339**(6127): p. 1546-58.
5. Hanahan, D. and R.A. Weinberg, *The hallmarks of cancer.* Cell, 2000. **100**(1): p. 57-70.
6. Hanahan, D. and R.A. Weinberg, *Hallmarks of cancer: the next generation.* Cell, 2011. **144**(5): p. 646-74.
7. Downing, J.R., et al., *The Pediatric Cancer Genome Project.* Nat Genet, 2012. **44**(6): p. 619-22.
8. Steliarova-Foucher, E., et al., *International Classification of Childhood Cancer, third edition.* Cancer, 2005. **103**(7): p. 1457-67.
9. Board, I.o.M.U.a.N.R.C.U.N.C.P., *Childhood Cancer Survivorship: Improving Care and Quality of Life*. 2003, Washington: National Academies Press.
10. Narod, S.A., C. Stiller, and G.M. Lenoir, *An estimate of the heritable fraction of childhood cancer.* Br J Cancer, 1991. **63**(6): p. 993-9.
11. Lindor, N.M., et al., *Concise handbook of familial cancer susceptibility syndromes - second edition.* J Natl Cancer Inst Monogr, 2008(38): p. 1-93.
12. Slater, O. and J. Shipley, *Clinical relevance of molecular genetics to paediatric sarcomas.* J Clin Pathol, 2007. **60**(11): p. 1187-94.
13. Goldie, J.H. and A.J. Coldman, *The genetic origin of drug resistance in neoplasms: implications for systemic therapy.* Cancer Res, 1984. **44**(9): p. 3643-53.
14. Bolus, N.E., *Basic Review of Radiation Biology and Terminology.* J Nucl Med Technol, 2017. **45**(4): p. 259-264.
15. John-Aryankalayil, M., et al., *Fractionated radiation therapy can induce a molecular profile for therapeutic targeting.* Radiat Res, 2010. **174**(4): p. 446-58.
16. Nakamura, K., et al., *Recent advances in radiation oncology: intensity-modulated radiotherapy, a clinical perspective.* International Journal of Clinical Oncology, 2014. **19**(4): p. 564-569.
17. Palm, A. and K.A. Johansson, *A review of the impact of photon and proton external beam radiotherapy treatment modalities on the dose distribution in field and out-of-field; implications for the long-term morbidity of cancer survivors.* Acta Oncol, 2007. **46**(4): p. 462-73.
18. Weber, D.C., et al., *Proton therapy for pediatric malignancies: Fact, figures and costs. A joint consensus statement from the pediatric subcommittee of PTCOG, PROS and EPTN.* Radiother Oncol, 2018.
19. Wang, H., et al., *Cancer Radiosensitizers.* Trends Pharmacol Sci, 2018. **39**(1): p. 24-48.
20. Adamson, P.C., *Improving the outcome for children with cancer: Development of targeted new agents.* CA Cancer J Clin, 2015. **65**(3): p. 212-20.
21. van Erp, A.E.M., et al., *Targeted Therapy-based Combination Treatment in Rhabdomyosarcoma.* Mol Cancer Ther, 2018. **17**(7): p. 1365-1380.
22. Yu, A.L., et al., *Anti-GD2 antibody with GM-CSF, interleukin-2, and isotretinoin for neuroblastoma.* N Engl J Med, 2010. **363**(14): p. 1324-34.
23. Chow, V.A., M. Shadman, and A.K. Gopal, *Translating anti-CD19 CAR T-Cell therapy into clinical practice for relapsed/refractory diffuse large B-Cell lymphoma.* Blood, 2018.

24. Morotti, R.A., et al., *An immunohistochemical algorithm to facilitate diagnosis and subtyping of rhabdomyosarcoma: the Children's Oncology Group experience.* Am J Surg Pathol, 2006. **30**(8): p. 962-8.
25. Cessna, M.H., et al., *Are myogenin and myoD1 expression specific for rhabdomyosarcoma? A study of 150 cases, with emphasis on spindle cell mimics.* Am J Surg Pathol, 2001. **25**(9): p. 1150-7.
26. Horn, R.C., Jr. and H.T. Enterline, *Rhabdomyosarcoma: a clinicopathological study and classification of 39 cases.* Cancer, 1958. **11**(1): p. 181-99.
27. Parham, D.M. and F.G. Barr, *Classification of rhabdomyosarcoma and its molecular basis.* Adv Anat Pathol, 2013. **20**(6): p. 387-97.
28. Fletcher CDM, B.J., Hogendoorn PCW, Mertens F, , *WHO Classification of Tumours of Soft Tissue and Bone. 4th ed. Lyon, France: International Agency for Research on Cancer*. World Health Organization Classification of Tumours, 2013. **5**.
29. Rudzinski, E.R., et al., *The World Health Organization Classification of Skeletal Muscle Tumors in Pediatric Rhabdomyosarcoma: A Report From the Children's Oncology Group.* Arch Pathol Lab Med, 2015. **139**(10): p. 1281-7.
30. Rudzinski, E.R., et al., *Histology, fusion status, and outcome in metastatic rhabdomyosarcoma: A report from the Children's Oncology Group.* Pediatr Blood Cancer, 2017. **64**(12).
31. Shern, J.F., et al., *Comprehensive genomic analysis of rhabdomyosarcoma reveals a landscape of alterations affecting a common genetic axis in fusion-positive and fusion-negative tumors.* Cancer Discov, 2014. **4**(2): p. 216-31.
32. Shern, J.F., M.E. Yohe, and J. Khan, *Pediatric Rhabdomyosarcoma.* Crit Rev Oncog, 2015. **20**(3-4): p. 227-43.
33. Wachtel, M., et al., *Gene expression signatures identify rhabdomyosarcoma subtypes and detect a novel t(2;2)(q35;p23) translocation fusing PAX3 to NCOA1.* Cancer Res, 2004. **64**(16): p. 5539-45.
34. Scheidler, S., et al., *The hybrid PAX3-FKHR fusion protein of alveolar rhabdomyosarcoma transforms fibroblasts in culture.* Proc Natl Acad Sci U S A, 1996. **93**(18): p. 9805-9.
35. Bernasconi, M., et al., *Induction of apoptosis in rhabdomyosarcoma cells through down-regulation of PAX proteins.* Proc Natl Acad Sci U S A, 1996. **93**(23): p. 13164-9.
36. Kikuchi, K., et al., *Effects of PAX3-FKHR on malignant phenotypes in alveolar rhabdomyosarcoma.* Biochem Biophys Res Commun, 2008. **365**(3): p. 568-74.
37. Davicioni, E., et al., *Identification of a PAX-FKHR gene expression signature that defines molecular classes and determines the prognosis of alveolar rhabdomyosarcomas.* Cancer Res, 2006. **66**(14): p. 6936-46.
38. Khan, J., et al., *Gene expression profiling of alveolar rhabdomyosarcoma with cDNA microarrays.* Cancer Res, 1998. **58**(22): p. 5009-13.
39. Ognjanovic, S., et al., *Trends in childhood rhabdomyosarcoma incidence and survival in the United States, 1975-2005.* Cancer, 2009. **115**(18): p. 4218-26.
40. Arndt, C.A.S., G. Bisogno, and E. Koscielniak, *Fifty years of rhabdomyosarcoma studies on both sides of the pond and lessons learned.* Cancer Treat Rev, 2018. **68**: p. 94-101.
41. Williamson, D., et al., *Fusion gene-negative alveolar rhabdomyosarcoma is clinically and molecularly indistinguishable from embryonal rhabdomyosarcoma.* J Clin Oncol, 2010. **28**(13): p. 2151-8.
42. Dantonello, T.M., et al., *Survival following disease recurrence of primary localized alveolar rhabdomyosarcoma.* Pediatr Blood Cancer, 2013. **60**(8): p. 1267-73.
43. Crist, W.M., et al., *Intergroup rhabdomyosarcoma study-IV: results for patients with nonmetastatic disease.* J Clin Oncol, 2001. **19**(12): p. 3091-102.

44. Li, F.P. and J.F. Fraumeni, Jr., *Rhabdomyosarcoma in children: epidemiologic study and identification of a familial cancer syndrome.* J Natl Cancer Inst, 1969. **43**(6): p. 1365-73.
45. Knudson, A.G., Jr., *Mutation and cancer: statistical study of retinoblastoma.* Proc Natl Acad Sci U S A, 1971. **68**(4): p. 820-3.
46. Raney, R.B., Jr., et al., *Disease patterns and survival rate in children with metastatic soft-tissue sarcoma. A report from the Intergroup Rhabdomyosarcoma Study (IRS)-I.* Cancer, 1988. **62**(7): p. 1257-66.
47. Maurer, H.M., et al., *The Intergroup Rhabdomyosarcoma Study-I. A final report.* Cancer, 1988. **61**(2): p. 209-20.
48. Koscielniak E, K.T., *CWS-guidance for risk adapted treatment of soft tissue sarcoma and soft tissue tumours, in children, adolescents, and young adults vol Version 1.6.1. Cooperative Weichteilsarkom Studie Group-CWS der GPOH,* . 2014.
49. Klingebiel, T., et al., *Treatment of children with metastatic soft tissue sarcoma with oral maintenance compared to high dose chemotherapy: report of the HD CWS-96 trial.* Pediatr Blood Cancer, 2008. **50**(4): p. 739-45.
50. Chisholm, J.C., et al., *Open-label, multicentre, randomised, phase II study of the EpSSG and the ITCC evaluating the addition of bevacizumab to chemotherapy in childhood and adolescent patients with metastatic soft tissue sarcoma (the BERNIE study).* Eur J Cancer, 2017. **83**: p. 177-184.
51. Mascarenhas, L., et al., *Randomized phase II trial of bevacizumab and temsirolimus in combination with vinorelbine (V) and cyclophosphamide (C) for first relapse/disease progression of rhabdomyosarcoma (RMS): A report from the Children's Oncology Group (COG).* Journal of Clinical Oncology, 2014. **32**(15_suppl): p. 10003-10003.
52. Geoerger, B., et al., *Phase II trial of temsirolimus in children with high-grade glioma, neuroblastoma and rhabdomyosarcoma().* Eur J Cancer, 2012. **48**(2): p. 253-62.
53. Anderson, J.L., et al., *Pediatric Sarcomas: Translating Molecular Pathogenesis of Disease to Novel Therapeutic Possibilities.* Pediatr Res, 2012. **72**(2): p. 112-21.
54. Villani, M.G., et al., *Identification of the fenretinide metabolite 4-oxo-fenretinide present in human plasma and formed in human ovarian carcinoma cells through induction of cytochrome P450 26A1.* Clin Cancer Res, 2004. **10**(18 Pt 1): p. 6265-75.
55. Hultin, T.A., M.S. Filla, and D.L. McCormick, *Distribution and metabolism of the retinoid, N-(4-methoxyphenyl)-all-trans-retinamide, the major metabolite of N-(4-hydroxyphenyl)-all-trans-retinamide, in female mice.* Drug Metab Dispos, 1990. **18**(2): p. 175-9.
56. Mehta, R.R., et al., *Metabolism of N-[4-hydroxyphenyl]retinamide (4-HPR) to N-[4-methoxyphenyl]retinamide (4-MPR) may serve as a biomarker for its efficacy against human breast cancer and melanoma cells.* Eur J Cancer, 1998. **34**(6): p. 902-7.
57. Formelli, F., et al., *Pharmacokinetics of oral fenretinide in neuroblastoma patients: indications for optimal dose and dosing schedule also with respect to the active metabolite 4-oxo-fenretinide.* Cancer Chemother Pharmacol, 2008. **62**(4): p. 655-65.
58. Garaventa, A., et al., *Phase I trial and pharmacokinetics of fenretinide in children with neuroblastoma.* Clin Cancer Res, 2003. **9**(6): p. 2032-9.
59. Sani, B.P., Y.F. Shealy, and D.L. Hill, *N-(4-hydroxyphenyl)retinamide: interactions with retinoid-binding proteins/receptors.* Carcinogenesis, 1995. **16**(10): p. 2531-4.
60. Graves, R.A., et al., *Formulation and evaluation of biodegradable nanoparticles for the oral delivery of fenretinide.* Eur J Pharm Sci, 2015. **76**: p. 1-9.
61. Ledet, G.A., et al., *Preparation and In Vitro Evaluation of Hydrophilic Fenretinide Nanoparticles.* Int J Pharm, 2015. **479**(2): p. 329-37.

62. Maurer, B.J., et al., *Improved oral delivery of N-(4-hydroxyphenyl)retinamide with a novel LYM-X-SORB organized lipid complex.* Clin Cancer Res, 2007. **13**(10): p. 3079-86.
63. Maurer, B.J., et al., *Phase I Trial of Fenretinide Delivered Orally in a Novel Organized Lipid Complex in Patients with Relapsed/Refractory Neuroblastoma: A Report from the New Approaches to Neuroblastoma Therapy (NANT) Consortium.* Pediatr Blood Cancer, 2013. **60**(11): p. 1801-8.
64. Kummar, S., et al., *Phase I trial of fenretinide lym-x-sorb oral powder in adults with solid tumors and lymphomas.* Anticancer Res, 2011. **31**(3): p. 961-6.
65. Lopez-Barcons, L., et al., *P450 inhibitor ketoconazole increased the intratumor drug levels and antitumor activity of fenretinide in human neuroblastoma xenograft models.* Int J Cancer, 2017. **141**(2): p. 405-413.
66. Mohrbacher, A.M., et al., *Phase I Study of Fenretinide Delivered Intravenously in Patients with Relapsed or Refractory Hematologic Malignancies: A California Cancer Consortium Trial.* Clin Cancer Res, 2017. **23**(16): p. 4550-4555.
67. Chen, N.E., et al., *Reactive Oxygen Species Mediates the Synergistic Activity of Fenretinide Combined with the Microtubule Inhibitor ABT-751 against Multidrug-Resistant Recurrent Neuroblastoma Xenografts.* Mol Cancer Ther, 2016. **15**(11): p. 2653-2664.
68. Villablanca, J.G., et al., *Phase I trial of oral fenretinide in children with high-risk solid tumors: a report from the Children's Oncology Group (CCG 09709).* J Clin Oncol, 2006. **24**(21): p. 3423-30.
69. Blomhoff, R. and H.K. Blomhoff, *Overview of retinoid metabolism and function.* J Neurobiol, 2006. **66**(7): p. 606-30.
70. Sheikh, M.S., et al., *N-(4-hydroxyphenyl)retinamide (4-HPR)-mediated biological actions involve retinoid receptor-independent pathways in human breast carcinoma.* Carcinogenesis, 1995. **16**(10): p. 2477-2486.
71. Delia, D., et al., *N-(4-hydroxyphenyl)retinamide induces apoptosis of malignant hemopoietic cell lines including those unresponsive to retinoic acid.* Cancer Res, 1993. **53**(24): p. 6036-41.
72. Fanjul, A.N., et al., *4-Hydroxyphenyl retinamide is a highly selective activator of retinoid receptors.* J Biol Chem, 1996. **271**(37): p. 22441-6.
73. Sani, B.P., Y.F. Shealy, and D.L. Hill, *N-(4-hydroxyphenyl)retinamide: interactions with retinoid-binding proteins/receptors.* Carcinogenesis, 1995. **16**(10): p. 2531-2534.
74. Yang, H., et al., *Induction and intracellular localization of Nur77 dictate fenretinide-induced apoptosis of human liver cancer cells.* Biochem Pharmacol, 2010. **79**(7): p. 948-54.
75. Suzuki, S., et al., *Implication of mitochondria-derived reactive oxygen species, cytochrome C and caspase-3 in N-(4-hydroxyphenyl)retinamide-induced apoptosis in cervical carcinoma cells.* Oncogene, 1999. **18**(46): p. 6380-7.
76. Osone, S., et al., *Fenretinide induces sustained-activation of JNK/p38 MAPK and apoptosis in a reactive oxygen species-dependent manner in neuroblastoma cells.* Int J Cancer, 2004. **112**(2): p. 219-24.
77. Goto, H., et al., *N-(4-Hydroxyphenyl)retinamide (4-HPR) induces leukemia cell death via generation of reactive oxygen species.* Int J Hematol, 2003. **78**(3): p. 219-25.
78. Tosetti, F., et al., *N-(4-hydroxyphenyl)retinamide inhibits retinoblastoma growth through reactive oxygen species-mediated cell death.* Mol Pharmacol, 2003. **63**(3): p. 565-73.
79. Cuperus, R., et al., *Fenretinide induces mitochondrial ROS and inhibits the mitochondrial respiratory chain in neuroblastoma.* Cell Mol Life Sci, 2010. **67**(5): p. 807-16.
80. Asumendi, A., et al., *Implication of mitochondria-derived ROS and cardiolipin peroxidation in N-(4-hydroxyphenyl)retinamide-induced apoptosis.* Br J Cancer, 2002. **86**(12): p. 1951-6.

81. Appierto, V., et al., *PLAB induction in fenretinide-induced apoptosis of ovarian cancer cells occurs via a ROS-dependent mechanism involving ER stress and JNK activation.* Carcinogenesis, 2009. **30**(5): p. 824-31.
82. Corazzari, M., et al., *Growth and DNA damage-inducible transcription factor 153 mediates apoptosis in response to fenretinide but not synergy between fenretinide and chemotherapeutic drugs in neuroblastoma.* Mol Pharmacol, 2003. **64**(6): p. 1370-8.
83. Anding, A.L., et al., *The unhydrolyzable fenretinide analogue 4-hydroxybenzylretinone induces the proapoptotic genes GADD153 (CHOP) and Bcl-2-binding component 3 (PUMA) and apoptosis that is caspase- dependent and independent of the retinoic acid receptor*. Cancer Res, 2007. **67**(13): p. 6270-7.
84. Kadara, H., et al., *Induction of endoplasmic reticulum stress by the pro-apoptotic retinoid N-(4-hydroxyphenyl)retinamide via a reactive oxygen species-dependent mechanism in human head and neck cancer cells.* Cancer Biol Ther, 2007. **6**(5): p. 705-11.
85. Hail, N., Jr. and R. Lotan, *Mitochondrial respiration is uniquely associated with the prooxidant and apoptotic effects of N-(4-hydroxyphenyl)retinamide.* J Biol Chem, 2001. **276**(49): p. 45614-21.
86. Myatt, S.S., C.P. Redfern, and S.A. Burchill, *p38MAPK-Dependent sensitivity of Ewing's sarcoma family of tumors to fenretinide-induced cell death.* Clin Cancer Res, 2005. **11**(8): p. 3136-48.
87. Lovat, P.E., et al., *Bak: a downstream mediator of fenretinide-induced apoptosis of SH-SY5Y neuroblastoma cells.* Cancer Res, 2003. **63**(21): p. 7310-3.
88. Kim, H.J., et al., *N-(4-hydroxyphenyl)retinamide-induced apoptosis triggered by reactive oxygen species is mediated by activation of MAPKs in head and neck squamous carcinoma cells.* Oncogene, 2006. **25**(19): p. 2785-94.
89. Lovat, P.E., et al., *Induction of GADD153 and Bak: novel molecular targets of fenretinide-induced apoptosis of neuroblastoma.* Cancer Lett, 2003. **197**(1-2): p. 157-63.
90. Makena, M.R., et al., *Reactive Oxygen Species-Mediated Synergism of Fenretinide and Romidepsin in Preclinical Models of T-cell Lymphoid Malignancies.* Mol Cancer Ther, 2017. **16**(4): p. 649-661.
91. Boya, P., et al., *The chemopreventive agent N-(4-hydroxyphenyl)retinamide induces apoptosis through a mitochondrial pathway regulated by proteins from the Bcl-2 family.* Oncogene, 2003. **22**(40): p. 6220-30.
92. Armstrong, J.L., et al., *Role of Noxa in p53-independent fenretinide-induced apoptosis of neuroectodermal tumours.* Apoptosis, 2007. **12**(3): p. 613-22.
93. Bassani, B., et al., *Fenretinide (4-HPR) Targets Caspase-9, ERK 1/2 and the Wnt3a/beta-Catenin Pathway in Medulloblastoma Cells and Medulloblastoma Cell Spheroids.* PLoS One, 2016. **11**(7): p. e0154111.
94. Fang, H., et al., *Synergistic activity of fenretinide and the Bcl-2 family protein inhibitor ABT-737 against human neuroblastoma.* Clin Cancer Res, 2011. **17**(22): p. 7093-104.
95. George, J., N.L. Banik, and S.K. Ray, *Survivin knockdown and concurrent 4-HPR treatment controlled human glioblastoma in vitro and in vivo.* Neuro Oncol, 2010. **12**(11): p. 1088-101.
96. Mukherjee, N., et al., *Combining a BCL2 inhibitor with the retinoid derivative fenretinide targets melanoma cells including melanoma initiating cells.* J Invest Dermatol, 2015. **135**(3): p. 842-850.
97. Raguenez, G., et al., *Fenretinide-induced caspase-8 activation and apoptosis in an established model of metastatic neuroblastoma.* BMC Cancer, 2009. **9**: p. 97.
98. Ulukaya, E., et al., *Additive enhancement of apoptosis by TRAIL and fenretinide in metastatic breast cancer cells in vitro.* Biomed Pharmacother, 2014. **68**(4): p. 477-82.

99. Herrero Martin, D., A. Boro, and B.W. Schafer, *Cell-based small-molecule compound screen identifies fenretinide as potential therapeutic for translocation-positive rhabdomyosarcoma.* PLoS One, 2013. **8**(1): p. e55072.
100. Cao, J., et al., *The oxidation states of DJ-1 dictate the cell fate in response to oxidative stress triggered by 4-hpr: autophagy or apoptosis?* Antioxid Redox Signal, 2014. **21**(10): p. 1443-59.
101. Lee, J., et al., *Sphingolipids as cell fate regulators in lung development and disease.* Apoptosis, 2015. **20**(5): p. 740-57.
102. Zheng, W., et al., *Ceramides and other bioactive sphingolipid backbones in health and disease: lipidomic analysis, metabolism and roles in membrane structure, dynamics, signaling and autophagy.* Biochim Biophys Acta, 2006. **1758**(12): p. 1864-84.
103. Hail, N., Jr., et al., *Dihydroorotate dehydrogenase is required for N-(4-hydroxyphenyl)retinamide-induced reactive oxygen species production and apoptosis.* Free Radic Biol Med, 2010. **49**(1): p. 109-16.
104. Hail, N., Jr., H.J. Kim, and R. Lotan, *Mechanisms of fenretinide-induced apoptosis.* Apoptosis, 2006. **11**(10): p. 1677-94.
105. Rahmaniyan, M., et al., *Identification of dihydroceramide desaturase as a direct in vitro target for fenretinide.* J Biol Chem, 2011. **286**(28): p. 24754-64.
106. Apraiz, A., et al., *Dihydroceramide accumulation and reactive oxygen species are distinct and non essential events in 4-HPR mediated leukemia cell death.* Biochem Cell Biol, 2012. **90**(2): p. 209-23.
107. Messner, M.C. and M.C. Cabot, *Cytotoxic responses to N-(4-hydroxyphenyl)retinamide in human pancreatic cancer cells.* Cancer Chemother Pharmacol, 2011. **68**(2): p. 477-87.
108. Droge, W., *Free radicals in the physiological control of cell function.* Physiol Rev, 2002. **82**(1): p. 47-95.
109. Brewer, T.F., et al., *Chemical approaches to discovery and study of sources and targets of hydrogen peroxide redox signaling through NADPH oxidase proteins.* Annu Rev Biochem, 2015. **84**: p. 765-90.
110. Goncalves, R.L., et al., *Sites of superoxide and hydrogen peroxide production by muscle mitochondria assessed ex vivo under conditions mimicking rest and exercise.* J Biol Chem, 2015. **290**(1): p. 209-27.
111. Murphy, M.P., *How mitochondria produce reactive oxygen species.* Biochem J, 2009. **417**(1): p. 1-13.
112. Marklund, S.L., *Extracellular superoxide dismutase and other superoxide dismutase isoenzymes in tissues from nine mammalian species.* Biochemical Journal, 1984. **222**(3): p. 649-655.
113. Bedard, K. and K.H. Krause, *The NOX family of ROS-generating NADPH oxidases: physiology and pathophysiology.* Physiol Rev, 2007. **87**(1): p. 245-313.
114. Winterbourn, C.C., *Toxicity of iron and hydrogen peroxide: the Fenton reaction.* Toxicol Lett, 1995. **82-83**: p. 969-74.
115. Valko, M., et al., *Free radicals, metals and antioxidants in oxidative stress-induced cancer.* Chem Biol Interact, 2006. **160**(1): p. 1-40.
116. Couto, N., J. Wood, and J. Barber, *The role of glutathione reductase and related enzymes on cellular redox homoeostasis network.* Free Radical Biology and Medicine, 2016. **95**: p. 27-42.
117. Lauer, A.C., et al., *Dose-dependent vitamin C uptake and radical scavenging activity in human skin measured with in vivo electron paramagnetic resonance spectroscopy.* Skin Pharmacol Physiol, 2013. **26**(3): p. 147-54.
118. Rhee, S.G., et al., *Peroxiredoxin functions as a peroxidase and a regulator and sensor of local peroxides.* J Biol Chem, 2012. **287**(7): p. 4403-10.

119. Berndt, C., C.H. Lillig, and A. Holmgren, *Thiol-based mechanisms of the thioredoxin and glutaredoxin systems: implications for diseases in the cardiovascular system.* Am J Physiol Heart Circ Physiol, 2007. **292**(3): p. H1227-36.
120. Ishii, T., et al., *Transcription factor Nrf2 coordinately regulates a group of oxidative stress-inducible genes in macrophages.* J Biol Chem, 2000. **275**(21): p. 16023-9.
121. Kobayashi, A., et al., *Oxidative stress sensor Keap1 functions as an adaptor for Cul3-based E3 ligase to regulate proteasomal degradation of Nrf2.* Mol Cell Biol, 2004. **24**(16): p. 7130-9.
122. Fourquet, S., et al., *Activation of NRF2 by nitrosative agents and H2O2 involves KEAP1 disulfide formation.* J Biol Chem, 2010. **285**(11): p. 8463-71.
123. Kobayashi, A., T. Ohta, and M. Yamamoto, *Unique function of the Nrf2-Keap1 pathway in the inducible expression of antioxidant and detoxifying enzymes.* Methods Enzymol, 2004. **378**: p. 273-86.
124. Kobayashi, M. and M. Yamamoto, *Molecular mechanisms activating the Nrf2-Keap1 pathway of antioxidant gene regulation.* Antioxid Redox Signal, 2005. **7**(3-4): p. 385-94.
125. Wu, K.C., J.Y. Cui, and C.D. Klaassen, *Beneficial role of Nrf2 in regulating NADPH generation and consumption.* Toxicol Sci, 2011. **123**(2): p. 590-600.
126. Reczek, C.R. and N.S. Chandel, *The Two Faces of Reactive Oxygen Species in Cancer.* Annual Review of Cancer Biology, 2017. **1**(1): p. 79-98.
127. Alfadda, A.A. and R.M. Sallam, *Reactive oxygen species in health and disease.* J Biomed Biotechnol, 2012. **2012**: p. 936486.
128. Glennon-Alty, L., et al., *Neutrophils and redox stress in the pathogenesis of autoimmune disease.* Free Radic Biol Med, 2018.
129. Sena, L.A. and N.S. Chandel, *Physiological roles of mitochondrial reactive oxygen species.* Mol Cell, 2012. **48**(2): p. 158-67.
130. Sabharwal, S.S. and P.T. Schumacker, *Mitochondrial ROS in cancer: initiators, amplifiers or an Achilles' heel?* Nat Rev Cancer, 2014. **14**(11): p. 709-21.
131. Trachootham, D., J. Alexandre, and P. Huang, *Targeting cancer cells by ROS-mediated mechanisms: a radical therapeutic approach?* Nat Rev Drug Discov, 2009. **8**(7): p. 579-91.
132. Toyokuni, S., et al., *Persistent oxidative stress in cancer.* FEBS Lett, 1995. **358**(1): p. 1-3.
133. Irani, K., et al., *Mitogenic signaling mediated by oxidants in Ras-transformed fibroblasts.* Science, 1997. **275**(5306): p. 1649-52.
134. Sablina, A.A., et al., *The antioxidant function of the p53 tumor suppressor.* Nature Medicine, 2005. **11**: p. 1306.
135. Cao, L., et al., *Absence of full-length Brca1 sensitizes mice to oxidative stress and carcinogen-induced tumorigenesis in the esophagus and forestomach.* Carcinogenesis, 2007. **28**(7): p. 1401-1407.
136. Kruiswijk, F., C.F. Labuschagne, and K.H. Vousden, *p53 in survival, death and metabolic health: a lifeguard with a licence to kill.* Nat Rev Mol Cell Biol, 2015. **16**(7): p. 393-405.
137. Oberley, L.W. and G.R. Buettner, *Role of superoxide dismutase in cancer: a review.* Cancer Res, 1979. **39**(4): p. 1141-9.
138. Egler, R.A., et al., *Regulation of reactive oxygen species, DNA damage, and c-Myc function by peroxiredoxin 1.* Oncogene, 2005. **24**(54): p. 8038-50.
139. No, J.H., Y.B. Kim, and Y.S. Song, *Targeting nrf2 signaling to combat chemoresistance.* J Cancer Prev, 2014. **19**(2): p. 111-7.
140. DeNicola, G.M., et al., *NRF2 regulates serine biosynthesis in non-small cell lung cancer.* Nat Genet, 2015. **47**(12): p. 1475-81.
141. Winterbourn, C.C. and D. Metodiewa, *Reactivity of biologically important thiol compounds with superoxide and hydrogen peroxide.* Free Radical Biology and Medicine, 1999. **27**(3): p. 322-328.

142. Halliwell, B. and J.M.C. Gutteridge, *Oxygen free radicals and iron in relation to biology and medicine: Some problems and concepts.* Archives of Biochemistry and Biophysics, 1986. **246**(2): p. 501-514.
143. Bienert, G.P., J.K. Schjoerring, and T.P. Jahn, *Membrane transport of hydrogen peroxide.* Biochimica et Biophysica Acta (BBA) - Biomembranes, 2006. **1758**(8): p. 994-1003.
144. Lee, S.R., et al., *Reversible inactivation of the tumor suppressor PTEN by H2O2.* J Biol Chem, 2002. **277**(23): p. 20336-42.
145. Salmeen, A., et al., *Redox regulation of protein tyrosine phosphatase 1B involves a sulphenyl-amide intermediate.* Nature, 2003. **423**: p. 769.
146. Son, Y., et al., *Mitogen-Activated Protein Kinases and Reactive Oxygen Species: How Can ROS Activate MAPK Pathways?* J Signal Transduct, 2011. **2011**: p. 792639.
147. Cantley, L.C., *The phosphoinositide 3-kinase pathway.* Science, 2002. **296**(5573): p. 1655-7.
148. Weinberg, F., et al., *Mitochondrial metabolism and ROS generation are essential for Kras-mediated tumorigenicity.* Proc Natl Acad Sci U S A, 2010. **107**(19): p. 8788-93.
149. Chandel, N.S., et al., *Role of oxidants in NF-kappa B activation and TNF-alpha gene transcription induced by hypoxia and endotoxin.* J Immunol, 2000. **165**(2): p. 1013-21.
150. Chandel, N.S., P.T. Schumacker, and R.H. Arch, *Reactive oxygen species are downstream products of TRAF-mediated signal transduction.* J Biol Chem, 2001. **276**(46): p. 42728-36.
151. Karin, M. and A. Lin, *NF-kappaB at the crossroads of life and death.* Nat Immunol, 2002. **3**(3): p. 221-7.
152. Jeon, S.M., N.S. Chandel, and N. Hay, *AMPK regulates NADPH homeostasis to promote tumour cell survival during energy stress.* Nature, 2012. **485**(7400): p. 661-5.
153. Huang, Y., et al., *Vascular normalization as an emerging strategy to enhance cancer immunotherapy.* Cancer Res, 2013. **73**(10): p. 2943-8.
154. Bell, E.L., B.M. Emerling, and N.S. Chandel, *Mitochondrial regulation of oxygen sensing.* Mitochondrion, 2005. **5**(5): p. 322-32.
155. Kaelin, W.G., Jr. and P.J. Ratcliffe, *Oxygen sensing by metazoans: the central role of the HIF hydroxylase pathway.* Mol Cell, 2008. **30**(4): p. 393-402.
156. Semenza, G.L., *Hypoxia-inducible factors in physiology and medicine.* Cell, 2012. **148**(3): p. 399-408.
157. Klimova, T. and N.S. Chandel, *Mitochondrial complex III regulates hypoxic activation of HIF.* Cell Death Differ, 2008. **15**(4): p. 660-6.
158. Masoud, G.N. and W. Li, *HIF-1alpha pathway: role, regulation and intervention for cancer therapy.* Acta Pharm Sin B, 2015. **5**(5): p. 378-89.
159. Tochhawng, L., et al., *Redox regulation of cancer cell migration and invasion.* Mitochondrion, 2013. **13**(3): p. 246-53.
160. Giannoni, E., et al., *Intracellular Reactive Oxygen Species Activate Src Tyrosine Kinase during Cell Adhesion and Anchorage-Dependent Cell Growth.* Mol Cell Biol, 2005. **25**(15): p. 6391-403.
161. Ichijo, H., et al., *Induction of apoptosis by ASK1, a mammalian MAPKKK that activates SAPK/JNK and p38 signaling pathways.* Science, 1997. **275**(5296): p. 90-4.
162. Saitoh, M., et al., *Mammalian thioredoxin is a direct inhibitor of apoptosis signal-regulating kinase (ASK) 1.* Embo j, 1998. **17**(9): p. 2596-606.
163. Han, J. and P. Sun, *The pathways to tumor suppression via route p38.* Trends Biochem Sci, 2007. **32**(8): p. 364-71.
164. Kaufmann, S.H. and W.C. Earnshaw, *Induction of apoptosis by cancer chemotherapy.* Exp Cell Res, 2000. **256**(1): p. 42-9.

165. Yun, J., et al., *Vitamin C selectively kills KRAS and BRAF mutant colorectal cancer cells by targeting GAPDH.* Science, 2015. **350**(6266): p. 1391-6.
166. Trachootham, D., et al., *Selective killing of oncogenically transformed cells through a ROS-mediated mechanism by beta-phenylethyl isothiocyanate.* Cancer Cell, 2006. **10**(3): p. 241-52.
167. Glasauer, A. and N.S. Chandel, *Targeting antioxidants for cancer therapy.* Biochem Pharmacol, 2014. **92**(1): p. 90-101.
168. Andringa, K.K., et al., *Inhibition of glutamate cysteine ligase activity sensitizes human breast cancer cells to the toxicity of 2-deoxy-D-glucose.* Cancer Res, 2006. **66**(3): p. 1605-10.
169. Fath, M.A., et al., *Enhancement of carboplatin-mediated lung cancer cell killing by simultaneous disruption of glutathione and thioredoxin metabolism.* Clin Cancer Res, 2011. **17**(19): p. 6206-17.
170. Glasauer, A., et al., *Targeting SOD1 reduces experimental non-small-cell lung cancer.* J Clin Invest, 2014. **124**(1): p. 117-28.
171. Magda, D. and R.A. Miller, *Motexafin gadolinium: a novel redox active drug for cancer therapy.* Semin Cancer Biol, 2006. **16**(6): p. 466-76.
172. Villeneuve, N.F., A. Lau, and D.D. Zhang, *Regulation of the Nrf2-Keap1 antioxidant response by the ubiquitin proteasome system: an insight into cullin-ring ubiquitin ligases.* Antioxid Redox Signal, 2010. **13**(11): p. 1699-712.
173. DeNicola, G.M., et al., *Oncogene-induced Nrf2 transcription promotes ROS detoxification and tumorigenesis.* Nature, 2011. **475**(7354): p. 106-9.
174. Wang, X.J., et al., *Nrf2 enhances resistance of cancer cells to chemotherapeutic drugs, the dark side of Nrf2.* Carcinogenesis, 2008. **29**(6): p. 1235-43.
175. Jaramillo, M.C. and D.D. Zhang, *The emerging role of the Nrf2-Keap1 signaling pathway in cancer.* Genes Dev, 2013. **27**(20): p. 2179-91.
176. Jeong, W.S., M. Jun, and A.N. Kong, *Nrf2: a potential molecular target for cancer chemoprevention by natural compounds.* Antioxid Redox Signal, 2006. **8**(1-2): p. 99-106.
177. Taguchi, K. and M. Yamamoto, *The KEAP1-NRF2 System in Cancer.* Front Oncol, 2017. **7**: p. 85.
178. Scott, C.C., F. Vacca, and J. Gruenberg, *Endosome maturation, transport and functions.* Semin Cell Dev Biol, 2014. **31**: p. 2-10.
179. Preston, J.E., N. Joan Abbott, and D.J. Begley, *Transcytosis of macromolecules at the blood-brain barrier.* Adv Pharmacol, 2014. **71**: p. 147-63.
180. Dutta, D. and J.G. Donaldson, *Search for inhibitors of endocytosis: Intended specificity and unintended consequences.* Cell Logist, 2012. **2**(4): p. 203-208.
181. Kumari, S., S. Mg, and S. Mayor, *Endocytosis unplugged: multiple ways to enter the cell.* Cell Res, 2010. **20**(3): p. 256-75.
182. Mayor, S. and R.E. Pagano, *Pathways of clathrin-independent endocytosis.* Nat Rev Mol Cell Biol, 2007. **8**(8): p. 603-12.
183. !!! INVALID CITATION !!! [181].
184. Kirchhausen, T., D. Owen, and S.C. Harrison, *Molecular structure, function, and dynamics of clathrin-mediated membrane traffic.* Cold Spring Harb Perspect Biol, 2014. **6**(5): p. a016725.
185. Kirchhausen, T., *Clathrin.* Annu Rev Biochem, 2000. **69**: p. 699-727.
186. Elkin, S.R., A.M. Lakoduk, and S.L. Schmid, *Endocytic pathways and endosomal trafficking: a primer.* Wien Med Wochenschr, 2016. **166**(7-8): p. 196-204.
187. Eschenburg, S. and T.F. Reubold, *Modulation of dynamin function by small molecules.* Biol Chem, 2018.
188. Kaksonen, M. and A. Roux, *Mechanisms of clathrin-mediated endocytosis.* Nat Rev Mol Cell Biol, 2018. **19**(5): p. 313-326.

189. Skruzny, M., et al., *An organized co-assembly of clathrin adaptors is essential for endocytosis.* Dev Cell, 2015. **33**(2): p. 150-62.
190. Sandvig, K., S. Kavaliauskiene, and T. Skotland, *Clathrin-independent endocytosis: an increasing degree of complexity.* Histochem Cell Biol, 2018. **150**(2): p. 107-118.
191. Kiss, A.L., *Caveolae and the regulation of endocytosis.* Adv Exp Med Biol, 2012. **729**: p. 14-28.
192. Shpetner, H.S. and R.B. Vallee, *Identification of dynamin, a novel mechanochemical enzyme that mediates interactions between microtubules.* Cell, 1989. **59**(3): p. 421-32.
193. van der Bliek, A.M. and E.M. Meyerowitz, *Dynamin-like protein encoded by the Drosophila shibire gene associated with vesicular traffic.* Nature, 1991. **351**(6325): p. 411-4.
194. Antonny, B., et al., *Membrane fission by dynamin: what we know and what we need to know.* Embo j, 2016. **35**(21): p. 2270-2284.
195. Sundborger, A.C., et al., *A dynamin mutant defines a superconstricted prefission state.* Cell Rep, 2014. **8**(3): p. 734-42.
196. Ferguson, S.M. and P. De Camilli, *Dynamin, a membrane-remodelling GTPase.* Nat Rev Mol Cell Biol, 2012. **13**(2): p. 75-88.
197. Chappie, J.S., et al., *A pseudoatomic model of the dynamin polymer identifies a hydrolysis-dependent powerstroke.* Cell, 2011. **147**(1): p. 209-22.
198. Mattila, J.P., et al., *A hemi-fission intermediate links two mechanistically distinct stages of membrane fission.* Nature, 2015. **524**(7563): p. 109-113.
199. Krueger, E.W., et al., *A dynamin-cortactin-Arp2/3 complex mediates actin reorganization in growth factor-stimulated cells.* Mol Biol Cell, 2003. **14**(3): p. 1085-96.
200. Schlunck, G., et al., *Modulation of Rac localization and function by dynamin.* Mol Biol Cell, 2004. **15**(1): p. 256-67.
201. Armstrong, S.M., et al., *Co-regulation of transcellular and paracellular leak across microvascular endothelium by dynamin and Rac.* Am J Pathol, 2012. **180**(3): p. 1308-23.
202. Park, R.J., et al., *Dynamin triple knockout cells reveal off target effects of commonly used dynamin inhibitors.* J Cell Sci, 2013. **126**(Pt 22): p. 5305-12.
203. Macia, E., et al., *Dynasore, a cell-permeable inhibitor of dynamin.* Dev Cell, 2006. **10**(6): p. 839-50.
204. Mohanakrishnan, A., et al., *A highly-sensitive high throughput assay for dynamin's basal GTPase activity.* PLoS One, 2017. **12**(9): p. e0185639.
205. McCluskey, A., et al., *Building a better dynasore: the dyngo compounds potently inhibit dynamin and endocytosis.* Traffic, 2013. **14**(12): p. 1272-89.
206. Dunn, V.K. and E. Gleason, *Inhibition of endocytosis suppresses the nitric oxide-dependent release of Cl- in retinal amacrine cells.* PLoS One, 2018. **13**(7): p. e0201184.
207. Yuan, M., et al., *Enhanced human enterovirus 71 infection by endocytosis inhibitors reveals multiple entry pathways by enterovirus causing hand-foot-and-mouth diseases.* Virol J, 2018. **15**(1): p. 1.
208. Persaud, A., et al., *Dynamin inhibitors block activation of mTORC1 by amino acids independently of dynamin.* J Cell Sci, 2018. **131**(1).
209. Preta, G., J.G. Cronin, and I.M. Sheldon, *Dynasore - not just a dynamin inhibitor.* Cell Commun Signal, 2015. **13**: p. 24.
210. Glucksmann, A., *Cell deaths in normal vertebrate ontogeny.* Biol Rev Camb Philos Soc, 1951. **26**(1): p. 59-86.
211. Kerr, J.F., *A histochemical study of hypertrophy and ischaemic injury of rat liver with special reference to changes in lysosomes.* J Pathol Bacteriol, 1965. **90**(2): p. 419-35.
212. Schweichel, J.U. and H.J. Merker, *The morphology of various types of cell death in prenatal tissues.* Teratology, 1973. **7**(3): p. 253-66.

213. Hotchkiss, R.S., et al., *Cell death.* N Engl J Med, 2009. **361**(16): p. 1570-83.
214. Galluzzi, L., et al., *Molecular definitions of cell death subroutines: recommendations of the Nomenclature Committee on Cell Death 2012.* Cell Death Differ, 2012. **19**(1): p. 107-20.
215. Zeiss, C.J., *The apoptosis-necrosis continuum: insights from genetically altered mice.* Vet Pathol, 2003. **40**(5): p. 481-95.
216. Galluzzi, L., et al., *Molecular mechanisms of cell death: recommendations of the Nomenclature Committee on Cell Death 2018.* Cell Death Differ, 2018. **25**(3): p. 486-541.
217. Galluzzi, L., et al., *Molecular mechanisms of cell death: recommendations of the Nomenclature Committee on Cell Death 2018.* Cell Death Differ, 2018. **25**(3): p. 486-541.
218. Kerr, J.F., A.H. Wyllie, and A.R. Currie, *Apoptosis: a basic biological phenomenon with wide-ranging implications in tissue kinetics.* Br J Cancer, 1972. **26**(4): p. 239-57.
219. Tata, J.R., *Requirement for RNA and protein synthesis for induced regression of the tadpole tail in organ culture.* Dev Biol, 1966. **13**(1): p. 77-94.
220. Sanders, E.J. and M.A. Wride, *Programmed cell death in development.* Int Rev Cytol, 1995. **163**: p. 105-73.
221. Riedl, S.J. and Y. Shi, *Molecular mechanisms of caspase regulation during apoptosis.* Nat Rev Mol Cell Biol, 2004. **5**(11): p. 897-907.
222. Savill, J. and V. Fadok, *Corpse clearance defines the meaning of cell death.* Nature, 2000. **407**(6805): p. 784-8.
223. Hacker, G., *The morphology of apoptosis.* Cell Tissue Res, 2000. **301**(1): p. 5-17.
224. Mohler, H., R.W. Pfirrmann, and K. Frei, *Redox-directed cancer therapeutics: Taurolidine and Piperlongumine as broadly effective antineoplastic agents (review).* Int J Oncol, 2014. **45**(4): p. 1329-36.
225. Wajant, H., *The Fas signaling pathway: more than a paradigm.* Science, 2002. **296**(5573): p. 1635-6.
226. Schutze, S., V. Tchikov, and W. Schneider-Brachert, *Regulation of TNFR1 and CD95 signalling by receptor compartmentalization.* Nat Rev Mol Cell Biol, 2008. **9**(8): p. 655-62.
227. Siegel, R.M., et al., *Fas preassociation required for apoptosis signaling and dominant inhibition by pathogenic mutations.* Science, 2000. **288**(5475): p. 2354-7.
228. Schulze-Osthoff, K., et al., *Apoptosis signaling by death receptors.* Eur J Biochem, 1998. **254**(3): p. 439-59.
229. Lavrik, I., A. Golks, and P.H. Krammer, *Death receptor signaling.* J Cell Sci, 2005. **118**(Pt 2): p. 265-7.
230. Delbridge, A.R., et al., *Thirty years of BCL-2: translating cell death discoveries into novel cancer therapies.* Nat Rev Cancer, 2016. **16**(2): p. 99-109.
231. Moldoveanu, T., et al., *Many players in BCL-2 family affairs.* Trends Biochem Sci, 2014. **39**(3): p. 101-11.
232. Shamas-Din, A., et al., *Mechanisms of action of Bcl-2 family proteins.* Cold Spring Harb Perspect Biol, 2013. **5**(4): p. a008714.
233. Dewson, G., et al., *Bax dimerizes via a symmetric BH3:groove interface during apoptosis.* Cell Death Differ, 2012. **19**(4): p. 661-70.
234. Gillies, L.A., et al., *Visual and functional demonstration of growing Bax-induced pores in mitochondrial outer membranes.* Mol Biol Cell, 2015. **26**(2): p. 339-49.
235. Antonsson, B., et al., *Inhibition of Bax channel-forming activity by Bcl-2.* Science, 1997. **277**(5324): p. 370-2.
236. Barclay, L.A., et al., *Inhibition of Pro-apoptotic BAX by a noncanonical interaction mechanism.* Mol Cell, 2015. **57**(5): p. 873-886.

237. Li, H., et al., *Cleavage of BID by caspase 8 mediates the mitochondrial damage in the Fas pathway of apoptosis.* Cell, 1998. **94**(4): p. 491-501.
238. Kroemer, G., L. Galluzzi, and C. Brenner, *Mitochondrial membrane permeabilization in cell death.* Physiol Rev, 2007. **87**(1): p. 99-163.
239. Li, P., et al., *Cytochrome c and dATP-dependent formation of Apaf-1/caspase-9 complex initiates an apoptotic protease cascade.* Cell, 1997. **91**(4): p. 479-89.
240. Tait, S.W. and D.R. Green, *Mitochondria and cell death: outer membrane permeabilization and beyond.* Nat Rev Mol Cell Biol, 2010. **11**(9): p. 621-32.
241. Roos, W.P., A.D. Thomas, and B. Kaina, *DNA damage and the balance between survival and death in cancer biology.* Nat Rev Cancer, 2016. **16**(1): p. 20-33.
242. Pihan, P., A. Carreras-Sureda, and C. Hetz, *BCL-2 family: integrating stress responses at the ER to control cell demise.* Cell Death Differ, 2017. **24**(9): p. 1478-1487.
243. Nunnari, J. and A. Suomalainen, *Mitochondria: in sickness and in health.* Cell, 2012. **148**(6): p. 1145-59.
244. Joza, N., et al., *Essential role of the mitochondrial apoptosis-inducing factor in programmed cell death.* Nature, 2001. **410**(6828): p. 549-54.
245. Li, L.Y., X. Luo, and X. Wang, *Endonuclease G is an apoptotic DNase when released from mitochondria.* Nature, 2001. **412**(6842): p. 95-9.
246. Chai, J., et al., *Structural and biochemical basis of apoptotic activation by Smac/DIABLO.* Nature, 2000. **406**(6798): p. 855-62.
247. Yang, Q.H., et al., *Omi/HtrA2 catalytic cleavage of inhibitor of apoptosis (IAP) irreversibly inactivates IAPs and facilitates caspase activity in apoptosis.* Genes Dev, 2003. **17**(12): p. 1487-96.
248. Srinivasula, S.M., et al., *Inhibitor of apoptosis proteins are substrates for the mitochondrial serine protease Omi/HtrA2.* J Biol Chem, 2003. **278**(34): p. 31469-72.
249. Krakstad, C. and M. Chekenya, *Survival signalling and apoptosis resistance in glioblastomas: opportunities for targeted therapeutics.* Mol Cancer, 2010. **9**: p. 135.
250. Laster, S.M., J.G. Wood, and L.R. Gooding, *Tumor necrosis factor can induce both apoptic and necrotic forms of cell lysis.* J Immunol, 1988. **141**(8): p. 2629-34.
251. Vanden Berghe, T., et al., *Regulated necrosis: the expanding network of non-apoptotic cell death pathways.* Nat Rev Mol Cell Biol, 2014. **15**(2): p. 135-47.
252. Vandenabeele, P., et al., *Molecular mechanisms of necroptosis: an ordered cellular explosion.* Nat Rev Mol Cell Biol, 2010. **11**(10): p. 700-14.
253. Abraham, M.C., Y. Lu, and S. Shaham, *A morphologically conserved nonapoptotic program promotes linker cell death in Caenorhabditis elegans.* Dev Cell, 2007. **12**(1): p. 73-86.
254. Chu-Wang, I.W. and R.W. Oppenheim, *Cell death of motoneurons in the chick embryo spinal cord. I. A light and electron microscopic study of naturally occurring and induced cell loss during development.* J Comp Neurol, 1978. **177**(1): p. 33-57.
255. Galluzzi, L., et al., *Molecular mechanisms of regulated necrosis.* Semin Cell Dev Biol, 2014. **35**: p. 24-32.
256. Kaiser, W.J., et al., *Toll-like receptor 3-mediated necrosis via TRIF, RIP3, and MLKL.* J Biol Chem, 2013. **288**(43): p. 31268-79.
257. Vercammen, D., et al., *Dual signaling of the Fas receptor: initiation of both apoptotic and necrotic cell death pathways.* J Exp Med, 1998. **188**(5): p. 919-30.
258. Vercammen, D., et al., *Tumour necrosis factor-induced necrosis versus anti-Fas-induced apoptosis in L929 cells.* Cytokine, 1997. **9**(11): p. 801-8.
259. Maelfait, J., et al., *Sensing of viral and endogenous RNA by ZBP1/DAI induces necroptosis.* Embo j, 2017. **36**(17): p. 2529-2543.

260. Vandenabeele, P., et al., *The role of the kinases RIP1 and RIP3 in TNF-induced necrosis.* Sci Signal, 2010. **3**(115): p. re4.
261. He, S., et al., *Toll-like receptors activate programmed necrosis in macrophages through a receptor-interacting kinase-3-mediated pathway.* Proc Natl Acad Sci U S A, 2011. **108**(50): p. 20054-9.
262. Jouan-Lanhouet, S., et al., *TRAIL induces necroptosis involving RIPK1/RIPK3-dependent PARP-1 activation.* Cell Death Differ, 2012. **19**(12): p. 2003-14.
263. Basit, F., S. Cristofanon, and S. Fulda, *Obatoclax (GX15-070) triggers necroptosis by promoting the assembly of the necrosome on autophagosomal membranes.* Cell Death Differ, 2013. **20**(9): p. 1161-73.
264. Saveljeva, S., et al., *Endoplasmic reticulum stress induces ligand-independent TNFR1-mediated necroptosis in L929 cells.* Cell Death Dis, 2015. **6**: p. e1587.
265. Festjens, N., et al., *RIP1, a kinase on the crossroads of a cell's decision to live or die.* Cell Death Differ, 2007. **14**(3): p. 400-10.
266. Dondelinger, Y., et al., *NF-kappaB-Independent Role of IKKalpha/IKKbeta in Preventing RIPK1 Kinase-Dependent Apoptotic and Necroptotic Cell Death during TNF Signaling.* Mol Cell, 2015. **60**(1): p. 63-76.
267. Zheng, L., et al., *Competitive control of independent programs of tumor necrosis factor receptor-induced cell death by TRADD and RIP1.* Mol Cell Biol, 2006. **26**(9): p. 3505-13.
268. Pasparakis, M. and P. Vandenabeele, *Necroptosis and its role in inflammation.* Nature, 2015. **517**(7534): p. 311-20.
269. Wang, L., F. Du, and X. Wang, *TNF-alpha induces two distinct caspase-8 activation pathways.* Cell, 2008. **133**(4): p. 693-703.
270. He, S., et al., *Receptor interacting protein kinase-3 determines cellular necrotic response to TNF-alpha.* Cell, 2009. **137**(6): p. 1100-11.
271. Dondelinger, Y., et al., *MLKL compromises plasma membrane integrity by binding to phosphatidylinositol phosphates.* Cell Rep, 2014. **7**(4): p. 971-81.
272. Sun, L., et al., *Mixed lineage kinase domain-like protein mediates necrosis signaling downstream of RIP3 kinase.* Cell, 2012. **148**(1-2): p. 213-27.
273. Murphy, J.M., et al., *The pseudokinase MLKL mediates necroptosis via a molecular switch mechanism.* Immunity, 2013. **39**(3): p. 443-53.
274. Huang, D., et al., *The MLKL Channel in Necroptosis Is an Octamer Formed by Tetramers in a Dyadic Process.* Mol Cell Biol, 2017. **37**(5).
275. Xia, B., et al., *MLKL forms cation channels.* Cell Res, 2016. **26**(5): p. 517-28.
276. Grootjans, S., T. Vanden Berghe, and P. Vandenabeele, *Initiation and execution mechanisms of necroptosis: an overview.* Cell Death Differ, 2017. **24**(7): p. 1184-1195.
277. Upton, J.W., W.J. Kaiser, and E.S. Mocarski, *DAI/ZBP1/DLM-1 complexes with RIP3 to mediate virus-induced programmed necrosis that is targeted by murine cytomegalovirus vIRA.* Cell Host Microbe, 2012. **11**(3): p. 290-7.
278. Dixon, Scott J., et al., *Ferroptosis: An Iron-Dependent Form of Nonapoptotic Cell Death.* Cell, 2012. **149**(5): p. 1060-1072.
279. Dixon, S.J., *Ferroptosis: bug or feature?* Immunol Rev, 2017. **277**(1): p. 150-157.
280. Dixon, S.J. and B.R. Stockwell, *The role of iron and reactive oxygen species in cell death.* Nat Chem Biol, 2014. **10**(1): p. 9-17.
281. Stockwell, B., et al., *Ferroptosis: A Regulated Cell Death Nexus Linking Metabolism, Redox Biology, and Disease*. Vol. 171. 2017.
282. Cao, J.Y. and S.J. Dixon, *Mechanisms of ferroptosis.* Cell Mol Life Sci, 2016. **73**: p. 2195-209.

283. Yang, W.S., et al., *Regulation of ferroptotic cancer cell death by GPX4.* Cell, 2014. **156**(1-2): p. 317-331.
284. Lachaier, E., et al., *Sorafenib induces ferroptosis in human cancer cell lines originating from different solid tumors.* Anticancer Res, 2014. **34**(11): p. 6417-22.
285. Kagan, V.E., et al., *Oxidized arachidonic and adrenic PEs navigate cells to ferroptosis.* Nat Chem Biol, 2017. **13**(1): p. 81-90.
286. Gaschler, M.M. and B.R. Stockwell, *Lipid peroxidation in cell death.* Biochemical and Biophysical Research Communications, 2017. **482**(3): p. 419-425.
287. Gao, M., et al., *Glutaminolysis and Transferrin Regulate Ferroptosis.* Mol Cell, 2015. **59**(2): p. 298-308.
288. Hou, W., et al., *Autophagy promotes ferroptosis by degradation of ferritin.* Autophagy, 2016. **12**(8): p. 1425-8.
289. Abeysinghe, R.D., et al., *The environment of the lipoxygenase iron binding site explored with novel hydroxypyridinone iron chelators.* J Biol Chem, 1996. **271**(14): p. 7965-72.
290. Yu, F., et al., *The role of lysosome in cell death regulation.* Tumour Biol, 2016. **37**(2): p. 1427-36.
291. Dielschneider, R.F., E.S. Henson, and S.B. Gibson, *Lysosomes as Oxidative Targets for Cancer Therapy.* Oxid Med Cell Longev, 2017. **2017**: p. 3749157.
292. Kroemer, G. and B. Levine, *Autophagic cell death: the story of a misnomer.* Nat Rev Mol Cell Biol, 2008. **9**(12): p. 1004-10.
293. Boya, P., et al., *Inhibition of macroautophagy triggers apoptosis.* Mol Cell Biol, 2005. **25**(3): p. 1025-40.
294. Denton, D., et al., *Autophagy, not apoptosis, is essential for midgut cell death in Drosophila.* Curr Biol, 2009. **19**(20): p. 1741-6.
295. Grander, D., et al., *Autophagy as the main means of cytotoxicity by glucocorticoids in hematological malignancies.* Autophagy, 2009. **5**(8): p. 1198-200.
296. Levine, B. and G. Kroemer, *Autophagy in the pathogenesis of disease.* Cell, 2008. **132**(1): p. 27-42.
297. Galluzzi, L., et al., *Cell death modalities: classification and pathophysiological implications.* Cell Death And Differentiation, 2007. **14**: p. 1237.
298. Levine, B. and D.J. Klionsky, *Development by self-digestion: molecular mechanisms and biological functions of autophagy.* Dev Cell, 2004. **6**(4): p. 463-77.
299. Lamb, C.A., T. Yoshimori, and S.A. Tooze, *The autophagosome: origins unknown, biogenesis complex.* Nat Rev Mol Cell Biol, 2013. **14**(12): p. 759-74.
300. Russell, R.C., H.X. Yuan, and K.L. Guan, *Autophagy regulation by nutrient signaling.* Cell Res, 2014. **24**(1): p. 42-57.
301. Chan, E.Y., *Regulation and function of uncoordinated-51 like kinase proteins.* Antioxid Redox Signal, 2012. **17**(5): p. 775-85.
302. Russell, R.C., et al., *ULK1 induces autophagy by phosphorylating Beclin-1 and activating Vps34 lipid kinase.* Nat Cell Biol, 2013. **15**(7): p. 741-50.
303. Kang, R., et al., *The Beclin 1 network regulates autophagy and apoptosis.* Cell Death Differ, 2011. **18**(4): p. 571-80.
304. Hanada, T., et al., *The Atg12-Atg5 conjugate has a novel E3-like activity for protein lipidation in autophagy.* J Biol Chem, 2007. **282**(52): p. 37298-302.
305. Dooley, H.C., et al., *WIPI2 links LC3 conjugation with PI3P, autophagosome formation, and pathogen clearance by recruiting Atg12-5-16L1.* Mol Cell, 2014. **55**(2): p. 238-52.
306. Kabeya, Y., et al., *LC3, GABARAP and GATE16 localize to autophagosomal membrane depending on form-II formation.* J Cell Sci, 2004. **117**(Pt 13): p. 2805-12.

307. Tanida, I., T. Ueno, and E. Kominami, *LC3 conjugation system in mammalian autophagy.* Int J Biochem Cell Biol, 2004. **36**(12): p. 2503-18.
308. Park, S., et al., *Choline dehydrogenase interacts with SQSTM1/p62 to recruit LC3 and stimulate mitophagy.* Autophagy, 2014. **10**(11): p. 1906-20.
309. Yang, Z., et al., *Atg22 recycles amino acids to link the degradative and recycling functions of autophagy.* Mol Biol Cell, 2006. **17**(12): p. 5094-104.
310. Overmeyer, J.H., et al., *Active ras triggers death in glioblastoma cells through hyperstimulation of macropinocytosis.* Mol Cancer Res, 2008. **6**(6): p. 965-77.
311. Kaul, A., J.H. Overmeyer, and W.A. Maltese, *Activated Ras induces cytoplasmic vacuolation and non-apoptotic death in glioblastoma cells via novel effector pathways.* Cell Signal, 2007. **19**(5): p. 1034-43.
312. Brel, V., et al., *Cytotoxicity and cell death mechanisms induced by the polyamine-vectorized anti-cancer drug F14512 targeting topoisomerase II.* Biochem Pharmacol, 2011. **82**(12): p. 1843-52.
313. Overmeyer, J.H., et al., *A chalcone-related small molecule that induces methuosis, a novel form of non-apoptotic cell death, in glioblastoma cells.* Mol Cancer, 2011. **10**: p. 69.
314. Minna, E., et al., *miR-199a-3p displays tumor suppressor functions in papillary thyroid carcinoma.* Oncotarget, 2014. **5**(9): p. 2513-28.
315. Trabbic, C.J., et al., *Differential Induction of Cytoplasmic Vacuolization and Methuosis by Novel 2-Indolyl-Substituted Pyridinylpropenones.* ACS Med Chem Lett, 2014. **5**(1): p. 73-77.
316. Reyes-Reyes, E.M., et al., *Mechanistic studies of anticancer aptamer AS1411 reveal a novel role for nucleolin in regulating Rac1 activation.* Mol Oncol, 2015. **9**(7): p. 1392-405.
317. Manara, M.C., et al., *CD99 triggering induces methuosis of Ewing sarcoma cells through IGF-1R/RAS/Rac1 signaling.* Oncotarget, 2016. **7**(48): p. 79925-79942.
318. Cingolani, F., et al., *Jaspine B induces nonapoptotic cell death in gastric cancer cells independently of its inhibition of ceramide synthase.* J Lipid Res, 2017. **58**(8): p. 1500-1513.
319. Sander, P., et al., *Vacquinol-1 inducible cell death in glioblastoma multiforme is counter regulated by TRPM7 activity induced by exogenous ATP.* Oncotarget, 2017. **8**(21): p. 35124-35137.
320. Sun, L., et al., *An Ursolic Acid Derived Small Molecule Triggers Cancer Cell Death through Hyperstimulation of Macropinocytosis.* J Med Chem, 2017. **60**(15): p. 6638-6648.
321. Huang, W., et al., *Discovery and Identification of Small Molecules as Methuosis Inducers with in Vivo Antitumor Activities.* J Med Chem, 2018. **61**(12): p. 5424-5434.
322. Maltese, W.A. and J.H. Overmeyer, *Methuosis: Nonapoptotic Cell Death Associated with Vacuolization of Macropinosome and Endosome Compartments.* The American Journal of Pathology, 2014. **184**(6): p. 1630-1642.
323. Lim, J.P. and P.A. Gleeson, *Macropinocytosis: an endocytic pathway for internalising large gulps.* Immunology And Cell Biology, 2011. **89**: p. 836.
324. Haigler, H.T., J.A. McKanna, and S. Cohen, *Rapid stimulation of pinocytosis in human carcinoma cells A-431 by epidermal growth factor.* J Cell Biol, 1979. **83**(1): p. 82-90.
325. Racoosin, E.L. and J.A. Swanson, *Macrophage colony-stimulating factor (rM-CSF) stimulates pinocytosis in bone marrow-derived macrophages.* J Exp Med, 1989. **170**(5): p. 1635-48.
326. Dharmawardhane, S., et al., *Regulation of macropinocytosis by p21-activated kinase-1.* Mol Biol Cell, 2000. **11**(10): p. 3341-52.
327. WH, L., *Pinocyosis.* John Hopkins Hospital Bulletin, 1931. **49**: p. 17-27.
328. Huotari, J. and A. Helenius, *Endosome maturation.* Embo j, 2011. **30**(17): p. 3481-500.
329. Di Paolo, G. and P. De Camilli, *Phosphoinositides in cell regulation and membrane dynamics.* Nature, 2006. **443**(7112): p. 651-7.

330. Hall, A. and C.D. Nobes, *Rho GTPases: molecular switches that control the organization and dynamics of the actin cytoskeleton.* Philos Trans R Soc Lond B Biol Sci, 2000. **355**(1399): p. 965-70.
331. Egami, Y., et al., *Small GTPases and phosphoinositides in the regulatory mechanisms of macropinosome formation and maturation.* Front Physiol, 2014. **5**.
332. Fujii, M., et al., *Dissecting the roles of Rac1 activation and deactivation in macropinocytosis using microscopic photo-manipulation.* Sci Rep, 2013. **3**: p. 2385.
333. Suetsugu, S., et al., *Differential roles of WAVE1 and WAVE2 in dorsal and peripheral ruffle formation for fibroblast cell migration.* Dev Cell, 2003. **5**(4): p. 595-609.
334. Samson, T., et al., *Endogenous RhoG is rapidly activated after epidermal growth factor stimulation through multiple guanine-nucleotide exchange factors.* Mol Biol Cell, 2010. **21**(9): p. 1629-42.
335. Zawistowski, J.S., et al., *A RhoC biosensor reveals differences in the activation kinetics of RhoA and RhoC in migrating cells.* PLoS One, 2013. **8**(11): p. e79877.
336. Bhanot, H., et al., *Induction of nonapoptotic cell death by activated Ras requires inverse regulation of Rac1 and Arf6.* Mol Cancer Res, 2010. **8**(10): p. 1358-74.
337. Chi, S., et al., *Oncogenic Ras triggers cell suicide through the activation of a caspase-independent cell death program in human cancer cells.* Oncogene, 1999. **18**(13): p. 2281-90.
338. Dendo, K., et al., *Induction of non-apoptotic programmed cell death by oncogenic RAS in human epithelial cells and its suppression by MYC overexpression.* Carcinogenesis, 2018. **39**(2): p. 202-213.
339. Kitanaka, C., et al., *Increased Ras expression and caspase-independent neuroblastoma cell death: possible mechanism of spontaneous neuroblastoma regression.* J Natl Cancer Inst, 2002. **94**(5): p. 358-68.
340. Porat-Shliom, N., Y. Kloog, and J.G. Donaldson, *A unique platform for H-Ras signaling involving clathrin-independent endocytosis.* Mol Biol Cell, 2008. **19**(3): p. 765-75.
341. Haga, Y., et al., *CtBP1/BARS is an activator of phospholipase D1 necessary for agonist-induced macropinocytosis.* Embo j, 2009. **28**(9): p. 1197-207.
342. Humphreys, D., et al., *Arf6 coordinates actin assembly through the WAVE complex, a mechanism usurped by Salmonella to invade host cells.* Proc Natl Acad Sci U S A, 2013. **110**(42): p. 16880-5.
343. Hoon, J.L., W.K. Wong, and C.G. Koh, *Functions and regulation of circular dorsal ruffles.* Mol Cell Biol, 2012. **32**(21): p. 4246-57.
344. Dowrick, P., et al., *Circular ruffle formation and closure lead to macropinocytosis in hepatocyte growth factor/scatter factor-treated cells.* Eur J Cell Biol, 1993. **61**(1): p. 44-53.
345. Palamidessi, A., et al., *Endocytic trafficking of Rac is required for the spatial restriction of signaling in cell migration.* Cell, 2008. **134**(1): p. 135-47.
346. Itoh, T. and J. Hasegawa, *Mechanistic insights into the regulation of circular dorsal ruffle formation.* J Biochem, 2013. **153**(1): p. 21-9.
347. Lanzetti, L., et al., *Rab5 is a signalling GTPase involved in actin remodelling by receptor tyrosine kinases.* Nature, 2004. **429**(6989): p. 309-14.
348. Legg, J.A., et al., *N-WASP Involvement in Dorsal Ruffle Formation in Mouse Embryonic Fibroblasts.* Mol Biol Cell, 2007. **18**(2): p. 678-87.
349. Cao, H., F. Garcia, and M.A. McNiven, *Differential Distribution of Dynamin Isoforms in Mammalian Cells.* Mol Biol Cell, 1998. **9**(9): p. 2595-609.
350. McNiven, M.A., et al., *Regulated interactions between dynamin and the actin-binding protein cortactin modulate cell shape.* J Cell Biol, 2000. **151**(1): p. 187-98.

351. Liu, Y.W., et al., *Isoform and splice-variant specific functions of dynamin-2 revealed by analysis of conditional knock-out cells.* Mol Biol Cell, 2008. **19**(12): p. 5347-59.
352. Kitanaka, C. and Y. Kuchino, *Caspase-independent programmed cell death with necrotic morphology.* Cell Death Differ, 1999. **6**(6): p. 508-15.
353. Nara, A., et al., *Methamphetamine induces macropinocytosis in differentiated SH-SY5Y human neuroblastoma cells.* Brain Res, 2010. **1352**: p. 1-10.
354. Nara, A., et al., *Hyperstimulation of macropinocytosis leads to lysosomal dysfunction during exposure to methamphetamine in SH-SY5Y cells.* Brain Res, 2012. **1466**: p. 1-14.
355. Li, C., et al., *Nerve growth factor activation of the TrkA receptor induces cell death, by macropinocytosis, in medulloblastoma Daoy cells.* J Neurochem, 2010. **112**(4): p. 882-99.
356. Li, C., et al., *Unravelling the Mechanism of TrkA-Induced Cell Death by Macropinocytosis in Medulloblastoma Daoy Cells.* Mol Cell Biol, 2016. **36**(20): p. 2596-611.
357. Robinson, M.W., et al., *Synthesis and evaluation of indole-based chalcones as inducers of methuosis, a novel type of nonapoptotic cell death.* J Med Chem, 2012. **55**(5): p. 1940-56.
358. Trabbic, C.J., et al., *Synthesis and biological evaluation of indolyl-pyridinyl-propenones having either methuosis or microtubule disruption activity.* J Med Chem, 2015. **58**(5): p. 2489-512.
359. Mbah, N.E., J.H. Overmeyer, and W.A. Maltese, *Disruption of endolysosomal trafficking pathways in glioma cells by methuosis-inducing indole-based chalcones.* Cell Biol Toxicol, 2017. **33**(3): p. 263-282.
360. Kitambi, S.S., et al., *RETRACTED: Vulnerability of glioblastoma cells to catastrophic vacuolization and death induced by a small molecule.* Cell, 2014. **157**(2): p. 313-328.
361. Ahlstedt, J., et al., *Evaluating vacquinol-1 in rats carrying glioblastoma models RG2 and NS1.* Oncotarget, 2018. **9**(9): p. 8391-8399.
362. Maltese, W.A. and J.H. Overmeyer, *Non-apoptotic cell death associated with perturbations of macropinocytosis.* Front Physiol, 2015. **6**: p. 38.
363. Connell, P.P. and S. Hellman, *Advances in Radiotherapy and Implications for the Next Century: A Historical Perspective.* Cancer Research, 2009. **69**(2): p. 383-392.
364. Powell, S. and T.J. McMillan, *DNA damage and repair following treatment with ionizing radiation.* Radiotherapy and Oncology, 1990. **19**(2): p. 95-108.
365. Lobo, V., et al., *Free radicals, antioxidants and functional foods: Impact on human health.* Pharmacogn Rev, 2010. **4**(8): p. 118-26.
366. Prise, K.M., et al., *New insights on cell death from radiation exposure.* Lancet Oncol, 2005. **6**(7): p. 520-8.
367. Dixon, R.L., *General equation for the calculation of nominal standard dose.* Acta Radiol Ther Phys Biol, 1972. **11**(4): p. 305-11.
368. Joiner, M.C., et al., *Low-dose hypersensitivity: current status and possible mechanisms.* Int J Radiat Oncol Biol Phys, 2001. **49**(2): p. 379-89.
369. Withers, H.R., *The Four R's of Radiotherapy*, in *Advances in Radiation Biology*, J.T. Lett and H. Adler, Editors. 1975, Elsevier. p. 241-271.
370. Steel, G.G., T.J. McMillan, and J.H. Peacock, *The 5Rs of radiobiology.* Int J Radiat Biol, 1989. **56**(6): p. 1045-8.
371. Pawlik, T.M. and K. Keyomarsi, *Role of cell cycle in mediating sensitivity to radiotherapy.* International Journal of Radiation Oncology*Biology*Physics, 2004. **59**(4): p. 928-942.
372. Robinson, M.F., et al., *Increased Tumor Oxygenation and Radiation Sensitivity in two Rat Tumors by A Hemoglobin-Based, Oxygen-Carrying Preparation.* Artificial Cells, Blood Substitutes, and Biotechnology, 1995. **23**(3): p. 431-438.
373. Kallman, R.F., *The phenomenon of reoxygenation and its implications for fractionated radiotherapy.* Radiology, 1972. **105**(1): p. 135-42.

374. Graeber, T.G., et al., *Hypoxia-mediated selection of cells with diminished apoptotic potential in solid tumours.* Nature, 1996. **379**(6560): p. 88-91.
375. Diehn, M., et al., *Association of reactive oxygen species levels and radioresistance in cancer stem cells.* Nature, 2009. **458**: p. 780.
376. E.J., H., *Radiobiology for the radiologist*. Vol. 7. 2012, Philadelphia, USA: Wolters Kluwer Lippincott Williams and Wilkins.
377. Wallace, S.S., *Enzymatic processing of radiation-induced free radical damage in DNA.* Radiat Res, 1998. **150**(5 Suppl): p. S60-79.
378. Moore, J.K. and J.E. Haber, *Cell cycle and genetic requirements of two pathways of nonhomologous end-joining repair of double-strand breaks in Saccharomyces cerevisiae.* Mol Cell Biol, 1996. **16**(5): p. 2164-73.
379. Wright, W.D., S.S. Shah, and W.D. Heyer, *Homologous recombination and the repair of DNA double-strand breaks.* J Biol Chem, 2018. **293**(27): p. 10524-10535.
380. Nagasawa, H. and J.B. Little, *Induction of sister chromatid exchanges by extremely low doses of alpha-particles.* Cancer Res, 1992. **52**(22): p. 6394-6.
381. Lehnert, B.E., E.H. Goodwin, and A. Deshpande, *Extracellular factor(s) following exposure to alpha particles can cause sister chromatid exchanges in normal human cells.* Cancer Res, 1997. **57**(11): p. 2164-71.
382. Khan, M.A., R.P. Hill, and J. Van Dyk, *Partial volume rat lung irradiation: an evaluation of early DNA damage.* Int J Radiat Oncol Biol Phys, 1998. **40**(2): p. 467-76.
383. Hinchcliffe, E.H., et al., *Chromosome missegregation during anaphase triggers p53 cell cycle arrest through histone H3.3 Ser31 phosphorylation.* Nat Cell Biol, 2016. **18**(6): p. 668-75.
384. Campisi, J., *Aging, cellular senescence, and cancer.* Annu Rev Physiol, 2013. **75**: p. 685-705.
385. He, S. and N.E. Sharpless, *Senescence in Health and Disease.* Cell, 2017. **169**(6): p. 1000-1011.
386. Macià i Garau, M., A. Lucas Calduch, and E.C. López, *Radiobiology of the acute radiation syndrome.* Rep Pract Oncol Radiother, 2011. **16**(4): p. 123-30.
387. Andreassen, C.N., *Can risk of radiotherapy-induced normal tissue complications be predicted from genetic profiles?* Acta Oncol, 2005. **44**(8): p. 801-15.
388. Follin, C. and E.M. Erfurth, *Long-Term Effect of Cranial Radiotherapy on Pituitary-Hypothalamus Area in Childhood Acute Lymphoblastic Leukemia Survivors.* Curr Treat Options Oncol, 2016. **17**(9): p. 50.
389. Johnston, K., et al., *Failure to lactate: a possible late effect of cranial radiation.* Pediatr Blood Cancer, 2008. **50**(3): p. 721-2.
390. Sfeir, J.G., et al., *Diagnosis of Growth Hormone Deficiency as a Late Effect of Radiotherapy in Survivors of Childhood Cancers.* J Clin Endocrinol Metab, 2018.
391. Constine, L.S., *Cured of Hodgkin lymphoma, but suffering a broken heart.* Leuk Lymphoma, 2008. **49**(8): p. 1433-5.
392. Mulhern, R.K., et al., *Late neurocognitive sequelae in survivors of brain tumours in childhood.* The Lancet Oncology, 2004. **5**(7): p. 399-408.
393. Constine, L.S., et al., *Subsequent malignancies in children treated for Hodgkin's disease: associations with gender and radiation dose.* Int J Radiat Oncol Biol Phys, 2008. **72**(1): p. 24-33.
394. Crump, M. and D. Hodgson, *Secondary breast cancer in Hodgkin's lymphoma survivors.* J Clin Oncol, 2009. **27**(26): p. 4229-31.
395. Fraass, B.A., *The development of conformal radiation therapy.* Med Phys, 1995. **22**(11 Pt 2): p. 1911-21.
396. Raziee, H., et al., *Improved outcomes with dose escalation in localized prostate cancer treated with precision image-guided radiotherapy.* Radiotherapy and Oncology, 2017. **123**(3): p. 459-465.

397. Kong, F., et al., *Clinical outcome of intensity modulated radiotherapy for carcinoma showing thymus-like differentiation.* Oncotarget, 2016. **7**(49): p. 81899-81905.
398. Gupta, T., et al., *Three-dimensional conformal radiotherapy (3D-CRT) versus intensity modulated radiation therapy (IMRT) in squamous cell carcinoma of the head and neck: A randomized controlled trial.* Radiotherapy and Oncology, 2012. **104**(3): p. 343-348.
399. Bentzen, S.M., *Preventing or reducing late side effects of radiation therapy: radiobiology meets molecular pathology.* Nat Rev Cancer, 2006. **6**(9): p. 702-13.
400. Bentzen, S.M., P.M. Harari, and J. Bernier, *Exploitable mechanisms for combining drugs with radiation: concepts, achievements and future directions.* Nat Clin Pract Oncol, 2007. **4**(3): p. 172-80.
401. Wolden, S.L., et al., *Indications for radiotherapy and chemotherapy after complete resection in rhabdomyosarcoma: A report from the Intergroup Rhabdomyosarcoma Studies I to III.* J Clin Oncol, 1999. **17**(11): p. 3468-75.
402. Weber, D.C., et al., *Proton therapy for pediatric malignancies: Fact, figures and costs. A joint consensus statement from the pediatric subcommittee of PTCOG, PROS and EPTN.* Radiotherapy and Oncology, 2018.
403. Breneman, J.C., et al., *The Children's Oncology Group Radiation Oncology Discipline: 15 Years of Contributions to the Treatment of Childhood Cancer.* Int J Radiat Oncol Biol Phys, 2018. **101**(4): p. 860-874.
404. Terezakis, S.A. and M.D. Wharam, *Radiotherapy for Rhabdomyosarcoma: Indications and Outcome.* Clinical Oncology, 2013. **25**(1): p. 27-35.
405. Paulino, A.C., et al., *Long-term effects in children treated with radiotherapy for head and neck rhabdomyosarcoma.* International Journal of Radiation Oncology • Biology • Physics, 2000. **48**(5): p. 1489-1495.
406. Donaldson, S.S., et al., *Results from the IRS-IV randomized trial of hyperfractionated radiotherapy in children with rhabdomyosarcoma--a report from the IRSG.* Int J Radiat Oncol Biol Phys, 2001. **51**(3): p. 718-28.
407. Wolden, S.L., et al., *Intensity-modulated radiotherapy for head-and-neck rhabdomyosarcoma.* Int J Radiat Oncol Biol Phys, 2005. **61**(5): p. 1432-8.
408. Combs, S.E., et al., *Intensity Modulated Radiotherapy (IMRT) and Fractionated Stereotactic Radiotherapy (FSRT) for children with head-and-neck-rhabdomyosarcoma.* BMC Cancer, 2007. **7**: p. 177.
409. Kozak, K.R., et al., *A dosimetric comparison of proton and intensity-modulated photon radiotherapy for pediatric parameningeal rhabdomyosarcomas.* Int J Radiat Oncol Biol Phys, 2009. **74**(1): p. 179-86.
410. Yock, T., et al., *Proton radiotherapy for orbital rhabdomyosarcoma: clinical outcome and a dosimetric comparison with photons.* Int J Radiat Oncol Biol Phys, 2005. **63**(4): p. 1161-8.
411. Baguley, B.C., *Multiple drug resistance mechanisms in cancer.* Mol Biotechnol, 2010. **46**(3): p. 308-16.
412. Fulda, S., *Targeting apoptosis resistance in rhabdomyosarcoma.* Curr Cancer Drug Targets, 2008. **8**(6): p. 536-44.
413. Fulda, S., *Therapeutic opportunities based on caspase modulation.* Seminars in Cell & Developmental Biology, 2017.
414. Cuperus, R., et al., *Fenretinide induces mitochondrial ROS and inhibits the mitochondrial respiratory chain in neuroblastoma.* Cell Mol Life Sci, 2010. **67**(5): p. 807-16.
415. Shubin, A.V., et al., *Cytoplasmic vacuolization in cell death and survival.* Oncotarget, 2016. **7**(34): p. 55863-89.

416. Sperandio, S., I. de Belle, and D.E. Bredesen, *An alternative, nonapoptotic form of programmed cell death.* Proc Natl Acad Sci U S A, 2000. **97**(26): p. 14376-81.
417. Weerasinghe, P. and L.M. Buja, *Oncosis: an important non-apoptotic mode of cell death.* Exp Mol Pathol, 2012. **93**(3): p. 302-8.
418. Orth, J.D., et al., *A novel endocytic mechanism of epidermal growth factor receptor sequestration and internalization.* Cancer Res, 2006. **66**(7): p. 3603-10.
419. Orth, J.D. and M.A. McNiven, *Get off my back! Rapid receptor internalization through circular dorsal ruffles.* Cancer Res, 2006. **66**(23): p. 11094-6.
420. Ha, S.J., et al., *Syringic acid prevents skin carcinogenesis via regulation of NoX and EGFR signaling.* Biochem Pharmacol, 2018.
421. Paulsen, C.E., et al., *Peroxide-dependent sulfenylation of the EGFR catalytic site enhances kinase activity*. Nature Chemical Biology, 2011. **8**: p. 57.
422. Aslan, M. and T. Ozben, *Oxidants in receptor tyrosine kinase signal transduction pathways.* Antioxid Redox Signal, 2003. **5**(6): p. 781-8.
423. Maltese, W.A. and J.H. Overmeyer, *Methuosis: nonapoptotic cell death associated with vacuolization of macropinosome and endosome compartments.* Am J Pathol, 2014. **184**(6): p. 1630-42.
424. Zhang, M., C.M. Linardic, and D.G. Kirsch, *RAS and ROS in Rhabdomyosarcoma.* Cancer Cell, 2013. **24**(6): p. 689-91.
425. Jaffray, D.A., *Delineating Organs at Risk in Radiation Therapy*. 2014: Springer Science & Business Media.
426. Raney, R.B., *The Intergroup Rhabdomyosarcoma Study Group (IRSG): Major Lessons From the IRS-I Through IRS-IV Studies as Background for the Current IRS-V Treatment Protocols.* 2001. **5**(1): p. 9-15.
427. Brown, J.M., *The hypoxic cell: a target for selective cancer therapy--eighteenth Bruce F. Cain Memorial Award lecture.* Cancer Res, 1999. **59**(23): p. 5863-70.
428. Masunaga, S.I., et al., *Effect of Tirapazamine, Metformin or Mild Hyperthermia on Recovery From Radiation-Induced Damage in Pimonidazole-Unlabeled Quiescent Tumor Cells.* World J Oncol, 2017. **8**(5): p. 137-146.
429. Ogawa, Y., et al., *Phase I study of a new radiosensitizer containing hydrogen peroxide and sodium hyaluronate for topical tumor injection: a new enzyme-targeting radiosensitization treatment, Kochi Oxydol-Radiation Therapy for Unresectable Carcinomas, Type II (KORTUC II).* Int J Oncol, 2009. **34**(3): p. 609-18.
430. Tsoli, M., et al., *DIPG-05. Combination of Synthetic Retinoid Fenretinide with Receptor Tyrosine Kinase Inhibitor as a Potential New Approach Against Diffuse Intrinsic Pontine Glimoma.* Neuro Oncol, 2017. **19**(Suppl 4): p. iv5-6.
431. Strasser-Wozak, E.M., et al., *Irradiation induces G2/M cell cycle arrest and apoptosis in p53-deficient lymphoblastic leukemia cells without affecting Bcl-2 and Bax expression.* Cell Death Differ, 1998. **5**(8): p. 687-93.
432. Cowan, A.J., et al., *Bortezomib and fenretinide induce synergistic cytotoxicity in mantle cell lymphoma through apoptosis, cell-cycle dysregulation, and IkappaBalpha kinase downregulation.* Anticancer Drugs, 2015. **26**(9): p. 974-83.
433. Schumacker, P.T., *Reactive oxygen species in cancer cells: Live by the sword, die by the sword.* Cancer Cell, 2006. **10**(3): p. 175-176.
434. Cooper, J.P., et al., *Clinical development of fenretinide as an antineoplastic drug: Pharmacology perspectives.* Exp Biol Med (Maywood), 2017. **242**(11): p. 1178-1184.